The Solar Assisted Smart Public Transportation System and its Coordination with the Grid

M. Bhaskar Naik

The Solar Assisted Smart Public Transportation System and its Coordination with the Grid

A

Thesis submitted

for the award of the degree of

DOCTOR OF PHILOSOPHY

By

M. Bhaskar Naik

Department of Electronics and Electrical Engineering

Indian Institute of Technology Guwahati

Guwahati-781039, Assam, India

August 2017

Dedicated to:

My Dear Wife and Son,
Eng. M. Pavani and M. Tarak Ram Naik;

My Beloved Parents,
M. Laxmi Bai and M. Chandya Naik;

My Supervisors,
Dr. Praveen Kumar and Dr. Somanath Majhi;

And

My Sisters,
M. Venkatlaxmi Bai, M. Lalitha Bai,
M. Amrutha Bai and M. Aruna Bai

Declaration

This is to certify that the thesis entitled "**The Solar Assisted Smart Public Transportation System and it's Coordination with the Grid**", submitted by me to the *Indian Institute of Technology Guwahati*, for the award of the degree of **Doctor of Philosophy**, under the supervision of Dr. Praveen Kumar and Dr. Somanath Majhi. The content of this thesis, in full or in parts, have not been submitted to any other University or Institute for the award of any degree or diploma.

Date: Signed: _____.

Place: Guwahati.

M. Bhaskar Naik

Electronics and Electrical Engineering Department,
Indian Institute of Technology Guwahati,
Guwahati - 781039, Assam, India.

Certificate

This is to certify that the thesis entitled "**The Solar Assisted Smart Public Transportation System and it's Coordination with the Grid**", submitted by **M. Bhaskar Naik** (11610220), a research scholar in the *Department of Electronics and Electrical Engineering, Indian Institute of Technology Guwahati*, for the award of the degree of **Doctor of Philosophy**, is a record of an original research work carried out by him under our supervision and guidance. The thesis has fulfilled all requirements as per the regulations of the institute and in our opinion has reached the standard needed for submission. The results embodied in this thesis have not been submitted to any other University or Institute for the award of any degree or diploma.

Date:

Place: Guwahati.

Signed: _____.

Dr. Praveen Kumar,
Electronics and Electrical Engineering Department,
Indian Institute of Technology Guwahati,
Guwahati - 781039, Assam, India.

Signed: _____.

Dr. Somanath Majhi,
Electronics and Electrical Engineering Department,
Indian Institute of Technology Guwahati,
Guwahati - 781039, Assam, India.

Acknowledgement

First of all its my privilege to express sincere gratitude to the thesis supervisors Dr. Praveen Kumar and Dr. Somanath Majhi. I respect both of these important persons of my life, from the bottom of my heart.

Dr. Praveen Kumar's strictness and punctuality at work taught me the importance of hard work. This provided the self-confidence to withstand all the difficult moments in life and to achieve the success. My heart full thanks to you sir, for your kind supervision, suggestions, motivation, patience, cooperation and forgiveness.

Dr. Somanath Majhi's teaching style attracted me immensely and created more interest towards the studies. His simple way of explanations, expressions and the communicating style with the students creates a hope towards beautiful feature. I am grateful to you sir, for your kind monitoring, attribute of help, valuable advices, and friendliness.

Further, my gratitude to the doctoral committee members: Prof. Sanjay Kumar Bose, Dr. Indrani Kar and Dr. Sisir Nayak for evaluating the progress of this thesis work. The time management, perfectness in every small topic and maintaining the confidence while delivering the presentation are the qualities that I have learned from these three respectable persons.

Also, I would like to thank the 'Head of the Department' and all other faculty members of EEE department for their kind cooperation to carry out this work. I appreciate the readiness of the non-teaching staff and technical assistants of EEE department, to help in any type of matter.

My special thanks to prof. R. Battacharjee, Prof. A.K. Gogoi, Prof. G.B. Shrestha and Prof. M. Chitra for their valuable support in critical situations while carrying this work. Also, I am thankful to Dr. P. Tripathy, Dr. A. Ravindranath, Dr. Shabarinath and Dr. S. Krisnaswami for their valuable suggestions.

I thank my seniors and fellow researchers Dr. Kannan, Dr. Mukesh, Dr. Ranjib and Dr. Reena for their extreme support and motivation to finish this work. Also, they assigned their valuable time to clarify the doubts which I had regarding this work.

I thank the fellow research students and B. Tech students: Mr. Mahesh, Mr. Aishwarya, Mr. Dharmendra, Mr. Ashish, Mr. Gunawath and Mr. S. Ghonzalo for their friendly interaction and cooperation regarding the thesis work.

My exclusive and individual thanks to: the important persons who are responsible for my happiest stay at IIT Guwahati. They are: Mr. Shanthi Kumar and his wife Anjali, Dr. Kannan, Dr. Suryaprakash, Dr. Ajay, Mr. Harikrishna, Mr. Nagender Naik, Dr. Bheem Raju, Dr. Nagesh, Dr. Yadav, Dr. Suresh, Mr. Kasi, Mr. K. Inala, Mr. Upendra and Mr. V. Jagath. I shared most of my feelings with these persons during happiest and saddest moments and they showed their love and affection towards me.

I express my special thanks to Ph.D. batch mates and friends: Dr. Bhajarangabali, Dr. Ankit, Dr. Saroj, Dr. Brajesh, Dr. S. Kundu, Dr. Sikandar, Dr. Holoi, Dr. Ramesh, Dr. Karam, Dr. S. Pandey, Dr. Nabanitha, Miss. Baita and Mrs. Sonali for their respect and friendliness with me.

I thank Dr. Shiva, Dr. Deepak, Dr. Anil, Dr. Vishwa, Dr. Kabir, Dr. Radha, Mr. Satya, Mr. Praveen and Mr. Ravi for their continuous encouragement while doing this thesis work. Also, I thank my school mates and college mates for their excellent support and friendship. Their motivation led me to do this work.

My sincere and deepest gratitude to: my parents (M. Chandya Naik and M. Laxmi Bai), my wife (Eng. M. Pavani) and my son (M. Tarak Ram Naik) for their continuous love, affection and support during my studies. Their sacrifices definitely stay at higher level and are the main reasons to achieve this position. Therefore, I pay attention with obedience towards them in any situation.

Further, my relatives played a great role to finish the thesis work. They are: M. Venktu, B. Baloji Naik, M. Lalli, M. Lachu Naik, M. Ambri, N. Chandra Naik, M. Aruna, S. Bhaskar Naik, my nieces: B. Vyshanavi and M. Jhansi, and my Nephews: B. Dinesh, M. Chaitu, N. Yugandhar, N. Vinay and S. Mahi. I am very grateful to them.

Finally, I believe this research experience will greatly benefit my carrier in the future.

M. Bhaskar Naik

Abstract

This thesis proposes the solar assisted smart public transportation system (SPTS) and it's interaction with the grid. SPTS consists of a specified number of electric bus stops that are present through the ring road of the Guwahati city, Assam, India. Every bus stop consists of a high capacity energy storage device (ESD) and these ESDs are responsible to communicate SPTS with the grid. ESDs receive energy from the grid during off-peak period and send its stored energy back to the grid during peak period. The charging and discharging performance of ESD mitigates the peak power demand of the grid (normally the grid remains under energy deficit condition during peak period). Also, ESD supplies energy to the electric buses (supercapacitor based energy storage system is used) for 24 h and performs the isolated operation of electric buses with the grid. The electric buses have been used to perform the mass transportation through the ring road of the Guwahati city.

SPTS completely depend on the grid if it is operated with only ESD. This may create severe failures in SPTS, if the grid is unable to supply energy to the SPTS. The assistance of solar energy plays an important role and reduces the grid dependency of SPTS. Therefore, the solar plants have been used in SPTS and connected to both, the grid and ESD at every bus stop. The controlled charging and discharging performance of ESD along with the solar plant performs the valley filling and peak shaving of the grid load profile.

In this thesis the active power has been controlled between the grid, ESD and the solar plant to improve the voltage profile of the grid during both the off-peak and peak periods. Also, the maximum priority has been given to utilize solar energy for SPTS support, while reducing the energy consumption from the grid. Therefore, an algorithm has been developed for the favorable energy support from both the grid and the solar plant to SPTS. This arrangement minimizes the SPTS reliance on the grid. Two types of days have been considered to show the variations in SPTS response through all the seasons of year. The random use of electric buses may trouble the functioning of both the grid and SPTS. Therefore, the exact numbers of electric buses should be required to perform the smooth operation of public transportation in SPTS. An algorithm has been developed to decide the optimal number of electric buses in SPTS. This algorithm determines the 'optimal number of electric buses' as a function of the load, the energy storage device, the solar plant and the passenger total. The electric buses halt

on their way if the consecutive bus stops failed to charge the electric buses. Therefore, the suitable communications have been provided at every bus stop and also, the suitable algorithms have been developed for the controllers that are required at every bus stop to manage the failure situations in SPTS. Finally, the capa-buses (supercapacitor based buses) and the electric vehicles have been utilized along with the electric buses to expand the electrified transportation network in the Guwahati city. Algorithm based controllers are responsible to control the energy flow between ESD and both, the capa-buses and electric vehicles. The fuzzy logic controller is present at every bus stop to control the energy flow between the grid, ESD and the solar plant. The complete system response has been verified through Simulations: for different situations in all the seasons of a year, and for the uncertain situations that exist in the system.

The main contributions of the thesis are given as follows:

- The favourable energy has been utilized from both, the grid and the solar plant to reduce the SPTS dependence on the grid.
- The optimal numbers of electric buses have been determined in SPTS and also, verified its self-sustainability for the different failures that exist in the SPTS.
- The smart public transportation network expansion has been carried out and also, verified its response: for all the seasons of a year and for the uncertain situations that exist in the system.

Index Terms: Capa-bus, electric bus, electric bus stop, electric vehicle, fuzzy logic controller, high capacity energy storage device, inductive charging system, smart public transportation system, solar irradiance, solar plant and supercapacitor.

CONTENTS

LIST OF FIGURES

LIST OF TABLES

भारतीय प्रौद्योगिकी संस्थान गुवाहाटी
Indian Institute of Technology Guwahati

LIST OF ACRONYMS

BS	Bus stop
CB	Capa-bus
CC	Communication channel
CTA	Central transportation authority
DOD	Depth of discharge of EV
DOF	The degree of fulfillment
DN	Distribution node
e-bus	Electric bus
EBS	Electric bus stop
ESD	High capacity energy storage device
EV	Electric vehicle
FLC	Fuzzy logic controller
ICS	Inductive charging system
ICSC	Inductive charging system controller
ISC	Isolation switch controller
ISP	Isolation switch position
KEBS	Khamakhya EBS
M	Monday
MEBS	Maligaav electric bus stop (EBS)
NB	Number of e-buses
ND	Normal day
NWD	Non-working day
NYCC	New York City Drive Cycle
ONB	Optimal number of e-buses
OPP	Off-peak period
$P\pm$	ESD receive/send power from/to the grid in OPP/PP
PP	Peak period
PVM	Photovoltaic module
R	Rainy season
S	Summer season

SCB	Set of CBs
SD	Special day
SEV	Set of EVs
SOC	State of charge of EV
SOC_{0i}	Initial *SOC* of EV
SP	Solar plant
SP±	SP send power to ESD/to the grid in OPP/PP
SPTS	Smart public transportation system
S_t	Saturday
S_u	Sunday
Vpu	Per unit voltage of the grid
W	Winter season
WD	Working day

LIST OF SYMBOLS

A	The frontal area of CB
B	Beam irradiance
B_0	Irradiance outside the atmosphere
$B(\theta)$	Beam irradiance with respect to θ
C	The sky clearness indicator
C_{CB}	The size of the supercapacitor in CB
C_D	Aerodynamic drag coefficient
C_i	The cloud amount in each layer
C_R	Charging rate of EV
D	Diffuse irradiance
$D(\theta)$	Diffuse irradiance with respect to θ
D_R	Discharging rate of EV
dV/dt	Acceleration of CB
EB_c	The passengers carrying capacity of e-bus
EB_f	The e-bus frequency
EB_{fd}	The daily e-bus frequency
EB_{fh}	The e-buses frequency in one hour
$E_{BT\ min/max}$	Minimum/maximum energy required by the e-bus
E_{CB}	Energy status of CB
E_{CBC}/E_{CBD}	Charge/discharge CBs from/to ESD
E_{CBmax}	Maximum charging limit of CB from ESD
$-E_{CBmax}$	Maximum discharging limit of CB to ESD
E_{CBnet}	The net energy availability of CBs
E_{CBR}	Energy required by CB
E_{CBT}	The amount of energy required by CB for completing a round trip of travel
E_{EB}	Energy given to the e-buses in a day
E_{EBRSH}	Total energy received by the e-buses from ESD in sunshine hours
E_{ESD}	ESD energy status
E_{ESDD}	The daily energy availability in the ESD
E_{ESDSH}	Energy remained in the ESD in sunshine hours

E_{ESDR}	Energy quantity received by ESD from $E_{SP\ node}$
E_{ESDmin}	Minimum energy status of ESD
E_{ESDmax}	Maximum energy status of ESD
E_{ESDT}	Total energy capacity of ESD
E_{ESDTS}	The energy required by the SPTS from ESD for 24 h
E_{EV}	Energy status of EV
E_{EVC}/E_{EVD}	Charge/discharge EVs from/to ESD
$E_{EVi\ C}$	Individual EV charging from ESD
$E_{EVi\ D}$	Individual EV discharging to ESD
$E_{EVi\ max}$	Maximum capacity of individual EV
$E_{EVi\ net}$	The net energy availability of individual EV
E_{EVmax}	Maximum charging limit of EV from ESD
$-E_{EVmax}$	Maximum discharging limit of EV to ESD
E_{EVnet}	A set of EVs net energy availability
E_{EVR}	The amount of energy remained in EV
E_{GG}	Energy given to the grid in peak hours
E_{PVM}	Energy produced by each photovoltaic module
E_R	Energy required by the e-bus
E_{RB}	The minimum energy required by the e-bus to travel between consecutive EBSs
E_{RCB}	Regenerative braking energy produced by the kinetic energy of CB
E_{RG}	Energy received from the grid in off-peak hours
E_{Scell}	Solar cell energy generation capacity
E_{SP}	SP energy status
$E_{SP\ \{(k)/\ (k-1)/\ (k-2)\}}$	E_{SP} at $k^{th}/\ k\text{-}1^{th}/\ k\text{-}2^{th}$ EBS
$E_{SP\ node}$	Extra bus bar provided through the ring road
E_T	Size of the solar plant
E_{TCB}	Tractive energy required by the CB
E_{TSP}	Total energy produced by the SP in a day
E_{TSPSH}	Total energy produced by SP in sunshine hours
F_A	Acceleration resistance

F_{AD}	Aero dynamic resistance
$F_{FLC\ \{(k)/\ (k-1)/\ (k-2)\}}$	FLC failed at k^{th}/ k-1^{th}/ k-2^{th} EBS
F_G	Grading resistance
F_R	Rolling resistance
f_r	Rolling resistance coefficient
F_{TCB}	Tractive force required by the CB
$F_{x\ \{(k)/\ (k-1)\}}$	Failure-x at k^{th}/ k-1^{th} EBS (x=1, 2, 4, 5)
$F_{x\ (k-2)}$	Failure-x at k-2^{th} EBS (x=4, 5)
G	Solar irradiance
G_{ex}	Extra-terrestrial irradiance
g	The gravitational acceleration
I	Output current of the solar cell
I_{ph}	Photocurrent
K_T	The clearness index
M	Mass of the CB
NB_1	NBs with respect to N_P
NB_2	NBs with respect to E_{ESD}
NB_3	NBs with respect to E_{SP}
N_P	Number of passengers per hour at EBS
$N_{P\ ND}$	Maximum passenger limit for ND
$N_{P\ SD}$	Maximum passenger limit for SD
ONB_{OPP}	ONB during OPP
ONB_{PP}	ONB during PP
P	The passengers
P_{ESDmax}	Maximum power limit of ESD during charging period in off-peak hours
$-P_{ESDmax}$	Maximum power limit of ESD during discharging period in peak hours
P_{EVC}	The amount of power received by EV in charging mode
P_{EVD}	The amount of power sent by EV to ESD in discharging mode
R_C	e-bus carrying capacity
RH	Relative humidity
SD1	Beehu (B_h)

SD2	Holi (H_o)
SD3	Dasara (D_u)
SD4	Diwali (D_i)
t	Time
V	The rated voltage of the supercapacitor
V_{actual}	Actual voltage of the grid with respect to load profile
V_{base}	The base voltage of the grid
Vpu_{max}	Maximum Vpu limit of the grid
Vpu_{min}	Minimum Vpu limit of the grid
σ	Longitude
$\emptyset$	Latitude
ω	Hour angle
δ	Solar declination angle
α	Solar elevation
ω_s	The sunrise angle
ψ	Solar azimuth
S	Solar constant
θ	The panel angle
β	The fraction of gravitational potential energy
ρ_a	Air mass density
μ	The grade of membership
μ(Vpu)	The grade of membership for Vpu
$\mu(E_{ESD})$	The grade of membership for E_{ESD}
μ(ONB)	The grade of membership for ONB
$\mu(E_{SP})$	The grade of membership for E_{SP}
$\mu(P\pm)$	The grade of membership for $P\pm$
$\mu(SP\pm)$	The grade of membership for $SP\pm$

1

Introduction

Contents

Introduction

The internal combustion engine vehicles (ICEVs) are the largest source of air pollution in urban regions. The superiority of ICEVs compared to other vehicles, is the major reason for their popularity [1]. The role of ICEVs in city traffic congestion aggravates the emission. The emission from ICEVs is a major contributor to the global warming and poor air quality in city regions [1]. Almost all Indian cities are victims of poor air quality [1].

Automobile utilization has become the major part of Indian lifestyle. For this reason, ICEVs become as the base for complete transportation sector. ICEVs use the petroleum as a source, to perform the mass transportation. Therefore, the transportation sector has become the largest user of petroleum products. Though the crude oil availability has increased in India, it is insufficient to meet the demand. India satisfies its total demand by importing the oil products from foreign countries [2]. The price variation of crude oil greatly affects the Indian economy [2]. Therefore, the use of petroleum based transportation systems should be minimized to achieve the improved air quality in city regions.

ICEV's replacement with the electric vehicles (EVs) is one of the possible solutions to mitigate such issues. EVs are more efficient than ICEVs [3]. EV based transportation system has the ability to use both, the renewable (wind, solar, biofuel etc.) and non-renewable (thermal, gas, nuclear etc.) electrical energy sources [3]. The advantages of EVs such as regenerative braking capability and wide range of output power make the electric based transportation system attractive in urban regions [3]. Therefore, the implementation of electrified transportation systems is essential in cities.

Electrical energy has contributed for the technological and economic growth of society across the globe. The basic needs of ever increasing population have raised the demand for electrical energy. This can be fulfilled by increasing the electricity generation capacity. India is the third largest power production country in the world. According to the central electricity authority of India (CEA), the total installed capacity in India is 307.278GW [4]. Power production from the different generating units in India is shown in Fig. 1.1. Thermal power plants produce 69.14% (60.69% from coal based plants, 8.15% from gas based plants and 0.29% from diesel based plants), the nuclear power plants produce 1.88%, the hydro power

plants produce 14.03% and the renewable energy sources produce 14.94% (9.41% from small-hydro plants, 61.15% from wind farms, 10.66% from bio-power plants and 18.54% from solar plants) [4]. The energy requirement in India is 1114.41 BU (TWh) against availability of 1090.85 BU with a shortage of 2.1% [4]. This energy gap is managed by load shedding. The peak power demand in India is 153.37 GW, but the available peak power is 148.47 GW with a deficit of 3.2% [4]. The power deficit can cause high stress on the grid during peak load hours. Also, it may lead to severe faults in the grid. The distributed energy generation systems and the grid integrated energy storage systems are capable of limiting the stress on the grid during peak load hours.

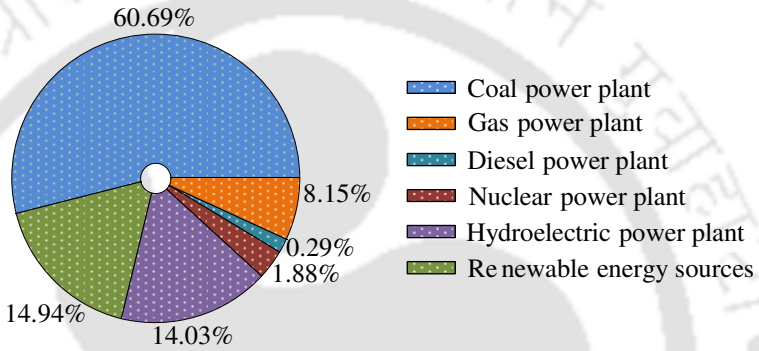

Fig. 1.1 The Power production from different generating units in India (as per year 2017)

The peak power-deficit is the common issue in all the regions of India. Assam state is located in the north-east region of India. The energy requirement in this state is 9.31 BU against the availability of 7.23 BU with a shortage of 22.4% [4]. This energy gap creates the power outage problems in Assam villages throughout the year. The peak power demand in Assam is 1.56 GW against the availability of 1.31 GW with a deficit of 16.02% [4]. Additional power plants installation can limit the energy-gap/power-deficit issues, but the high infrastructure cost is the main hurdle to their installation.

The peak load power management is one of the possible solutions to reduce stress of the grid in peak period. Normally, the grid remains under energy deficit condition during peak period. Therefore, the voltage profile remains unstable. Integration of the distributed energy storage systems, renewable energy sources and EVs with the grid regulates the voltage profile of the grid and also, performs the load leveling process of the grid load profile. The base load is termed as the minimum level of load demand on the distribution grid over 24 h. The grid remains under off-peak/peak period when the load profile of the grid stays below/above the based load. The load profile data is collected from the state electricity board

of Assam, India [5]. A sample load profile is shown in Fig. 1.2 [5]. The grid has surplus energy during off-peak period (from 23:00 to 07:00 h and from 12:30 to 16:30 h) (ref. Fig. 1.2). Therefore, this energy can be stored in the high capacity energy storage device (ESD) during off-peak period and the stored energy of ESD can be fed back into the grid during peak period (from 07:00 to 12:30 h and from 16:30 to 23:00 h) (ref. Fig. 1.2). ESD act as a load/source to the grid during off-peak/peak period [6]. The resultant load profile in Fig. 1.2 shows that the ESD has performed the valley filling and peak shaving of the grid load profile, during off-peak and peak period. Therefore, this process of energy transfer between the grid and ESD during off-peak and peak period improves the voltage profile of the grid.

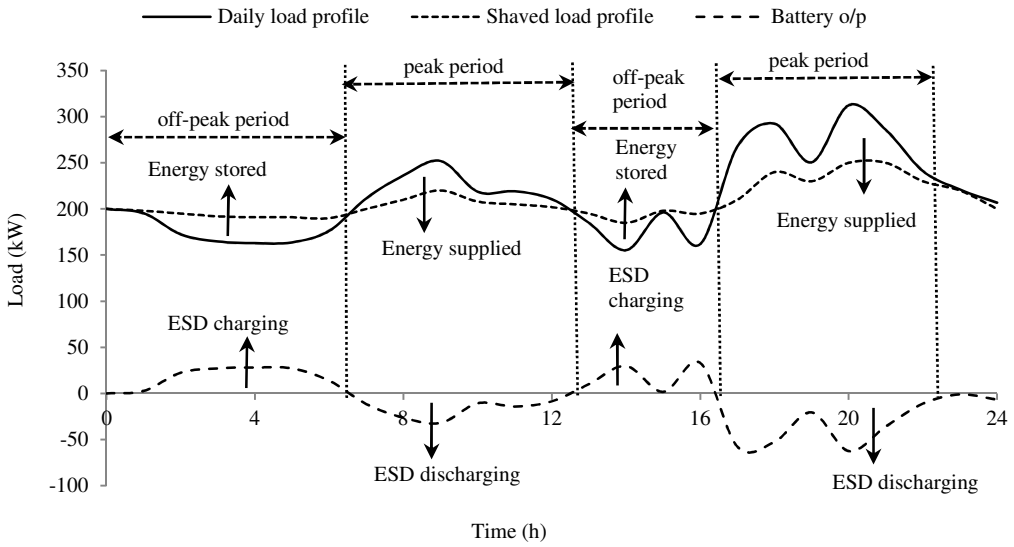

Fig. 1.2 Load profile of the distribution grid with energy storage device

The revolution in the storage technology has been started in the 21st century. High cost and small capacity of batteries were the major reasons for their limited use in power systems. However, new battery technologies have been developed in the 1st decade of the 21st century to provide the load-leveling capabilities. The different energy storage methods are therefore: chemical, electrical (capacitor, supercapacitor etc.), electrochemical (rechargeable and flow batteries), thermal and mechanical [7]. The selection of energy storage system should have to satisfy the following criteria such as:

- High charge and discharge cycle.
- The price per kWh stored energy must be competitive.
- It has to perform well for high current, short time discharges.
- Low maintenance cost

Development in the battery technology is shown in Table 1.1 [7]. Batteries can be divided into three types such as primary, secondary and specialized batteries. The primary batteries are non-rechargeable (use and throw type) batteries. The secondary batteries are rechargeable batteries. The specialized batteries are designed for specific applications and these are rechargeable batteries [7]. Among all the specialized batteries, the batteries for electrical energy storage applications are suitable to perform the load leveling process of the distribution grid. The vanadium redox flow battery (VRB) is one type in this category which satisfies the above mentioned criteria and is suitable to manage the peak load power demand in the Guwahati City, Assam, India.

Table 1.1: Battery types and their development [7]

S.no.	**Primary Batteries**	**Secondary Batteries**	**Specialized Batteries**
1.	Zinc-Carbon batteries (1866)	Lead-Acid batteries (1859)	Batteries for Electric and Hybrid Vehicles (1837)
2.	Magnesium and Aluminum batteries	Valve Regulated Lead-Acid batteries (1980)	Batteries for Electrical Energy Storage Applications (1988)
3.	Alkaline-Manganese Dioxide batteries (1959)	Iron Electrode batteries (1897)	Batteries for Biomedical Applications (1958)
4.	Mercuric Oxide batteries (1939)	Industrial and Aerospace Nickel-Cadmium batteries	Batteries for consumer electronics
5.	Silver Oxide-Zinc batteries (1960)	Vented Sintered Nickel-Cadmium batteries (1898)	Metal/Air Batteries
6.	Zinc-Air batteries (1961)	Portable Sealed Nickel-Cadmium batteries	Magnesium Water-Activated Batteries (1940)
7.	Lithium Primary batteries (1970)	Nickel-Metal Hydride batteries (1989)	Zinc/Silver Oxide Reserve Batteries (1942)
8.	-	Nickel –Zinc batteries (1901)	Ambient-Temperature Lithium Anode Reserve Batteries
9.	-	Nickel-Hydrogen Batteries	Spin-Dependent Reserve (1970)
10.	-	Silver Oxide Batteries (1800)	Thermal Batteries (1947)
11.	-	Lithium Ion Batteries (1991)	-
12.	-	Rechargeable Lithium Metal Batteries (1980)	-
13.	-	Rechargeable Zinc/Alkaline/Manganese Dioxide Batteries (1970)	-

The battery powered electrical vehicles (EVs) were introduced in 19th century. Thereafter, EV technology has achieved a progressive development. EVs show the following benefits such as: acts as the distributed energy storage, supports the transportation system, supports the grid during peak period and also, performs the load leveling process of the distribution grid. Introduction of Lithium-ion batteries has raised the EV market to a significant level with their prominent features [7]. Mostly, EVs are available in the daytime except their cruising period. This creates the possibility to communicate EVs with the distribution grid for

the maximum time period in a day (24 h). The grid coordinated EVs is a branch of smart grid technology. Andres Carvallo introduced the smart grid technology in 2004 [8]. The smart grid is the integration of an electric grid, a communication network, software and hardware to manage the generation, energy consumption and storage [8]. An advanced smart grid enables the integration of utility infrastructure with buildings, homes, EVs, distributed generation, batteries and smart devices to increase the energy efficiency, renewable energy use and customer satisfaction [8].

The expensive price and the battery maintenance of EVs (lifetime of the battery) are the major hurdles for their popularity. Therefore, EVs are unable to satisfy the requirements of common citizen. The public transportation systems such as: tram, trolleybus and supercapacitor based buses overcome such difficulty. All these systems are compatible to the common passenger to travel in city regions. However, these systems are grid powered and may create an extra stress on the grid during peak period (grid has to sustain these systems along with the load). Therefore, the grid dependency of transportation system should be minimized and also, the stress of the grid during peak period should be minimized. Utilization of ESDs and the solar power systems in public transportation systems may show the possibility to reduce the grid dependency of the transportation system and to reduce the stress of the grid during peak period. Therefore, the public transportation systems should satisfy the requirements of both, the grid and passengers. The supercapacitor based mass transportation systems are suitable to satisfy the above mentioned criteria. Therefore, these systems are gaining momentum, due to its safe operation, less operating cost, durable in harsh environment and friendly nature with the grid [62, 138].

This chapter is organized in the following manner. Section 1.1 describes the role of EVs in the smart grid technology including the concepts of ‘grid to vehicle’ and ‘vehicle to grid’, drawbacks of EVs and the importance of public transportation systems in city regions. Section 1.2 explains the literature review including the tram systems, trolleybus systems and supercapacitor based bus systems for urban transit. Also, explains the need of high capacity energy storage systems, importance of supercapacitors, contactless charging systems and the solar power systems in the smart grid technology. Section 1.3 explains the motivation of the thesis. Aim of the thesis is defined in Section 1.4. The contributions of the thesis are described in Section 1.5. Finally, the thesis organization is given in Section 1.6

1.1. EVs role in the smart grid technology

EV charging systems are of two types. One is the unidirectional charging system (grid to vehicle) and the other is bidirectional charging system (vehicle to grid). Energy flows from grid to vehicle in the unidirectional charging system. In this type of charging system, EVs utilize the total energy for transportation purpose so that EVs perform only the valley filling of the grid load profile. In the bidirectional charging system, energy flows from grid to vehicle as well as from vehicle to grid. In this type of charging system, EVs utilize energy for transportation purpose as well as to support the grid during peak period. Therefore, EVs perform both the valley filling and peak shaving of the grid load profile. Also, EVs charge from the grid with low tariff in off-peak period and discharge to the grid with high tariff during peak period. A fleet of EVs utilization at the distribution grid level provides the economic benefit to both, the grid and EV's owner. Bidirectional charging system suffices the grid as well as EVs.

1. 1.1 Grid to Vehicle

The plug-in EVs have gained popularity due to their clean performance in urban regions. These vehicles charge instantaneously when they are connected to an ordinary plug/standard outlet at home/at other locations. This type of EVs charging is known as the uncoordinated charging system and it may cause the voltage fluctuations in the grid. Therefore, Kristen *et al* [9] proposed the coordinated charging of EVs for improving power loss and grid load factor. They computed an optimal charging profile for EVs. The rise of plug-in EVs charging may lead to the potential stress, performance degradation and overloads to the distribution grid. Deilmai *et al* [10] proposed the load management solution for the coordinated charging of multiple plug-in EVs in the smart grid system. Also, they developed real time integration of plug-in EV charging system to reduce the total generating cost plus the losses associated with the grid. Kejun *et al* [11] proposed the modeling of the load demand in distribution system with EV charging. They also observed the different types of uncontrolled charging of EVs and their effects in different situations. In [12], control of EV charging loads with respect to time of use price has been proposed. This work has focused on the optimized charging pattern of EVs that benefit cost reduction and flattering the load curve [12]. In [13], the unidirectional vehicle to grid regulation with the help of an aggregator has been proposed.

They have tested the optimal algorithm on ten thousand EVs, while reducing system load impacts and consumer costs [13].

Medhi *et al* [14] proposed the electric service station, which is similar to that of oil-filling station for travelling longer distances with EVs. Here, the fast charging of batteries is needed over small period of time. This work investigates the effect of fast charging EVs on distribution grid. Progress in the research of unidirectional charging system can be observed from the above literature and some other discussions are given in [15]-[21]. Both, the charging and discharging performance of EVs should be required to reduce the stress on the grid during peak period.

1. 1.2 Vehicle to Grid

The interaction of EVs with the grid for maximum time period creates the possibility to manage the peak load power demand. The charging/discharging of EVs from/to the grid in off-peak/peak period flattens the load profile of the grid. The increased EVs and their random arrivals create difficulty in the scheduled charging. Optimal scheduling schemes are needed to overcome such difficulty. Therefore, Yifeng *et al* [22] proposed a global and local optimal scheduling scheme to charge and discharge the EVs. They optimized charging power to reduce the total cost of all EVs. This work is useful for the dynamic arrivals of EVs and scalable to large EV population. Yuchao *et al* [23] described a model of storage system using EVs and coordinated with a power system. They decided battery energy deployment based on the time, vehicle charging requirements and electricity prices.

The discussion about vehicle to grid support, regulation of active power, load balancing and filtering the current harmonics are given in [24]. Also, they proposed three elements for successful vehicle to grid operation such as: power connection to the grid, intelligent metering and the communication between the grid and vehicles. Success of vehicle to grid concept relies on the battery technology and smart scheduling schemes, standardization of requirements and infrastructure decisions [25]. In [26], a review of the energy storage for transport and grid applications has been presented. This work focuses on storage and the power converters used in storage technologies for peak shaving. In [27], the vehicle fleet evaluation and vehicle energy demand simulations combined with the transportation simulation has been proposed. They determined the daily behavior of EVs with battery energy levels [27].

Mukesh *et al* [28] proposed various possibilities and their impacts for implementing vehicle to grid technology in Indian scenario. They proposed the grid coordinated EVs for improving the voltage profile and to minimize the power transmission losses [29]. Also, they modeled the EVs charging station that can fulfill different demands of EVs owner such as: state of charge (*SOC*)/ charging rate (c-rate)/ power management of battery [30]. A multi charging station which can handle a large fleet of EVs without affecting the grid performance has been proposed in [31]-[32]. In [33], the controlled charging and discharging performance of a fleet of EVs depending on their battery energy status and grid condition has been proposed.

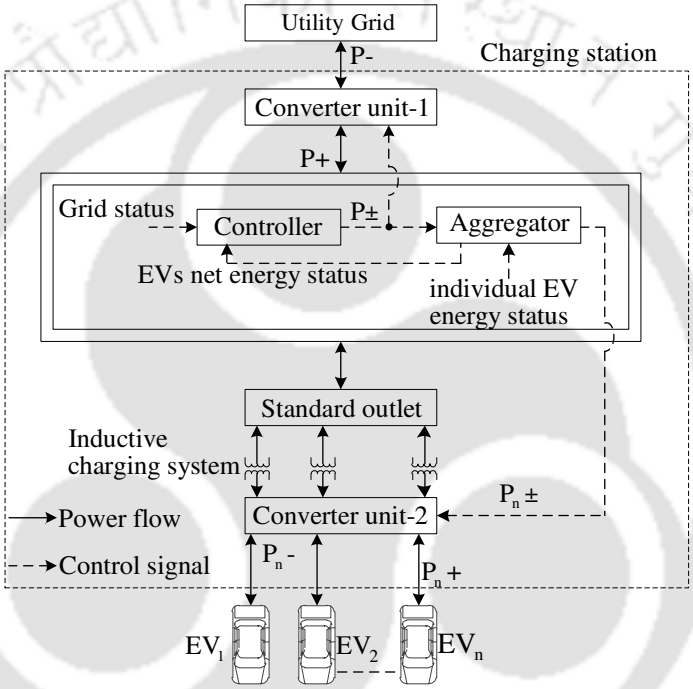

Fig. 1.3 Bidirectional power flow between the grid and EVs

Fig. 1.3 shows the conceptual representation of the bidirectional power flow between the grid and EVs. A fleet of EVs (EV_1, EV_2, --- EV_n) have been connected to the charging station to charge/discharge energy from/to the grid. Charging station is connected to the grid via converter unit-1. A controller is present at the charging station to control the energy between the grid and EVs. This controller works based on two inputs and one output. The inputs are: the grid energy status and EVs net energy status. Output is $P\pm$ ($P+$ is the power flow from the grid to EVs and $P-$ is the power flow from EVs to the grid). Controller sends output signal to converter unit-1 as well as to the aggregator. The aggregator works based on two inputs and two outputs. Inputs are: $P\pm$ and the individual EV energy status. One output is the net energy status of EVs (this signal goes to the controller as input) and the other is $P_n\pm$

(power to/from the individual EV) (this signal goes to the converter unit-2). A fleet of EVs have been connected to the standard outlet via converter unit-2. EVs receive power from the standard outlet via inductive charging system as shown in Fig. 1.3. Also, a controller should be required to manage the EVs in and out timings at the charging station. This controller should coordinate with the main controller.

Above mentioned literature represents a progressive research on the vehicle to grid concept. The grid integrated EVs shows the significant benefits from both, the environmental and economic aspects. The expensive price and the battery maintenance of EVs are the main hurdles for their growth. This creates less interest to the common citizen towards EV utilization. Also, a group of EVs occupy more space on the streets of the city to perform low mass transportation. The public transportation systems such as tram, trolleybus and the supercapacitor based buses etc… are the possible options to limit such difficulty. The public transportation system occupies less space on the streets of the city to perform maximum mass transportation. The passenger's price sharing is the base for public transportation system. Therefore, it creates the possibility for every citizen to take part in the clean energy based transportation system. Also, this system is economical to the common passenger to travel end to end of the city. The public transportation systems such as trolley bus systems and tram systems were operated in the middle of the 8^{th} decade of 19^{th} century [36]. These systems are the base for enhancement in public transportation system technology and also, brought a revolution in the transportation sector. The different types of public transportation systems and their technological growth are given in the following sub-section.

1.2. The literature review

The mass transportation performance using EVs has a long history and it can be divided into two categories. First one is EVs run with the on-board energy storage and the second one is EVs run without on-board energy storage.

1). *EVs with on-board energy storage systems*: The battery powered EVs such as electric cars, motor cycles, electric buses etc. are used in these systems. The limited battery capacity of EVs set the distance limit for these systems.

2). *EVs without on-board energy storage systems*: EVs run on tracks or definite routes such as railway trains, tram systems and trolley bus systems etc. are used in these systems. Their

ability to use renewable energy sources and the consumption of less energy make them strong to use for urban and inter urban transportation systems. The distance limit is not applicable for these systems due to the electrical lines availability through the specified routes in the urban and inter-urban regions.

The energy efficient transportation systems are extremely important in city regions due to the rising prices and environmental concerns. Moving to electric based transportation systems, most of the cities often opt for either tram or trolleybus systems. Thus both, the tram and trolleybus systems have gained popularity. The public transportation systems in cities depend on the following factors: the capital cost and the life time running cost of the tram and trolley bus systems.

1.2.1. Tram systems for urban transit

Russia operated the first trolley car/tram system in 1880. Tram is a rail vehicle which runs on the tracks, laid along the streets of urban region. Tramways are the networks operated by tramcars. The details of overhead line equipment and the electric energy required for the tramways are discussed in [34]. Also, the details of electric tramways used for goods carriage are given in [35].

The petrol buses superiority in many cases as that of tram systems led the degraded demand towards the tram systems. Most of the tram and trolleybus networks were dismantled in 1950's to replace with ICEVs. The cities that were canceled these networks are present with high pollution levels. The rapid rise of air pollution level in cities is the major reason to create the demand for electrified transportation systems. Joachim *et al* [36] compared the two most common electric public transportation systems in cities. They considered the same route for both the tram and trolleybus systems and compared the traction energy consumption per passenger. Also, they considered the acceleration, braking, deceleration, maximum speed and travelling time are all same to model both the systems. Tram system is heavier than that of trolleybus system in all the cases. However, the rolling resistance of the tram system is lower than that of trolleybus system. Therefore, the tram system consumes less energy (in coasting, the tram systems have the higher kinetic energy and the lower coefficient of friction) [36].

Garcia *et al* [37, 38] proposed the hybrid tramway system. They performed the energy management by using fuel cell as the primary source and battery as the secondary energy

source. This system shows the benefits such as: provides fast and additional power during acceleration, reduces the size of the fuel cell and enables the recovery of regenerative braking energy. Also, they included supercapacitors to reduce the grid dependence while the tram is at the stoppage [38]. Flavio *et al* [39] developed a control strategy to manage the power flow in the supercapacitor based energy storage system of tramway network. They optimized the energy flow among substations and running tram cars, improved the energy saving and reduced the voltage drops in the supply network. In [40], the stochastic tram model has been developed from a real traffic data which is reliable to power flow, losses and the efficiency of storage system. Also, they investigated the fuzzy energy management system for supercapacitor based storage in tram systems [41]. The on board supercapacitors show the benefits such as: reduction of peak power demands, decrease of power consumption, improvement in the performance and efficiency. They predicted tram position, using the global positioning system through an algorithm [41]. Next sub-section explains the importance of the trolleybus systems for urban transit.

1.2.2. Trolleybus systems for urban transit

The urbanization and industrialization has created the demand towards transportation system in city regions. Electrification of the transportation sector shows the following benefits such as: more efficient, reduced energy consumption, renewable energy usage via grid, reduced noise level, pollution free performance, creates more comfort with fine acceleration and is effective to mitigate global warming. Tramway systems are the nuisance under modern city traffic conditions and their replacement with the trolleybuses is one of the better options [42]. The trolleybuses were introduced in the early 19^{th} century. The trolleybuses have an advantage that they run on the locally generated power in preference to an imported fuel [42]. They used rheostat braking to produce the regenerative braking energy in trolleybuses [42]. This energy is fed back into the power lines and simultaneously the other trolleybuses utilize that energy. The lack of advancement in the storage technology was the major reason for such kind of operations. In [43], the trolleybuses working principle has been explained including with the mechanical features, electrical equipment used, regenerative control, traction motors use, current collectors, overhead line equipment and the

sub-stations. Also, they conducted a tilt test on the trolleybus. This work claimed that a 10% of regenerative braking energy is possible with the full use of regenerative brake [43].

Trolley coach is the most economical transit vehicle than other mechanical vehicles [44]. One trolley coach line's capacity to handle the passengers is equal to a 7-lane highway normally handles by automobiles [44]. The unlimited power availability for acceleration of trolley coach provides, the ability to maintain faster speed schedule than any other similar services [44]. Trolley coach achieves the faster speed schedule with the high capacity electric motor that can handle 150 to 200 percent load for a short period of time. Also, it has wider aisle and doors which enable the movement of passengers on and off the coach faster. Therefore, it provides the increased schedule speeds [44]. Also, this work discusses about the comparison of trolley coach (operating cost and benefits) with mechanical buses [44]. In [45], the faster performance of the electric car than other automobiles has been presented. In [46], it has been discussed that the EV has more power compared to gasoline engine vehicle and are more economical to operate in cities.

Trolleybuses are the vehicles derived from the buses. These vehicles require electrical infrastructure for their supply. In [47], the possibility of trolleybus system implementation has been reported. In [48], the electric current, voltage and power of trolleybus system have been determined with respect to time and location. They used input data such as: vehicle and control parameters. In [49], a new current collector for electric trolleybus has been designed. They discussed about, the associated problems and operational limitations of the current collector in the trolleybus system.

The continuous connection of trolleybuses to a contact line shows some demerits such as: it needs infrastructure, the maintenance has limited flexibility (events like road works or accidents may have a severe impact on operational capabilities) and the regenerative braking energy dissipates in a braking resistor if there is no demand for power in the feeding line of trolleybus [50]. They also highlighted the possible ways to electrify the public transportation systems such as: hybrid buses, buses with hydrogen fuel, battery buses, trolleybuses and battery augmented trolley coaches [50].

The use of trolleybuses in the smart grid systems to reduce the greenhouse emission and the energy savings in public transport have been presented in [51, 52]. They discussed about the smart grid vehicle features such as: electrification of existing transportation system,

management of regenerative energy, grid for both buses and users, and the bus for public transportation in the smart grid. Trolleybus line performs the same transport capacity as that of light rail, tram and metro-transit systems. In [53], the benefits of the storage technology in the electrified transport systems have been presented. They discussed about the cable car implementation and the energy services with the storage system such as: security, power quality and energy efficiency. In [54], the use of energy storage in trolleybus lines for urban mobility has been presented. The potential upgrading actions on the trolleybus lines improve its energy performance. The implementation of on board energy storage system, based on supercapacitors exploits the braking energy and improves the energy performance of the trolley buses [54]. Supercapacitor based energy storage system can help to smooth the strong and short time power solicitations of a distribution network. In [55], a solid state supercapacitor bank has been used as a storage device and interfaced using the power electronic converters. They decided the size of supercapacitor bank based on the energy requirement of an electric bus to start. Next sub-section explains the importance of supercapacitors in the public transportation systems and their technological growth.

1.2.3. Supercapacitor based bus systems for urban transit

The transportation system's life time can be estimated depending on the lifespan of the components used in it. The energy storage systems such as battery, supercapacitors etc. are the important parts of the electrical transportation systems. Supercapacitors are ranked as the powerful alternative energy resource for future. Supercapacitors have less energy density compared to lithium-ion batteries. Therefore, the supercapacitors are not suitable for passenger vehicles. The frequent stop and go pattern of the public transportation system in cities require high power density repeatedly. Therefore, the batteries are unfit for public transportation systems due to their low power density. Supercapacitors are well suited for the public transportation systems due to their high power density and quick charge/discharge performance. The raw materials used in supercapacitor such as: aluminum and carbon shows long life span (one million cycles). This shows the supercapacitor fitness for innovation in the mass transportation systems. Supercapacitors have less fire hazards and comparatively safer than batteries.

The vehicles with on board supercapacitors travel very short distance between consecutive stoppages (usually less than half a kilometer). The use of conventional battery along with

supercapacitor inside the vehicle provides relief in worst operating conditions such as: traffic jams, higher distance to be covered and the extra energy required in abnormal situations [56]. Ayad *et al* [57] discussed about the supercapacitor use in EVs and their modeling, sizing and control. Supercapacitor based urban mass transit systems target to minimize the power fluctuations, voltage drops and regenerative power lapses [58]-[61]. Fabbri *et al* [62] developed the supercapacitors based sustainable public transportation system. The main components of this system (K-bus) are: the on board supercapacitors, a bus stop tied with electrical network as well as photovoltaic panels and a charging system to charge the supercapacitors. K-bus carries the limited energy storage that is necessarily required to reach the next bus stop. Therefore, the potential range of K-bus increases and the operative cost which is the real bottleneck for the EVs get reduces [62].

Camara *et al* [63] presented an approach of supercapacitors integration in transport applications. The electrical and analytical model for the capacitance variation has been introduced in [64]. They considered the sizing aspects to reduce the electrical losses in the supercapacitor [64]. The supervisory energy management of hybrid energy storage systems used in EVs is one of the key issues for their development. Yin *et al* [65] proposed an adaptive fuzzy logic based energy management strategy to determine the power split between the battery and supercapacitor packs. This system maximizes the system efficiency, minimizes the battery current variation and also, minimizes the supercapacitor state of charge difference [65].

Yoichi Hori [66] has discussed about the future EV's development which employ three techniques: supercapacitors, electric motors and inductive power transfer. This system avoids the requirement of batteries, engines and quick charging stations. Electric motors used in EVs show the advantages such as: motor can be attached to each wheel; torque generation is quick, accurate and can be estimated precisely. Supercapacitors dominate the batteries for the charging of future EVs and show the benefits such as: large current density, long operating life and environmentally friendly composition [66]. William *et al* [67] simulated the series hybrid and pure EVs employing lead-acid battery and supercapacitor combinations. They showed that the series hybrid EVs consume less fuel (when the lead-acid batteries linked with supercapacitors) as that of a vehicle with only batteries.

The electric based transportation system achieves the high efficiency using electric drives. Energy storage systems such as: supercapacitors, fuel-cells and batteries integration can improve efficiency further in these systems. Allegre *et al* [68] proposed a new subway system without supply rail between two stations. They have improved energy saving in subway system with on-board supercapacitors bank (charges from the station and discharges to the subway when it accelerates). If the subway decelerates/braking applied, then the regenerative braking energy charges the supercapacitor bank [68]. Next subsection explains the role of high capacity energy storage systems in the smart grid technology.

1.2.4. High capacity energy storage systems in the smart grid technology

The high capacity energy storage systems play dominant role in the smart grid technology and are used to integrate the fluctuated power generated from renewable energy sources to the grid. These systems play an important role to maintain the stability and power quality in the power system. For the large scale energy storage applications, the Vanadium Redox flow Battery (VRB) is suitable as that of other energy storage devices [69]. VRB has long life span compared to other batteries. The independent power and energy rating of VRB increases its scalability. VRB shows the following advantages such as: it is having large capacity, low maintenance requirements, flexibility in design, low manufacturing cost for large scale, recyclable electrolytes and fast response to rapid changes [69]. VRB enables the flexibility in the design of energy storage system. These batteries are developed for stationary applications and are used at high power ratings. VRB technology shows the following benefits compared to conventional battery technology.

a. Environmental Advantages:

- VRB is having the ability to integrate with renewable energy sources (solar, wind etc.).
- VRB is termed as 'the green battery' (the materials used in it are environmental friendly).
- VRB has an indefinite life of electrolytes (reusable and no disposal issues).

b. Technical Advantages:

i. Operational:

- VRB remains fully charged. No charge is lost when the battery is not in use.
- The solution can be used for an indefinite time.
- VRB's does not have the life degradation for repeated charge/discharge.

- VRB can operate with one or more electrical inputs and outputs at multiple voltage levels.
- VRB response is instantaneous (<1 m. sec).
- Low maintenance cost and low operating temperature (10-45^{0}C).
- VRB can charge and discharge up to 15,000 times without the need of membrane replacement.

ii. Charge and Discharge:

- VRB can charge/discharge at any voltage level. It can be overcharged with no loss or damage.
- VRB is capable of rapid charge and discharge. Self-discharge is negligible.

iii. Energy Storage Capacity:

- The electrolyte volume is proportional to VRB storage capacity.

The study of different energy storage systems shows that the flow type battery technology is more suitable for hours of energy storage, due to deep discharge ability and flexibility in power or energy sizing. Zhou *et al* [70] proposed the grid connected marine current turbine system using VRB to handle the output power and to manage the grid side demand on a daily basis. They performed the modeling and the parameter calculation process of VRB [70]. The power sharing between different technologies are responsible to create the hybrid energy storage systems. Wang *et al* [71] proposed a hybrid energy storage system using VRB and supercapacitor technologies to smooth the oscillating output power of the grid connected photovoltaic system. They reduced the required power rating of supercapacitor bank to only one-fifth of the VRB rating to avoid the VRB operation at low power levels [71]. The details about VRB modeling and their usage in different power applications are given in [72]-[78]. Supercapacitors and their benefits in the smart grid technology are given in the next sub-section.

1.2.5. Role of the supercapacitors in the smart grid technology

The supercapacitor shows the following benefits such as: long life cycle, high power density, wide range of temperature, high durability, large cycling range and the low maintenance cost. Supercapacitors are used in the following applications: transmission and distribution stabilization in power systems, voltage control and regulation, to start the motor, power system protection, boosting the batteries performance and cold start of engines.

Supercapacitors are used as a stand-alone storage module and also, used along with batteries/fuel-cells in cars, aircrafts and railway vehicles. An equivalent electric model of the supercapacitor is required to perform the simulations of the aforementioned applications. Electrical models of supercapacitor can be categorized in two groups such as: the models which represent all the physical and chemical phenomena for both charging and discharging mode, and the models that are suitable for system level studies and real-time applications.

Yasha *et al* [79] presented a validated lumped and computationally efficient electrical and thermal model for a cylindrical supercapacitor cell. They estimated the electric model parameters and also, presented the equivalent electric circuit model with capacitance and open-circuit voltage [79]. Supercapacitors behavior is a function of various parameters such as: size of electrodes, temperature, electrolyte state, aging etc… and they express more stability for wider temperature range. German *et al* [80] used a simple and reproducible method for multi-pore model for the identification of supercapacitor parameters. They presented a method, which is based on the physics of ions penetration in supercapacitor electrodes [80]. Also they studied about the specific impact of supercapacitor ageing on different pore sizes using a multi-pore model [81]. The voltage balancing should be performed for the series connected modules of supercapacitor bank to limit the ageing and safety issues. The voltage balancing methods of supercapacitor are of three groups such as: passive dissipative, active dissipative (switched resistors) and active lossless (energy transfer between cells without dissipating). Yuhimenko *et al* [82] utilized the advanced method to achieve the voltage balancing of series connected modules of supercapacitor bank. The different methods that are used for dynamic modeling of supercapacitors and the model based energy control schemes are presented in [83]-[88]. Next sub-section explains the importance of contactless charging system in smart grid technology.

1.2.6. Contactless power transfer

The contactless charging system is also known as inductive/wire-less/hands-free/plug-less charging system. This system shows the following benefits such as: protected connections, safer for human beings, convenience in maintenance, easier than plug-in power cable and more durable. Also, this system overcomes the disadvantages associated with the wired charging systems such as: electrical injuries, fire sparks, heating of sockets and cables. The important applications of this system are: transcutaneous transformers, linear motors, coil

guns, inductive charging system for EVs etc. The electromagnetic field is used as a medium between the excitation coil (the coil which is excited from the source side) and observation coil (the coil where the variations in output can be observed from the load side) in this system [89]. The design of contactless EV charging system which focuses on the transmitter and receiver coils is presented in [90]. The optimization of multi-objective magnetics without moving the mechanical parts show the limitations such as: efficiency, power density and low stray field for high power inductive charging systems [90].

Reena *et al* [89] described an analytical approach to compute the mutual inductance between two coils. They investigated all the possible angular and lateral misalignments with the vertical and horizontal variations between two coils. They reduced the complex mathematical equations using this approach for all the positions of the coil [89]. Also, they studied on variable load, frequency and distance of a planar inductive power transfer system [91] and parallel connected multipoint bidirectional contactless charging station [92]. They also described four compensation topologies of magnetic coupling system by connecting capacitors at the terminals of the coils to achieve the resonance between coils [93]. Kannan *et al* [94] proposed the control and modeling of inductive charging station in vehicle to grid scenario. They developed a multi-point bidirectional inductive charging station with its control structure. Also, they developed a smart control algorithm that decides the power flow between grid and EVs via contactless charging system [94]. Solar energy and its importance in the smart grid systems are presented in the next sub-section.

1.2.7. Solar energy in the smart grid systems

The solar power systems have the ability to provide power to the whole world. For that, it requires less space (roughly equal to the area of Spain). The use of maximum solar energy can limit the global warming. The momentum of solar systems has been started due to the subsidized policies from government, falling price of solar panels and increased research on solar systems [95]. Solar power systems are of two types: standalone solar power system and grid interfaced solar power system. The energy storage systems are required for standalone solar power systems; whereas the grid integrated solar power systems do not require energy storage. However, these systems need to satisfy the standard power quality to integrate with the grid. Bhim Singh *et al* [95] proposed the solar photovoltaic system with the objectives of

maximum power point tracking and sending solar energy to the grid. Also, this system improves the power quality in the grid.

The fluctuated power generation is the stochastic nature of renewable energy sources. The stability and power quality of the distribution grid can be affected with the increased penetration of such renewable energy sources to the grid. ESD is the possible solution to mitigate such difficulties. Wang *et al* [96] proposed an algorithm to manage the power and to enable the small-scale photo voltaic power plant with a hybrid energy storage system including VRB as primary and the supercapacitor bank as a complementary energy storage system. Solar power generation is more/grid-load is less during midday. This may create the voltage rise issues in the grid. Such issues can be limited by charging EVs during midday. Alam *et al* [97] utilized the plug-in EV battery capacity to mitigate the solar photovoltaic impact and to support the grid. Also, they developed a controllable charging and discharging system to optimize the use of limited plug-in EV battery capacity to mitigate photovoltaic impacts [97].

Solar power systems change the total load demand in power system. Hamid *et al* [98] proposed a method to estimate the generation capacity of invisible solar power sites. Paul *et al* [99] described the vehicle-solar-grid concept. This system provides ancillary services to the grid by using the grid connected solar inverters and batteries of EVs. The bidirectional power flow can reduce the cost of the photovoltaic system and EVs [99]. Baleke *et al* [100] reviewed the forecasting techniques to increase the renewable energy penetration to the grid. The reliable forecast techniques reduce the power curtailments and also, increase the power plant's revenue in electricity market [100]. Some other discussions on solar energy systems are listed in [101]-[102].

1.3. Motivation

The layout of the literature review is shown in Fig. 1.4. The literature shows that the grid has been utilized in three directions. In the first direction, the grid is used as a source for the different types of transportation systems. In the second direction, the grid is used as a source and also, as a node (to feed the stored energy back to the grid). In the third direction, the grid is used as a node (to send the renewable energy to the grid). The details are given as follows.

Energy flows from grid to vehicle (tram/trolleybus/supercapacitor based bus systems) when 'the gird is used as a source' (ref. Fig. 1.4). These vehicles utilize total energy to perform the mass transportation and unable to support the grid during peak period. The grid powered transportation systems can be observed from the literature [34]-[68]. These systems receive energy from the grid irrespective of the grid condition. The introduction of super-capacitor based buses represents the technological growth in the mass transportation systems. These buses do not require electrical line infrastructure between the consecutive bus stops, but frequently need energy from the bus stops. However, these buses are also directly charge from the grid. This technology is well suited for the public transportation in cities, but the grid does not receive any support from this system. The supercapacitor equipped tram networks are established in Spain, Portugal and China [138]. However, these systems are also grid dependent. The on-board supercapacitors manage the energy required by the tram systems to travel between consecutive stations. Grid dependence of the above mentioned transportation systems, is the major drawback and these systems may create an extra stress on the grid (the grid has to sustain these systems along with the normal load) during peak load hours. Also, there is a possibility that these systems may undergo in failure mode if the grid is unable to support. The possible solution to overcome such difficulty is to provide ESDs between the grid and the transportation sector. This arrangement is helpful to curtail the transportation system dependence on the grid.

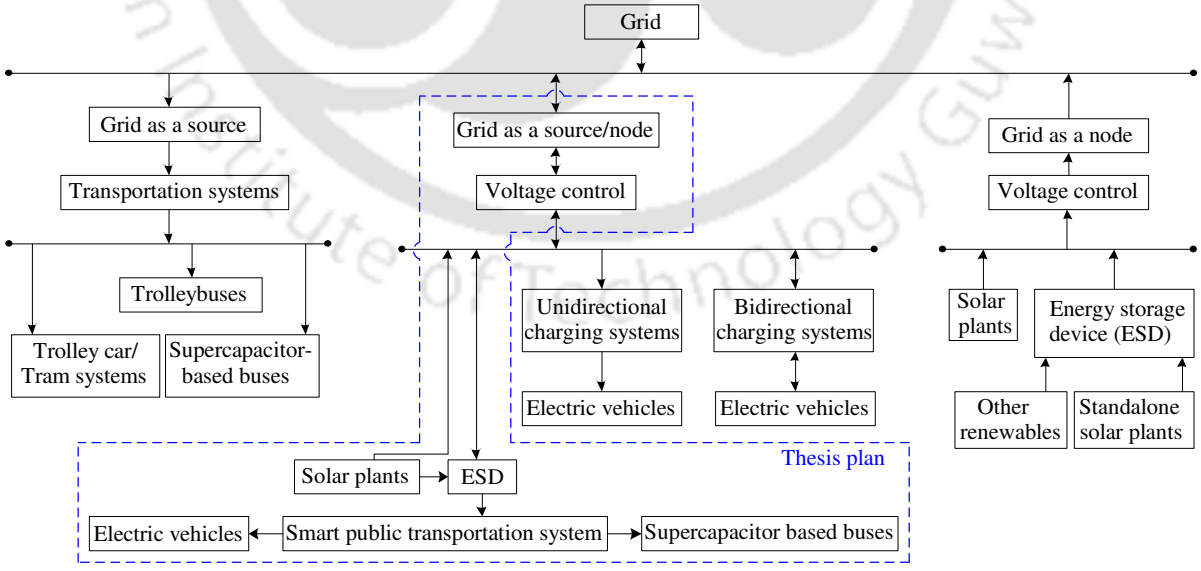

Fig. 1.4 Layout of the literature review and thesis plan

Energy flows from grid to vehicle (EVs/ESD) as well as from vehicle to grid when 'the gird is used as a source/node' (ref. Fig. 1.4). The literature from [9] to [21] shows that the unidirectional coordinated charging systems are used the grid as a source. EVs perform the valley filling of the grid load profile by receiving energy from the grid during off-peak period. This means EVs act as a load to the grid during off-peak period and subsequently improves the net load to the grid. EVs utilize total energy for transportation purpose, so that EVs are unable to support the grid during peak period. Charging and discharging performance of EVs should be required to overcome such difficulty. EVs charge from the grid during off-peak period and discharge to the grid during peak period in the bidirectional charging systems. The bidirectional energy flow between the grid and EVs creates the possibility to perform the valley filling and peak shaving of the grid load profile. The literature from [22] to [33] shows that the bidirectional coordinated charging systems used the grid as a source as well as a node. EVs act as a load/source to the grid during off-peak/peak period. Literature also shows that a fleet of EVs utilization at the distribution grid level regulates the voltage profile of the grid as well as maintains the power quality in the grid. Such systems are beneficial to both, the grid and EVs. However, a common citizen cannot take part in this activity due to the expensive price of EVs. The electrified public transportation systems are well suited to satisfy the common citizen requirements. These systems are driven on the price sharing base. Therefore, a common citizen is able to afford the price to travel in the electric bus through the city. The public transportation systems should provide better services to the common citizen as well as to the grid.

Energy flows from renewable energy sources (solar plants/other renewables/standalone solar plants) to the grid when 'the gird is used as a node' (ref. Fig. 1.4). The literature from [95] to [102] shows that the renewable energy is integrated to the grid by considering the grid as a node. Solar power system is the leading technology among renewable energy sources. The presence of irradiance availability at all the locations shows the flexibility to install the solar power systems at any region. Solar power integration to the grid is of two types: one is the direct integration with suitable inverter technology and the other is integration via ESDs (standalone solar systems). The solar power system performs the voltage regulation process by sharing a part of the grid load. Literature also shows that the total solar power is sent to the grid irrespective of grid condition. Possibilities are there to utilize the solar energy in

multi directions, instead of sending solar energy only to the grid. The use of solar energy in electrified transportation systems can enable the green energy based transportation systems in city regions. This can reduce the transportation system dependence on the grid. The air pollution is the rough and complex issue in city regions from decades. It creates many difficulties to the citizens who live in the city regions. Nowadays this problem has crossed its maximum limit in most of the important cities across the world. The green energy based transportation systems in cities is one of the possible solutions to limit such issue. If the complete transportation sector run on the solar energy, then it is possible to overthrow the air pollution from the city regions.

Extensive research is required to provide the efficient electrified transportation systems in cities. The following issues are perceived from the literature.

i. The bidirectional energy flow between the grid and EVs limit the voltage instability in the grid. The energy transfer between the grid and the transportation systems should be required to achieve the smooth performance of the transportation systems as well as to provide the energy support to the grid during peak load hours.
ii. Mostly the solar energy is used to interface with the grid. Possibilities are there to utilize solar energy in multi directions. Solar energy should be utilized to support the transportation system as well as to support the grid.
iii. All the present electrified transportation systems are grid powered (runs depending on the grid). The transportation system dependence on the grid should be reduced.
iv. ESD should perform both the charging and discharging operation from/to the grid. This arrangement provides benefit to the grid as well as to the transportation system.
v. The supercapacitor based buses and EVs should run in harmony with ESD to perform the mass transportation in cities. The energy transfer between EVs and ESD is also beneficial to the grid during peak period.

The present work introduces the smart public transportation system (SPTS) which fulfills the above mentioned issues. SPTS has created a new area of research in the wing of grid as a source/load (ref. Fig. 1.4). SPTS shows the following advantages: it is beneficial to the grid, to the transportation system, to the passengers, to EV owners and also it is helpful to provide the pollution free environment in the city region. SPTS utilize the grid as a source/load

during off-peak/peak period and subsequently improves the voltage profile of the grid. The basic idea about the working principle of SPTS and the thesis plan are shown in Fig. 1.4.

Fig. 1.5 Guwahati city ring road circuit and SPTS structure

ESD is placed between the grid and SPTS. ESD receives energy from the grid during off-peak period and send its stored energy back to the grid during peak period. ESD performs the

valley filling and peak shaving of the grid load profile during off-peak and peak period. The energy flow between the grid and ESD during off-peak and peak period improves the voltage profile of the grid. ESD is also connected to photovoltaic based solar plant (SP) and receives energy from SP during sunshine hours depending on the grid condition. SP is helpful to reduce the grid dependence of SPTS. Also, SP avoids the failure situations in SPTS.

The proposed transportation network is located along the ring road circuit of the Guwahati city, Assam, India as shown in Fig. 1.5. This circuit covers four different types of loads such as: home load (H), home plus commercial load (H+C), commercial load (C) and industrial load (I). The important places in the ring road circuit are shown in Fig. 1.5 (Jalukbari, Maligaav, Fancy, MG-road, Dispur, Basista, Balaji, and Boragaon). Home load is present in the area between Jalukbari and Maligaav, the home plus commercial load is present in the area between Kamakhya and Paltanbazar, the commercial load is expanded in the areas of MG road, Dispur and Basista, and finally the industrial load is present in the area between Balaji and Jalukbari as shown in Fig. 1.5. The off-peak and peak periods are regardless of one another in all these types of loads. The frequent stop and go pattern is the most common feature for the city transportation systems. Therefore, the bus stops are required within 1 to 2 km distance. A total of 32 electric bus stops (EBSs) are present through the ring road circuit. The average distance between consecutive EBSs is considered as 2 km. The EBSs used in SPTS are given in Table 1.2. The ring road circuit covers a total distance of 47.5 km.

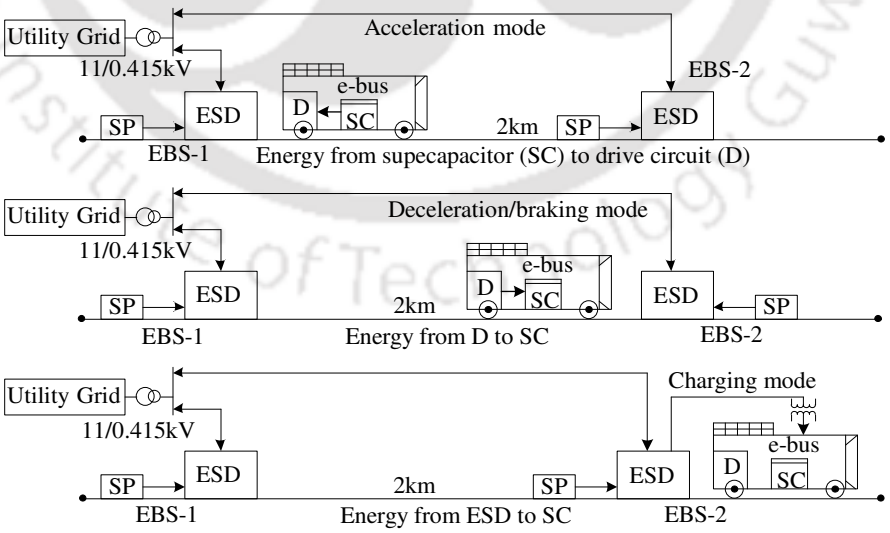

Fig. 1.6 The working principle of e-bus

The electric buses (e-buses) ply on the ring road circuit to perform the mass transportation in the Guwahati city. The supercapacitors are used as the energy storage in e-buses due their salient features [114]-[116]. The e-buses receive energy from the current EBS via inductive charging system and reaches to the next EBS as shown in Fig. 1.6. This arrangement reduces the weight of the energy storage in the e-bus (battery weight is the main concern in EVs). Also, the on board supercapacitors in the e-bus reduces the electric line infrastructure needed between consecutive EBSs. Therefore, the connections between EBSs are not required in SPTS but all the EBSs should be connected to the utility grid via ESD. The bidirectional energy flow between supercapacitor and drive circuit inside the e-bus is shown in Fig. 1.6. Supercapacitor supplies energy to the drive circuit during acceleration mode of the e-bus. Therefore, supercapacitor experiences the gradual energy decrease during this mode. The drive circuit supplies energy to the supercapacitor during deceleration/braking mode of the e-bus (regenerative braking energy). Therefore, the super-capacitor's energy increases again. In this work, it has been considered that a 40% of total energy is produced by the regenerative braking energy. Once the e-bus reaches to the next EBS, the supercapacitor receives energy from the ESD of that EBS. This process continues throughout the ring road of the city. ESD is present at every EBS of the ring road circuit and it receives energy from the grid as well as from SP. ESD utilizes this energy to support the e-buses throughout the day (for 24 h). The passenger's in/out duration to/from the e-bus is considered as 2 minutes. This means that the e-buses halt at every EBS for 2 minutes. In this duration, the e-buses fully charge from the EBS. The quick charge/discharge performance of supercapacitors play major role in reducing the halt time of e-buses at EBS. SPTS shows the convenience to the passengers as well as to the grid.

Table 1.2: EBSs in SPTS

1.	Jalukbari	7.	Santipur	13.	RBI	19.	Ganeshguri	25.	Lohia	31.	Nursary
2.	Aaadabari	8.	Machkowa	14.	Paanbazar	20.	Nayapur	26.	Sarusajai	32.	Nagsari
3.	Boripora	9.	Ferry	15.	Bishaal	21.	Dispur	27.	Lokhra		
4.	Maligaav	10.	Fancy	16.	Paltanbazar	22.	Jaya Nagar	28.	Balaji		
5.	Kamakhya	11.	Kachari	17.	Ullubari	23.	khanapara	29.	Gorchuk		
6.	Kahilipara	12.	High court	18.	GMC	24.	Basista	30.	Boragaon		

The structure of the distribution network that covers the entire ring road of the Guwahati city is shown in Fig. 1.7. EBSs are connected to the 11/0.415 kV distribution nodes (DN). The main grid is present at the Sarusajai, in the Guwahati city. From there, a 132kV

transmission line passes to the substation (132 kV node) located at Kahilipara, Guwahati. This place is at the middle of the ring road circuit as shown in Fig. 1.5. From this node, an adequate number of 33 kV transmission lines travel to the city. A total of ten 33 kV nodes are present inside the ring road circuit [121,122].

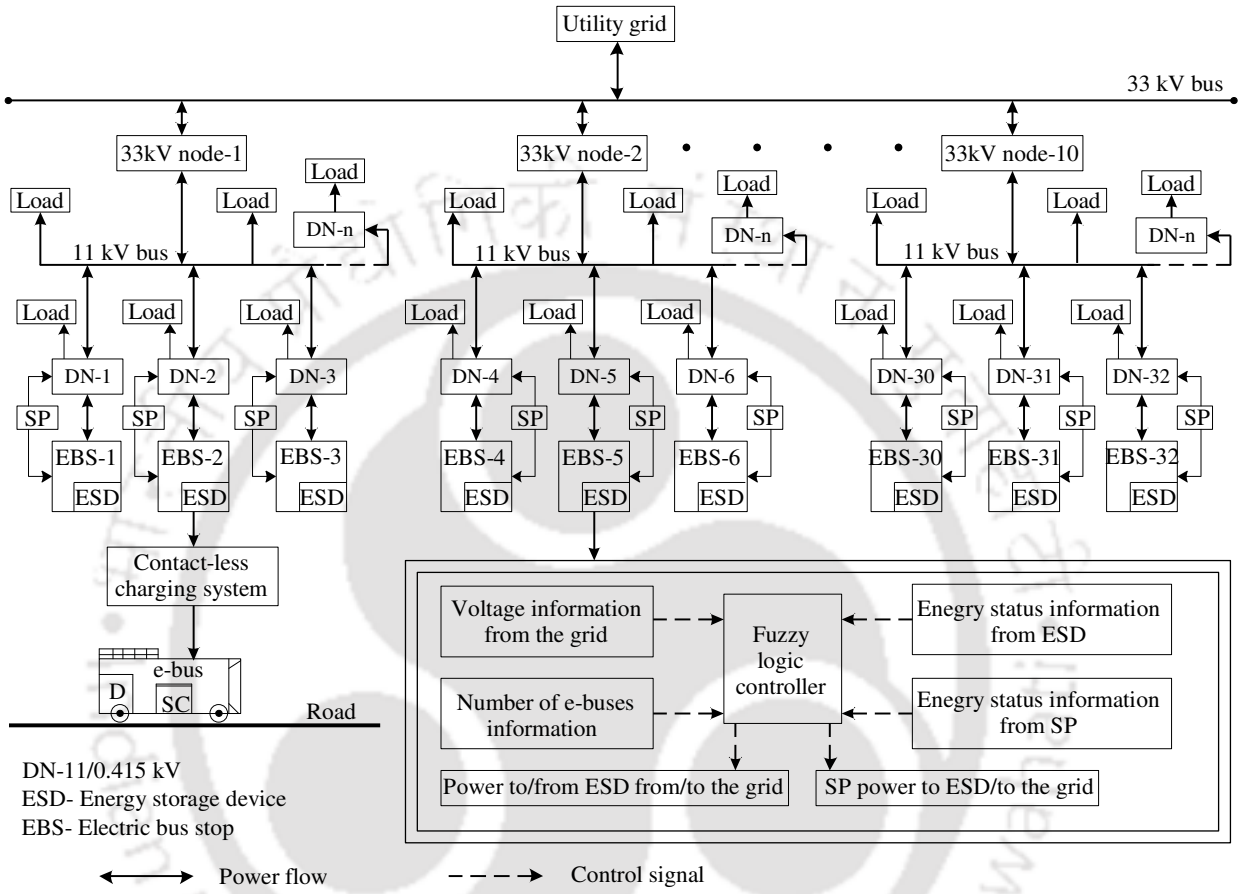

Fig. 1.7 The structure of the distribution network

Under each 33 kV node, moderate 11 kV nodes are present according to the load demand of that particular region. Some of these nodes consist of EBSs and the remaining nodes are dedicated to loads. A maximum of three EBSs are present under an 11 kV node. ESD is present at every EBS and it is connected to both, SP and the distribution node. SP is connected to both, ESD and the distribution node. ESD receive/send energy from/to the distribution node and also receive energy from SP according to the fuzzy logic controller's (FLC) command. FLC, works based on four inputs and two outputs. Inputs are: the voltage information of the grid, the number of e-buses information, the information of ESD energy status and the information of SP energy status. Outputs are: first one is: ESD receive/send energy from/to the grid, and the second one is: SP send energy to ESD/to the grid.

Contactless charging system is connected to ESD. The e-buses receive energy from ESD via contactless charging system. This system shows better advantages compared to wired charging system [89]-[94]. Therefore, SPTS utilizes the contactless charging system and the efficiency of this system is considered about 85% to 90%. A total of 32 distribution nodes are used for 32 EBSs, in SPTS. The distribution nodes are also consists of normal loads along with EBSs as per Fig. 1.7.

1.4. Aim of the thesis

The main aim of the thesis is to integrate the solar assisted smart public transportation system with the grid. This can be achieved through, the proper knowledge of vehicle-dynamics, the size of supercapacitor in the e-bus, the size of ESD, solar irradiance availability in all the seasons of a year, the size of SP, load profile of the grid and its variation throughout the year, commuter's profile, suitable controllers and aggregators. The primary objective of the thesis is to perform the smooth operation of SPTS and reduce the grid dependence of SPTS using the favorable energy from both the grid and SP. Further, to perform the controlled energy flow between the grid, SP and SPTS during off-peak and peak period. The energy transfer rate between SP, SPTS and the grid relies on the node voltage variations, SP energy availability, number of e-buses required for public transportation and the amount of energy required for SPTS support. Motives of the primary work are as follows:

i. The vehicle-dynamics calculations should be required to estimate the amount of energy needed by the e-bus to travel between the consecutive EBSs.
ii. The solar irradiance should be determined to estimate the solar energy availability in SPTS network region through all the seasons of a year.
iii. The load profile data of the grid for entire year should be required to verify the SPTS sustainability in all the seasons of a year.
iv. The commuter's data should be required to determine the number of e-buses needed to perform the mass transportation in the Guwahati city. The real time data of the solar, commuters and the load is required for better understanding of SPTS response in all the seasons of a year.
v. The maximum capacities of ESD and SP should be determined for achieving the smooth performance of SPTS. The size of SP and ESD should not affect the performance of both, the grid and SPTS.

vi. A control algorithm should be required to perform the charging/discharging operation of ESD from/to the grid and also, to send the SP energy to ESD/ to the grid during off-peak/peak period. This algorithm should decide the favorable energy from both the grid and SP for the SPTS support.

vii. SPTS performance verification with ‘only ESD’ and 'ESD along with SP' should be required for all the seasons of a year.

The second objective of the thesis is to determine the optimal number of e-buses in SPTS and also, to achieve the fail proof performance of SPTS. The optimal number of e-buses determination relies on the node voltage variation, SP energy status, commuters profile and ESD energy status. The failure analysis of SPTS explains the self-sustainability of SPTS for different failures that exist in the system. The motives of second work are therefore:

i. The real time data of three dynamic profiles such as: load, solar and commuters should be required to determine the optimal number of e-buses (ONB) in SPTS.

ii. ONB determination should be required to use the precise number of e-buses in SPTS and it should not affect the performance of both, the grid and SPTS.

iii. A suitable algorithm should be required to determine ONB for different types of days in all the seasons of a year.

iv. SPTS response verification should be required for the failures that exist in the system from both, hardware and software sides.

v. SPTS should achieve the fail-proof performance in all the seasons of a year.

vi. Appropriate controllers and aggregators should be required to perform the energy management in the failure situations of SPTS.

vii. A suitable controller is needed to manage the energy between the grid, SP and SPTS.

viii. SPTS response verification should be required as a function of both, ONB and the failures that exist in the system.

The third objective of the thesis is to expand the electrified transportation network in the Guwahati city using EVs and the capa-buses (supercapacitor based buses) (CBs) along with e-buses. This system maximizes the use of electric based transportation system in the city region as well as maintains the power quality in the grid. The smart public transportation network response relies on the node voltage variations, SP energy status, EVs energy status, CBs energy status and ESD energy status. The motives of the third work are as follows:

i. The vehicle-dynamics calculations including with the road angle should be required to determine the energy needed by the CB to travel between EBSs.
ii. Different types of electric vehicles such as CBs, EVs and e-buses are necessarily required to expand the electrified transportation network in the Guwahati city.
iii. The proper knowledge of SP energy availability, load profile of the grid and commuters profile should be required to verify the smart public transportation network response in all the seasons of a year.
iv. Appropriate controllers and aggregators are needed to perform the energy management between ESD, SP and the grid, and also, between ESD and both, CBs and EVs.
v. Smart public transportation network response verification should be required for all the seasons of a year and also, for the uncertain situations that exist in the system.

1.5. Main contributions of thesis

The main contributions of thesis are listed in the following manner:

i. The vehicle-dynamics (the tractive energy required by the e-bus to overcome all the resistive forces) have been calculated. Also, the amount of energy required by the e-bus to travel between the consecutive EBSs is determined.
ii. The real time data based dynamic profiles such as: load, solar and commuters have been used in SPTS simulations.
iii. An algorithm has been developed (real time solar data is used) to determine the solar irradiance availability through all the seasons of a year. The size of both, ESD and SP is decided according to the energy requirement of SPTS.
iv. ESD along with SP has been integrated with the grid through an FLC. An algorithm has been developed to reduce the SPTS reliance on the grid. Also, SPTS response for three seasons of a year has been verified through simulations.
v. An algorithm has been developed to determine ONB for normal and special days as a function of the load profile, SP energy status, commuters profile and ESD energy status.

vi. SPTS failure analysis has been carried out through the algorithm based controllers and aggregators. The complete system is integrated with the grid using FLC and simulated through MATLAB.

vii. The vehicle-dynamics including the road angle is calculated using EMPARX driving cycle and determined the amount of energy required by CB to travel between EBSs. SPTS network expansion has been performed using CBs and EVs along with e-buses in the Guwahati city transportation network. Both CB's and EV's, charging/discharging performance from/to ESD during off-peak/peak period is controlled through the algorithm based controllers and aggregators.

viii. The entire system has been integrated with the grid using FLC. SPTS network response has been verified for three seasons of a year, with ESD alone and with 'ESD along with CBs and EVs'. Also, the SPTS network response for uncertain situations that exist in the system has been verified.

1.6. Thesis organization

Thesis is organized in the following manner. Chapter-2 explains the details of small-scale solar plants coupled with SPTS and its coordination with the grid. The modeling of SPTS has been performed in the following manner. The vehicle dynamics have been calculated using the New York City Drive Cycle (NYCC) to decide the amount of energy required by the e-bus to travel between the consecutive EBSs. The size of ESD at each EBS is decided based on the e-bus energy requirement and the number of e-buses required for 24 h. An algorithm has been developed to calculate the irradiance availability throughout the year based on the real time solar data. The size of SP is decided based on the irradiance availability. The main aim of this work is to minimize the SPTS dependence on the grid. Therefore, an algorithm has been developed for the favorable energy support from both the grid and SP to the SPTS. A single month in every season and two types of days (working day and non-working day) in every month have been considered to verify the SPTS response. A suitable FLC has been developed to control the energy flow between the grid, ESD and SP. Two types of case studies have been considered to explain the simulated results. First case explains the benefits with only ESD and with both 'ESD and SP' in SPTS. The second case explains the SPTS response for three seasons of a year.

Chapter-3 explains the details of the optimal number of e-buses in the solar assisted smart public transit system and its failure analysis. The main aim of this work is to determine ONB in SPTS and also, the failure analysis in SPTS. An algorithm has been developed to determine the ONB in SPTS. Two types of days such as normal and special days have been considered to show the variations in ONB for both types of days. ONB is determined as a function of the load profile, passenger's profile, the energy status of ESD and the energy status of SP. The failure analysis in SPTS has been carried out by considering two types of failures such as: failures from hardware side (four types of failures have been considered) and the failures from software side (two types of failures have been considered). Three isolation switch controllers (ISC) (suitable algorithms have been developed), an inductive charging system controller (ICSC) and the aggregator are responsible to manage the energy between EBSs during failure situations in SPTS. A suitable FLC has been developed to control the energy flow between the grid, ESD and SP. Two types of case studies have been considered to explain the simulated results. First case explains the performance of SPTS for ND and SDs with respect to ONB. The second case explains the SPTS response in failure situations.

Chapter-4 explains the details of SPTS network expansion and its interaction with the grid. The main aim of this work is to expand the electrified transportation network in the Guwahati city using CBs and EVs along with the e-buses. A specified EBS has been considered in SPTS network to charge the CBs and EVs along with the e-buses. Suitable algorithms have been developed for both CB controller and EV controller. These controllers are responsible to manage the energy between ESD and both CBs and EVs. SPTS network response with 'only ESD' and 'ESD with CBs and EVs' has been verified for three seasons of a year. A suitable FLC has been developed to control the energy flow between the grid, ESD and SP. Two types of case studies have been considered to explain the simulated results. First case explains the SPTS network response for three seasons of a year. The second case explains the SPTS network response for uncertain situations that exist in the system.

Finally the conclusion and future works are given in Chapter-5

2

Small-scale Solar Plants coupled with Smart Public Transport System and its Coordination with the Grid

Contents

Introduction

The present transportation system in modern cities is predominantly dependent on petroleum as its fuel. This is a major source of air pollution in cities across the globe. Such issues are partly solved by the implementation of electric vehicles (EVs) [103, 104]. EVs benefit from several energy sources like renewable and non-renewables. However, EVs need the coordinated charging to avoid the voltage and frequency fluctuations in the grid [105]. EV technology has been improved by the implementation of trolleybuses and supercapacitor based buses for public transportation in urban regions [106]-[109]. The online operation of these systems with the grid creates an extra burden on the grid during the peak period. In [110], the on-line operation of EV with the grid has been proposed and EVs charge via wireless-charging system installed under the road. This system is beneficial in transportation system point of view but in grid point of view it creates an extra stress on the grid. To overcome such difficulties, a high capacity energy storage device (ESD) is needed between the transportation sector and the grid [111, 112].

A study [113] was carried out to merge the transportation system with the grid by using the energy storage systems. However, this system shows the complete reliance of the transportation system on the grid and also has the chances of failure, if the grid is unable to support the transportation system. An attempt has been made in this work to curtail the transportation system reliance on the grid by utilizing solar energy. The present work focuses on the following objectives:

- The favorable energy utilization from both, the grid and the small-scale solar plant (SP) to run the smart public transportation system (SPTS) smoothly.
- To show the SPTS response for three seasons of a year in different situations.

The present work maximizes the green energy utilization by depleting energy from the grid for SPTS support. The e-buses are used for mass transportation in the Guwahati city in view of the ring road as a case study. The supercapacitors are used as prime energy storage in the e-buses owing to their prominent features [114]-[116]. The energy points are provided through the ring road to charge the e-buses during their journey. At each EBS, the ESD as well as SP are connected to run the SPTS smoothly and to improve the voltage profile of the grid. ESD receives energy from both, the grid and SP in the off-peak period. The ESD and SP (in sunshine hours) together send energy to the grid during peak period. The combined

use of both, ESD and SP in SPTS achieves the process of load leveling in off-peak/peak period of the grid. The solar irradiance has been determined by using the real-time solar data and the size of SP is decided based on the irradiance availability. An algorithm has been developed for the favorable energy utilization from both, the grid and SP to run the SPTS smoothly. The overall response of SPTS is shown through the results for three seasons of a year. Every EBS consists of a Fuzzy Logic Controller (FLC) to perform the control actions [117]-[120].

The rest of this chapter is organized in the following manner. Modeling of SPTS is given in Section 2.1. Section 2.2, shows the minimization of SPTS dependence on the grid. Results and discussions are given in Section 2.3 and finally the summery is given in section 2.4.

2.1 Modeling of the SPTS

This section explains the modeling of SPTS including the SPTS structure, the EBS structure, ESD sizing, irradiance availability determination and SP sizing. Fig. 2.1 shows the ring road of the Guwahati city covered by a number of EBSs (X_1, X_2… X_{32}) (the distance between EBSs is considered as 2 km) and distribution nodes (DN_1, DN_2… DN_{32}).

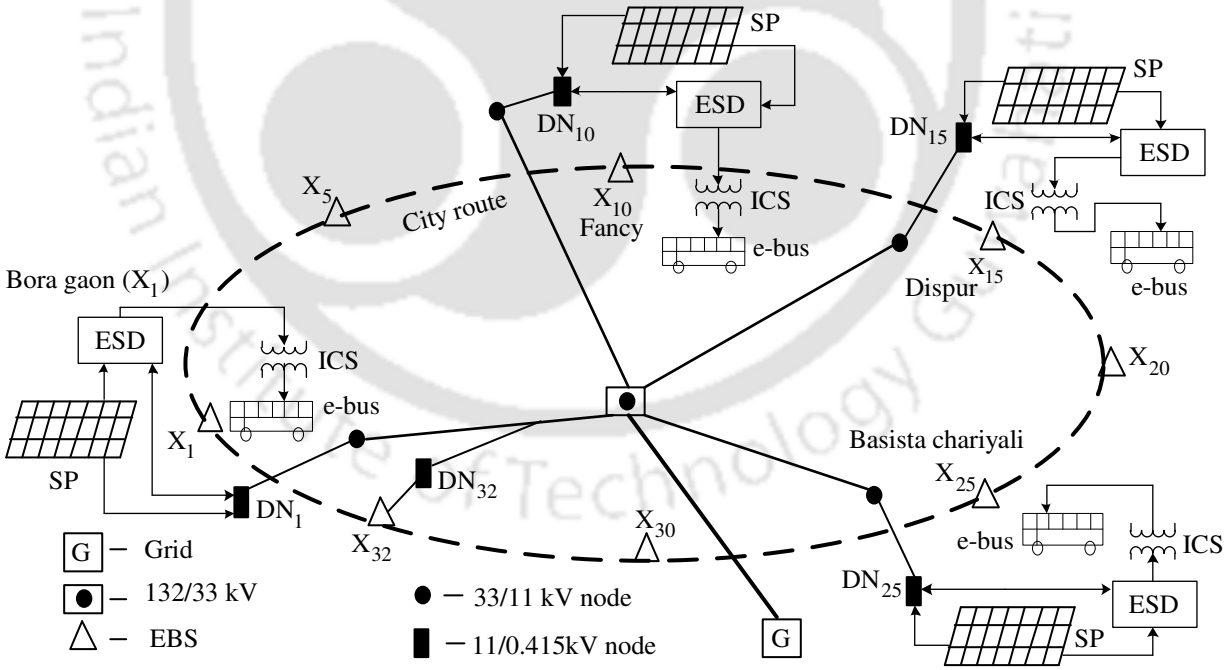

Fig. 2.1 SPTS structure

The structure of the real-time distribution network that covers the entire ring road is represented in the following manner: The grid is located at Sarusajai (outskirts of Guwahati

city and have 12 km distance from the city) and from the grid a 132 kV transmission line goes to the sub-station, located at Kahilipara (which is at middle of the Guwahati city ring road circuit) [121, 122]. 33 kV lines go to the city from this place and some of them cover the ring road. Each 33 kV node has 11 kV feeders according to the load demand [121, 122]. The ESD and SP are connected at all EBSs, but in Fig. 2.1, only 4 EBSs are shown and the analysis of SPTS has been carried out at X_1 EBS. The e-bus receives energy from ESD situated at current EBS via inductive charging system (ICS) and moves to the next EBS (stopping time of the e-bus at EBS is considered as 2 minutes and the e-bus get charged within this duration. The amount of power received by the e-bus from ESD in 2 minutes duration is 39.7 kW). This process continues throughout the ring road.

2.1.1. The structure of EBS

The EBS structure is shown in Fig. 2.2. SP is connected to the grid as well as to ESD. Both, SP and ESD are connected to the grid via 11/0.415 kV node and a small load is also present at the same node. ESD receives/sends energy from/to the grid in off-peak/peak period. SP sends energy to ESD/to the grid in off-peak/peak period. EBS consists of a fuzzy logic controller to manage the energy among ESD, SP and the grid. FLC receives four inputs: ESD energy status (E_{ESD}), EB frequency (EB_f), SP energy status (E_{SP}) and the per unit voltage of the grid (V_{pu}). FLC generate two outputs: one as $P\pm$ (power from/to grid to/from ESD in off-peak/peak period) and the other as $SP\pm$ (power from SP to ESD/to the grid in off-peak/peak period).

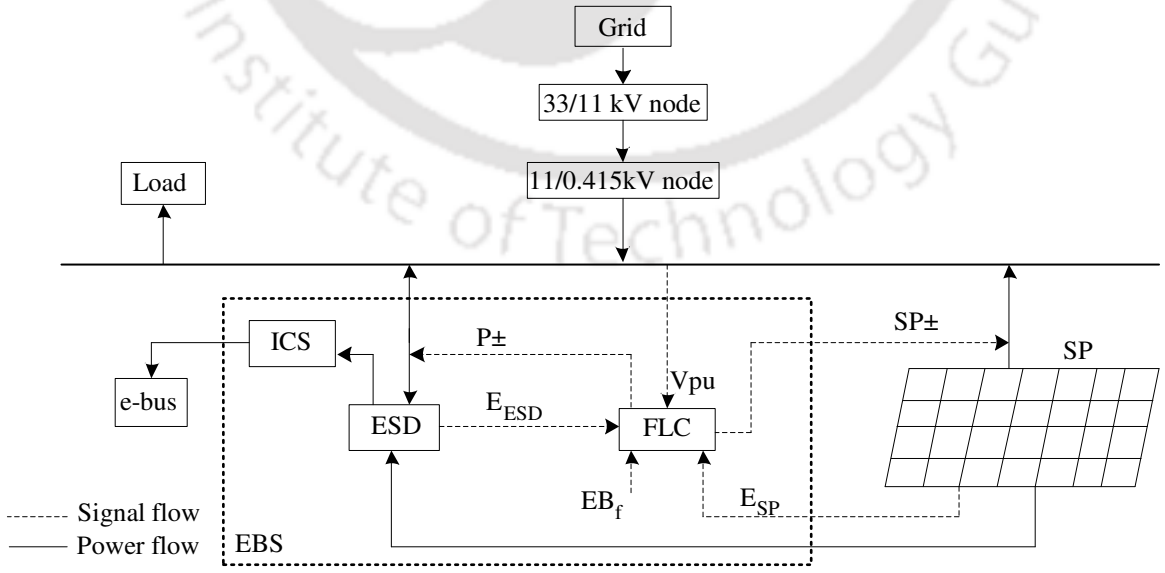

Fig. 2.2 The structure of electric bus stop (EBS)

2.1.2. ESD sizing

The e-bus frequency (EB_f) is the number of e-buses pass from one EBS and is calculated according to the number of passengers. The e-bus capacity is limited to 30 passengers. The hourly EB_f is expressed as

$$EB_{fh} = \left(\sum_{i=1}^{n} P_i\right) / (EB_c) \tag{2.1}$$

EB_{fh} is the e-buses frequency in one hour, P is the passengers (i=1, 2… n), EB_c is the passengers carrying capacity of the e-bus. The EB_f in a day is given by

$$EB_{fd} = \sum_{j=1}^{m} EB_{fh\ j} \tag{2.2}$$

EB_{fd} is the daily e-bus frequency, 'j' is the number of hours (j=1, 2… m). According to EB_{fd}, the total energy required by the e-buses from ESD is therefore

$$E_{ESDTS} = EB_{fd} \times E_{RB} \tag{2.3}$$

$$E_{ESDT} = 2 \times E_{ESDTS} \tag{2.4}$$

E_{ESDTS} is the energy required by the SPTS from ESD for 24 h, E_{ESDT} is the total energy capacity of ESD and E_{RB} is the minimum energy required by the e-bus to travel between consecutive EBSs (two times of E_{RB} is the maximum energy rating of the e-bus (considered to avoid the emergency situations)) and is calculated by using 'New York City Drive Cycle' (NYCC) [113], [123]. The factor 2 in (2.4) shows that the half ESD energy is required to support SPTS. The remaining half is used to store SP energy as well as to support the grid in peak period. E_{RB} and ESD specifications are given in Table 2.1.

Table 2.1: The ESD specifications and EB energy requirement [113]

Variable	*Rating*
Minimum energy required by the e-bus (E_{RB})	1.31 kWh
ESD total energy	300 kWh
DC voltage rated	125 V
DC current rated	370 A
Range of DC voltage	100-155 V

2.1.3 Solar irradiance availability determination

The algorithm for solar irradiance calculation is shown in Fig. 2.3. Real-time solar data is collected from the India meteorological department (IMD), Guwahati, Assam, India [124]. The SP energy generation depends on (proportional to) the solar irradiance availability. The collected solar data has the details of longitude (σ), latitude ($\emptyset$), relative humidity (RH), air

temperature (T). The solar irradiance is determined by following the procedure: first, specify the day number (d=1, 2… 365), σ, $\emptyset$ and solar constant (S) values and initialize RH values. From these values calculate hour angle (ω), solar declination angle (δ), solar elevation (α), the sunrise angle (ω_s), solar azimuth (ψ) and irradiance outside the atmosphere (B_0) [125, 126].

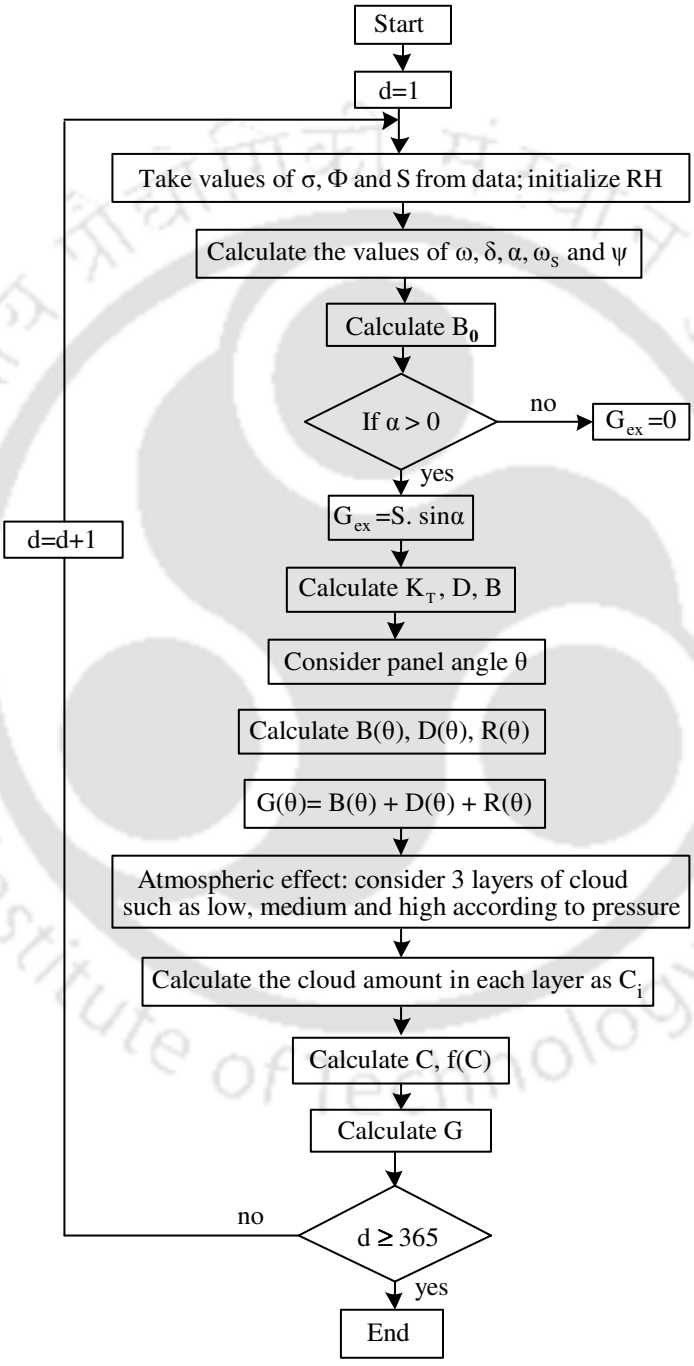

Fig. 2.3 Algorithm for solar irradiance calculation

Check the If condition: if $\alpha > 0$ calculate extra-terrestrial irradiance (G_{ex}), otherwise (if $\alpha < 0$) G_{ex} is zero. If the condition has been satisfied, then proceed to calculate the clearness index (K_T), diffuse irradiance (D) and beam irradiance (B). After that, consider the panel angle (θ) and with respect to 'θ' calculate beam irradiance $B(\theta)$, diffuse irradiance $D(\theta)$, irradiance reflected from the ground $R(\theta)$ and the global irradiance $G(\theta)$ [125]-[127]. Subsequently, calculate the atmospheric effect by considering three layers of the cloud (low, medium and high according to the pressure) and calculate the cloud amount in each layer (C_i). Then, calculate the sky clearness indicator (C), the function of C as $f(C)$ and actual global solar irradiance (G) [128]. The mathematical expressions used for G calculation have been followed from [125]-[128]. A closed loop has been formed for calculating the G for 365 days of a year. The power generation capacity of a solar cell has been calculated based on the irradiance [125],[126],[129]. The G availability in the Guwahati city region for a complete year is calculated through the algorithm given in Fig. 2.3. The mathematical expressions for the power generation of a solar cell and the equivalent circuit are not shown in this work. G under the standard test condition has been considered as 1 kW/m^2.

2.1.4 SP sizing

The SP sizing depends on the photovoltaic module (PVM) energy generation capacity and the number of PVMs, required to meet the selected size of SP [130]. The generation capacity of each solar cell (depends on the following equivalent circuit parameters) is expressed as

$$E_{Scell} = f(G, T, I, I_{Ph}, V) \tag{2.5}$$

E_{Scell} is the solar cell output energy, G is the solar irradiance, T is the temperature, I_{ph} is the photocurrent, I is the output current, and V is the output voltage of solar cell. The energy produced by PVM (solar cells connected in the series) is therefore

$$E_{PVM} = n \times E_{Scell} \tag{2.6}$$

where 'n' is the number of solar cells and the block diagram of PVM is shown in Fig. 2.4.

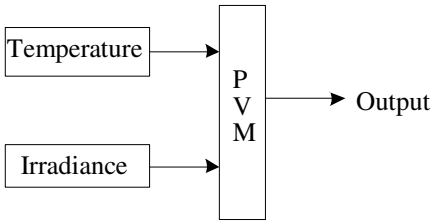

Fig. 2.4 Photovoltaic module (PVM)

Temperature and irradiance are the inputs to PVM block and the mathematical expressions are utilized inside the PVM block for determining the output power of PVM. Total energy produced by the SP is given by

$$E_T = m \times E_{PVM} \tag{2.7}$$

E_{PVM} is the output energy of PVM, m is the number of modules and E_T is the total energy generation capacity of SP. The energy produced by the SP in a day is therefore

$$E_{TSP} = \sum_{c=1}^{24} E_{T\,c} \tag{2.8}$$

E_{TSP} is the total energy produced by the SP in a day and 'c' is the number of sunshine hours. The daily SP generation capacity is considered in such a way that, it should be less than or equal to half of the ESD capacity plus the energy received by the e-buses in sunshine hours and is expressed as

$$E_{TSP} \leq (0.5 \times E_{ESDT}) + E_{EBRSH} \tag{2.9}$$

E_{ESDT} is the total energy capacity of ESD (2.4) and E_{EBRSH} is the total energy received by the e-buses from ESD in sunshine hours (from 08:00 to 17:00 h.). E_{EBRSH} can be expressed as

$$E_{EBRSH} = \sum_{x=1}^{n} E_{EBfh\,x} \tag{2.10}$$

E_{EBfh} is the energy required by the e-buses with respect to hourly e-bus frequency (2.1) and 'x' is sunshine hours (x= 1, 2 … n). The energy remained in the ESD, in sunshine hours is given by

$$E_{ESDSH} = E_{TSPSH} - E_{EBRSH} \tag{2.11}$$

E_{TSPSH} is the total energy produced by SP in sunshine hours and E_{ESDSH} is the energy remained in the ESD in sunshine hours. This means that the e-buses indirectly receiving energy from SP in sunshine hours via ESD. The daily energy availability in the ESD is expressed as

$$E_{ESDD} = \sum_{t=1}^{x} E_{RG\,t} - \sum_{p=1}^{y} E_{GG\,p} + \sum_{t=1}^{x} E_{TSP\,t} - \sum_{i=1}^{n} E_{EB\,i} \tag{2.12}$$

E_{EB} is the energy given to the e-buses in a day (i= 1, 2… n), E_{TSP} is the total energy received from SP in off-peak hours (t=1, 2… x), E_{GG} is the energy given to the grid in peak hours (p= 1, 2… y), E_{RG} is the energy received from the grid in off-peak hours (t= 1, 2… x). The SP size is given in Table 3.

2.1.5 Assumptions

This work carries out the system level modelling of the entire network so that the modelling of ESD and converters, the losses due to ESD and the solar panel are not included. The losses with ICS are very small. The efficiency of ICS depends on the distance between the transmitting and receiving coils and the coupling co-efficient. The range of ICS efficiency is considered as 85% to 90%. The ESD energy rating assumed to be same at all the EBSs.

2.2 Minimization of SPTS dependence on the grid

According to [113], the grid has been utilized as an energy source for running the public transportation system. However, this work shows the complete reliance of transportation system on the grid. The present work has focused on this issue and made an attempt to reduce the transportation system reliance on the grid by utilizing solar energy. The transportation system benefits from solar energy when a situation arises like ESD is unable to receive energy from the grid (SPTS has such arrangement that when ESD is disconnected from the grid then SP is open circuited from the grid irrespective of grid condition and SP send its total energy to ESD). Critical situations in SPTS can be handled smoothly by the favorable energy utilization from both, the grid and SP. The conceptual representation of SPTS (basic working model of SPTS) is shown in Fig. 2.5.

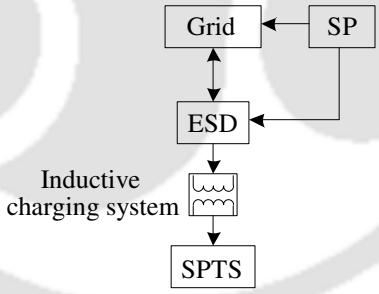

Fig. 2.5 SPTS basic model

The SP is connected to ESD as well as to the grid. Solar energy is utilized in two directions (SP sends energy to ESD/to the grid), depending on the grid condition throughout the day. The controller has to perform the control actions in such a manner that: if the grid stays under peak period in the day-time, SP has to send energy to the grid otherwise SP has to send energy to ESD. A high capacity ESD is placed between the grid and the transportation system owing to its multiple benefits to the grid as well as to the transportation system. ESD performs in such a manner: it charges from the grid in off-peak period and discharges to the

grid in peak period. Also, ESD charges the e-buses for 24 h. The distinct benefits that the ESD shows in SPTS are therefore:

- ESD run online with the grid by isolating the super-capacitors (e-buses) to the grid. ESD reduces the risk of transients that occur in the grid due to the direct connection of super-capacitors to the grid.
- ESD acts as a load to the grid in off-peak period (the valley filling of the grid load profile) and acts as a source to the grid in peak period (peak shaving of the grid load profile). ESD also work as a source to the transportation system for 24 h.
- ESD supports the transportation system for 48 h (The energy required by the e-bus to travel between the two EBSs is 1.31 kWh. 112 number of e-buses pass from one ESD for 24 h. The total energy is 112 x 1.31 kWh which is 146.72 kWh. 300 kWh is the ESD full capacity. Now, for 48 h duration 146.72 x 2 is 293.44 kWh) with the help of SP when ESD failed to receive energy from the grid.

The importance of SPTS is represented as:

- To electrify the existing transportation system and to provide the pollution free environment in city regions.
- To use the maximum SP energy for SPTS support and to check the possibility of the only solar energy based SPTS.

The proposed work has been carried out by collecting the real time data of three dynamic parameters (load, solar and commuters) that are involved in SPTS. The real-time data is collected from the following departments.

- Solar data from India meteorological department [124].
- Commuter's data from central transportation authority.
- Load data from the state electricity board, Assam, India [121, 122].

The motive of the proposed work is expressed as:

- The favorable energy utilization from both, the grid and SP to run the SPTS smoothly. The maximum priority has been given to utilize the SP energy for SPTS support.
- To check the SPTS response as a function of three dynamic profiles (load, solar and commuters) for three seasons of a year.

2.2.1 Favorable energy utilization from both, the grid and SP for SPTS support

Fig. 2.6 shows an algorithm for the favorable energy utilization from both, the grid and SP for SPTS support.

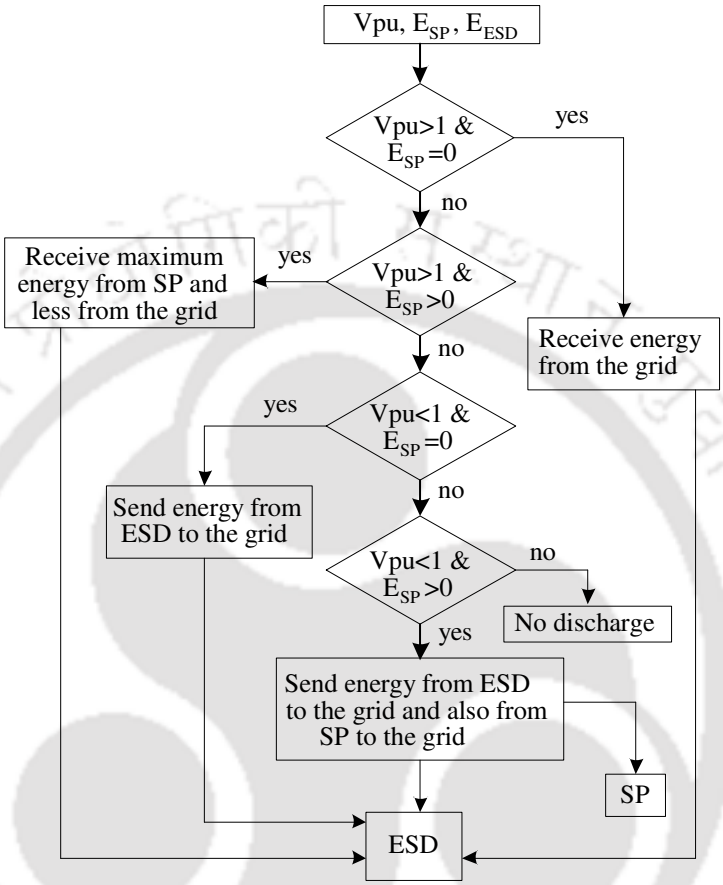

Fig. 2.6 Algorithm for the energy support from both, the grid and SP to SPTS

The proposed algorithm works in the following manner: first, initialize three inputs such as: Vpu, E_{SP} and E_{ESD}. If the condition (Vpu is greater than 1 pu and E_{SP} is zero) has been satisfied then ESD receives energy from the grid otherwise go to the next condition. If Vpu is greater than 1 pu and E_{SP} is greater than zero then ESD receives maximum energy from SP and less energy from the grid. If this condition is not satisfied then go to the next condition. If Vpu is less than 1 pu and E_{SP} is zero, then ESD has to discharge energy to the grid otherwise go to the next condition. If Vpu is less than 1 pu and E_{SP} is greater than zero then ESD has to discharge energy to the grid and also SP has to send energy to the grid. This algorithm allows the maximum SP energy utilization for SPTS support and subsequently reduces the energy consumption from the grid. All these logics of an algorithm have been included inside the

controller to give the best control actions for managing the energy among SP, ESD and the grid.

2.2.2 SPTS response for three seasons of a year

The SPTS response for three seasons of a year as a function of three dynamic profiles is explained through Fig. 2.7 at X_1 EBS (ref. Fig. 2.1).

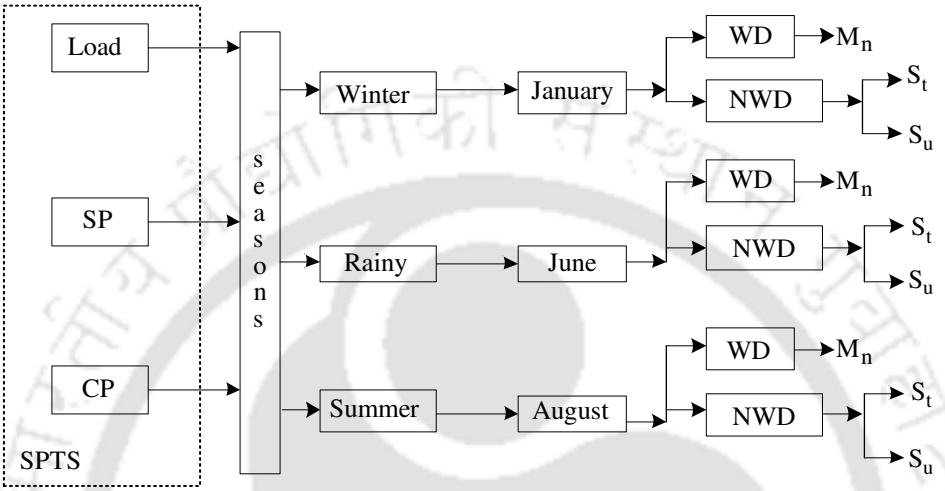

Fig. 2.7 SPTS response for three seasons of a year

Three seasons of a year such as winter (W), Summer (S) and rainy (R) have been considered. In every season, a single month such as January in winter, June in rainy and August in the summer have been considered. In every month, two types of days have been considered: one as the working day (WD) and the other as non-working day (NWD). Under NWD both, Saturday (S_t) and Sunday (S_u) are considered and under WD only Monday (M_n) is considered. The load profile and commuter's profile differ for WD and NWDs throughout the year. This is the reason why two types of days have been considered for giving the better understanding about the SPTS response throughout the year. The SPTS response verification is a challenging task due to the dynamic behavior of the load, SP and commuter's profiles. The daily variations in SP profile depend on weather conditions. The generation capacity of SP is determined by calculating the solar irradiance availability for one year (Sec. 2.1.3 & 2.1.4). The seasonal variation in the energy support from SP to SPTS is given in Table 2.2.

Table 2.2: Seasonal variation in the energy support from SP to ESD and from the grid to ESD

Season	*Energy from SP to ESD*	*Energy from the grid to ESD*
Winter	Minimum	Maximum
Rainy	Medium	Medium
Summer	Maximum	Minimum

In the summer season, SP has maximum energy generation compared to other seasons. SP gives its full support to SPTS in this season and subsequently reduces the energy consumption from the grid. Three dynamic profiles for the considered days of three seasons are shown from Fig. 2.8 to 2.16. These profiles are used in SPTS simulations. The response of SPTS depends on the following factors and is expressed as

$$SPTS_R = f(\text{LG}) + f(\text{CP}) + f(\text{SP}) \tag{2.13}$$

$$\text{LG} = f\ (\text{Year, Season, Month, Day type}) \tag{2.14}$$

$$\text{CP} = f\ (\text{Commuters, Day type}) \tag{2.15}$$

$$\text{SP} = f\ (\text{Irradiance, Season, Day type}) \tag{2.16}$$

where, $SPTS_R$ is the response of SPTS, f (LG) is the function of the load of the grid, f (CP) is the function of commuter's profile and f (SP) is the function of the solar plant. The day type is either WD or NWD. The irradiance availability for M_n, S_t and S_u in three seasons is shown in Fig. 2.8, 2.9 and 2.10 respectively. In all these figures, the solid line represents the irradiance for W season, the medium dotted line represents the irradiance for S season and the small dotted line represents the irradiance for R season. The solar irradiance availability is low in W, moderate in R and high in S season and that can be observed from Fig. 2.8 to 2.10.

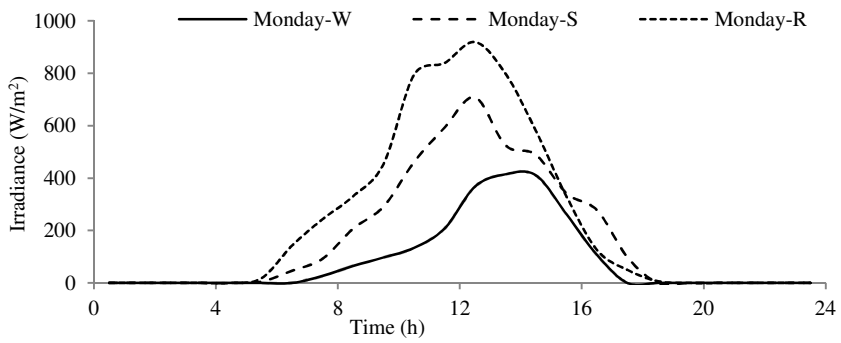

Fig. 2.8 The irradiance availability for 'M_n' in three seasons

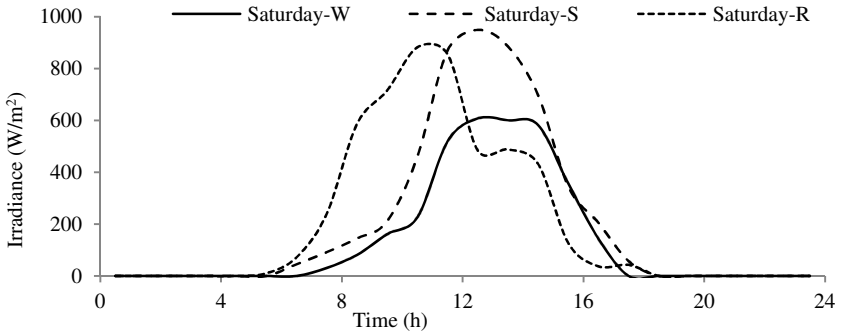

Fig. 2.9 The irradiance availability for 'S_t' in three seasons

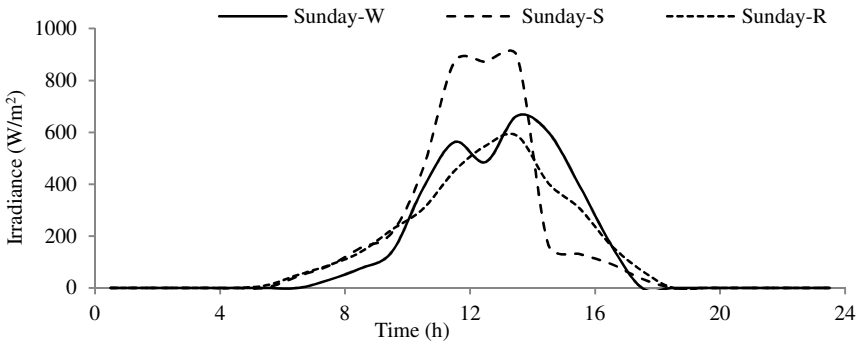

Fig. 2.10 The irradiance availability for 'S_u' in three seasons

The number of e-buses according to commuter's profile for M_n, S_t and S_u in three seasons is shown in Fig. 2.11, 2.12 and 2.13 respectively. In all these figures, the solid line represents the EB_f for W season, the medium dotted line represents the EB_f for S season and the small dotted line represents the EB_f for R season. The commuter's peak period starts from 07:00 to 11:00 h and from 16:00 to 22:00 h for M_n (considered the commuters travel for office and other purposes) and the peak period starts from 08:00 to 22:00 h for S_t and S_u (considered the commuters travel for shopping and other purposes). The total number of e-buses pass from one EBS in 24 h is given in Table 2.3.

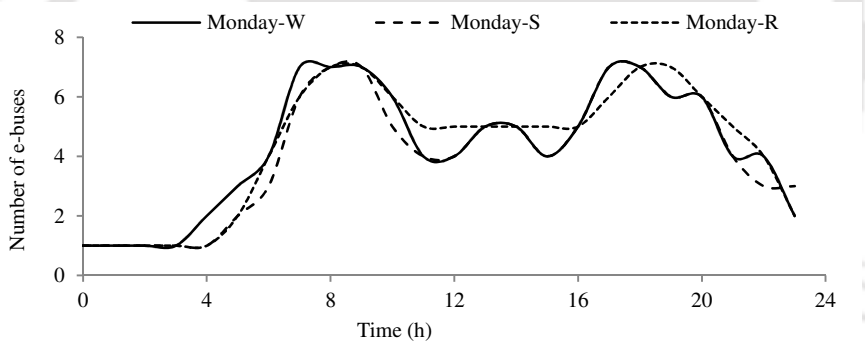

Fig. 2.11 The e-bus frequency for 'M_n' in three seasons

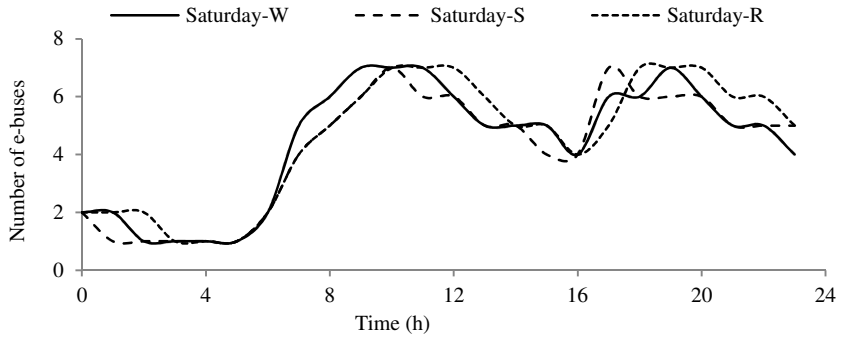

Fig. 2.12 The e-bus frequency for 'S_t' in three seasons

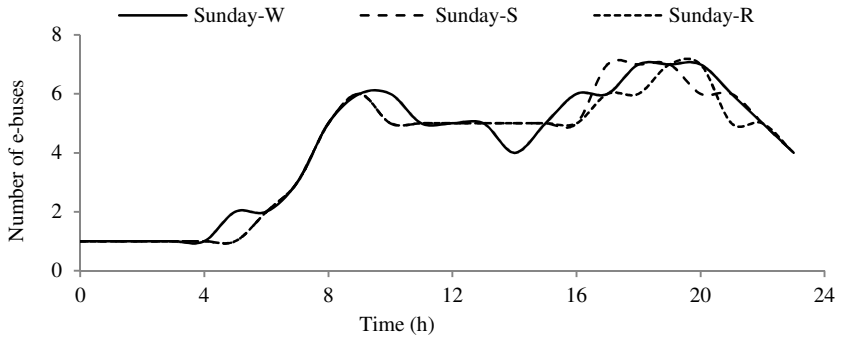

Fig. 2.13 The e-bus frequency for 'S_u' in three seasons

Fig. 2.14 to 2.16 shows the dynamic load profiles at X_1 EBS for M_n, S_t and S_u in three seasons. The solid, medium dotted and small dotted lines represent the load profiles for W, S and R seasons respectively. These load profiles are used in SPTS simulations.

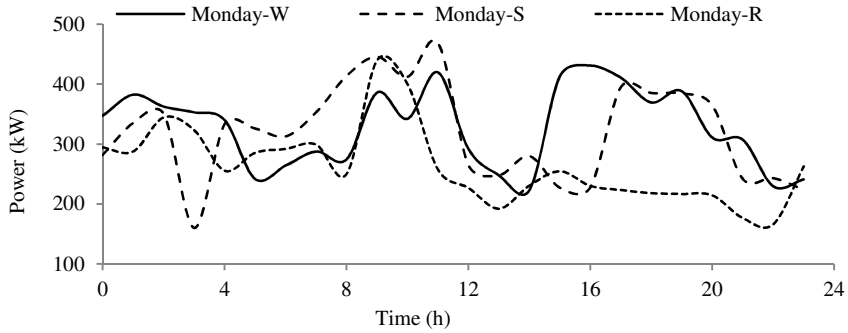

Fig. 2.14 The load profiles of the grid for 'M_n' in three seasons

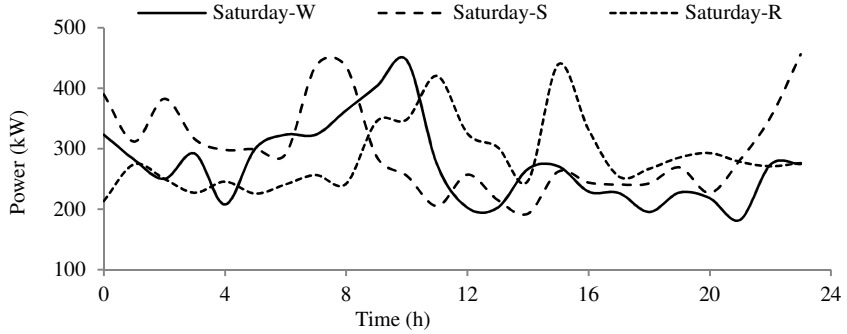

Fig. 2.15 The load profiles of the grid for 'S_t' in three seasons

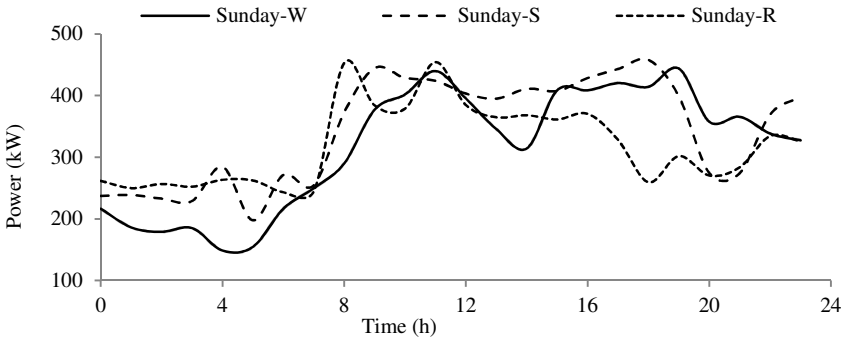

Fig. 2.16 The load profiles of the grid for 'S_u' in three seasons

Table 2.3: The SPTS and SP specifications

Variable	*Rating*
The total number of e-buses pass from one EBS for 24 h	112
SP capacity	50 kW

2.2.3 The Fuzzy logic controller

EBS consists of a fuzzy logic controller (FLC) to control the charging/discharging of ESD from/to the grid in off-peak/peak period and also to control the SP energy to ESD/to the grid in off-peak/peak period. The advantages that FLC shows are: simple mathematical concepts, flexible and is based on natural language [117]-[120]. The FLC has followed the logics as per the algorithm given in the earlier subsection and decides the controlled power flow among ESD, SP and the grid. The idea behind the FLC shows that the practical thinking and intelligence of a human is represented by the collection of If-Then rules. Fig. 2.17 shows the basic working model of FLC with inputs: Vpu, E_{ESD}, EB_f, E_{SP} and outputs: $P\pm$, $SP\pm$. Fuzzification (Mamdani inference system is used) is the process of converting input crisp set values into linguistic variables. Defuzzification is the process of converting linguistic variables into output crisp set values. These conversions are done by means of triangular membership functions and are used due to their simple representation and ease of mathematical expressions. The rule base in FLC performs the control strategy and the outputs from each rule are reduced by inference logic. The Defuzzification process has been performed by the center of area method.

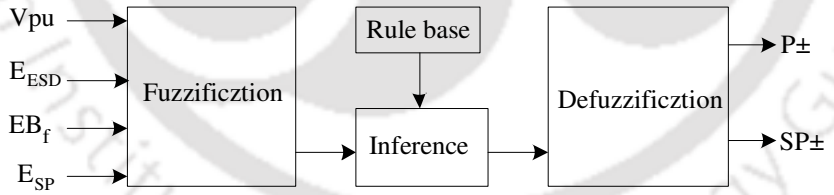

Fig. 2.17 The basic working model of FLC

The input and output membership functions of FLC are shown in Fig. 2.18 and 2.19 respectively. The Vpu thresholds are considered from 0.85 pu to 1.05 pu [105]. The universe of discourse ranges for inputs are: for Vpu (0.85 to 1.05), for E_{ESD} (0 to 300 kWh), for EB_f (0 to 6) and for E_{SP} (0 to 50 kWh). Each input is divided into three membership functions and represented with the linguistic variables such as low (L), medium (M) and high (H). The grade of the membership range for all inputs and outputs are from 0 to 1. The two outputs are divided into 7 and 6 membership functions and represented with the linguistic variables such

as negative low (NL) negative medium (NM), negative high (NH), zero (Z) and positive low (PL), positive medium (PM), positive high (PH). The universe of discourse for $P\pm$ is from -40 kW to 40 kW and for $SP\pm$ is from -50 kW to 50 kW. The FLC rule base is given in Table 2.4 and the inputs are Vpu, E_{ESD}, EB_f and E_{SP} respectively. The outputs are $P\pm$ and $SP\pm$.

Table 2.4: Rule base of the FLC

Input				*Output*			*Input*				*Output*	
Vpu	E_{ESD}	EB_f	E_{SP}	$P\pm$	$SP\pm$		*Vpu*	E_{ESD}	EB_f	E_{SP}	$P\pm$	$SP\pm$
H	M	H	H	Z	PH		M	L	H	H	Z	NH
H	M	H	M	Z	PM		M	L	H	M	Z	NM
H	M	H	L	Z	PL		M	L	H	L	Z	NL
H	M	M	H	Z	PH		M	L	M	H	Z	NH
H	M	M	M	Z	PM		M	L	M	M	Z	NM
H	M	M	L	Z	PL		M	L	M	L	Z	NL
H	M	L	H	Z	PH		M	L	L	H	Z	NH
H	M	L	M	Z	PM		M	L	L	M	Z	NM
H	M	L	L	Z	PL		M	L	L	L	Z	NL
H	L	H	H	PL	PH		L	H	H	H	NH	NH
H	L	H	M	PL	PH		L	H	H	M	NH	NM
H	L	H	L	PL	PM		L	H	H	L	NH	NM
H	L	M	H	PL	PH		L	H	M	H	NH	NH
H	L	M	M	PL	PH		L	H	M	M	NH	NM
H	L	M	L	PL	PM		L	H	M	L	NH	NM
H	L	L	H	PL	PH		L	H	L	H	NH	NH
H	L	L	M	PL	PH		L	H	L	M	NH	NM
H	L	L	L	PL	PM		L	H	L	L	NH	NM
M	H	H	H	NH	NH		L	M	H	H	NM	NH
M	H	H	M	NH	NM		L	M	H	M	NM	NM
M	H	H	L	NH	NL		L	M	H	L	NM	NL
M	H	M	H	NH	NH		L	M	M	H	NM	NH
M	H	M	M	NH	NM		L	M	M	M	NM	NM
M	H	M	L	NH	NL		L	M	M	L	NM	NL
M	H	L	H	NH	NH		L	M	L	H	NM	NH
M	H	L	M	NH	NM		L	M	L	M	NM	NM
M	H	L	L	NH	NL		L	M	L	L	NM	NL
M	M	H	H	NH	NH		L	L	H	H	Z	PH
M	M	H	M	NH	NM		L	L	H	M	Z	PM
M	M	H	L	NH	NL		L	L	H	L	Z	PL
M	M	M	H	NH	NH		L	L	M	H	Z	PH
M	M	M	M	NH	NM		L	L	M	M	Z	PM
M	M	M	L	NH	NL		L	L	M	L	Z	PL
M	M	L	H	NH	NH		L	L	L	H	Z	PH
M	M	L	M	NH	NM		L	L	L	M	Z	PM
M	M	L	L	NH	NL		L	L	L	L	Z	PL

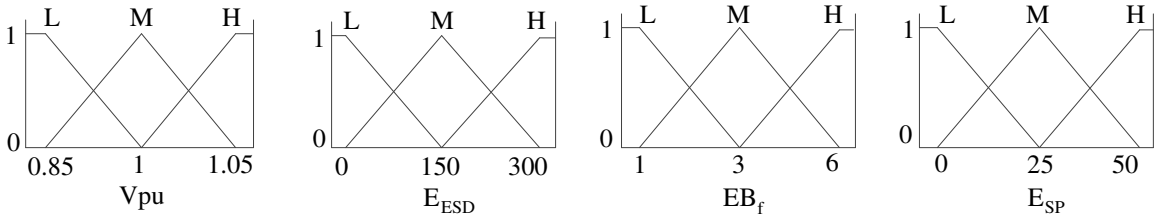

Fig. 2.18 Input membership functions of FLC

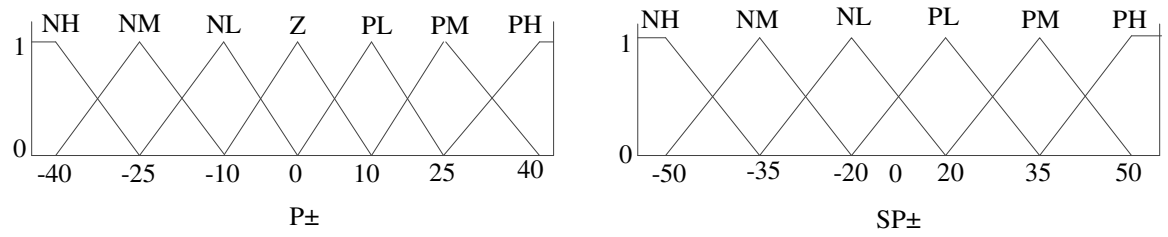

Fig. 2.19 Output membership functions of FLC

2.3 Results and discussion

The SPTS response for three seasons of a year and the favorable energy utilization from both, the grid and SP for SPTS support has been explained through two case studies:

1) The benefits with only ESD and with both ESD and SP in SPTS are given in case-1.

2) SPTS response for three seasons of a year is given case-2.

The maximum e-buses frequency is considered for simulations in both the cases as per Table 2.3. The results show that the voltage profile flattening of the grid using the energy from both, the ESD and SP in SPTS.

2.3.1 Case-1: SPTS response with only ESD and with both, the ESD and SP

The SPTS response has been explained through, Vpu profiles of the grid and the energy behavior bar-charts of ESD and SP. In this work Vpu is maintained between 0.98 pu and 1.015 pu. The off-peak period is considered when Vpu is greater than 1 pu otherwise peak period. The Vpu response with and without ESD and with both, the ESD and SP are shown in Fig. 2.20.

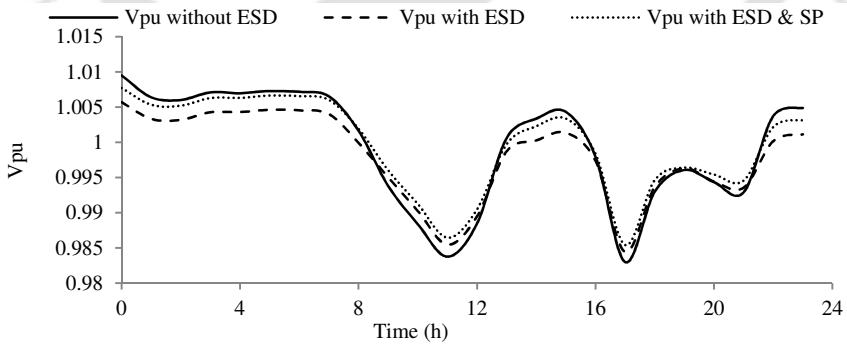

Fig. 2.20 Vpu response of the grid with and without ESD and with both, the ESD and SP

The Vpu curve with only ESD shows that the ESD is receiving maximum energy from the grid in off-peak period so that the Vpu curve is reaching near to 1 pu (the valley filling in the load point of view). The ESD is supporting to the grid in peak period so that the Vpu curve is above the actual Vpu (peak shaving in the load point of view). The Vpu with both the ESD

and SP shows that the ESD is receiving less energy from the grid in off-peak period (due to the SP energy availability) and giving more support to the grid in peak period (support from both, ESD and SP when peak period occur in the day-time). The joint use of ESD and SP sets the Vpu profile in the improved fashion compared to ESD only in SPTS.

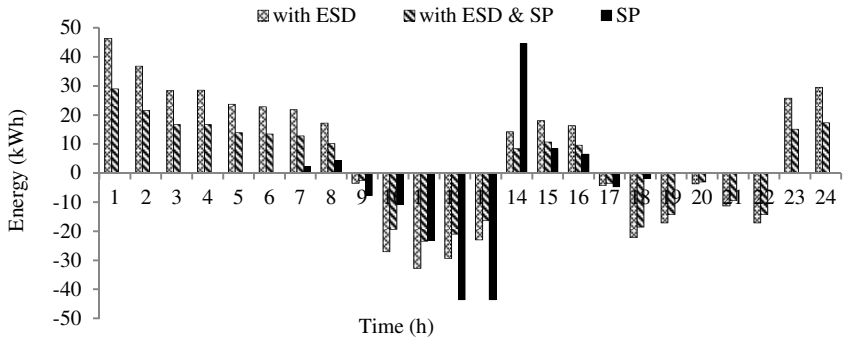

Fig. 2.21 The energy behavior with only ESD and with both, the ESD and SP after integrating with the grid

The energy behavior with only ESD and with both the ESD and SP after integrating with the grid is shown in Fig. 2.21. The positive bars of ESD represent the amount of energy received from the grid and the negative bars represent the amount of energy fed back to the grid by ESD. The positive bars of SP represent the amount of energy from SP to ESD and the negative bars represent the amount of energy from SP to the grid. The bars with the only ESD have more energy value than the bars with both ESD and SP in off-peak period. This shows that the SPTS only with ESD is completely depending on the grid and also supporting less to the grid in peak period as compared to both ESD and SP.

2.3.2 Case-2: SPTS response for three seasons of a year

The SPTS response is given separately for M_n, S_t and S_u in W, S and R seasons from Fig. 2.22 to 2.35. The results show that both, the grid and SP support to the SPTS for 24 h via ESD, the SP energy to ESD/to the grid in off-peak/peak period and the ESD energy from/to the grid in off-peak/peak period.

2.3.2.1 Winter (W) season

The Vpu profile of M_n in W is shown in Fig. 2.22. The solid line represents the actual Vpu and the dotted line represents the resultant Vpu. The same sequence has been followed for all the Vpu profiles of three seasons. The Vpu curves follow the dynamic load profiles (off-peak and peak period vary throughout the day) of the grid (ref. Fig. 2.14 to 2.16). In all the Vpu curves the resultant Vpu curve is below the actual Vpu curve in off-peak period. This means that the ESD is receiving energy from the grid. The resultant Vpu curve is above the actual

Vpu curve in peak period. This means that the ESD is sending its stored energy back to the grid along with SP. Likewise; the Vpu profile has been improved in off-peak and peak period by utilizing energy from both, the ESD and SP in SPTS.

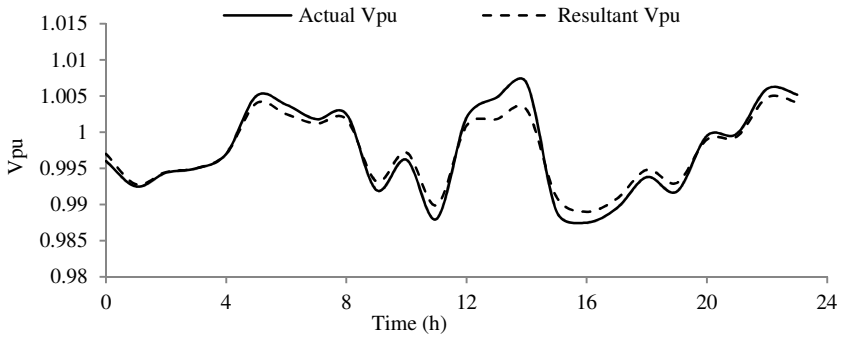

Fig. 2.22 Vpu of M_n in W season

The energy behavior of ESD and SP for M_n in W is shown in Fig. 2.23. The small dotted bars represent the ESD energy to/from the grid, the crossed line bars represent the SP energy to ESD/to the grid and the solid line bars represent the energy received by the e-buses (EBs) from ESD. The e-bus is represented with EB in all the bar charts of three seasons. This sequence has been followed in all the energy behavior figures of three seasons.

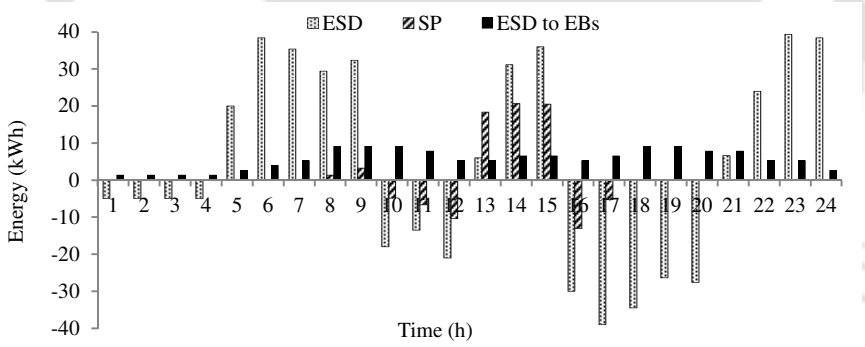

Fig. 2.23 The energy behavior of ESD and SP for M_n in W season

ESD positive bars represent the amount of energy from the grid to ESD in off-peak period and the negative bars represent the amount of energy from ESD to the grid in peak period. The positive bars of SP represent the amount of energy from SP to ESD in off-peak period and the negative bars represent the amount of energy from SP to the grid in peak period. ESD sends energy to the e-buses for 24 h (by receiving energy from both the grid and SP in off-peak period) so that ESD to e-bus bars are always remaining positive according to e-bus frequency throughout the day. The favorable energy utilization from both, the grid and SP for e-buses support can be observed from Fig 2.23. The SP is sending energy to the grid, from

10:00 to 12:00 h when the grid is under peak period in the day-time. SP is sending energy to ESD, from 13:00 to 15:00 h when the grid is under off-peak period. This shows the decent energy utilization from SP, for both the grid and SPTS support. The Vpu profile for S_t in W is shown in Fig. 2.24. The improvement in Vpu profile of the grid in both, off-peak and peak periods can be observed from Fig. 2.24.

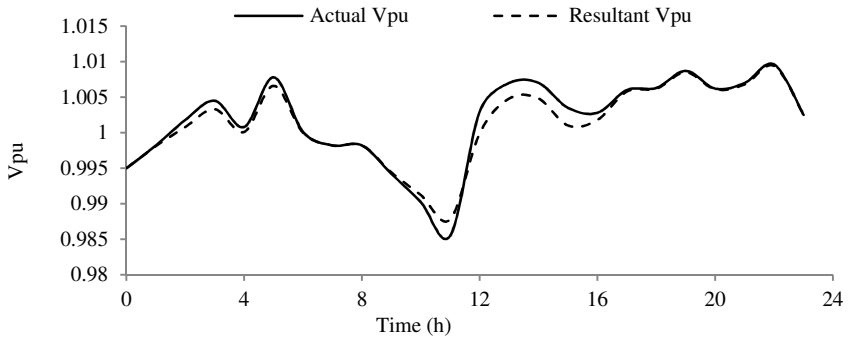

Fig. 2.24 Vpu of S_t in W season

The energy behavior of ESD and SP for S_t in W is shown in Fig. 2.25. The Vpu profile of the grid has stayed under peak period from 10:00 to 12:00 h, so that SP has sent energy to the grid during this period. The Vpu profile of the grid has stayed under off-peak period from 13:00 to 24:00 h. Therefore, SP has sent energy to ESD from 13:00 to 17:00 h, as shown in Fig. 2.25. ESD is receiving less energy from the grid after 18:00 h due to the energy status of the ESD has reached to its maximum state.

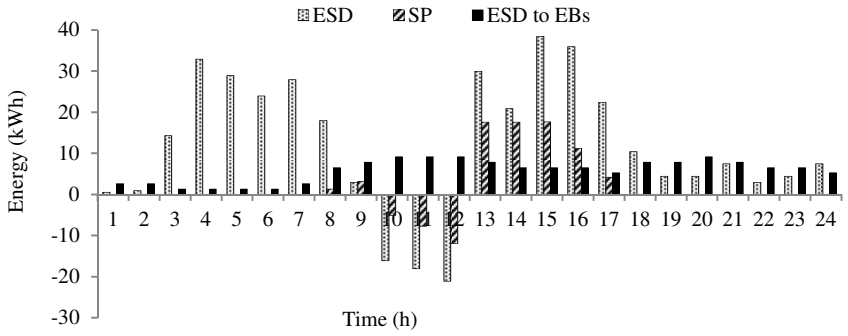

Fig. 2.25 The energy behavior of ESD and SP for S_t in W season

The Vpu profile for S_u in W is shown in Fig. 2.26. The area between the actual and resultant Vpu curve shows that the amount of energy received from the grid in off-peak period and the amount of energy fed back to the grid in peak period by the ESD.

The energy behavior of ESD & SP for S_u in W is shown in Fig. 2.27. The ESD receives moderate energy from the grid during off-peak period as it needs to keep the space for receiving energy from SP. The FLC intelligently decides the rate of energy from the grid to

ESD and from SP to ESD. The FLC performs this control action based on the rule base designed in it. The FLCs of every EBS work individually without interacting the other FLCs. The Vpu profile has stayed under peak period from 11:00 to 24:00 h so that SP has sent its total energy to the grid.

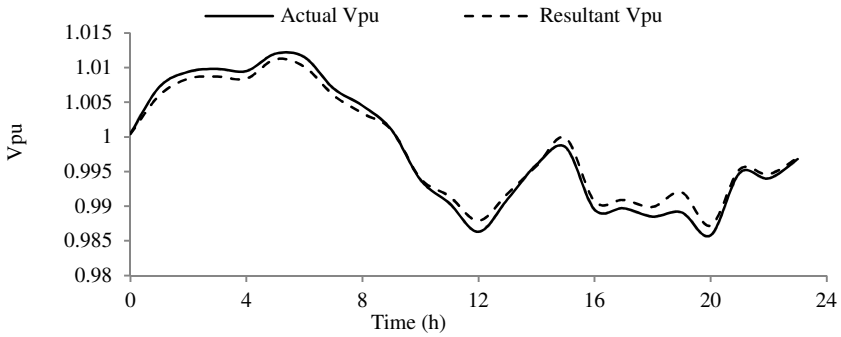

Fig. 2.26 Vpu of S_u in W season

ESD support the grid as well as the e-buses with the energy received from the grid in off-peak period and that can be observed from Fig. 2.27. The solar irradiance availability is less during W season (ref. Fig. 2.8 to 2.10) so that the SP is sending less energy to the grid/to ESD during peak/off-peak period. It can be observed from Fig. 2.22 to 2.27 that SPTS is getting less energy support from SP in this season compared to other seasons.

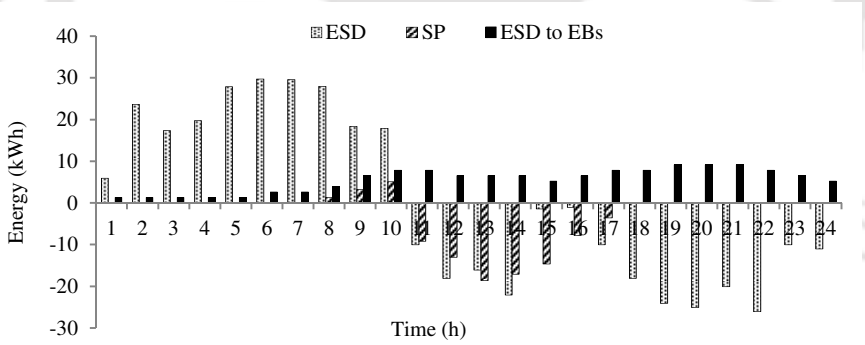

Fig. 2.27 The energy behavior of ESD and SP for S_u in W season

2.3.2.2 Summer (S) season

Vpu profile for M_n in S is shown in Fig. 2.28. The valley filling and peak shaving of Vpu profile using the energy from both, ESD and SP can be observed from Fig. 2.28. ESD send energy to the grid during peak period and SP send energy to the grid when it remains under peak period during sunshine hours. ESD and SP together perform the valley filling of the Vpu profile. ESD alone perform the peak shaving of the Vpu profile by receiving energy from the grid during off-peak period and that can be observed from Fig. 2.28.

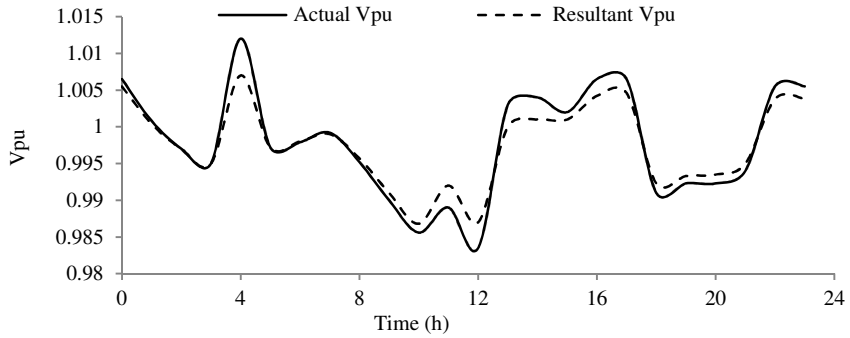

Fig. 2.28 Vpu of M_n in S season

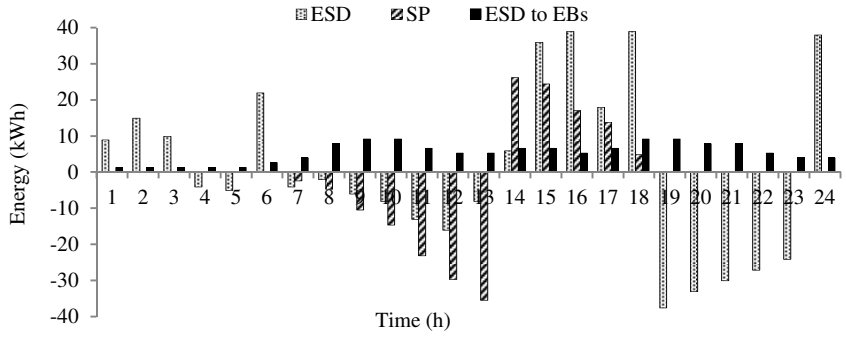

Fig. 2.29 The energy behavior of ESD and SP for M_n in S season

The energy behavior of ESD and SP for M_n in S is shown in Fig. 2.29. The Vpu profile has stayed under peak period from 07:00 to 13:00 h so that both, the ESD and SP are sending energy to the grid. The off-peak period is from 14:00 to 18:00 h so that SP is sending energy to ESD during this period. ESD is supporting maximum energy to the grid from 19:00 to 23:00 h.

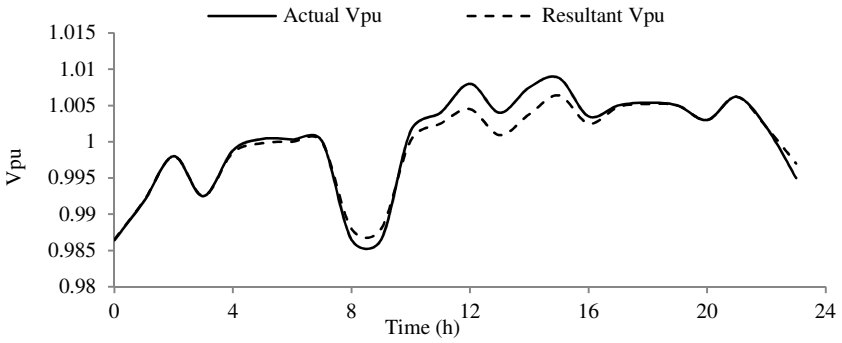

Fig. 2.30 Vpu of S_t in S season

Vpu profile for S_t in S is shown in Fig. 2.30. The improvement in Vpu profile during off-peak and peak period can be observed from Fig. 2.30. The energy behavior of ESD and SP for S_t in S is shown in Fig. 2.31. The Vpu profile has remained under off-peak period from 07:00 to 08:00 h and 11:00 to 23:00 h so that ESD is receiving energy from the grid. Also,

SP is sending maximum energy to ESD from 11:00 to 18:00 h so that ESD is receiving less energy from the grid during this period. ESD is also sending energy to the e-buses for 24 h with respect to EB_f (ref. Fig. 2.12). The Vpu profile has remained under peak period from 24:00 to 06:00 h and 09:00 to 10:00 h. Therefore, ESD is sending its stored energy back to the gird during this period and that can be observed from Fig. 2.31.

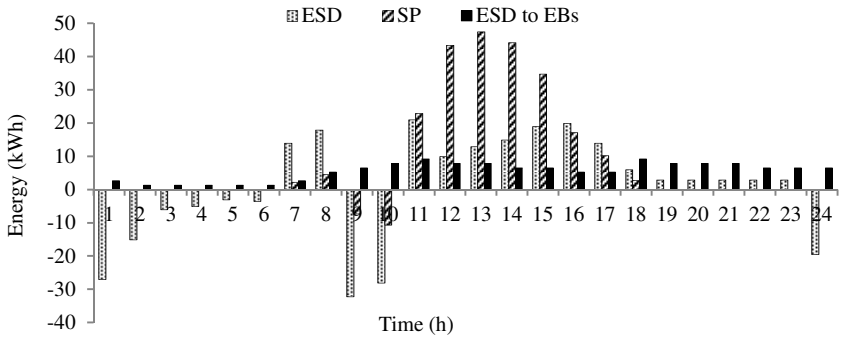

Fig. 2.31 The energy behavior of ESD and SP for S_t in S season

Vpu profile for S_u in S is shown in Fig. 2.32. The improvement in Vpu profile during off-peak and peak period can be observed from Fig. 2.32.

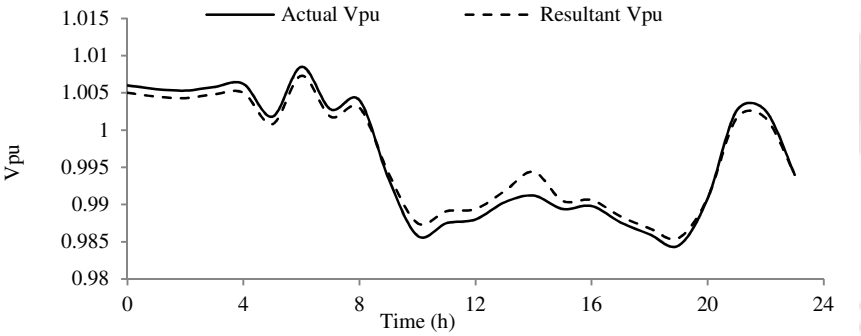

Fig. 2.32 Vpu of S_u in S season

The energy behavior of ESD and SP for S_u in S is shown in Fig. 2.33. The Vpu profile has remained under off-peak period from 22:00 to 10:00 h so that ESD is receiving energy from the grid. The Vpu profile has remained under peak period from 11:00 to 21:00 h so that ESD is sending its stored energy back to the gird during this period. Also, SP is sending its maximum energy to the grid from 11:00 to 18:00 h and that can be observed from Fig. 2.33. The solar irradiance availability is more during S season and SP energy generation is proportional to solar irradiance availability. Therefore, SP is sending its maximum energy to the grid/to ESD during peak/off-peak period in this season. It can be observed from Fig. 2.28 to 2.33 that SPTS is getting maximum energy support from SP in this season compared to

other seasons. The complete SP energy can be utilized for SPTS support if the grid stays continuously under off-peak period in the day-time. If this situation exists then SPTS runs, only based on SP energy. This means that the SPTS become independent of the grid.

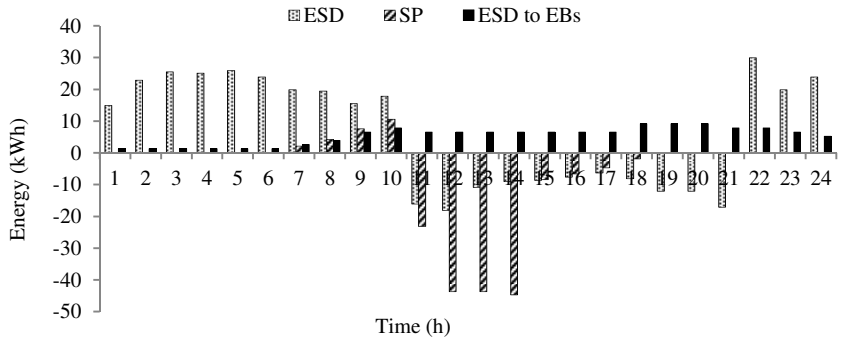

Fig. 2.33 The energy behavior of ESD and SP for S_u in S season

2.3.2.3 Rainy (R) season

Vpu profile for M_n in R is shown in Fig. 2.34. The area between actual and resultant Vpu profile during peak and off-peak period shows that the valley filling and peak shaving of the Vpu profile. The Vpu profile improvement during off-peak and peak period can be observed from Fig. 2.34.

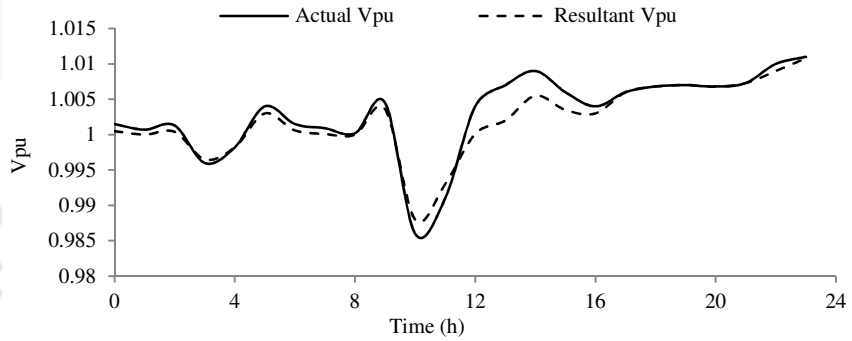

Fig. 2.34 Vpu of M_n in R season

The energy behavior of ESD and SP for M_n in R is shown in Fig. 2.35. The Vpu profile has remained under off-peak period from 13:00 to 03:00 h and 06: to 10:00 h so that ESD is receiving energy from the grid. The Vpu profile has remained under peak period from 04:00 to 05:00 h and 11:00 to 12:00 h so that ESD is sending its stored energy back to the gird during this period. Also, SP is sending energy to the grid from 11:00 to 12:00 h and that can be observed from Fig. 2.35.

Vpu profile for S_t in R is shown in Fig. 2.36. The energy behavior of ESD and SP for S_t in R is shown in Fig. 2.37. The Vpu profile has stayed under peak period from 10:00 to 13:00 h and from 16:00 to 17:00 h so that both, the ESD and SP are sending energy to the grid. The

off-peak period is from 18:00 to 09:00 h and from 14:00 to 15:00 h so that ESD is receiving energy from the grid. Also, SP is sending energy to ESD from 07:00 to 09:00 h, 14:00 to 15:00 h and 18:00 to 19:00 h. ESD and SP are supporting maximum energy to the grid during peak period.

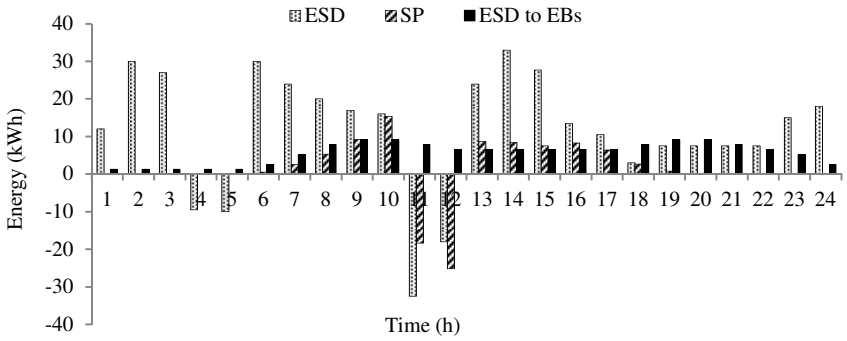

Fig. 2.35 The energy behavior of ESD and SP for M_n in R season

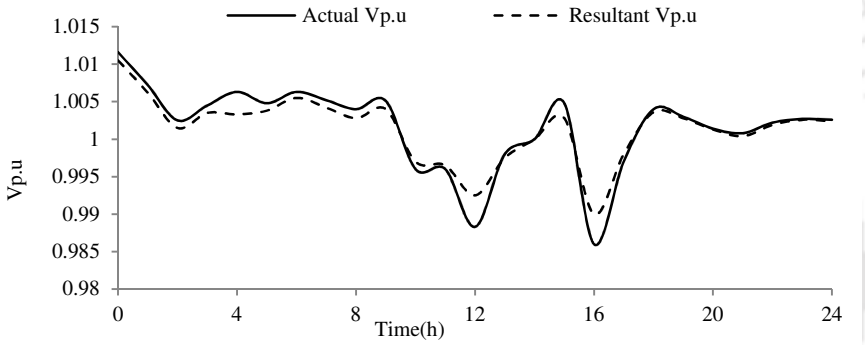

Fig. 2.36 Vpu of S_t in R season

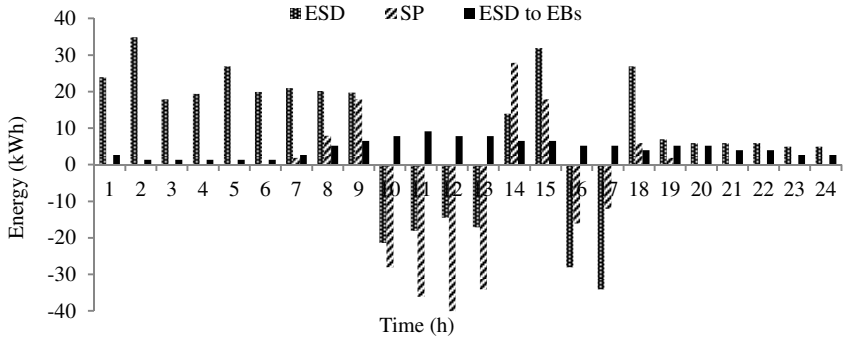

Fig. 2.37 The energy behavior of ESD and SP for S_t in R season

Vpu profile for S_u in R is shown in Fig. 2.38. The energy behavior of ESD and SP for S_u in R is shown in Fig. 2.39. The Vpu profile has stayed under peak period from 09:00 to 18:00 h so that both, the ESD and SP are sending energy to the grid. The off-peak period is from 19:00 to 08:00 h so that ESD is receiving energy from the grid. Also, SP is sending energy to ESD from 07:00 to 08:00 h. The solar irradiance availability is medium during 'R' season.

Therefore, SP is sending moderate energy to the grid/to ESD during peak/off-peak period in this season. It can be observed from Fig. 2.34 to 2.39 that SPTS is getting moderate energy support from SP in this season compared to other seasons.

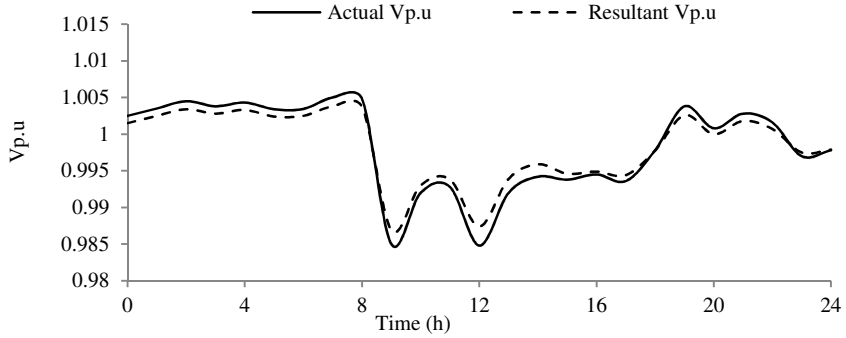

Fig. 2.38 Vpu of S_u in R season

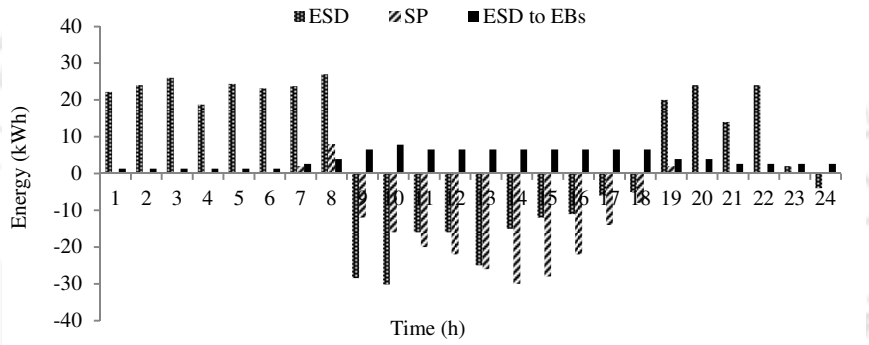

Fig. 2.39 The energy behavior of ESD and SP for S_u in R season

The above discussion (results for three seasons) concludes that the SPTS is getting more benefit from SP in the summer season than other seasons. The intelligent energy utilization from both, ESD and SP has reduced the SPTS reliance on the grid. This system is beneficial to the grid, to the SPTS and to the passengers. Also, this system provides clean environment in city regions and is helpful in improving the air quality in the urban regions.

2.4 Summary

- In this chapter, SPs coupled with SPTS has been modeled and coordinated with the grid.
- The e-buses are used for mass transportation in the Guwahati city, Assam, India.
- The EBSs have been provided through the ring road of the city to charge the e-buses during their journey. Both, the ESD and SP are connected to each EBS to improve the voltage profile of the grid.
- The maximum SP energy has been utilized by reducing the energy consumption from the grid for SPTS support.

- The SP sizing and the energy generation capacity of SP has been calculated by determining the solar irradiance availability.
- The smooth performance of SPTS has been obtained by utilizing the favorable energy from both, the grid and SP.
- The SPTS response is shown for two types of days (working day and non-working day) in three seasons of a year at X_1 EBS.
- FLC performed the control actions to manage the energy flow among the grid, SP and SPTS.
- The intelligent energy utilization from both, ESD and SP has reduced the SPTS dependence on the grid.

In the next chapter, the optimal number of e-buses has been determined as a function of the load, SP energy status, ESD energy status and the passenger profile for both normal and special days. Also, the failure analysis of SPTS has been carried out to achieve the fail proof performance of SPTS.

Note: This work, "small-scale solar plants coupled with smart public transport system and its coordination with the grid" is published in IET Journal on 'Electrical systems in transportation'.

3

Optimal number of e-buses in the Solar Assisted Smart Public Transit System and its Failure Analysis

Contents

Introduction

The clean energy based transportation system implementation is one of the possible solutions to limit air pollution in cities. The electric vehicle (EV) based transportation system is introduced prior to the internal combustion engine vehicles. However, EVs lost their popularity due the limited battery capacity of EVs [104], [123]. Certainly, the need of clean energy based transportation system and the systematic enhancement in storage technology led the demand towards EVs [104]. However, EVs need the coordinated charging to avoid the voltage and frequency fluctuations in the grid [103], [105]. Enhancement in the public transportation system has been started with the introduction of trolleybuses and the supercapacitor based buses [106]-[109]. These electric buses are grid powered and may halt on their way if the grid is unable to support the electric buses. In [110], the grid powered transportation system has been proposed. In this system, EVs receive energy from the grid via wireless-charging system installed under the road. The transportation system is convenient with this arrangement, but it creates an extra stress on the grid during the peak period. Placing a high capacity energy storage device (ESD) between the grid and the transportation system may overcome such difficulty [111, 112].

In [113], the energy storage devices have been used to combine the transportation system with the grid. This system may collapse due to the limited capacity of supercapacitor based buses and the lack of communication among the bus stops. The proposed work focuses on these aspects and provides the fail-proof performance of the smart public transit system (SPTS). Objectives of the present work are therefore:

- To decide the optimal number of electric buses (the total number of electric buses that are required to manage the passenger traffic per hour) as a function of the load, passengers, ESD and the solar plant (SP).
- To achieve the fail-proof performance of SPTS.

Electric buses (e-buses) are used to perform the mass transportation in the Guwahati city, Assam, India. The charging points have been provided through the ring road of the city to charge the e-buses. Supercapacitors are the prime energy storage in e-buses due to their salient features [114, 115], [131]. Every charging point consists of a high capacity energy storage device as well as the solar plant to achieve the smooth performance of SPTS. This arrangement improves the voltage profile of the grid in both, the off-peak and peak period. SP generation capacity is proportional to the solar irradiance availability and is calculated

based on the real-time solar data. Optimal number of e-buses (ONB) has been determined as a function of the load, passengers, ESD and SP. ONB impact, on the performance of both the grid and SPTS has been verified through simulations. Three isolation switch controllers (ISC), an inductive charging system controller (ICSC) and an aggregator have been provided at every charging point to overcome the failure situations in SPTS. The fuzzy logic controller (FLC) controls the power flow among ESD, SP and the grid [117]-[120], [132].

The remainder of this chapter is organized as follows. The structure of SPTS network is given in Section 3.1. Section 3.2, explains the ONB determination and failure analysis in SPTS. The results and discussions are given in Section 3.3 and finally the summary is given in Section 3.4.

3.1 Structure of the SPTS network

This section explains the structure of both, the charging point (electric bus stop (EBS)) and the SPTS network. Fig. 3.1 shows the ring road of the Guwahati city covered by a number of EBSs (B_1, B_2 …B_{32}) including SPs as well as the distribution nodes (11/0.415 kV) (DN_1, DN_2… DN_{32}).

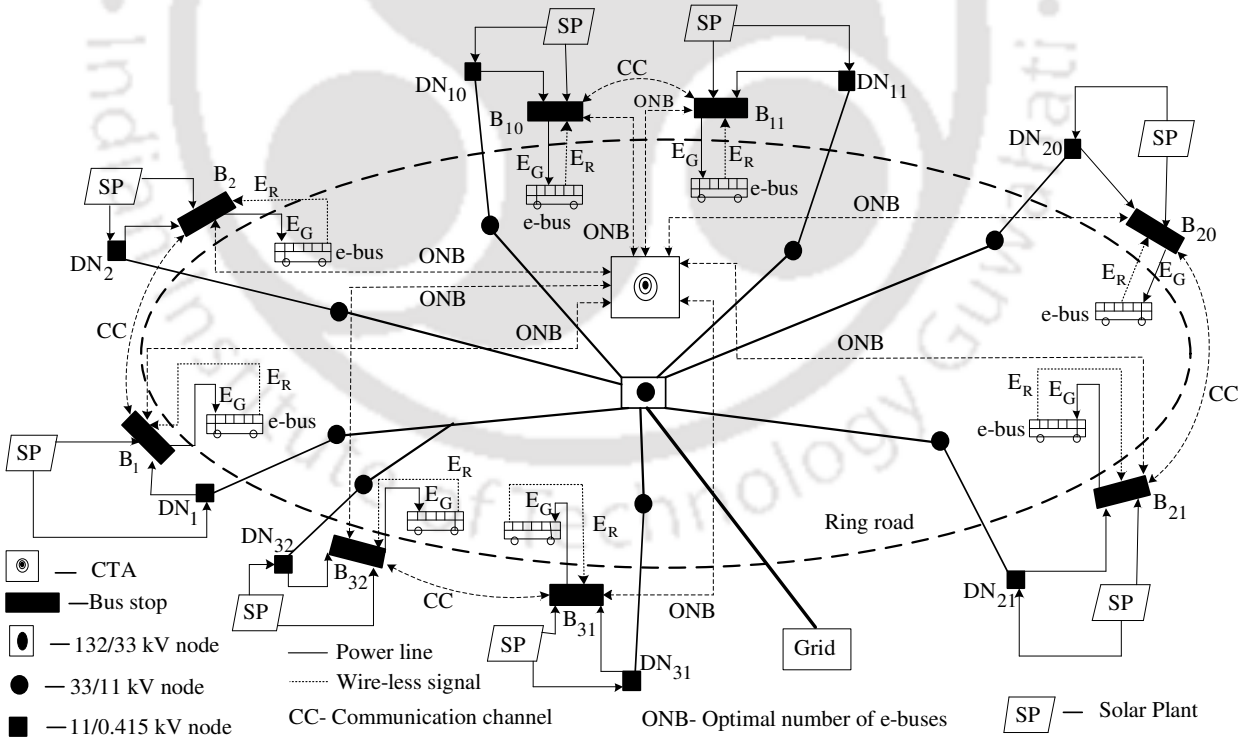

Fig. 3.1 SPTS network structure

A 10 number of 33 kV nodes cover the ring road [121, 122]. Under each 33 kV node, 11 kV nodes are present. Some of the 11 kV nodes consist of EBSs and the remaining are dedicated

to load. Both, ESD and SP are connected to the grid via 11/0.415 kV node. The e-bus receives energy from ESD situated at the current EBS via inductive charging system (ICS) and moves to the next EBS. This process continues throughout the ring road. At every EBS, the passengers get down/in duration from/to the e-bus is considered as 2 minutes. The e-bus receives sufficient energy in this duration (39.7 kW) from ESD. The minimum energy required by the e-bus to travel between consecutive EBSs is considered as 1.31 kWh ($E_{BT\ min}$) [133]. The e-bus maximum energy ($E_{BT\ max}$) is considered as 2 times of $E_{BT\ min}$ to avoid the emergency situations in SPTS. The communication channels (CC) have been provided between every EBS and also, among the central transportation authority (CTA) and the bus stops, to handle the failure situations in SPTS.

3.1.1 The bus stop structure

The structure of EBS is shown in Fig. 3.2. Both, ESD and SP are connected to the grid via DN. SP is connected to both, DN and ESD. ICS is connected to ESD through which the e-buses receive energy.

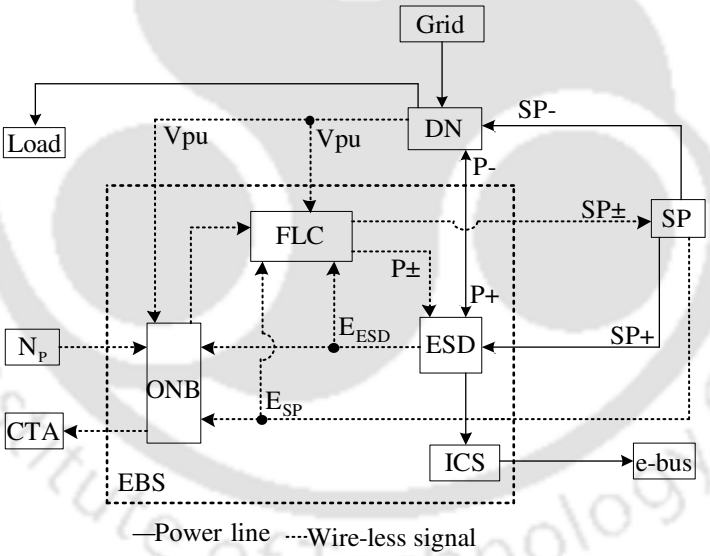

Fig. 3.2 The electric bus stop structure

The ONB block works based on four inputs and one output. Inputs are: per unit voltage of the grid (Vpu), ESD energy status (E_{ESD}), SP energy status (E_{SP}) and the number of passengers per hour (N_P). Output of ONB goes to both, FLC and CTA. The FLC, works based on four inputs and two outputs. Inputs are: Vpu, E_{ESD}, E_{SP}, and ONB. Outputs are: $P\pm$ (ESD receive/send power from/to the grid in off-peak/peak period) and $SP\pm$ (SP send power to ESD/to grid in off-peak/peak period). DN consists of a usual load along with EBS as shown

in Fig. 3.2. The ESD sizing, solar irradiance availability determination and SP sizing are given in Chapter-2, Section 2.1.2 to 2.1.4 respectively.

3.1.2 Assumptions

This work carries out the system level modelling of the entire network so that the modelling of ESD and converters, the losses due to ESD and ICS are not included.

3.2 The ONB determination and failure analysis in SPTS

The capa-bus (supercapacitor based buses) based public transportation system is presented in [113]. This system appears to be vulnerable for the increased number of passengers per hour (N_P) at EBSs. Capa-bus limited capacity and the lack of communication among EBSs may lead to the complete system failure. The present work conquers these issues and provides the fail-proof performance of SPTS. The increased N_P may trouble the functioning of both, the grid and SPTS. Therefore, ONB is required to manage the N_P demand. ONB determination is a challenging task due to the dynamic behaviour of the load, passengers, SP and ESD. ONB should not affect the performance of both, the grid and SPTS. Algorithm of ONB has insight of all such issues while deciding ONB [135], and it shows the following benefits:

- Decides ONB based on four dynamic profiles.
- Achieves the smooth functionality of SPTS using energy form both, the grid and SP.
- Avoids stress on the grid, which may occur due to the increased number of e-buses (NBs).
- Utilize the solar energy in proportion to the increased NBs.

The e-buses halt on their way if the consecutive EBSs failed to charge the e-buses. Such kinds of situations are restricted with the smart communication among the EBSs. The salient features of failure analysis in SPTS are, therefore:

- Optimal power utilization from both, the grid and SP.
- Fail proof.
- Smart communication.
- Intelligent energy management within EBS and among EBSs.

The major issues investigated in the failure analysis are:

- Different types of failures that exist in SPTS.
- The solution for each type of failure to ensure smooth functioning of SPTS.

- The solution for each type of failure to ensure grid support.
- Support from SP to SPTS in failure situations.

The real time data of the load, solar and passengers have been collected from the following departments.

- Load data from the state electricity board, Assam, India [121, 122].
- Solar data from the India meteorological department [124].
- Commuter's data from the central transportation authority.

The details about ONB determination, failure analysis and FLC are given in the following sub-sections.

3.2.1 The ONB determination

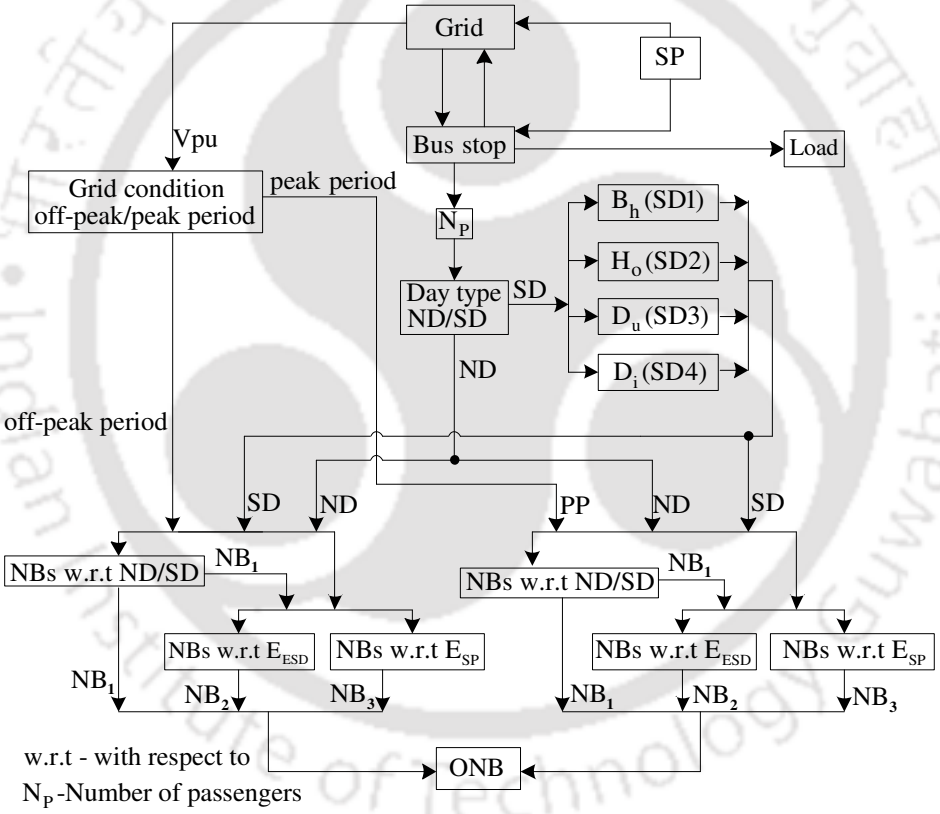

Fig. 3.3 ONB determination for ND and SDs in SPTS

The algorithm for ONB determination is explained through Fig. 3.3. Two types of days have been considered based on N_P. One is the normal day (ND) and the other as a special day (SD). N_P varies from minimum to medium for NDs (considered the passengers travel for office and other purposes) and varies from medium to maximum for SDs (considered the devotees travel to the temples). Four types of festival days have been considered under SD: Beehu (B_h) (SD1), Holi (H_o) (SD2), Dasara (D_u) (SD3) and Diwali (D_i) (SD4). Preference

has been given for the smooth functionality of SPTS, so that the NB is considered as an objective function. The maximum NBs are proportional to N_P. Off-peak period is considered when Vpu is greater than 1pu otherwise peak period.

The proposed algorithm decides ONB in the following manner: first, it checks the grid condition, whether it is in off-peak/peak period. Then it decides the day type, whether it is ND/SD. After that it decides: the NBs with respect to ND/SD, the NBs with respect to E_{ESD} and the NBs with respect to E_{SP} during off-peak and peak period separately as shown in Fig. 3.3. ONB is the average of NB_1 (NBs with respect to N_P), NB_2 (NBs with respect to E_{ESD}) and NB_3 (NBs with respect to E_{SP}) for ND/SD during off-peak/peak period (3.5). Therefore, ONB during off-peak period (ONB_{OPP}) and in peak period (ONB_{PP}) can be expressed as

$$\left.\begin{matrix}\mathrm{ONB_{OPP}}\\ \mathrm{ONB_{PP}}\end{matrix}\right\} = \mathrm{f(NB_1, NB_2, NB_3)} \tag{3.1}$$

If the grid stays under off-peak period, then ONB is determined in the following manner.

ONB_{OPP}: NBs according to N_P is given by

$$\mathrm{NB_1} = \begin{cases} \left(\dfrac{N_P}{R_C}\right) & (0 < N_P \le N_{P\,ND}) \,/\, (N_{P\,ND} < N_P < N_{P\,SD}) \\ \left(\dfrac{N_{P\,SD}}{R_C}\right) & otherwise \\ 0 & N_P = 0 \end{cases} \tag{3.2}$$

R_C is the e-bus carrying capacity (limited to 30 passengers), $N_{P\,ND}$ is the maximum passenger limit for ND (180 passengers/ h) and $N_{P\,SD}$ is the maximum passenger limit for SD (360 passengers/ h). NBs with respect to E_{ESD} (ESD total capacity (E_{ESDT}) is considered as 300 kWh) [133] is expressed as

$$\mathrm{NB_2} = \begin{cases} \mathrm{NB_1} & E_{ESD} \ge 20\% \\ \left(\dfrac{E_{ESD}}{E_{ESD\,min}}\right) & otherwise \\ 0 & E_{ESD} = 0 \end{cases} \tag{3.3}$$

Minimum energy always remain in the ESD ($E_{ESD\,min}$) is considered as 20%. ESD is able to support the maximum NBs when E_{ESD} is greater than 20%. The supporting formulas such as: ESD sizing and SP sizing can be observed from Chapter-2, Section 2.1.2 to 2.1.4 [133]. NBs with respect to E_{SP} (SP capacity is considered as 50 kW) [133] is therefore

$$NB_3 = \begin{cases} \left(\dfrac{E_{SP}}{E_{BT\,min}}\right) & (E_{SP} \le 15.75\% \quad \text{for ND}) / (E_{SP} \le 31.5\% \quad \text{for SD}) \\ NB_1 & (E_{SP} > 15.75\% \quad \text{for ND}) / (E_{SP} > 31.5\% \quad \text{for SD}) \\ 0 & otherwise \end{cases} \tag{3.4}$$

E_{SP} varies from 0 to 50 kWh with respect to solar irradiance availability during sunshine hours (ref. Fig. 3.4), 31.5% of SP energy is required to support the maximum NBs in SDs (the maximum NBs for SD are 12 and $E_{BT\,min}$ is 1.31 kWh [133], which is 15.72 kWh. A 31.5% of E_{SP} is 15.75 kWh). The maximum NBs for ND are 6. Therefore, E_{SP} limit is 15.75%. The resultant ONB in off-peak period is therefore

$$ONB_{OPP} = \left(\frac{(NB_1 + NB_2 + NB_3)}{(T_1 + T_2 + T_3)}\right) \tag{3.5}$$

where T_1, T_2 and T_3 are the temporary variables as a function of NB_1, NB_2, and NB_3. Individually, T_1, T_2 and T_3 become '0', if NB_1, NB_2 and NB_3 are '0', otherwise '1'. If the grid stays under peak period, then ONB is determined in the following manner.

ONB_{PP}: NBs according to N_P is same as that of (3.2). NBs according to E_{ESD} is given by

$$NB_2 = \begin{cases} NB_1 & E_{ESD} \ge 30\% \\ \left(\dfrac{E_{ESD}}{E_{ESD\,min}}\right) & otherwise \\ 0 & E_{ESD} = 0 \end{cases} \tag{3.6}$$

NBs according to E_{SP} are same as that of (3.4). The resultant ONB with respect to NB_1, NB_2 and NB_3 in peak period is same as that of (3.5). Table 3.1 shows the total use of NBs in 24 h for both, ND and SD.

Table 3.1: SP specification and the number of e-buses for ND and SD

Variable	*Rating*
The number of e-buses for ND (in 24 h)	112
The number of e-buses for SD (in 24 h)	180
SP capacity	50 kW

Fig. 3.4 shows the solar irradiance availability and its seasonal variation. The solar irradiance availability is calculated based on the real time solar data collected from the India meteorological department (IMD). The solar irradiance availability is low in winter, moderate in rainy and high in the summer season. SDs cover all the seasons of a year, which can be seen in Fig. 3.4. The load profiles used for SPTS simulations are shown in Fig. 3.5.

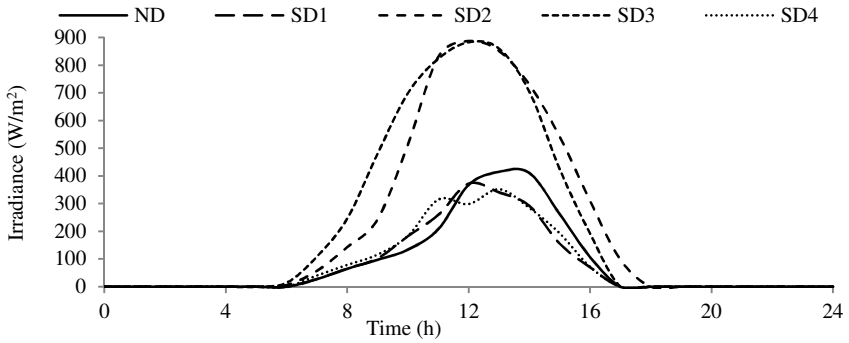

Fig. 3.4 Solar irradiance availability for ND and SDs

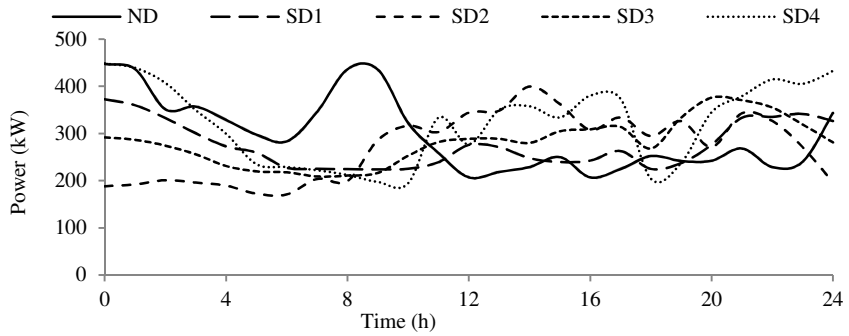

Fig. 3.5 Load profiles of the grid for ND and SDs

3.2.2 Failure Analysis in SPTS

Failures in SPTS are divided into two categories. First category explains the failures from hardware side, and the second category explains the failures from software side.

1. **Failures from hardware side:** Four types of failures have been considered under this category.

- When ESD is disconnected from the grid is failure-1 (F_1).
- When ICS is disconnected from ESD is failure-2 (F_2).
- When SP is disconnected from the grid is failure-3 (F_3).
- Failure-4 is of two types. First, one is when SP is disconnected from ESD (F_4) and the other is when ESD is disconnected from $E_{SP\ node}$ (F_5).

2. **Failures from software side:** This failure is of two types. First, one is when FLC is failed (F_{FLC}) and the other is when both F_{FLC} and F_5 exist in SPTS.

The communications required to overcome the failure situations in SPTS are shown in Fig. 3.6. An extra bus-bar ($E_{SP\ node}$) has been provided through the ring road of the Guwahati city to manage the energy among EBSs in failure situations. The controllers present at every EBS are therefore:

- A failure sensor (FS) (ref. Fig. 3.6) that sends the failure information of the current bus stop (k^{th} EBS) to the next two bus stops ($k+1^{th}$ and $k+2^{th}$ EBSs).
- An inductive charging system controller (ICSC) which decides the amount of energy given to the e-bus from ESD (E_G).
- The isolation switch controller (ISC-1) which decides the isolation switch position (ISP)-0/1/2 among SP, $E_{SP\ node}$ and the grid.
- The ISC-2 which decides ISP-0/1 between ICS and ESD.
- The ISC-3 which decides ISP-1/2 among ESD, $E_{SP\ node}$ and the grid.
- The aggregator which decides the amount of energy received by ESD from $E_{SP\ node}$ (E_{ESDR}).

The working principles of above-mentioned controllers are given in the following subsections.

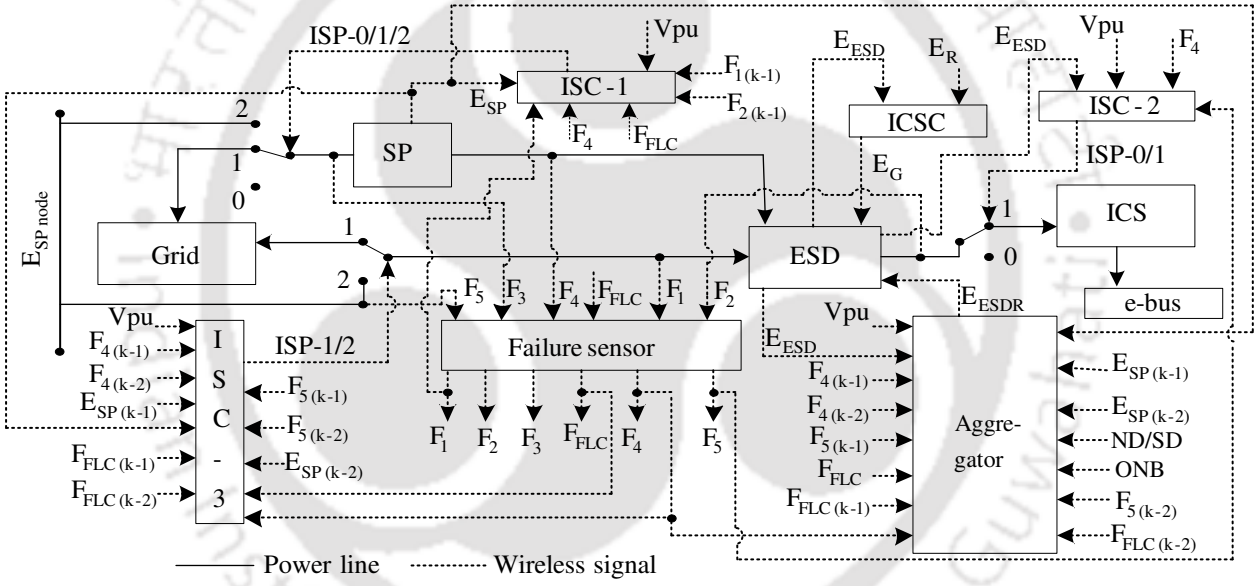

Fig. 3.6 The communications required in the electric bus stop

ISC-1: The ISC-1 works based on seven inputs and one output (ref. Fig. 3.6). The inputs are Vpu, $F_{1\ (k)}$ (F_1 of k^{th} EBS), $F_{4\ (k)}$ (F_4 of k^{th} EBS), $F_{FLC\ (k)}$ (F_{FLC} of k^{th} EBS), $F_{1\ (k-1)}$ (F_1 of $k\text{-}1^{th}$ EBS), $F_{2\ (k-1)}$ (F_2 of $k\text{-}1^{th}$ EBS) and $E_{SP\ (k)}$ (E_{SP} of k^{th} EBS). The output is ISP-0/1/2 (SP is open circuited from the grid/ connected to the grid/ connected to $E_{SP\ node}$). Algorithm of ISC-1 is shown in Fig. 3.7. If $F_{1\ (k)}$/ $F_{1\ (k-1)}$/ $F_{2\ (k-1)}$ exists then output is ISP-0 otherwise check the next condition. If $F_{4\ (k)}$ / $F_{FLC\ (k)}$ exists and also satisfy the conditions such as: Vpu of k^{th} EBS is under off-peak period and $E_{SP\ (k)}$ is greater than zero then output is ISP-2 otherwise ISP-1.

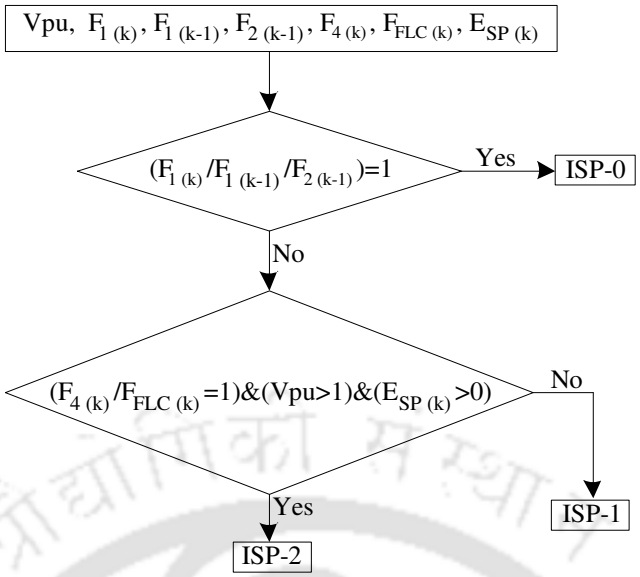

Fig. 3.7 Algorithm of ISC-1

ISC-2: The ISC-2 works based on four inputs and one output (ref. Fig. 3.6). The inputs are Vpu, E_{ESD}, $F_{4\,(k)}$ and $F_{5\,(k)}$. The output is ISP-0/1 (ICS is open circuited/connected from/to ESD). Algorithm of ISC-2 is shown in Fig. 3.8. If no failure exists then output is ISP-1. If Vpu of k^{th} EBS is under off-peak period and also both, $F_{4\,(k)}$ and $F_{5\,(k)}$ exist then output is ISP-0 otherwise ISP-1.

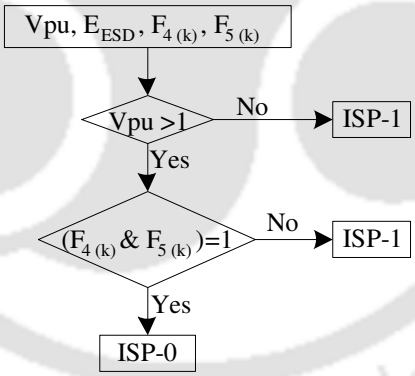

Fig. 3.8 Algorithm of ISC-2

ISC-3: The ISC-3 works based on twelve inputs and one output (ref. Fig. 3.6). The inputs are Vpu, $F_{4\,(k)}$, $F_{FLC\,(k)}$, $F_{4\,(k-1)}$ (F_4 of k-1^{th} EBS), $F_{5\,(k-1)}$ (F_5 of k-1^{th} EBS), $F_{4\,(k-2)}$ (F_4 of k-2^{th} EBS), $F_{5\,(k-2)}$ (F_5 of k-2^{th} EBS), $F_{FLC\,(k-1)}$ (F_{FLC} of k-1^{th} EBS), $F_{FLC\,(k-2)}$ (F_{FLC} of k-2^{th} EBS), $E_{SP\,(k)}$ (E_{SP} of k^{th} EBS), $E_{SP\,(k-1)}$ (E_{SP} of k-1^{th} EBS) and $E_{SP\,(k-2)}$ (E_{SP} of k-2^{th} EBS). The output is ISP-1/2 (ESD is connected to the grid/ connected to $E_{SP\,node}$). Algorithm of ISC-3 is shown in Fig. 3.9. If no failure exists then output is ISP-1. If Vpu is in off-peak period and if $F_{4\,(k)}$/ $F_{FLC\,(k)}$/ ($F_{4\,(k-1)}$ & $F_{5\,(k-1)}$)/ ($F_{4\,(k-2)}$ & $F_{5\,(k-2)}$)/ ($F_{FLC\,(k-1)}$ & $F_{5\,(k-1)}$)/ ($F_{FLC\,(k-2)}$ & $F_{5\,(k-2)}$) exist and also

satisfies the conditions for ND/SD then output is ISP-2, otherwise ISP-1. A 31.5% of SP energy is required to support ONB at the k^{th} EBS in SDs.

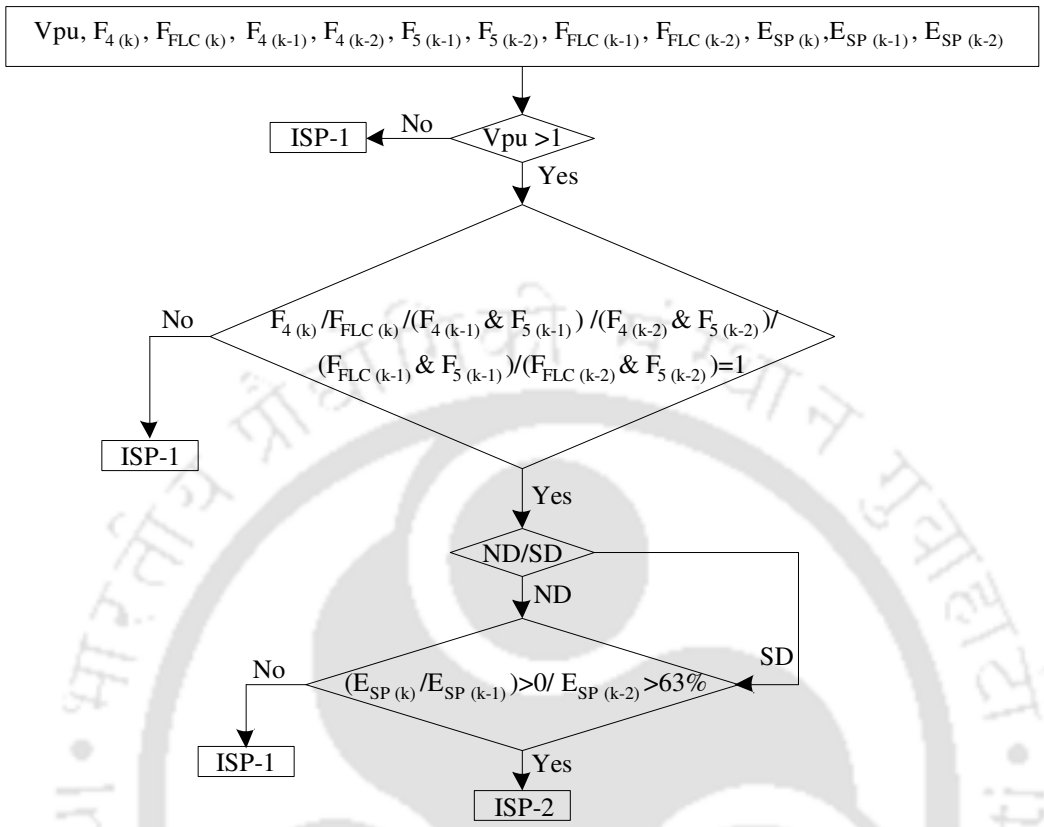

Fig. 3.9 Algorithm of ISC-3

Aggregator: The aggregator works based on fifteen inputs and one output (ref. Fig. 3.6). The inputs are Vpu, $F_{4\,(k)}$, $F_{FLC\,(k)}$, $F_{4\,(k-1)}$, $F_{5\,(k-1)}$, $F_{4\,(k-2)}$, $F_{5\,(k-2)}$, $F_{FLC\,(k-1)}$, $F_{FLC\,(k-2)}$, $E_{SP\,(k)}$, $E_{SP\,(k-1)}$, $E_{SP\,(k-2)}$, ND/SD, E_{ESD} of k^{th} EBS and ONB. The output is E_{ESDR}. If the grid stays under peak period, then E_{ESDR} is zero.

For ND: If the grid stays under off-peak period then E_{ESDR} is expressed as

$$E_{ESDR} = \begin{cases} E_{SP\,(k)}\,; & \text{for } (F_{4\,(k)} / F_{FLC\,(k)}) = 1 \text{ and } E_{SP\,(k)} > 0 \\ \left(\dfrac{(\sum_{i=1}^{n} 4 \times \text{ONB} \times E_{BT\,min})}{(\sum_{j=1}^{m} E_{SP\,(k-1)})} \right) \times \left(\sum_{j=1}^{m} E_{SP\,(k-1)} \right); & \\ \qquad \text{for } (F_{4\,(k-1)} \,\&\, F_{5\,(k-1)}) / (F_{FLC\,(k-1)} \,\&\, F_{5\,(k-1)}) = 1 \,\&\, (0 < E_{SP\,(k-1)} \le 63\%) & \\ \left(\dfrac{(\sum_{i=1}^{n} 2 \times \text{ONB} \times E_{BT\,min})}{(\sum_{j=1}^{m} E_{SP\,(k-2)})} \right) \times \left(\sum_{j=1}^{m} E_{SP\,(k-2)} \right); & \\ \qquad \text{for } (F_{4\,(k-2)} \,\&\, F_{5\,(k-2)}) / (F_{FLC\,(k-2)} \,\&\, F_{5\,(k-2)}) = 1 \,\&\, (E_{SP\,(k-2)} > 63\%) & \\ 0\,; \quad \text{for } E_{ESD} = E_{ESDT} & \end{cases} \tag{3.7}$$

where, i and j are the number of sunshine hours. If $F_{4\ (k)}$ / $F_{FLC\ (k)}$ exists and also, $E_{SP\ (k)}$ is greater than zero then ESD receives total $E_{SP\ (k)}$ via $E_{SP\ node}$. If ($F_{4\ (k-1)}$ & $F_{5\ (k-1)}$)/ ($F_{FLC\ (k-1)}$ & $F_{5\ (k-1)}$) exist and $E_{SP\ (k-1)}$ is in-between 0 to 63% then E_{ESDR} is a fraction of $E_{SP\ (k-1)}$ with respect to ONB. The factor 4 for this output in (3.7) shows that four times of ONB energy in NDs is equal to 63% of $E_{SP\ (k-1)}$. If ($F_{4\ (k-2)}$ & $F_{5\ (k-2)}$)/ ($F_{FLC\ (k-2)}$ & $F_{5\ (k-2)}$) exist and $E_{SP\ (k-2)}$ is greater than 63% then E_{ESDR} is a fraction of $E_{SP\ (k-2)}$ with respect to ONB. When ESD is in filled state (E_{ESDT}) then E_{ESDR} is zero. If such situation arises then mobile ESDs are arranged to rectify the problem. E_{ESDR} for SDs is same as that of (3.7) and the factor 2 divides the second and third output of (3.7) due to the increased ONB for SDs.

ICSC: The ICSC works based on two inputs and one output (ref. Fig. 3.6). Inputs are: E_{ESD} and the energy required by the e-bus (E_R). Output is E_G and is expressed as

$$E_G = \begin{cases} E_R & E_{ESD} > 20\% \\ E_{BT\ min} & E_{ESD} < 20\% \end{cases} \tag{3.8}$$

The details about the failures that exist in SPTS and the proper solutions to overcome these failures are as follows.

Failure-1: In this case, the breakdown of the connection between the grid and ESD has been considered at the k^{th} EBS (Fig. 3.6). In this situation, ESD is able to support the e-buses for 24 h but unable to receive/send energy from/to the grid in off-peak /peak period.

Solution: FS sends F_1 information to ISC-1 of k^{th} and $k+1^{th}$ EBSs. ISC-1 disconnects SP from the grid at k^{th} and $k+1^{th}$ EBSs (Fig. 3.7). SP is open circuited from the grid at these two EBSs irrespective of the grid condition and the total SP energy flows into ESD. If the situation arises like E_{ESD} is low and also, SP energy is not available at k^{th} EBS, then $k+1^{th}$ EBS shares the k^{th} EBS energy.

Failure-2: In this case, ICS is disconnected from ESD at k^{th} EBS (Fig. 3.6). Therefore, ESD is unable to charge the e-buses, but able to receive/send energy from/to the grid.

Solution: FS sends F_2 information of k^{th} EBS to ISC-1 of $k+1^{th}$ EBS. ISC-1 disconnects SP from the grid at $k+1^{th}$ EBS (Fig. 3.7). This creates the total SP energy availability at $k+1^{th}$ EBS. Therefore, the e-buses increased energy thirst (travel from k^{th} EBS to $k+1^{th}$ EBS) is fulfilled at $k+1^{th}$ EBS.

Failure-3: In this case, SP is disconnected from the grid (Fig. 3.6).

Solution: FS sends F_3 information to CTA. ESD of the k^{th} EBS manages the total SP energy. CTA activates the F_3 alarm to rectify the existed failure.

Failure-4: In this case, the breakdown of the connection between SP and ESD has been considered (Fig. 3.6). In this situation, SP energy has to be managed among the EBSs, if the grid stays under off-peak period during sunshine hours.

Solution: $E_{SP\ node}$ has been utilized to manage the SP energy (Fig. 3.6) under this failure. The communication among the EBSs and $E_{SP\ node}$ provides the flexibility in such a way that: the next two EBSs ($k+1^{th}$ and $k+2^{th}$ EBSs) share the current/failed EBS's (k^{th} EBS) SP energy. Two cases have been considered under this failure.

Case-a: F_4 exists at k^{th} EBS: FS sends F_4 information of k^{th} EBS to the aggregator, ISC-1 and ISC-3 of k^{th} EBS. ISC-1 disconnects SP from the grid and connects to $E_{SP\ node}$ (Fig. 3.6 and 3.7). ISC-3 disconnects ESD from the grid and connects to $E_{SP\ node}$ (Fig. 3.6 and 3.9). This arrangement shows that SP is bypassed to ESD via $E_{SP\ node}$. The aggregator decides E_{ESDR} according to (3.7) for NDs/SDs.

Case-b: Both, F_4 and F_5 exist at k^{th} EBS: FS sends the F_4 and F_5 information of k^{th} EBS to the ISC-1 and ISC-2 of k^{th} EBS. ISC-1 connects SP to $E_{SP\ node}$ (Fig. 3.6 and 3.7) and ISC-2 disconnects ICS from ESD (Fig. 3.6 and 3.8). This means an increased energy demand has been created by the e-buses without giving energy at k^{th} EBS and that energy is compensated at $k+1^{th}$ and $k+2^{th}$ EBSs. Also, FS sends the F_4 and F_5 information of k^{th} EBS to the aggregator and ISC-3 of $k+1^{th}$ and $k+2^{th}$ EBSs. ISC-3 of $k+1^{th}$ and $k+2^{th}$ EBSs disconnect ESD from the grid and connect to $E_{SP\ node}$ (Fig. 3.9). This means, ESDs of $k+1^{th}$ and $k+2^{th}$ EBSs share the total SP energy of k^{th} EBS. Aggregator decides E_{ESDR} at $k+1^{th}$ and $k+2^{th}$ EBSs according to (3.7) for NDs/SDs. Under this failure $k+1^{th}$ EBS shares 63% of $E_{SP\ (k)}$ and $k+2^{th}$ EBS shares the remaining $E_{SP\ (k)}$ (ref. (3.7)).

FLC failure: In this case, failure of FLC at the k^{th} EBS has been considered. In this situation, FLC is unable to command both, ESD and SP.

Solution: The e-buses receive energy from ESD of k^{th} EBS. $k+1^{th}$ and $k+2^{th}$ EBSs share SP energy of k^{th} EBS.

Case-a: F_{FLC} exist at k^{th} EBS: FS sends the F_{FLC} information of k^{th} EBS to ISC-1, ISC-3 and the aggregator of k^{th} EBS. ISC-1 connects SP to $E_{SP\ node}$ (Fig. 3.7), ISC-3 connects ESD to $E_{SP\ node}$ (Fig. 3.9) and the aggregator decides E_{ESDR} according to (3.7).

Case-b: Both, F_{FLC} and F_5 exist at k^{th} EBS: FS sends the F_{FLC} information of k^{th} EBS to the ISC-1 of k^{th} EBS. ISC-1 connects SP to $E_{SP\ node}$ (Fig. 3.7). Also, FS sends the F_{FLC} and F_5 information of k^{th} EBS to the aggregator and ISC-3 of $k+1^{th}$ and $k+2^{th}$ EBSs. ISC-3 of $k+1^{th}$ and $k+2^{th}$ EBSs disconnect ESDs from the grid and connect to $E_{SP\ node}$ (Fig. 3.9). Aggregator decides E_{ESDR} at $k+1^{th}$ and $k+2^{th}$ EBSs according to (3.7).

3.2.3 The Fuzzy logic controller

Every EBS in SPTS consists of an FLC to control the charging/discharging of ESD from/to the grid in off-peak/peak period and also, to control the SP energy to ESD/to the grid in off-peak/peak period (ref. Fig. 3.2). FLC shows the features like simple representation for complex systems, flexible, ease in mathematics and natural language based [117]-[120], [132]. Fig. 3.10 shows the block diagram of FLC with four inputs (Vpu, E_{ESD}, ONB and E_{SP}) and two outputs ($P\pm$ and $SP\pm$).

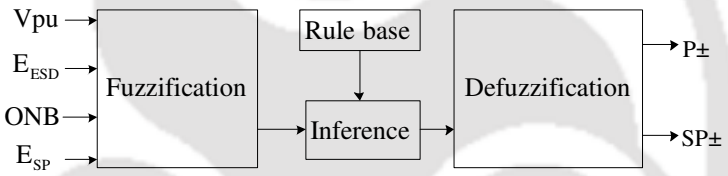

Fig. 3.10 The block diagram of FLC

Fuzzification is the process of converting input crisp set values into fuzzy variables through membership functions. The triangular membership functions have been used due to their simple representation and ease in mathematics. The grade of membership (μ) is the output value of the membership function represented with a number between 0 and 1. The rule base of FLC has been designed based on the antecedents and consequents. The degree of fulfilment of each rule decides the corresponding output membership function (Mamdani inference system is used). Aggregation of all the outputs of individual rules is the fuzzy output. Defuzzification is the process of converting fuzzy output into crisp set values. The centre of area method is used to perform the Defuzzification process. The increased inputs to the FLC create more complexity to design the rule base of FLC. The FLC decide the output crisp set values as a function of input membership functions based on the rule base designed in it. The membership functions for inputs of FLC are shown in Fig. 3.11.

Table 3.2: Rule base of the FLC

Input				*Output*			*Input*				*Output*	
Vpu	E_{ESD}	*ONB*	E_{SP}	*P*±	*SP*±		*Vpu*	E_{ESD}	*ONB*	E_{SP}	*P*±	*SP*±
H	M	H	H	Z	PH		M	L	H	H	Z	NH
H	M	H	M	Z	PM		M	L	H	M	Z	NM
H	M	H	L	Z	PL		M	L	H	L	Z	NL
H	M	M	H	Z	PH		M	L	M	H	Z	NH
H	M	M	M	Z	PM		M	L	M	M	Z	NM
H	M	M	L	Z	PL		M	L	M	L	Z	NL
H	M	L	H	Z	PH		M	L	L	H	Z	NH
H	M	L	M	Z	PM		M	L	L	M	Z	NM
H	M	L	L	Z	PL		M	L	L	L	Z	NL
H	L	H	H	PL	PH		L	H	H	H	NH	NH
H	L	H	M	PL	PH		L	H	H	M	NH	NM
H	L	H	L	PL	PM		L	H	H	L	NH	NM
H	L	M	H	PL	PH		L	H	M	H	NH	NH
H	L	M	M	PL	PH		L	H	M	M	NH	NM
H	L	M	L	PL	PM		L	H	M	L	NH	NM
H	L	L	H	PL	PH		L	H	L	H	NH	NH
H	L	L	M	PL	PH		L	H	L	M	NH	NM
H	L	L	L	PL	PM		L	H	L	L	NH	NM
M	H	H	H	NH	NH		L	M	H	H	NM	NH
M	H	H	M	NH	NM		L	M	H	M	NM	NM
M	H	H	L	NH	NL		L	M	H	L	NM	NL
M	H	M	H	NH	NH		L	M	M	H	NM	NH
M	H	M	M	NH	NM		L	M	M	M	NM	NM
M	H	M	L	NH	NL		L	M	M	L	NM	NL
M	H	L	H	NH	NH		L	M	L	H	NM	NH
M	H	L	M	NH	NM		L	M	L	M	NM	NM
M	H	L	L	NH	NL		L	M	L	L	NM	NL
M	M	H	H	NH	NH		L	L	H	H	Z	PH
M	M	H	M	NH	NM		L	L	H	M	Z	PM
M	M	H	L	NH	NL		L	L	H	L	Z	PL
M	M	M	H	NH	NH		L	L	M	H	Z	PH
M	M	M	M	NH	NM		L	L	M	M	Z	PM
M	M	M	L	NH	NL		L	L	M	L	Z	PL
M	M	L	H	NH	NH		L	L	L	H	Z	PH
M	M	L	M	NH	NM		L	L	L	M	Z	PM
M	M	L	L	NH	NL		L	L	L	L	Z	PL

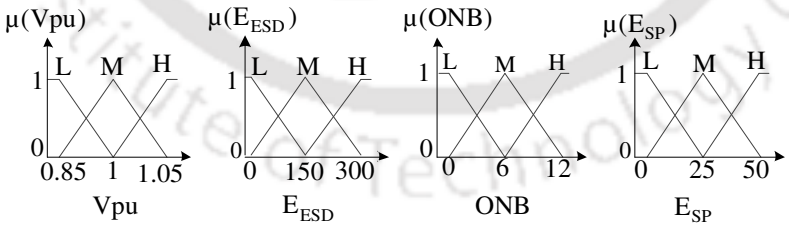

Fig. 3.11 Input membership functions of FLC

Vpu thresholds have been considered from 0.85 pu to 1.05 pu [103]. The universe of discourse ranges for inputs are: for Vpu (0.85 to 1.05), for E_{ESD} (0 to 300 kWh), for ONB (0 to 12) and for E_{SP} (0 to 50 kWh). The membership functions for each input are represented with the linguistic variables such as: low (L), medium (M) and high (H). The grade of

membership range for all inputs (μ(Vpu), $\mu(E_{ESD})$, μ(ONB) and $\mu(E_{SP})$) and outputs ($\mu(P\pm)$ and $\mu(SP\pm)$) are from 0 to 1.

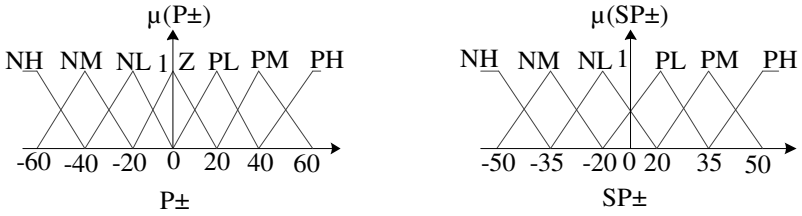

Fig. 3.12 Output membership functions of FLC

The membership functions for outputs of FLC are shown in Fig. 3.12. The universe of discourse for $P\pm$ is from -60 kW to 60 kW and for $SP\pm$ is from -50 kW to 50 kW. The membership functions for the first output $P\pm$ are represented with the linguistic variables such as: negative low (NL), negative medium (NM), negative high (NH), zero (Z), positive low (PL), positive medium (PM) and positive high (PH). The membership functions for the second output $SP\pm$ are represented with the linguistic variables such as: NH, NM, NL, PL, PM and PH as shown in Fig. 3.12. The FLC decides the power flow among ESD, SP and the grid based on the rule base designed in it. The rule base of FLC is shown in Table 3.2.

3.3 Results and discussion

Two types of case studies have been considered to explain the simulated results of the proposed system.

1) First case explains the performance of SPTS for ND and SDs with respect to ONB.

2) The second case explains the response of SPTS for different failures that exist in SPTS.

3.3.1 Case-1: SPTS performance for normal and special days

ONB impact on the performance of both, the grid and SPTS for ND and SDs are shown from Fig. 3.13 to 3.24. The improvement in Vpu profile of the grid and the energy behaviour of ESD and SP during both, the off-peak and peak periods have been explained through these results.

For ND: Vpu response of the grid for ND is given in Fig. 3.13. ESD is receiving energy from both the grid and SP during off-peak period. ESD is sending its stored energy back to the grid along with SP during peak period. The area between the actual and resultant Vpu curves show that the valley filling/peak shaving in off-peak/peak period. Mostly the Vpu

profile has stayed under off-peak period during sunshine hours, so that the SP is sending its total energy to ESD as shown in Fig. 3.13.

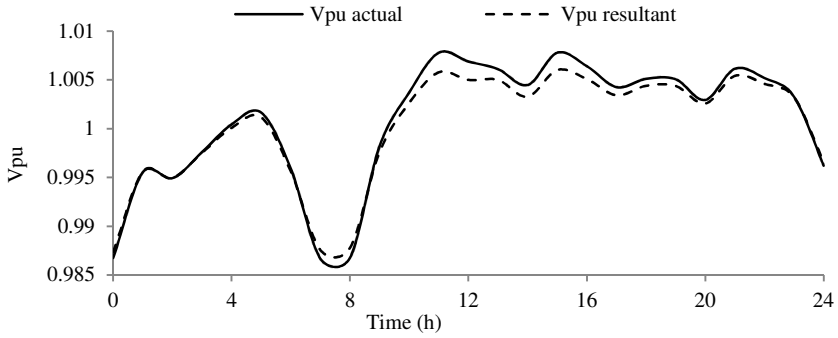

Fig. 3.13 Vpu profile of the grid for ND

The energy behaviour of ESD and SP for ND is shown in Fig. 3.14. The positive/negative values of ESD curve represents the amount of energy received/sent by ESD from/to the grid. The positive/negative values of SP curve represents the amount of energy sent to ESD/to the grid. The Vpu profile has remained under off-peak period from 10:00 to 24:00 h and 04:00 to 06:00 h so that ESD is receiving energy from the grid. Also, SP is sending its total energy to ESD from 10:00 to 17:00 h. In this duration ESD is receiving energy in two directions: one is from the grid and the other is from SP. The Vpu profile has remained under peak period from 24:00 to 03:00 h and from 06:00 to 10:00 h. ESD is sending its stored energy back to the gird during this period. Also, SP is sending energy to the grid from 06:00 to 10:00 h and that can be observed from Fig. 3.14. The e-buses receive energy from ESD for 24 h with respect to ONB (ref. (3.5)). SP energy generation is proportional to solar irradiance availability for ND and SDs (ref. Fig. 3.4).

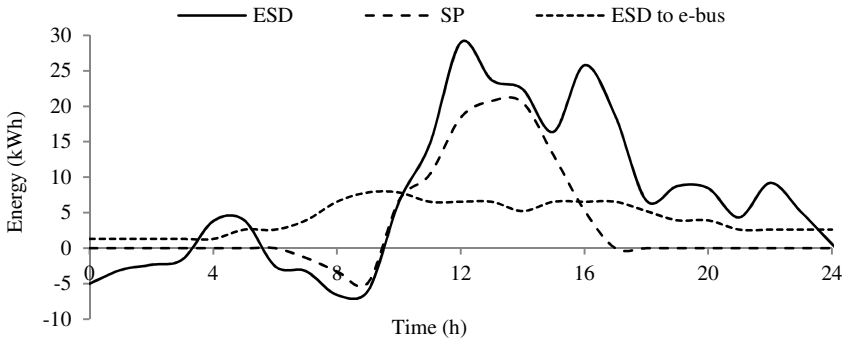

Fig. 3.14 The energy behaviour of ESD and SP for ND

For SDs: Vpu profile for SD1 is shown in Fig. 3.15. ESD is receiving/sending more/less energy from/to the grid during off-peak/peak period. Improvement in the Vpu profile of the

grid during off-peak and peak period (using the energy support from both, ESD and SP to the grid) can be observed from Fig. 3.15.

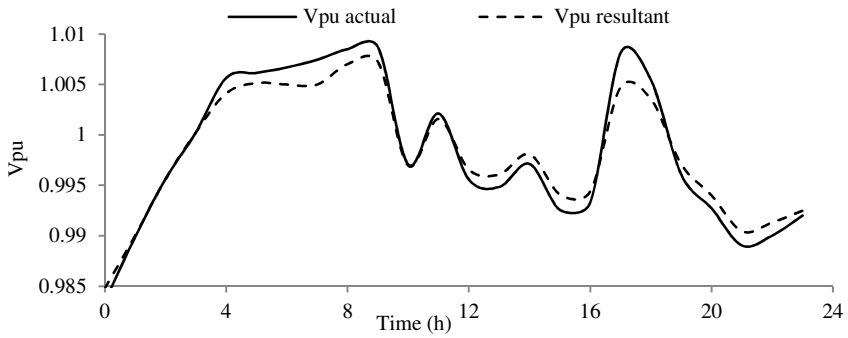

Fig. 3.15 Vpu profile of the grid for SD1

The energy behaviour of ESD and SP for SD1 is shown in Fig. 3.16. The Vpu profile of the grid has stayed under peak period from 20:00 to 03:00 h, from 10:00 to 11:00 h and from 12:00 to 17:00 h, so that ESD is sending energy to the grid during this period. SP sent energy to the grid from 10:00 to 11:00 h and from 12:00 to 17:00 h, as shown in Fig. 3.16. The Vpu profile of the grid has stayed under off-peak period from 17:00 to 20:00 h, from 03:00 to 10:00 h and from 11:00 to 12:00 h, so that ESD is receiving energy from the grid during this period. Also, SP has sent energy to ESD from 08:00 to 10:00 h, from 11:00 to 12:00 h and from 17:00 to 18:00 h, as shown in Fig. 3.16. After 20:00 h, the energy status of ESD is reached to its 30%. Therefore, ESD is supporting less energy to both the grid and NBs. The comparison of ESD to e-bus curves from Fig. 3.14 and 3.16 shows the difference in ONB for ND and SD.

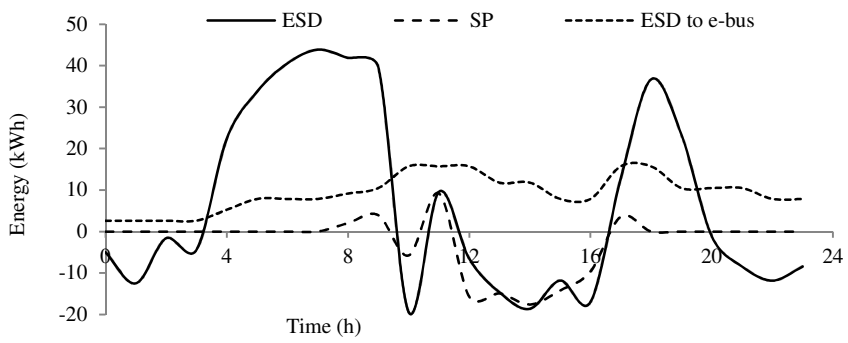

Fig. 3.16 The energy behaviour of ESD and SP for SD1

Vpu profile for SD2 is shown in Fig. 3.17. The energy behaviour of ESD and SP for SD2 is shown in Fig. 3.18. The Vpu profile of the grid has stayed under peak period during sunshine hours, so that the total SP energy has been sent to the grid and that can be observed from Fig.

3.18. The off-peak period is existed from 21:00 to 09:00 h, from 15:00 to 16:00 h and from 17:00 to 19:00 h, so that ESD is receiving energy from the grid. Also, ESD is receiving energy from SP during 06:00 to 09:00 h, 15:00 to 16:00 h and 17:00 to 18:00 h, as shown in Fig. 3.18. The peak period is existed from 09:00 to 15:00 h, from 16:00 to 17:00 h and from 19:00 to 21:00 h, so that ESD is sending energy to the grid. Also, SP is sending energy to the grid from 09:00 to 15:00 h and from 16:00 to 17:00 h, as shown in Fig. 3.18.

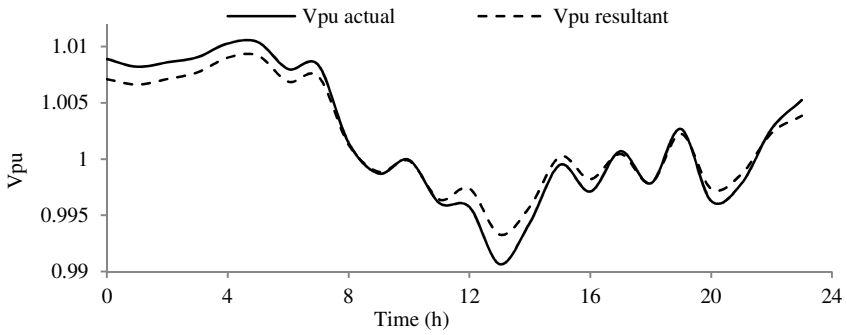

Fig. 3.17 Vpu profile of the grid for SD2

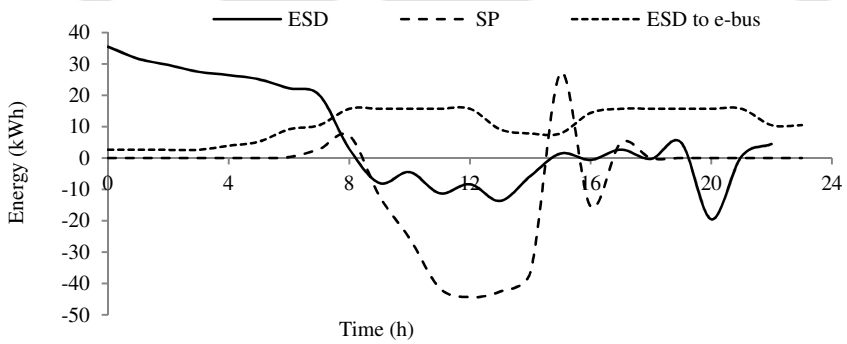

Fig. 3.18 The energy behaviour of ESD and SP for SD2

The energy stored in ESD for ND, SD1 and SD2 are shown in Fig. 3.19.

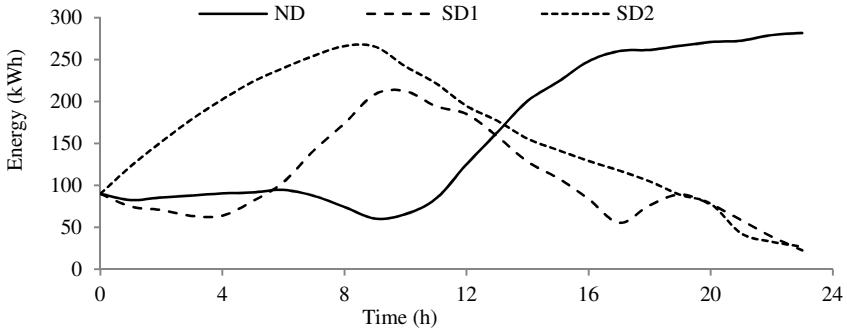

Fig. 3.19 Energy stored in the ESD for ND, SD1 and SD2

Variations in the stored energy of ESD with respect to the load profiles of the grid can be observed from Fig. 3.19. For ND, the load profile of the grid has stayed under off-peak period during the daytime and also, the energy demand from e-buses is low. So that the

maximum amount of energy is available in ESD. For both SD1 and SD2, the load profile of the grid has stayed under peak period during the daytime and also, the energy demand from e-buses is high. Therefore, the minimum amount of energy is available in ESD.

ONB profiles for ND, SD1 and SD2 are shown in Fig. 3.20. Maximum priority has been given to provide the comfortable journey to the passengers in SDs. So that the maximum number of e-buses have been determined through ONB algorithm during peak periods of the passenger profile and that can be observed from Fig. 3.20.

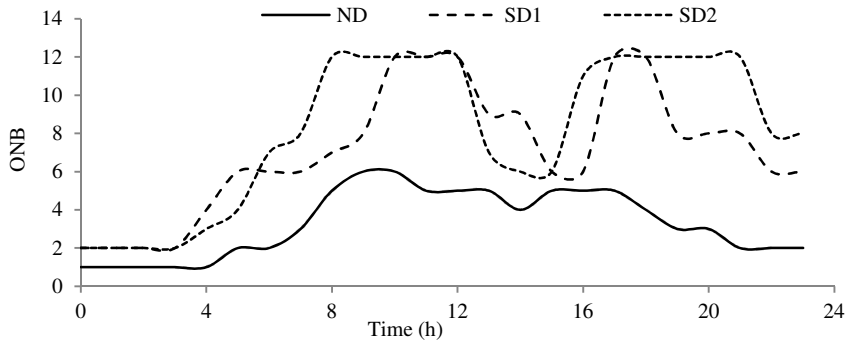

Fig. 3.20 ONB profiles for ND, SD1 and SD2

Vpu profile for SD3 is shown in Fig. 3.21. The Vpu profile mostly stayed under off-peak period during the day-time. The maximum charging/discharging performance of ESD from/to the grid during off-peak /peak period can be observed from Fig. 3.21.

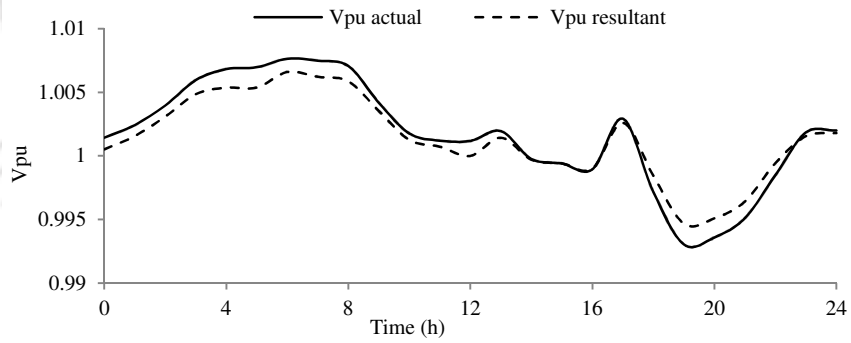

Fig. 3.21 Vpu profile of the grid for SD3

The energy behaviour of ESD and SP for SD3 is shown in Fig. 3.22. Vpu profile of the grid has stayed under off-peak period during sunshine hours, so that the total SP energy has been sent to ESD and that can be observed from Fig. 3.22. The off-peak period is existed from 23:00 to 18:00 h, so that ESD is receiving energy from the grid. The peak period is existed from 18:00 to 23:00 h, so that ESD is sending energy to the grid during this period. The e-buses are receiving energy from ESD according to ONB for SDs. The ESD is

receiving less energy from the grid and maximum energy from SP. This means that the e-buses mostly travel with solar energy in SD3 and that can be observed from Fig. 3.22. The grid has remained under off-peak period during sunshine hours so that the SP is sending its total energy to ESD (solar irradiance availability is high for SD3) as shown in Fig. 3.22.

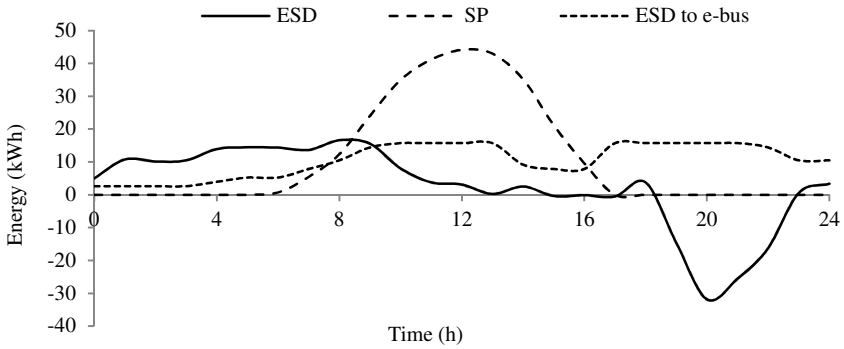

Fig. 3.22 The energy behaviour of ESD and SP for SD3

Vpu profile for SD4 is shown in Fig. 3.23. The SPTS receives maximum energy support from SP, if the grid stays under off-peak period during sunshine hours. For SD4, the Vpu profile mostly stayed under off-peak period during the day-time. Therefore, SPTS has utilized total SP energy in SD4 and that can be observed from Fig. 3.23. The maximum charging/discharging performance of ESD from/to the grid during off-peak/peak period and subsequent improvement in the Vpu profile for SD4 can be observed from Fig. 3.23.

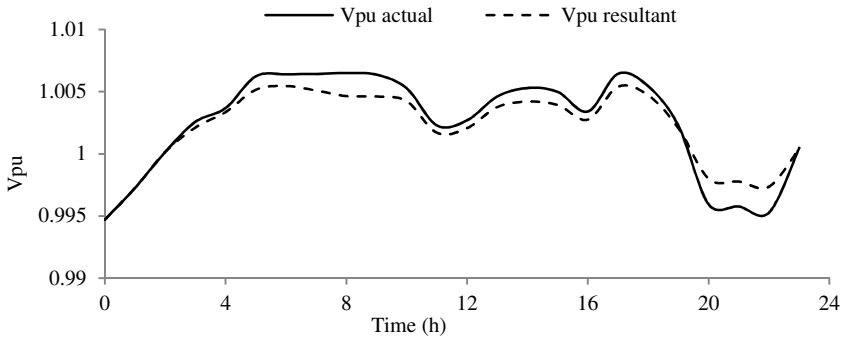

Fig. 3.23 Vpu profile of the grid for SD4

The energy behaviour of ESD and SP for SD4 is shown in Fig. 3.24. The Vpu profile of the grid has stayed under off-peak period during sunshine hours, so that the total SP energy has been sent to the ESD and that can be observed from Fig. 3.24. The off-peak period is existed from 02:00 to 19:00 h, so that ESD is receiving energy from the grid. The peak period is existed from 19:00 to 02:00 h, so that ESD is sending energy to the grid during this period. The e-buses are receiving energy from ESD according to ONB for SDs. The ESD is receiving moderate energy from the grid and less energy from SP. The solar irradiance

availability is less for SD4, so that SP is sending less energy to ESD and that can be observed from Fig. 3.24.

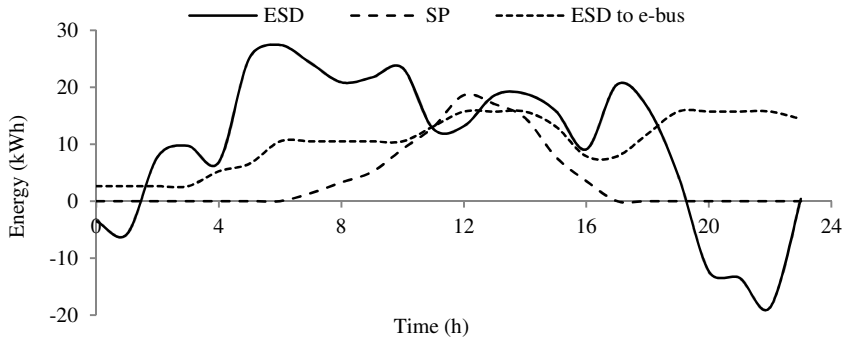

Fig. 3.24 The energy behaviour of ESD and SP for SD4

3.3.2 Case-2: SPTS response in failure situations

SPTS response for both categories of failures are shown separately and also explained about the energy harnessing among EBSs under failure situations.

1. Failures from hardware side:

Failure-1: Vpu response of $k+1^{th}$ EBS when F_1 exists at the k^{th} EBS is shown in Fig. 3.25. ESD is disconnected from the grid at k^{th} EBS, so that the Vpu profile of k^{th} EBS is similar to that of the actual Vpu curve. ESD of $k+1^{th}$ EBS, is receiving/sending more/less energy from/to the grid in off-peak/peak period. The maximum irradiance and NB_{max} have been considered for the failure analysis in SPTS.

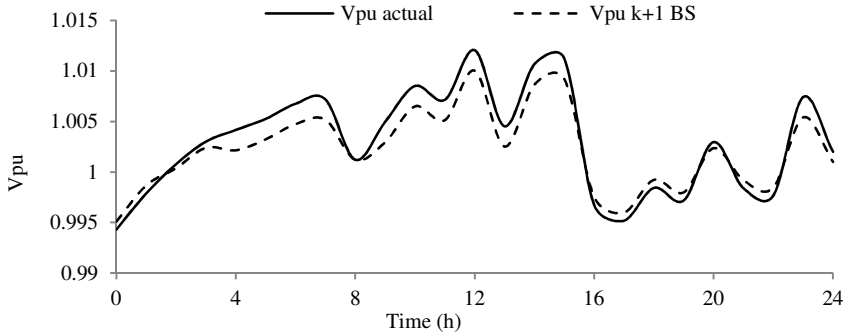

Fig. 3.25 Vpu profile of $k+1^{th}$ EBS when F_1 exist at k^{th} EBS

The energy behaviour of ESD and SP, when F_1 exist at k^{th} EBS is shown in Fig. 3.26. At k^{th} EBS, the ESD curve is at zero energy state for 24 h and the total SP energy is sent to ESD as shown in Fig. 3.26. If E_{ESD} is low and also, SP energy is not available at k^{th} EBS, then $k+1^{th}$ EBS shares the k^{th} EBS energy as shown in Fig. 3.27.

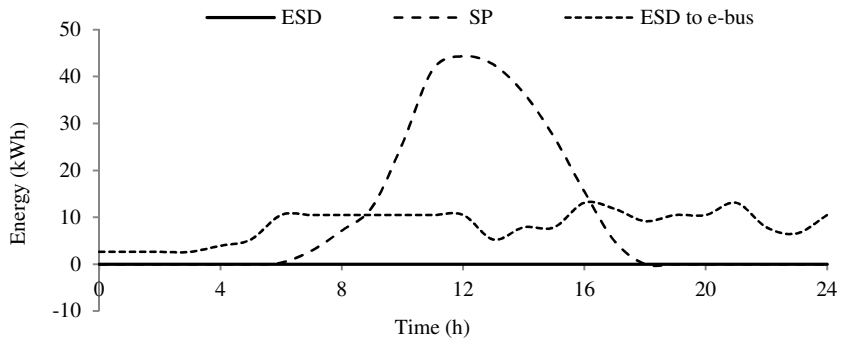

Fig. 3.26 The energy behaviour of ESD and SP of k^{th} EBS

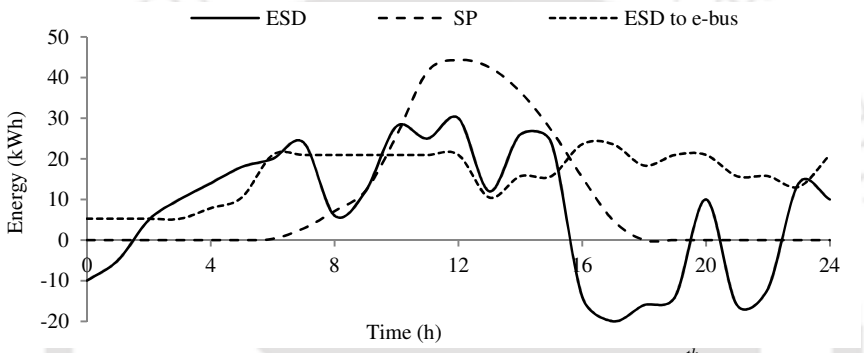

Fig. 3.27 The energy behaviour of ESD and SP of $k+1^{th}$ EBS

Failure-2: Vpu response of the grid at k^{th} and $k+1^{th}$ EBSs when F_2 exists at the k^{th} EBS is shown in Fig. 3.28. ESD is receiving/sending less/more energy from/to the grid during off-peak/peak period. ESD of $k+1^{th}$ EBS is receiving/sending more/less energy from/to the grid in off-peak/peak period.

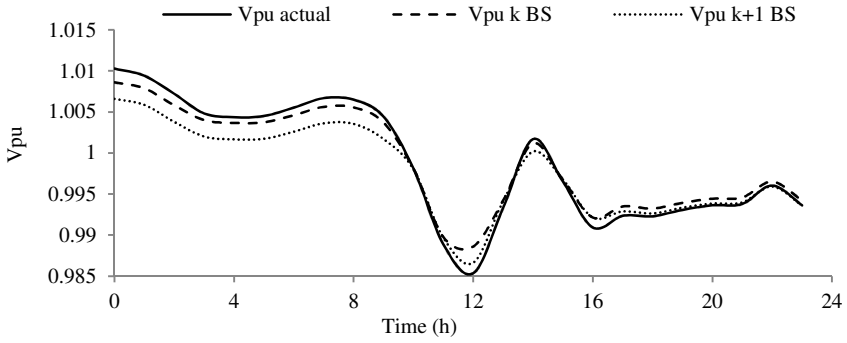

Fig. 3.28 Vpu profile of k^{th} and $k+1^{th}$ EBS when F_2 exist at k^{th} EBS

The energy behaviour of ESD and SP of k^{th} EBS is shown in Fig. 3.29. ESD to e-bus curve is at the zero energy state for 24 h. This means that the e-buses move from k^{th} EBS to $k+1^{th}$ EBS with the energy deficit and that energy is recovered at $k+1^{th}$ EBS as shown in Fig. 3.30.

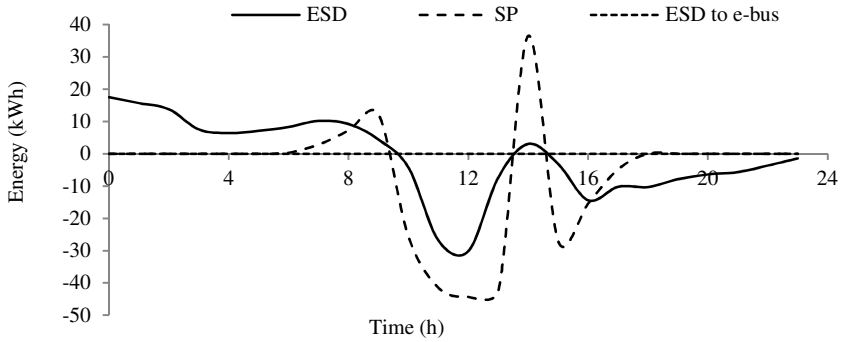

Fig. 3.29 The energy response of ESD and SP of k^{th} EBS

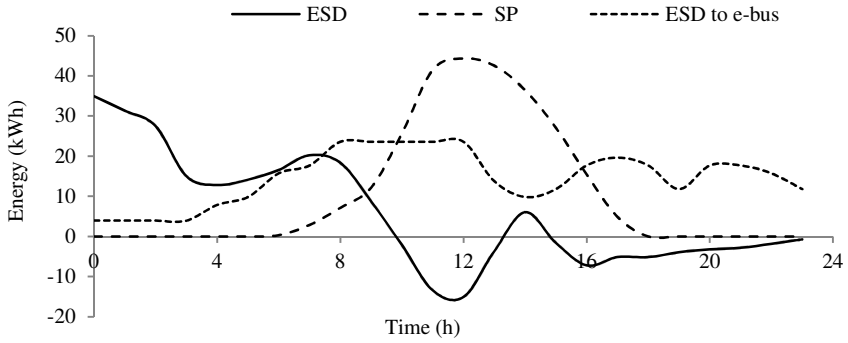

Fig. 3.30 The energy response of ESD and SP of $k+1^{th}$ EBS

Failure-3: ESD receives total SP energy at k^{th} EBS and is same as that of Fig. 3.26. Therefore, the results for this failure are not shown.

Failure-4:

Case-a: Under this failure only F_4 exists at the k^{th} EBS. Vpu profile for this failure is same as that of Vpu profile of $k+1^{th}$ EBS in Fig. 3.31. SP of k^{th} EBS is bypassed to ESD via $E_{SP\ node}$ and ESD is receiving total SP energy at k^{th} EBS during 06:00 to 18:00 h (ref. Fig. 3.9). The energy behaviour of ESD and SP is same as that of Fig. 3.33, except the SP energy curve of k^{th} EBS.

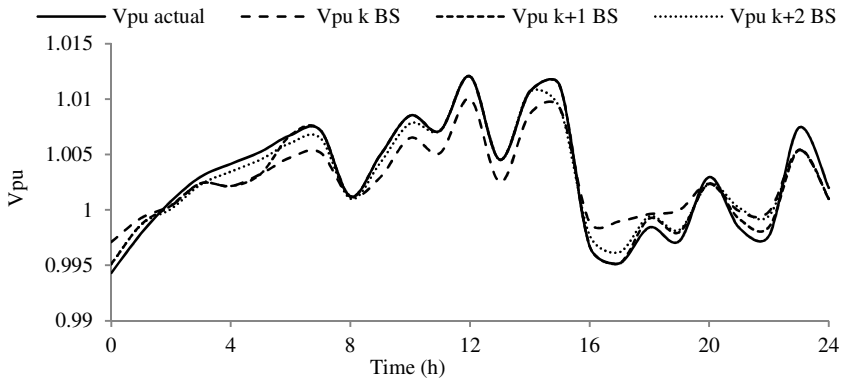

Fig. 3.31 Vpu profile of k^{th}, $k+1^{th}$ and $k+2^{th}$ EBSs when F_4 and F_5 exist at k^{th} EBS

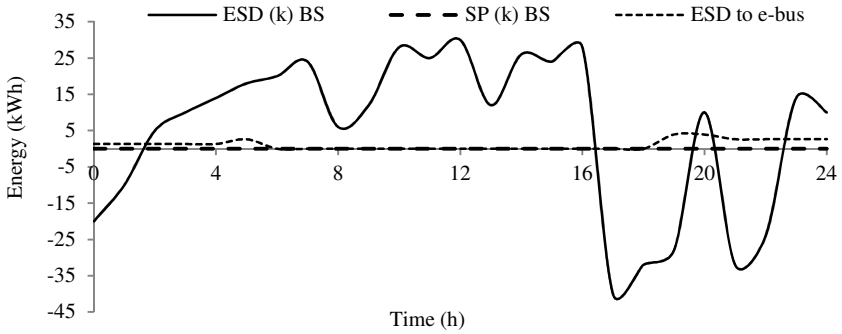

Fig. 3.32 The ESD and SP energy behaviour of k^{th} EBS

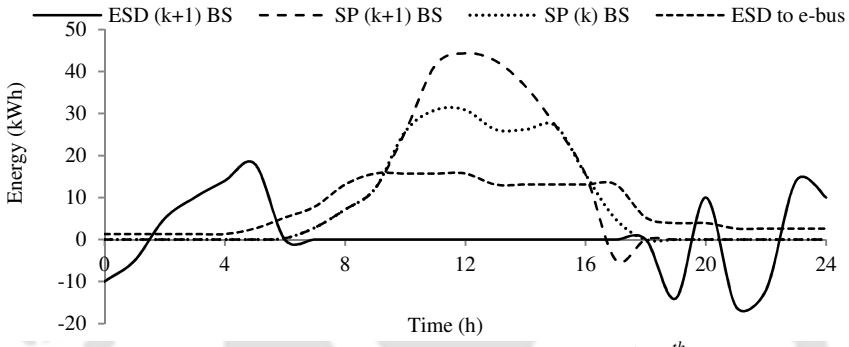

Fig. 3.33 The ESD and SP energy behaviour of $k+1^{th}$ EBS

Case-b: Under this failure, both F_4 and F_5 exist at k^{th} EBS. Vpu profiles of k^{th}, $k+1^{th}$ and $k+2^{th}$ EBSs are shown in Fig. 3.31. The k^{th} EBS is receiving/sending more energy from/to the grid during off-peak/peak period. Both, the $k+1^{th}$ and $k+2^{th}$ EBSs are receiving/sending less/more energy from/to the grid. The energy behaviour of ESD and SP at the k^{th} EBS is shown in Fig. 3.32. SP energy curve is at the zero energy state for 24 h. ESD to e-bus curve is at the zero energy state from 06:00 to 18:00 h. The increased energy thirst of e-buses is compensated at $k+1^{th}$ EBS as shown in Fig. 3.33. ESD is open circuited from the grid at $k+1^{th}$ EBS from 06:00 to 18:00 h for receiving $E_{SP\,(k)}$ up to 63%. Also, ESD is open circuited from the grid at $k+2^{th}$ EBS from 10:00 to 15:00 h for receiving $E_{SP\,(k)}$ when it is greater than 63% as shown in Fig. 3.34. ESDs of the $k+1^{th}$ and $k+2^{th}$ EBSs run the e-buses with only SP energy under this failure.

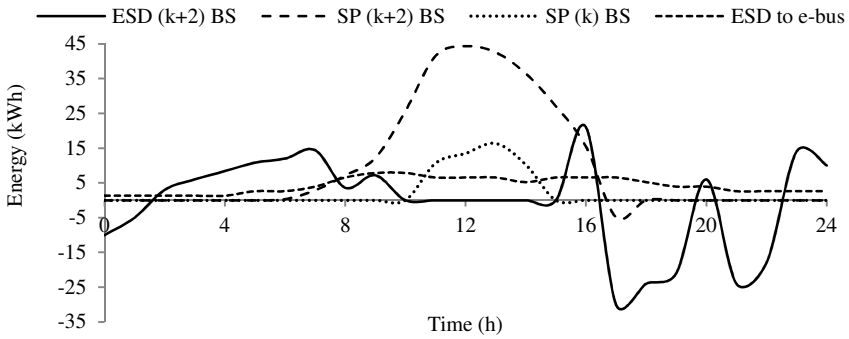

Fig. 3.34 The ESD and SP energy behaviour of $k+2^{th}$ EBS

2. Failures from software side:

FLC failure:

Case-a: Vpu profile for this failure is same as that of actual Vpu in Fig. 3.25. The energy behavior of ESD and SP is same as that of Fig. 3.26. ESD is unable to receive/send energy from/to the grid, so that ESD energy status is at the zero state for 24 h. SP is bypassed to ESD via $E_{SP\ node}$ at k^{th} EBS so that the total SP energy flows into ESD as shown in Fig. 3.26.

Case-b: Vpu profile for the k^{th} EBS is same as that of actual Vpu in Fig. 3.31. Vpu profiles for $k+1^{th}$ and $k+2^{th}$ EBSs are same as that of Vpu profiles of $k+1^{th}$ and $k+2^{th}$ EBSs in Fig. 3.31. The energy status of both, ESD and SP are at the zero state for 24 h at k^{th} EBS (ref. Fig. 3.26 for ESD and ref. Fig. 3.32 for SP). The energy behaviour of ESD and SP for $k+1^{th}$ and $k+2^{th}$ EBSs are same as that of Fig. 3.33 and Fig. 3.34. Under this failure, ESD of $k+1^{th}$ EBS disconnected from the grid, if $E_{SP\ (k)}$ is in-between 0 to 63%. Also, ESD of $k+2^{th}$ EBS disconnected from the grid, if $E_{SP\ (k)}$ is greater than 63%. Likewise the energy harnessing has been performed and achieved the fail proof performance of SPTS.

3.4 Summary

- In this chapter, the solar assisted smart public transit system has been modelled and integrated with the grid.
- The specified numbers of electric bus stops along the ring road of the Guwahati city charge the e-buses.
- The smooth performance of SPTS and the improvement in the voltage profile of the grid have been achieved by placing ESD as well as SP at every EBS.
- Two types of days such as: normal and special days have been considered to determine the optimal number of e-buses in SPTS.
- The optimal number of e-buses has been determined through an algorithm as a function of the load, the energy status of ESD, the energy status of SP and the passenger's total.
- The fail-proof performance of SPTS has been achieved by placing three isolation switch controllers (ISC), an inductive charging system controller (ICSC) and an aggregator at every EBS in SPTS.

- The optimal number of e-buses determination and the failure analysis in SPTS shows the self-sustainability of SPTS for the failure situations that exist in the system through all the seasons of a year.
- FLC intelligently decided the power flow between the grid, ESD, and SP.

In the next chapter, the smart public transportation network expansion (using the capa-buses and the electric vehicles along with the e-buses) and its interaction with the grid has been presented.

Note: This work, "Optimal number of e-buses in the Solar Assisted Smart Public Transit System and its Failure Analysis" is published in IET Journal on 'Electrical systems in transportation'.

4

Smart Public Transportation Network expansion and its interaction with the grid

Contents

Introduction

The petroleum based transportation system and the luxurious lifestyle of ever increasing population are the major sources of air pollution across the globe. Transforming the present transportation system from petroleum based to electric based is one of the possible solutions to curtail such issue. The revolution in the electric-based transportation system has been started with the trolleybuses and tram systems (used for mass transportation in the city regions) [104], [109],[123],[136,137]. In [138], the super-capacitor equipped tram networks have been introduced in Spain, Portugal, and China. Also, the supercapacitor based buses have been introduced for the public transportation in urban regions of China [108]. The on-board supercapacitor based transportation networks reduce the electrical line infrastructure needed between consecutive stops. However, in these systems, the supercapacitors receive energy from the grid periodically and act as a load to the grid for short durations. This may create transients in the grid. In [110], the on-line operation of electric vehicles (EVs) with the grid has been introduced. EVs charge from the grid via wireless-charging system installed under the road. This system is beneficial in the transportation system point of view, but from the grid point of view it creates an extra stress on the grid during the peak period. The current trend of research is the electric vehicles that run with onboard solar energy [139]. This system works very effectively during sunny days, but the electric vehicles may stop working in cloudy days. In such situation, the electric vehicles need to receive energy from the grid. The use of high capacity energy storage device (ESD) between the grid and the transportation system is one of the possible solutions for such difficulties [111], [140,141].

As per [113], the interaction between the grid and the transportation system has been performed by using the energy storage systems. However, this system completely depends on the grid and has the chances of failure if the grid is unable to support the transportation system. Solar energy utilization is one of the possible options to curtail this system dependence on the grid and to escape failure situations. The proposed work focuses on these issues and achieves the smooth performance of the smart public transportation network by reducing the grid dependence. Therefore, the objectives of the present work are as follows:

- The smart public transportation network response verification in all the seasons of a year.
- The smart public transportation network behavior for uncertain situations that exist in the system.

A specified number of electric bus stops (EBSs) are present through the ring road of the Guwahati city, Assam, India. Electric buses receive energy from each of the EBS to perform the mass transportation through the city. The ring road circuit is considered as a case study in this work. Supercapacitors are the prime energy storage in the electric buses due to their significant features [114,115]-[131]. At every EBS, the solar plant as well as ESD have been connected to improve the voltage profile of the gird and also, to perform the smooth functioning of the smart public transportation network. The real time solar data is used to calculate the solar irradiance availability. The solar energy generation is proportional to the solar irradiance availability in all the seasons of a year. A specified EBS (Maligaav EBS (MEBS)) of the smart public transportation network has been considered to charge the capa-buses (CBs) and EVs along with the electric buses. The supercapacitors are used in CBs and Li-ion batteries in EVs due to their individual benefits. The use of CBs and EVs in the smart public transportation network shows the possibility to expand the electrified transportation network in the Guwahati city. Also, CBs and EVs usage along with ESD creates the possibility to perform more improvement in the voltage profile of the grid as that of ESD alone in the smart public transportation network. An algorithm based controllers have been developed for controlling the energy flow between ESD and CBs and also between ESD and EVs. CB controller takes care of charging/discharging of CBs from/to ESD and EV controller takes care of charging/discharging of EVs from/to ESD. Every EBS in the smart public transportation network consists of a fuzzy logic controller (FLC) to control the energy flow between the grid, ESD and the solar plant [117]-[120], [132]. The simulations have been performed, to verify the smart public transportation network response for three seasons of a year and for the uncertain situations that exist in the system.

The remainder of this chapter is organized as follows. The structure of the smart public transportation network is given in Section 4.1. Section 4.2, explains the smart public transportation network expansion using CBs and EVs. The results and discussions are given in Section 4.3 and the summary is given in Section 4.4.

4.1. Structure of the smart public transportation network

This section explains the structure of the smart public transportation network including with the MEBS structure, solar irradiance availability determination and the solar plant sizing. The smart public transportation network structure is shown in Fig. 4.1.

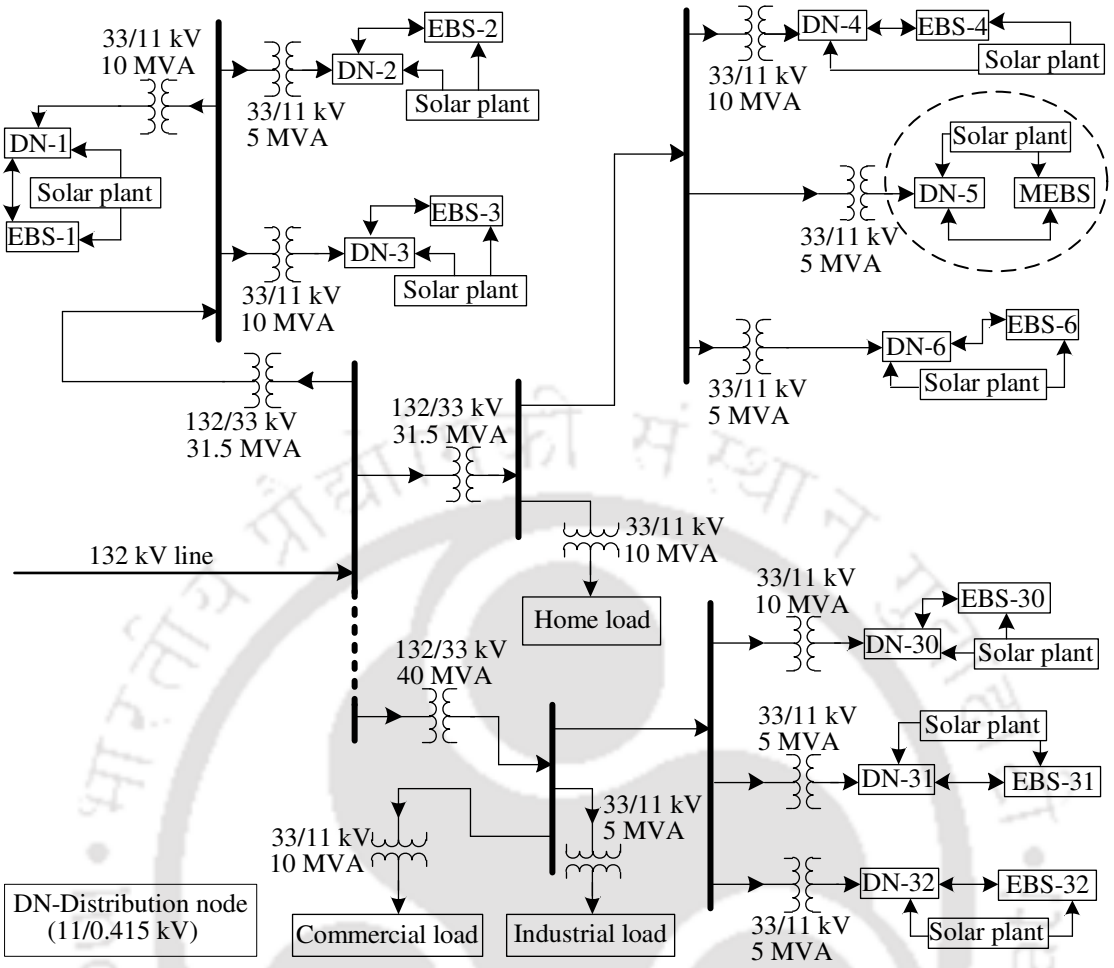

Fig. 4.1 Structure of the smart public transportation network

A total of 32 EBSs are present through the ring road circuit of the Guwahati city and Fig. 4.1 shows some of them. The average distance between consecutive EBSs is considered as 2 km. The electric bus receives energy from the current EBS and travels to the next EBS. This process continues through the ring road circuit. Each EBS has been connected to a separate distribution node (11/0.415 kV) along with the solar plant as shown in Fig. 4.1. The capacity of solar plants which are present at all the EBSs are same (considered as 50 kW). A 132 kV node covers the entire ring road of the Guwahati city. A total of ten 33 kV nodes are sufficient to cover all the EBSs in the smart public transportation network. Each 33 kV node consists of 11 kV nodes according to the load demand of that particular area [121,122]. The distribution network which covers the entire ring road circuit consists of different loads such as: the industrial load, the home load and the commercial load as shown in the Fig. 4.1. MEBS fall under the home load region. Thick lines in Fig. 4.1 show the bus bars of the respective nodes. The smart public transportation network response verification has been

carried out at MEBS and is represented with a circle in Fig. 4.1. The details of MEBS structure are given in the following sub-sections.

4.1.1 MEBS structure

A total of 32 distribution nodes (11/0.415 kV) covers the entire ring road circuit and the MEBS is connected to the distribution node-5 as shown in Fig. 4.2. The details about MEBS structure are given in the following manner. The solar plant is connected to the distribution node as well as to ESD. Both, the solar plant and ESD are connected to the grid via distribution node. ESD is connected to the inductive charging system-1 (ICS-1) to charge the electric buses, connected to ICS-2 to send/receive energy to/from CB (E_{CBC}/ E_{CBD}), connected to the standard outlet to send/receive energy to/from EV (E_{EVC}/ E_{EVD}) and also connected to the grid to receive/send power from/to the grid ($P\pm$). The energy management at MEBS has been performed in three directions. In the first direction, FLC controls the energy flow between the grid, the solar plant and ESD. In the second direction, the EV controller along with an aggregator controls the energy flow between ESD and EVs. In the third direction, the CB controller controls the energy flow between ESD and CBs.

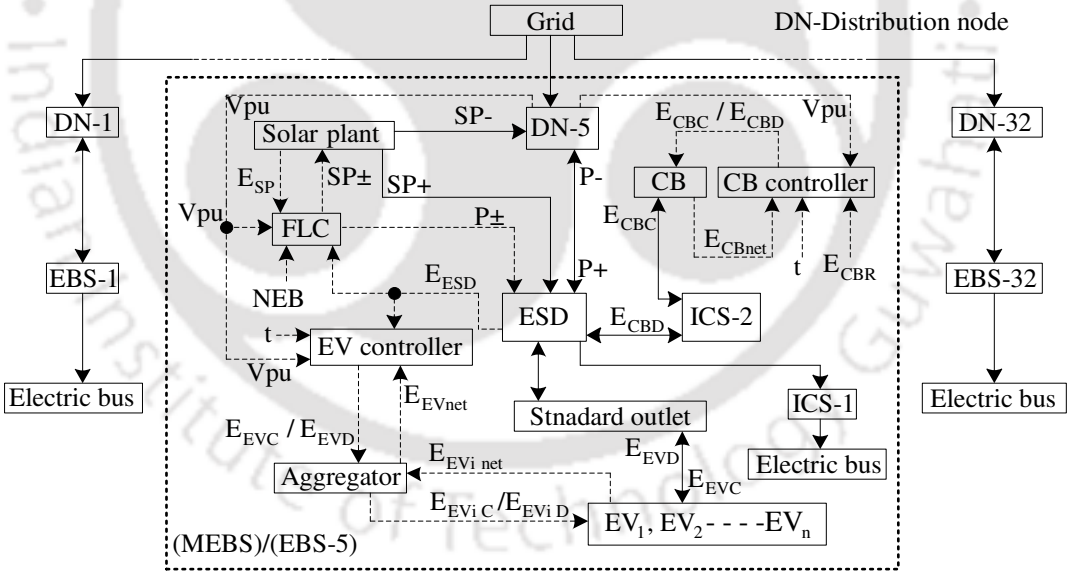

Fig. 4.2 The structure of MEBS

FLC, works based on four inputs and two outputs. The inputs are: energy status of the ESD (E_{ESD}), energy status of the solar plant (E_{SP}), the number of e-buses (NEB) and the per unit voltage of the grid (Vpu). The outputs are: $P\pm$ (power from/to the grid to/from ESD) and $SP\pm$ (power from the solar plant to ESD/to the grid). The EV controller works based on four inputs and one output. The inputs are: Vpu, E_{ESD}, time (t) and the net energy availability of

EVs (E_{EVnet}). Output is E_{EVC}/E_{EVD} (charge/discharge EVs from/to ESD). The aggregator works based on two inputs and two outputs. The inputs are: E_{EVC}/E_{EVD} and the net energy availability of individual EVs ($E_{EVi\ net}$). The outputs are: E_{EVnet} and $E_{EVi\ C}/E_{EVi\ D}$ (individual EV charging/discharging from/to ESD). The CB controller works based on four inputs and one output. The inputs are: Vpu, t, the energy required by CB (E_{CBR}) and the net energy availability of CB (E_{CBnet}). Output is E_{CBC}/E_{CBD} (charge/discharge CB from/to ESD).

4.1.2 ESD sizing

The size of the ESD is decided based on the energy requirement of the electric bus (to travel between the consecutive EBSs) (E_{EB}) and the total number of electric buses which passes from an EBS for 24 h (EB_d). An average speed of 11 km/h is suitable to cover the distance between the consecutive EBSs in the smart public transportation network. So that, the New York City Drive Cycle (NYCC) is used to calculate the energy needed by the electric bus and the details are given in [134]. The total number of electric buses pass from an EBS per hour (EB_h) is therefore

$$EB_h = \left(\frac{(\sum_{i=1}^{n} P_i)}{(EB_c)} \right)_h \tag{4.1}$$

P is the passengers (i=1, 2… n), EB_c is the carrying capacity of the electric bus (limited to 30 passengers). EB_d is therefore

$$EB_d = \sum_{j=1}^{m} EB_{h\ j} \tag{4.2}$$

j is the number of hours (j=1, 2… m). The total energy required by the electric buses from ESD for 24 h (E_{EBT}) is given by

$$E_{EBT} = EB_d \times E_{EB} \tag{4.3}$$

The size of the ESD (E_{ESDS}) is therefore

$$E_{ESDS} = 2 \times E_{EBT} \tag{4.4}$$

The factor 2 in (4.4) shows that half of the ESD capacity is required to support the electric buses for 24 h. The remaining half energy is used to support the grid during peak period and also, to support the electric buses for another 24 h when ESD is failed to receive energy from the grid. Specifications of both, the electric bus and ESD are given in Table 4.1.

Table 4.1: Specifications of the electric bus and ESD [113]

Variable	*Rating*
Minimum energy required by the electric bus (E_{EB})	1.31 kWh
ESD total energy	300 kWh
DC voltage rated	125 V
DC current rated	370 A
Range of DC voltage	100-155 V

4.1.3 Solar irradiance availability determination

The collected solar data has the details of longitude (σ), latitude ($\emptyset$), relative humidity (RH) and the air temperature (T) [124]. The following steps are used to calculate solar irradiance.

Step-1: Use the available values from solar data to calculate the hour angle (ω), solar declination angle (δ), solar elevation (α), sunrise angle (ω_s) and the solar azimuth (ψ).

Step-2: Use step-1 to calculate the solar irradiance outside the atmosphere (B_0) [125,126], [142].

Step-3: If α is less than zero then extraterrestrial irradiance (G_{ex}) is zero. If α is greater than zero then calculate G_{ex} and clearness index (K_T).

Step-4: Calculate the diffuse irradiance $D(\theta)$, beam irradiance $B(\theta)$, the irradiance reflected from the ground $R(\theta)$ and the global solar irradiance $G(\theta)$ with respect to the panel angle (θ).

Step-5: Calculate the cloud amount in 3 layers (C_i) and sky clearness indicator (C) [128], [143].

Step-6: Calculate the actual global solar irradiance (G).

Solar irradiance under the standard test condition is considered as 1 kW/m^2. The energy generation capacity of each solar cell (E_{Scell}) plays a key role in deciding the size of the solar plant. Therefore, E_{Scell} depends on the following factors (the equivalent circuit of the solar cell is not shown) and is expressed as

$$E_{Scell} = f(G, T, I, I_{Ph}, V) \tag{4.5}$$

G is solar irradiance, T is temperature, I is output current, I_{ph} is photocurrent, and V is the output voltage of the solar cell. Energy produced by each photovoltaic module (the number of solar cells connected in series) (E_{PVM}) is given by

$$E_{PVM} = n \times E_{Scell} \tag{4.6}$$

where, n is the number of solar cells. The size of the solar plant (E_T) is therefore

$$E_T = m \times E_{PVM} \tag{4.7}$$

where, m is the number of modules. Solar plant capacity is given in Table 4.3 [144].

4.1.4 Assumptions

This work carries out the system level modeling of the entire network so that the modeling of the converters and ESD are not included. Also, the losses due to ESD, ICS and the solar panel are not included. The ICS efficiency is considered as 80-90% in this work. The ESD energy rating assumed to be same at all the EBSs.

4.2. Smart public transportation network expansion using CBs and EVs

The present work made an attempt to expand the electrified transportation network in the Guwahati city, Assam, India. Moreover, the proposed system shows the following benefits such as: improves the voltage profile of the grid during both the off-peak and peak period (as a result it maintains the power quality in the grid), utilizes the solar energy to support the transportation network as well as to the grid during off-peak/peak period, supports the electric buses for 24 h and also, supports both the CBs and EVs according to the timings given in Table 4.2. CBs (the mini-buses with a carrying capacity of 30 passengers) are used to transport the devotees to/from the Khamakhya EBS (KEBS) (located on the top of "Neelachala" hills in Guwahati city) from/to MEBS. EVs (the school vans with a carrying capacity of 15 students) are used to transport the students from/to the school to/from their respective stoppages. A particular EBS (MEBS) of the smart public transportation network has been considered to charge CBs and EVs along with the electric buses (ref. Fig. 4.2). The use of both, CBs and EVs along with ESD achieves more improvement in Vpu profile as that of 'ESD only' in the smart public transportation network.

Fig. 4.3, shows the basic working model of the smart public transportation network at MEBS. Solar plant is connected to both the grid and ESD. Solar plant sends energy to ESD/to the grid during the off-peak/peak period in sunshine hours. The controllers have to perform the control actions to manage the energy flow between the grid, solar plant, ESD, CBs and EVs. ESD is placed between the grid and the transportation network (combination of the electric buses, CBs and EVs) owing to its multiple benefits to the grid as well as to the transportation network.

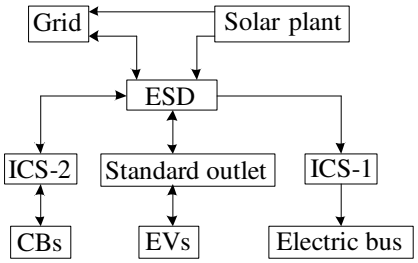

Fig. 4.3 The basic model of the smart public transportation network at the MEBS

ESD shows the following benefits.

- ESD isolates the transportation network from the grid and reduces the risk of transients in the grid (which may occur due to the direct connection of the transportation network with the grid).
- ESD receives/sends energy from/to the grid during the off-peak/peak period and also, receives energy from the solar plant if the grid stays under off-peak period during sunshine hours.
- ESD sends/receives energy to/from both, CBs and EVs according to the timings given in Table 4.2. Also, ESD supports the electric buses for 24 h.

Table 4.2: Working and non-working periods of school and temple

Time	*School*	*Temple*
Working period	09:00 to 15:00 h	05:00 to 11:30 h and 13:30 to 20:00 h
Non-working period	15:00 to 09:00 h	11:30 to 13:30 h and 20:00 to 05:00 h

The importance of the proposed work is represented in the following manner:

- The electrified transportation system lessens the use of internal combustion engine vehicles in the city regions and brings the public consciousness towards the EVs utilization. This system shows the possibility to rid of the poor air quality in cities.
- To maintain the power quality in the grid by improving the voltage profile of the grid. Also, to provide the clean energy based transportation system accessibility to the common citizen.
- To perform the intelligent energy management between the grid, the solar plant, energy storage devices and the energy consuming devices in the smart public transportation network.

The energy management between the grid, ESD and the solar plant is a challenging task due the dynamic behaviors of the passenger's profile, grid load profile and the solar energy

availability. Real time data of the above-mentioned profiles have been collected from their respective departments.

- Passenger's data from central transportation authority India.
- Solar data from India meteorological department [124].
- Load data from state electricity board Assam, India [121,122].

The motives of the present work are therefore:

- To expand the electrified transportation network in the Guwahati city.
- To show the difference in Vpu profile improvement with only ESD and with 'CBs, EVs and ESD' in the smart public transportation network.
- Favorable energy usage from both the grid and the solar plant to reduce the transportation network dependence on the grid.
- Smart public transportation network response verification in all the seasons of a year.
- Smart public transportation network behavior for uncertain situations that exist in the system.

Algorithm based controllers such as CB controller and EV controller have been developed to control the energy flow between ESD and both, CBs and EVs. The details about CBs, EVs and their algorithm-based controllers are given in the following sub-sections.

4.2.1 The capa-buses (CBs)

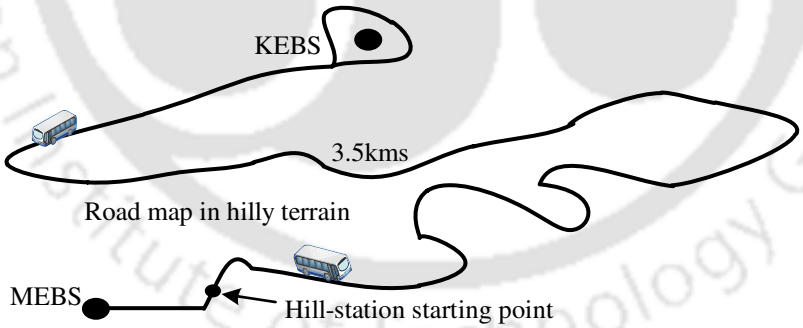

Fig. 4.4 The route map between the MEBS and KEBS

CB travels between MEBS and KEBS in the hilly terrain. The route map between these two bus stops is shown in Fig. 4.4. CB travels between these two bus stops. The considered route has the road angle 'θ' as shown in Fig. 4.4 and 4.6. The distance from MEBS to KEBS is considered as 3.5 km. CB need to travel 7 km distance in order to complete a loop of travel. CB utilizes the traction energy while travelling in the uphill mode and produces the regenerative braking energy while travelling in downhill mode. CBs are fully charged before

05:00 h according to the Vpu profile of the grid. CB receives the only half energy from ESD after 05:00 h and the remaining half energy receive from the regenerative braking energy. If ESD fails to charge CBs at MEBS, then mobile ESDs are arranged to avoid emergency situations. CBs show the following benefits:

- CB requires energy to travel from MEBS to KEBS (uphill route). CB travels from KEBS to MEBS with zero energy requirements (downhill root) (simultaneously produces the regenerative braking energy).
- Half of the CB's rated energy capacity is sufficient to complete a loop of travel (up and down the hill).
- CB supports the grid via ESD in peak period. CBs are beneficial to the grid, to the passengers and also, to the transportation network.

The calculations of CB energy requirement are given in the following sub-section.

4.2.1.1 CB's energy requirement calculations

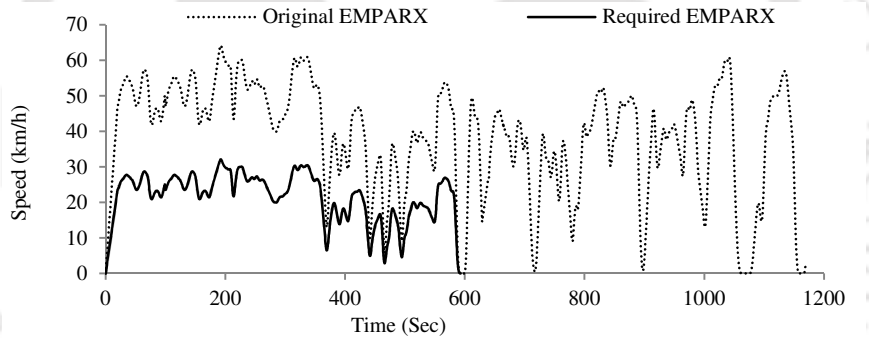

Fig. 4.5 EMPARX driving cycle

The original EMPARX driving cycle is shown in Fig. 4.5 [145]. Also, the required EMPARX driving cycle to complete the distance between MEBS and KEBS (Fig. 4.4) is shown in Fig. 4.5. Half of the EMPARX driving cycle's speed and time (represented with a solid line in Fig. 4.5) are suitable to complete the route map given in Fig. 4.4. The acceleration and deceleration periods of the required EMPARX driving cycle are suitable to complete the curves and slopes of the considered route (Fig. 4.4). Therefore, this driving cycle is used to determine the CB's energy requirement [145]. The considered distance between MEBS and KEBS is 3.5 km and stoppages are not required between these two bus stops. The required EMPARX driving cycle is also, not having the stoppage before 600 sec and covers a distance of 3.6 km in this duration. Also, an average speed of 21.6 km/h is suitable to complete the

considered route. Therefore, EMPARX driving cycle is considered in this work. The details of original and the required EMPARX driving cycle are given in Table 4.3.

Table 4.3: Time period, the distance covered and the average speed of EMPARX driving cycle

Driving cycle	*Time (sec)*	*Distance (km)*	*Average speed (km/h)*
Original EMPARX	1169	12.4	38.2
Required EMPARX	593	3.6	21.6

The vehicle dynamics have been calculated in the following manner. The different resistive forces that oppose the motion of CB are shown in Fig. 4.6 [123].

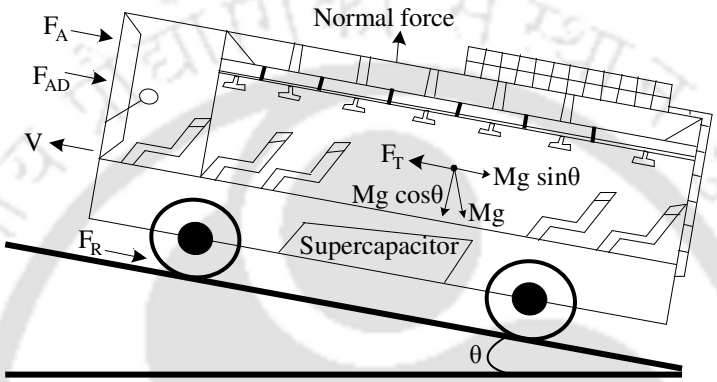

Fig. 4.6 various forces acting on CB

The tractive force required by the CB (F_{TCB}) to overcome these resistive forces is expressed as

$$F_{TCB} = (F_R + F_{AD} + F_G + F_A) = (Mgf_r cos\theta + 0.5\rho_a C_D A V^2 + Mgsin\theta + M\delta\frac{dV}{dt}) \quad (4.8)$$

where, F_R is the rolling resistance, F_{AD} is the aero dynamic resistance, F_G is the grading resistance and F_A is the acceleration resistance. M is the mass of CB (10^4 kg), g is gravitational acceleration (9.81 m/s^2), f_r is the rolling resistance coefficient (0.01), θ is the grading angle (20^0), ρ_a is the air mass density (1.184 kg/m^3), C_D is the aerodynamic drag coefficient (0.5), A is the frontal area of CB (6 m^2), V is the vehicle speed (m/s), δ is the rotational inertia factor (1.1), and dV/dt is the acceleration of CB (m/s^2). The tractive energy (E_{TCB}) required by the CB is expressed as

$$E_{TCB} = F_{TCB} \times D \quad (4.9)$$

where, D is the displacement (m). The regenerative braking energy produced by the kinetic energy of CB (E_{RCB}) [146] in the deceleration period is therefore

$$E_{RCB} = \beta \times E_{TCB} \quad (4.10)$$

β is the fraction of gravitational potential energy (0<β<1) and is considered as 0.5. 'β' is less than 0.5, for non-downhill journey segments. Therefore, CB needs to receive more energy from ESD when it travels on the flat root (θ=0). Actual CB energy (E_{CB}) is therefore

$$E_{CB} = E_{TCB} - E_{RCB} \tag{4.11}$$

The size of the supercapacitor in CB (C_{CB}) is expressed as

$$C_{CB} = (2 \times E_{TCB}) / (V^2) \tag{4.12}$$

V is the rated voltage of the supercapacitor as 125 V. The amount of energy required by CB for completing a round trip (E_{CBT}) is therefore

$$E_{CBT} = E_{CB\,max} - E_{TCB} + E_{RCB} \tag{4.13}$$

E_{CBmax} is the maximum energy of CB and is given as

$$E_{CB\max} = 2 \times E_{TCB} \tag{4.14}$$

The factor 2 in (4.14) is considered to avoid the emergency situations (CB completes maximum three loops with E_{CBmax} when CB failed to receive energy from ESD).

4.2.1.2 Algorithm of CB controller

CB's charging/discharging performance from/to ESD is decided through the algorithm of the CB controller. CB receives energy from ESD irrespective of the grid condition (during both the off-peak and peak periods) and discharges energy to ESD during the peak period after satisfying the specific conditions of (4.18). CB's charging/discharging performance should not affect the functioning of ESD. So that the energy limit, has been decided for CB, to receive/send energy from/to ESD. Therefore, CB's energy range is given as

$$-E_{CBj\,max} \le E_{CBj} \le E_{CBj\,max} \qquad \forall j \in SCB \tag{4.15}$$

where, E_{CB} is the energy status of CB, E_{CBmax} is the maximum charging limit of CB from ESD and $-E_{CBmax}$ is the maximum discharging limit of CB to ESD and SCB is the set of CBs (j=1, 2 --- n). It has been considered that Vpu is greater/less than 1pu when the grid stays under off-peak/peak period (Vpu profile varies with respect to the load profile of the grid shown in Fig. 4.10). The amount of energy received by CB (E_{CBC}) during the off-peak period (Vpu>1pu) is expressed as

$$E_{CBC} = \begin{cases} E_{CBR} & for\ (0 < E_{CBR} < E_{CB\max}) \\ 0 & otherwise \end{cases} \tag{4.16}$$

E_{CBR} is the amount of energy required by the CB and E_{CBmax} is the CB's maximum energy limit. CB receives energy from ESD when E_{CBR} stays between zero and E_{CBmax}. E_{CBR} may vary due to uncertain situations such as driving style of the driver, weather condition, over loading and the traffic congestion, etc. Therefore E_{CBR} is given as

$$E_{CBR} = E_{CBmax} - E_{RCB} - E_{CBmin} \tag{4.17}$$

E_{CBmin} is the minimum energy remains in CB and it may vary from zero to E_{CBmin} when uncertain situations exist (if CB utilizes other than E_{TCB} then E_{CBmin} decreases, otherwise E_{CBmin} remains the same). The amount of energy sent/received by CB (E_{CBD} /E_{CBC}) to/from ESD during the peak period (Vpu<1pu) is therefore

$$E_{CBD}/E_{CBC} = \begin{cases} E_{CBnet} & for\ (t > 20{:}00\ \text{h}\ \&\ E_{CBnet} > 0) \\ E_{CBC} & otherwise \end{cases} \tag{4.18}$$

E_{CBnet} is the net energy availability of CBs and 't' is the time period in hours (24 h). CBs discharge their total energy to ESD when both the conditions such as 't' is greater than 20:00 h and E_{CBnet} is greater than zero are satisfied. Otherwise, CBs receive energy from ESD with respect to (4.16). A total of four CBs have been considered in this work and the maximum energy rating of each CB (E_{CBmax}) is given in Table 4.4.

4.2.2 Electric vehicles (EVs)

EVs travel through the city from 07:00 to 09:00 h (1st loop), and from 15:00 to 17:00 h (2nd loop), to pick up/drop the students from/to their respective bus stops. EVs receive sufficient energy from ESD before their first trip of travel. Again, EVs are connected to ESD between 09:00 to 15:00 h to receive energy from ESD. After completion of the second trip of travel, EVs support the grid with the remained energy if the peak period exists after 18:00 h otherwise EVs charge from ESD. EVs do not receive energy from ESD if the grid stays under the peak period from 09:00 to 15:00 h. Under this situation, EVs utilize half energy for the 1st loop of travel and the remaining half energy for 2nd loop of travel. This means that EVs utilize total energy for transportation purpose. Therefore, EVs are unable to support the grid. EVs show the following benefits:

- EVs curtail the use of internal combustion engine vehicles.

- EVs charge from the grid via ESD in the off-peak period and discharge to the grid via ESD in peak period.
- EVs strengthen the ESD in the process of voltage profile flattening of the grid.
- EVs can be operated with the only solar energy if the grid stays under off-peak period during sunshine hours.
- EVs work in harmony with the grid and with the smart public transportation network, and are beneficial to the students, to the transportation network and also, to the grid.

The details of EV's energy requirement and the algorithms of both, the EV controller and the aggregator are given in the following sub-section.

4.2.2.1 EVs energy requirement and the algorithm of EV controller

A total of four EVs have been considered and the carrying capacity of each EV is limited to 15 students. The travelling distance of each EV is considered as 34 miles. The energy rating of EV is given in Table 4.4. EV travel two loops (each loop cover 17 miles) in a day and each loop consumes 12 kWh. EVs should not create the extra burden on the ESD during the peak period. So that the energy limit, has been decided for charging/discharging of EVs from/to ESD during off-peak/peak period. Therefore, the EVs energy range is given as

$$-E_{EVimax} \le E_{EVi} \le E_{EVimax} \qquad \forall i \in SEV \tag{4.19}$$

where E_{EV} is the energy status of EV, E_{EVmax} is the maximum charging limit of EV from ESD and $-E_{EVmax}$ is the maximum discharging limit of EV to ESD and SEV is the set of EVs (i=1, 2 --- n). EV's charging/discharging performance from/to ESD is decided through the algorithms of both, the EV controller and the aggregator. The amount of energy received by EVs from ESD during the off-peak period (E_{EVC}) (Vpu>1pu) is expressed as

$$E_{EVC} = \begin{cases} \left(\left(\dfrac{E_{ESD} - E_{ESD\min}}{E_{ESD\max}} \right) \times E_{EV\max} \right) & for\ (E_{ESD} > E_{ESD\min}\ \&\ E_{EVnet} < E_{EV\max}) \\ 0 & otherwise \end{cases} \tag{4.20}$$

E_{ESDmin} is the minimum energy status of ESD (40% of E_{ESD} is considered), E_{ESDmax} is the maximum energy status of ESD, E_{EVmax} is the set of EVs maximum energy limit, and E_{EVnet} is the set of EVs net energy availability. EVs receive energy from ESD with respect to the expression given in (4.20) when both the conditions such as E_{ESD} is greater than E_{ESDmin} and E_{EVnet} is less than E_{EVmax} are satisfied. ESD allows EVs to charge when it crosses its

minimum energy limit (E_{ESDmin}) (this is the minimum energy required to support the electric buses for 24 h). The charging rate (C_R) and the discharging rate (D_R) of EV are therefore

$$C_R = \frac{P_{EVC}}{E_{EVR}}; \quad D_R = \frac{P_{EVD}}{E_{EVR}} \tag{4.21}$$

P_{EVC} is the amount of power received by EV in charging mode, E_{EVR} is the amount of energy remained in EV and P_{EVD} is the amount of power sent by EV in discharging mode. P_{EVC}/P_{EVD} has the limited power range according to (4.19). The amount of energy from EVs to ESD during the peak period (E_{EVD}) (Vpu<1pu) is expressed as

$$E_{EVD} = \begin{cases} 0.5D_R & for\ (t > 18{:}00\ \text{h}\ \ \&\ E_{EVnet} > 0) \\ 0 & otherwise \end{cases} \tag{4.22}$$

The state of charge (SOC)/ the depth of discharge (DOD) at the end of charging/discharging of EV are given as

$$SOC_i = SOC_{0\,i} + \left(\frac{E_{EVC}}{E_{EVnet}}\right)_i \qquad \forall i \in SEV \tag{4.23}$$

$$DOD_i = SOC_{0\,i} + \left(\frac{E_{EVD}}{E_{EVnet}}\right)_i \qquad \forall i \in SEV \tag{4.24}$$

$SOC_{0\,i}$ is the initial SOC of EV. The aggregator distributes/collects energy to/from individual EV and the details are as follows.

Table 4.4: The specifications of CB, EV and the solar plant

Variable	*Rating*
The maximum energy rating of CB (E_{CBmax})	9 kWh
The energy rating of EV	24 kWh
Solar plant capacity	50 kW

4.2.2.2 Aggregator

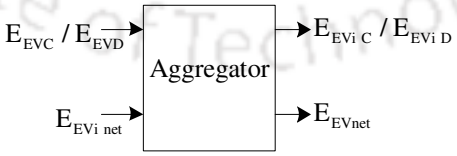

Fig. 4.7 Block diagram of an aggregator

The block diagram representation of an aggregator is shown in Fig. 4.7. The aggregator works based on two inputs and two outputs. The inputs are E_{EVC}/E_{EVD} (signals receive from the EV controller) and the net energy availability of individual EV ($E_{EVi\ net}$) (this signal

receives from EVs) (ref. Fig. 4.2). The outputs are $E_{EVi\ C}$/$E_{EVi\ D}$ (energy to/from individual EV) and E_{EVnet}. $E_{EVi\ C}$ is expressed as

$$E_{EVi\ C} = \begin{cases} \left(\dfrac{(E_{EVC})}{(\sum_{i=1}^{n} EV_i)} \right) & E_{EVi\ net} < E_{EVi\ \max} \\ 0 & otherwise \end{cases} \tag{4.25}$$

where, $E_{EVi\ net}$ is the net energy availability of individual EV and $E_{EVi\ max}$ is the maximum capacity of individual EV. Therefore $E_{EVi\ D}$ is given as

$$E_{EVi\ D} = \begin{cases} \left(\dfrac{(E_{EVD})}{(\sum_{i=1}^{n} EV_i)} \right) & E_{EVi\ net} > 0 \\ 0 & otheriwse \end{cases} \tag{4.26}$$

E_{EVnet} is expressed as

$$E_{EVnet} = \sum_{i=1}^{n} E_{EVi\ net} \tag{4.27}$$

Smart public transportation network response verification for three seasons of a year is given in the following sub-section.

4.2.3 Smart public transportation network response for three seasons of a year

The improvement in Vpu profile of the grid at MEBS with 'only ESD' and ESD with both 'CBs and EVs' for three seasons of a year has been explained through Fig. 4.8.

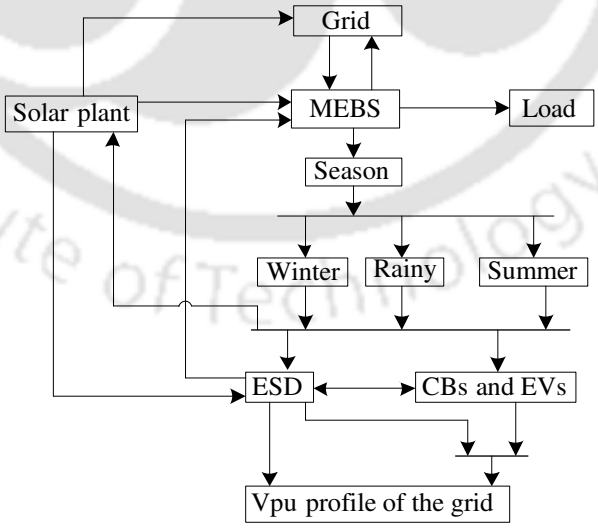

Fig. 4.8 The smart public transportation network response for three seasons of a year at MEBS

Three seasons such as winter, rainy and summer have been considered to verify the response of a smart public transportation network in different situations. Solar power

generation is directly proportional to the solar irradiance availability through all these seasons of a year (ref. Sec. 4.1.3). ESD acts as a load/source to the grid during off-peak/peak period and accordingly performs the improvement in Vpu profile of the grid. EVs and CBs strengthen the ESD to receive/send more energy from/to the grid during the off-peak/peak period. This arrangement improves the load/source to the grid during off-peak/peak period so that the improved Vpu as that of ESD alone in the smart public transportation network at MEBS. Vpu of the grid is therefore

$$\text{Vpu} = \frac{V_{actual}}{V_{base}} \tag{4.28}$$

where, V_{actual} is the actual voltage of the grid with respect to load profile and V_{base} is the base voltage of the grid. Vpu should vary within the permissible voltage limit to maintain the power quality in the grid [147,148]. So that, the Vpu limit of the grid has been considered and is expressed as

$$Vpu_{\min} \le \text{Vpu} \le Vpu_{max} \tag{4.29}$$

Vpu_{min} and Vpu_{max} are the minimum and the maximum Vpu limit of the grid and accordingly the controller performs the voltage control actions in the grid (ref. Fig. 4.14). ESD's maximum power limit (ESD receive/send power from/to the grid) is expressed as

$$-P_{ESDmax} \le P_{ESD} \le P_{ESDmax} \tag{4.30}$$

P_{ESDmax} is the maximum power limit of ESD during the charging period in off-peak hours and $-P_{ESDmax}$ is the maximum power limit of ESD during the discharging period in peak hours (ref. Fig. 4.15). FLC perform the controlled power flow between the grid and ESD with respect to this power limit.

The energy management at MEBS has been performed by using three controllers such as FLC, EV controller and CB controller, and the details are given through Fig. 4.9. The working principles of the three controllers in the smart public transportation network are expressed through the algorithm given in Fig. 4.9 and works in the following manner: first, initialize inputs such as Vpu, E_{SP}, E_{ESD}, E_{EVnet}, E_{EVmax}, E_{CBR}, E_{CBnet}, E_{CBmax}, and 't'. Algorithm works based on six conditions (C) such as: *C-1:* Vpu is greater than 1 pu and E_{SP} is greater than zero, *C-2:* E_{ESD} is greater than E_{ESDmin} and E_{EVnet} is less than E_{EVmax}, *C-3:* E_{CBR} is less than E_{CBmax}, *C-4:* Vpu is less than 1 pu and E_{SP} is greater than zero, *C-5:* E_{EVnet} is

greater than zero and '*t*' is greater than 18:00 h, and *C-6:* E_{CBnet} is greater than zero and '*t*' is greater than 20:00 h.

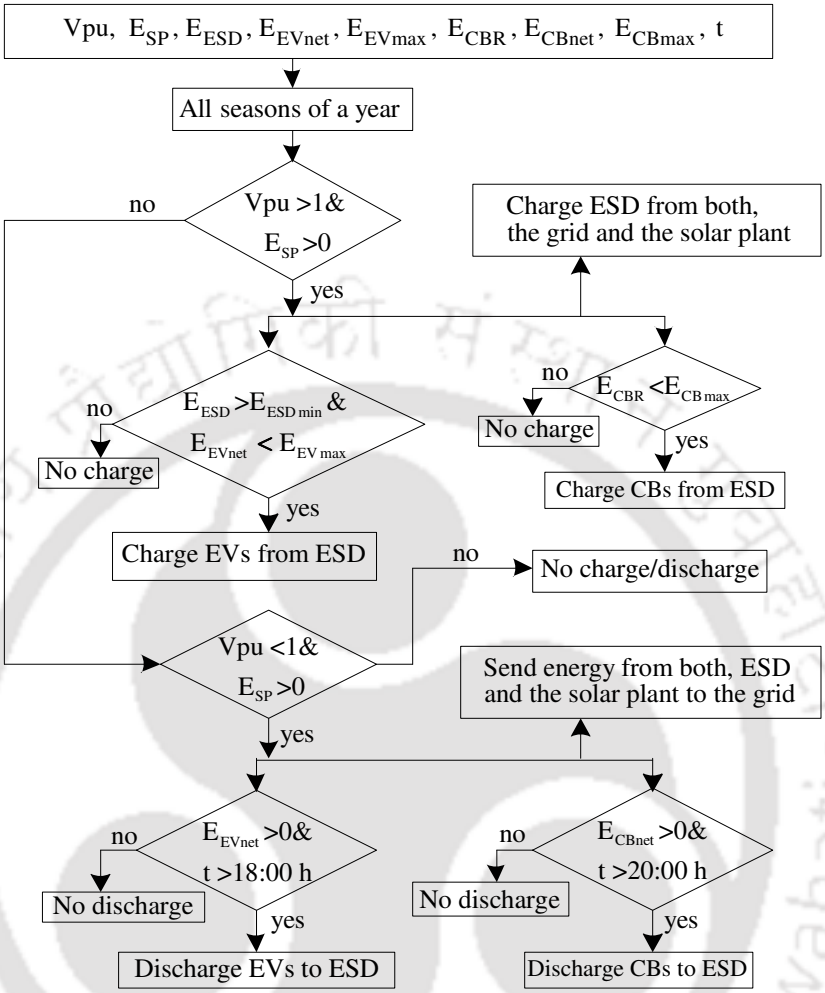

Fig. 4.9 Algorithm for energy management in the smart public transportation network

If *C-1* is satisfied then ESD receives energy from both the grid and the solar plant according to FLC commands. If both, *C-1* and *C-2* are satisfied then EVs receive energy from ESD otherwise no charge. If both, *C-1* and *C-3* are satisfied then CBs receive energy from ESD otherwise no charge. If *C-1* and *C-4* are not satisfied then no charge/discharge. If *C-4* is satisfied then both ESD and solar plant send energy to the grid. If *C-4* and *C-5* satisfied then EVs send energy to ESD otherwise no discharge. If *C-4* and *C-6* are satisfied then CBs send energy to ESD otherwise no discharge.

The average load profile, solar irradiance availability and the electric bus profile for three seasons of a year have been used in the simulations and are shown in Fig. 4.10, 4.11 and 4.12 respectively.

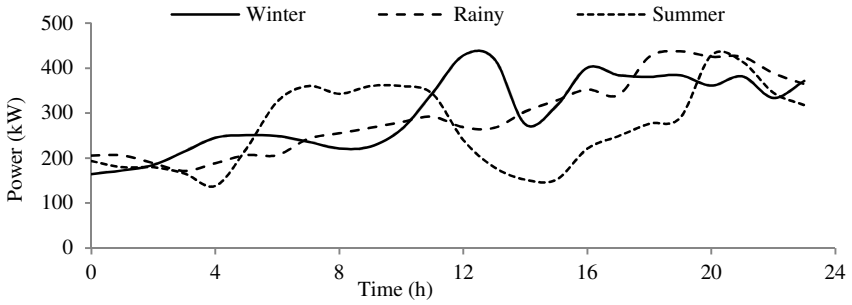

Fig. 4.10 Load profiles of the grid for three seasons

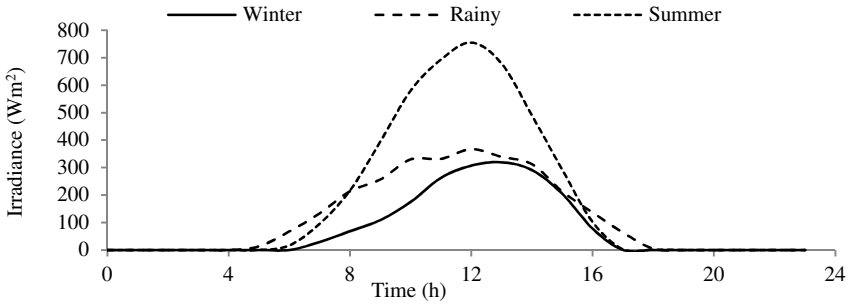

Fig. 4.11 The irradiance for three seasons

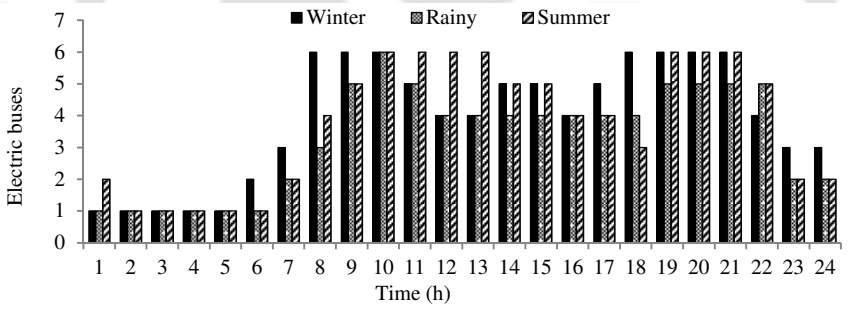

Fig. 4.12 Electric buses for three seasons

4.2.4 Fuzzy logic controller

Every EBS in the smart public transportation network consists of an FLC to control the charging/discharging of ESD from/to the grid during the off-peak/peak period and also to control the solar plant's energy to ESD/to the grid during the off-peak/peak period (Fig. 4.2). FLC is used in this work owing to its numerous features like ease in mathematics, simple representation in complex systems, flexible and natural language based [117]-[120], [132]. Fig. 4.13 shows the block diagram of FLC with four inputs (Vpu, E_{ESD}, NEB and E_{SP}) and two outputs ($P\pm$ and $SP\pm$). FLC works in the following manner: input crisp set values are converted into linguistic variables by using the fuzzification process (Mamdani inference system is used). The linguistic variables are converted into crisp set values by using the Defuzzification process. These conversions are done by means of triangular membership

functions and are used due to their simple representation and ease in mathematics. The rule base performs the control strategy and the output from each rule, are reduced by inference logic. The center of area method is used for the Defuzzification process. The membership functions for inputs are shown in Fig. 4.14.

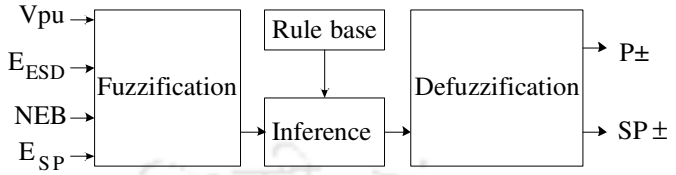

Fig. 4.13 FLC block diagram

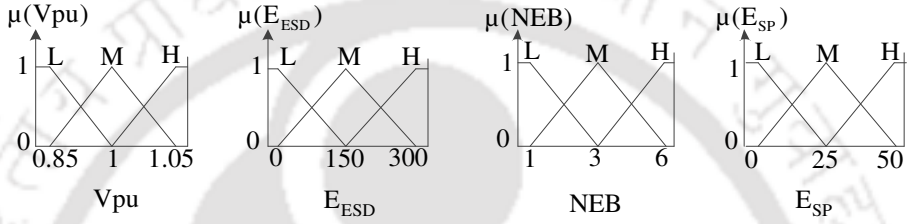

Fig. 4.14 FLC input membership functions

Vpu thresholds have been considered from 0.85 pu to 1.05 pu [136]. The universe of discourse ranges for inputs are: for Vpu (0.85 to 1.05), for E_{ESD} (0 to 300 kWh), for NEB (0 to 6) and for E_{SP} (0 to 50 kWh). Each input is divided into three membership functions represented with linguistic variables low (L), medium (M) and high (H). The degree of membership range for all inputs and outputs are from 0 to 1.

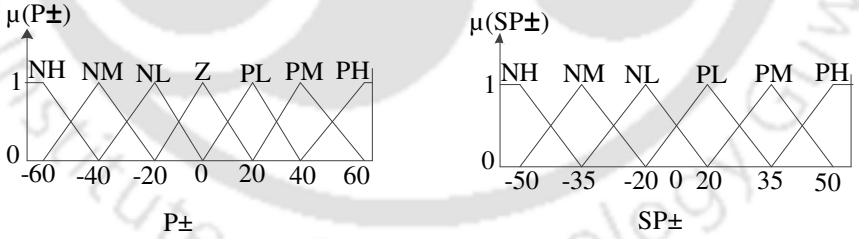

Fig. 4.15 FLC output membership functions

The membership functions for outputs are shown in Fig. 4.15. Two outputs are divided into 7 and 6 membership functions respectively and represented with the linguistic variables: negative (N) {L, M, H}, zero (Z) and positive (P) {L, M, H}. The universe of discourse for $P\pm$ is from -60 kW to 60 kW and for $SP\pm$ is from -50 kW to 50 kW. FLC decides the power flow among ESD, the solar plant and the grid based on the rule base designed in it. The rule base of FLC is shown in Table 4.5. The degree of fulfillment (*DOF*) for the individual rule is expressed as

Table 4.5: FLC rule base

Input				Output			Input				Output	
Vpu	E_{ESD}	NEB	E_{SP}	P±	SP±		Vpu	E_{ESD}	NEB	E_{SP}	P±	SP±
H	M	H	H	Z	PH		M	L	H	H	Z	NH
H	M	H	M	Z	PM		M	L	H	M	Z	NM
H	M	H	L	Z	PL		M	L	H	L	Z	NL
H	M	M	H	Z	PH		M	L	M	H	Z	NH
H	M	M	M	Z	PM		M	L	M	M	Z	NM
H	M	M	L	Z	PL		M	L	M	L	Z	NL
H	M	L	H	Z	PH		M	L	L	H	Z	NH
H	M	L	M	Z	PM		M	L	L	M	Z	NM
H	M	L	L	Z	PL		M	L	L	L	Z	NL
H	L	H	H	PL	PH		L	H	H	H	NH	NH
H	L	H	M	PL	PH		L	H	H	M	NH	NM
H	L	H	L	PL	PM		L	H	H	L	NH	NM
H	L	M	H	PL	PH		L	H	M	H	NH	NH
H	L	M	M	PL	PH		L	H	M	M	NH	NM
H	L	M	L	PL	PM		L	H	M	L	NH	NM
H	L	L	H	PL	PH		L	H	L	H	NH	NH
H	L	L	M	PL	PH		L	H	L	M	NH	NM
H	L	L	L	PL	PM		L	H	L	L	NH	NM
M	H	H	H	NH	NH		L	M	H	H	NM	NH
M	H	H	M	NH	NM		L	M	H	M	NM	NM
M	H	H	L	NH	NL		L	M	H	L	NM	NL
M	H	M	H	NH	NH		L	M	M	H	NM	NH
M	H	M	M	NH	NM		L	M	M	M	NM	NM
M	H	M	L	NH	NL		L	M	M	L	NM	NL
M	H	L	H	NH	NH		L	M	L	H	NM	NH
M	H	L	M	NH	NM		L	M	L	M	NM	NM
M	H	L	L	NH	NL		L	M	L	L	NM	NL
M	M	H	H	NH	NH		L	L	H	H	Z	PH
M	M	H	M	NH	NM		L	L	H	M	Z	PM
M	M	H	L	NH	NL		L	L	H	L	Z	PL
M	M	M	H	NH	NH		L	L	M	H	Z	PH
M	M	M	M	NH	NM		L	L	M	M	Z	PM
M	M	M	L	NH	NL		L	L	M	L	Z	PL
M	M	L	H	NH	NH		L	L	L	H	Z	PH
M	M	L	M	NH	NM		L	L	L	M	Z	PM
M	M	L	L	NH	NL		L	L	L	L	Z	PL

$$DOF_i = min\{\mu_{i\,MFin}(\text{Vpu}, E_{ESD}, \text{NEB}, E_{SP})\} = \mu_{i\,MFout}(P\pm) \quad (4.31)$$

where, '*i*' is the individual *DOF* for the respective rule from the rule base (*i*= 1, 2 --- *n*), $\mu_{i\ MFin}$ is the degree of membership for individual input along with input membership function (L, M and H) (ref. Fig. 4.14). *DOF* can be decided according to the 'minimum/maximum' method, and here the 'minimum' method has been utilized (4.31). $\mu_{i\ MFout}$ ($P\pm$) is the corresponding output's degree of membership along with the membership function (NH, NM, NL, Z, PL, PM and PH) with respect to DOF_i.

The Defuzzification process has been performed to express the linguistic variables into crisp set values and is given as

$$(P\pm) = \frac{\sum_{i=1}^{n}\left((P\pm)_i \times \mu(P\pm)_i\right)}{\sum_{i=1}^{n}\mu(P\pm)_i} \tag{4.32}$$

where, $(P\pm)_i$ is the output power value on x-axis (i= 1, 2 --- n) (ref. Fig. 4.15), $\mu\,(P\pm)_i$ is the degree of MF for the corresponding output power on y-axis (ref. Fig. 4.15) and $P\pm$ is the crisp set value of net output power for the corresponding input values. Similar procedure has been followed (from (4.31) to (4.32)) for deciding the FLC's second output $SP\pm$.

4.3. Results and discussion

Two types of case studies have been considered to explain the simulated results of the proposed system.

1) The first case explains the smart public transportation network response for all the three seasons of a year.
2) The second case explains the smart public transportation network behavior for uncertain situations that exist in the system.

Also, the results explain the benefits of using 'CBs and EVs along with ESD' as that of 'only ESD' in the smart public transportation network. In both the cases, the smart public transportation network response depends on the dynamic nature of the load, passengers and the solar irradiance availability. Vpu profiles for both the cases vary with respect to the load profiles of the grid shown in Fig. 4.10. EVs and CBs can run with only solar energy, if the grid stays under the off-peak period during sunshine hours.

4.3.1 Case-1: The smart public transportation network response for three seasons of a year

The smart public transportation network response verification for the three seasons of a year at MEBS has been explained through Fig. 4.16 to 4.26. The irradiance availability is low in winter, medium in rainy and high in the summer season (Fig. 4.11). Solar plant supports the grid as well as the transportation network as per the irradiance availability.

4.3.1.1 Winter season

The Vpu profile of the grid with 'only ESD', and 'ESD along with CBs and EVs' for the winter season is shown in Fig. 4.16.

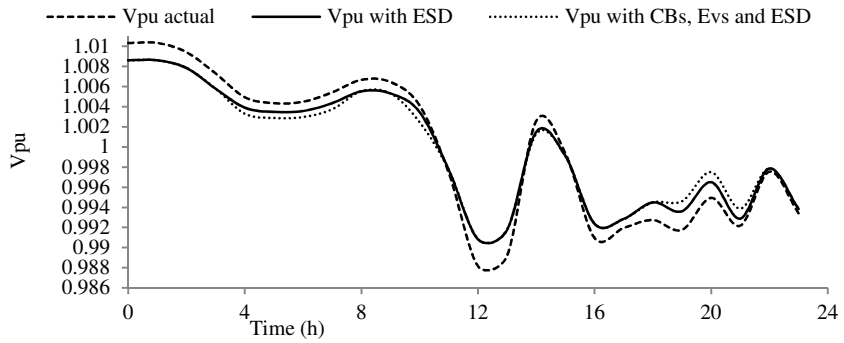

Fig. 4.16 Vpu profile of the grid with ESD only and 'ESD with CBs and EVs' for the winter season

The 'Vpu with ESD' curve shows that the ESD is receiving energy from the grid during the off-peak period so that the Vpu curve is below the actual Vpu curve (the valley filling in load point of view). ESD is sending its stored energy back to the grid during peak period so that the Vpu curve is above the actual Vpu curve (peak shaving in load point of view). The 'Vpu with CBs, EVs and ESD' curve shows that the ESD is receiving more energy from the grid between 03:00 to 07:00 h, 09:00 to 10:00 h, and 14:00 to 15:00 h with the presence of EVs and CBs (ESD is receiving additional energy from the grid). So that, the 'Vpu with CBs, EVs and ESD' curve is below the 'Vpu with ESD' curve and also, reaching close to 1 pu (more valley filling in load point of view). ESD is sending more energy to the grid between 19:00 to 23:00 h with the presence of EVs and CBs (more peak shaving in load point of view). So that, the 'Vpu with CBs, EVs and ESD' curve is above the 'Vpu with ESD' curve during this period. Therefore, more improvement in Vpu profile with 'CBs, EVs and ESD' as that of only ESD in the smart public transportation network and that can be observed from Fig. 4.16.

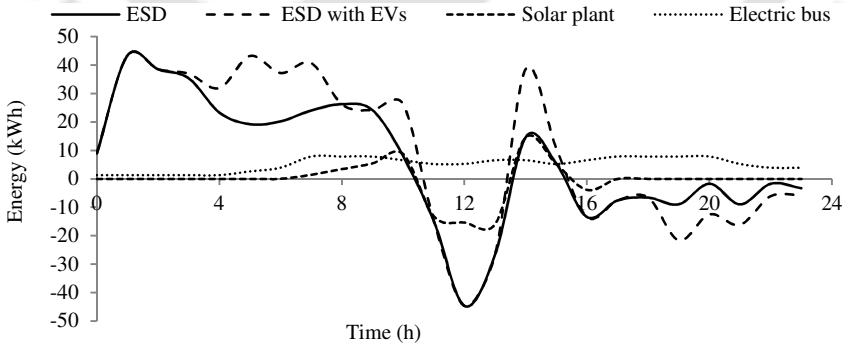

Fig. 4.17 Energy behavior of ESD, the solar plant, ESD with EVs and the electric bus for the winter season

The energy behavior of ESD, the solar plant, ESD with EVs and the electric bus for the winter season is shown in Fig. 4.17. The positive/negative values of ESD curve represent the amount of energy received/sent by ESD from/to the grid. The positive/negative values of

'ESD with EVs' curve represent the amount of energy received/sent by ESD with the presence of EVs from/to the grid. The positive/negative values of the solar plant curve represent the amount of energy sent to ESD/to the grid by the solar plant. The positive values of the electric bus curve represent the amount of energy received by the electric buses from ESD at MEBS. This sequence has been followed in all the energy behavior curves for three seasons of a year. The energy behavior of the ESD curve shows that the ESD is receiving/sending energy from/to the grid during off-peak/peak period with respect to load profile of the grid as shown in Fig. 4.17. The energy behavior of 'ESD with EVs' curve shows that the ESD is receiving extra energy from the grid between 03:00 to 07:00 h, 09:00 to 10:00 h and 14:00 to 15:00 h, with the presence of EVs and sending extra energy to the grid between 19:00 to 23:00 h, as shown in Fig. 4.17. The energy behavior of the solar plant curve shows that the solar plant is sending energy (less solar energy is available in the winter season (ref. Fig. 4.11)) to ESD between 06:00 to 10:00 h and 14:00 to 15:00 h, and sending energy to the grid between 10:00 to 14:00 h and 15:00 to 17:00 h, as shown in Fig. 4.17.

The energy status of ESD, 'ESD with CBs and EVs' and ESD with EVs for the winter season are shown in Fig. 4.18.

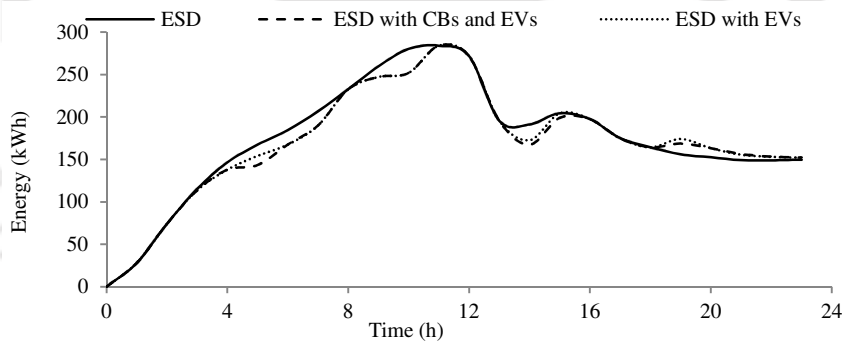

Fig. 4.18 The energy status of ESD for the winter season

The load profile of the grid has stayed under the off-peak period from 00:00 h to 10:00 h, so that ESD energy is reached to its maximum state. After 10:00 h, the load profile of the grid has stayed under peak period so that the ESD energy is reached to its minimum state. ESD is sending energy to EVs from 03:00 to 07:00 h, 09:00 to 10:00 h and 14:00 to 15:00 h, so that this curve is below the ESD curve. Also, EVs are sending energy to ESD between 19:00 to 23:00 h, so that this curve is above the ESD curve. CBs energy capacity is less as that of EVs, so that the variations between 'ESD with EVs' curve and 'ESD with EVs and CBs' curve is small. Also, the variations between the ESD curve and 'ESD with CBs and EVs'

curve is small between 08:00 to 09:00 h, 11:00 to 13:00 h and 16:00 to 18:00 h. This is due to the reason that CBs receive less energy from ESD (EVs do not receive energy from ESD during this period).

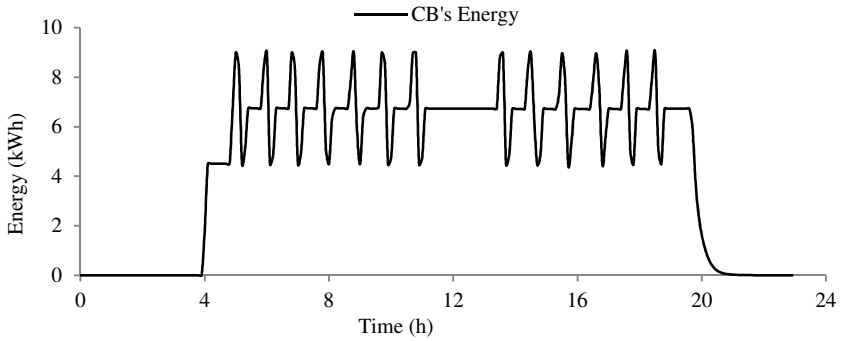

Fig. 4.19 The charging/discharging performance of CB from/to ESD for all the seasons of a year

The charging/discharging performance of CB from/to ESD for all the seasons of a year is shown in Fig. 4.19. CB receives maximum energy from ESD before its first trip of travel (ply from 05:00 h). The rising curve of CB before 05:00 h represents the amount of energy received by CB from ESD. The falling curve of CB represents the amount of energy utilized by CB while travelling from MEBS to KEBS (uphill route). After 05:20 h, the first half rising curve shows the amount of energy received by CB via regenerative braking energy (downhill root) and the second half rising curve shows the amount of energy received by CB from ESD. The constant line between two half rising curves of CB shows that CB remains idle for 20 minutes at MEBS for collecting the passengers. CB also remains idle from 11:30 to 13:30 h (ref. Table 4.2). The remained energy in CB (regenerative braking energy plus half of its rated energy) after the completion of the last trip of travel is used to support the grid via ESD as shown in Fig. 4.19.

4.3.1.2 Rainy season

The Vpu response of the grid with 'only ESD' and ESD with CBs and EVs for the rainy season is shown in Fig. 4.20. The area between the actual Vpu curve and the 'Vpu with ESD' curve shows the amount of energy received/sent by the ESD from/to the grid during off-peak/peak period. The comparison of Vpu profiles such as: 'Vpu actual' and 'Vpu with ESD' shows the improvement in Vpu profile during both the off-peak and peak period. The 'Vpu with CBs, EVs and ESD' curve shows that the ESD is receiving more energy from the grid between 03:30 to 07:00 h and 09:00 to 11:00 h. So that the Vpu curve is below the 'Vpu with

ESD' curve. Also, ESD is sending more energy to the grid from 19:00 to 23:00 h with the presence of EVs and CBs. So that the Vpu curve is above the 'Vpu with ESD' curve. The area between the actual Vpu curve and the 'Vpu with CBs, EVs and ESD' curve shows more improvement in Vpu profile as that of only ESD in the smart public transportation network and that can be observed from Fig. 4.20. This Vpu profile maintains the power quality in the grid during both the off-peak and peak period.

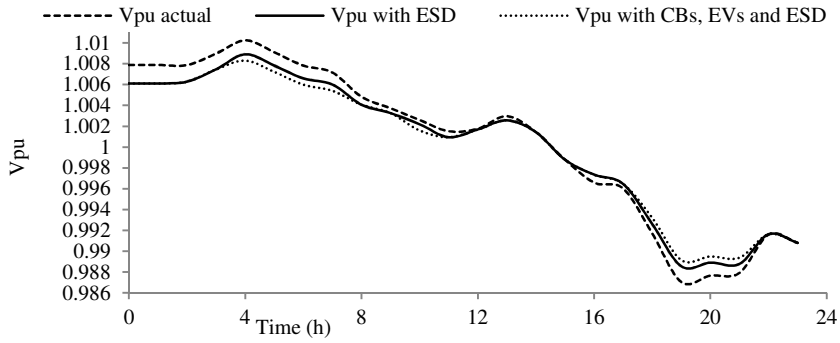

Fig. 4.20 Vpu profile of the grid with ESD only and 'ESD with CBs and EVs' for the rainy season

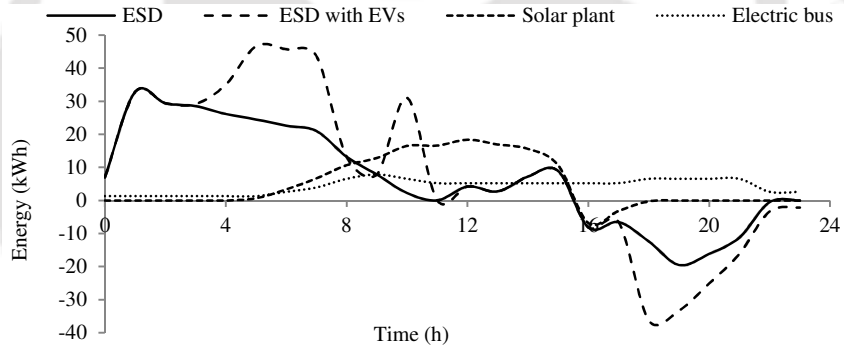

Fig. 4.21 Energy behavior of ESD, the solar plant, ESD with EVs and the electric bus for the rainy season

The energy behavior of ESD, the solar plant, ESD with EVs and the electric bus for the rainy season is shown in Fig. 4.21. The energy behavior of ESD curve shows that the ESD is receiving/sending energy from/to the grid during the off-peak/peak period with respect to load profile of the grid. The energy behavior of 'ESD with EVs' curve shows that the ESD is receiving more energy from the grid between 03:30 to 07:00 h and 09:00 to 11:00 h with the presence of EVs and sending extra energy to the grid, from 17:00 to 24:00 h. The energy behavior of the solar plant curve shows that the solar plant is sending energy (moderate solar energy is available in the rainy season (ref. Fig. 4.11)) to ESD from 06:00 to 15:00 h and also, sending energy to the grid from 15:00 to 18:00 h. The energy status of ESD, ESD with 'CBs and EVs', and ESD with EVs for the rainy season is shown in Fig. 4.22. The Vpu

profile of the grid has stayed close to 1pu between 10:00 to 11:00 h, so that ESD is not receiving energy from the grid (ref. Fig. 4.21). ESD charge the EVs during this period with the support of solar energy as shown in Fig. 4.21.The energy status of ESD with EVs curve shows that EVs are charging from ESD between 03:30 to 07:00 h and 09:00 to 11:00 h and also, discharging to ESD from 18:00 to 23:00 h, as shown in Fig. 4.22.

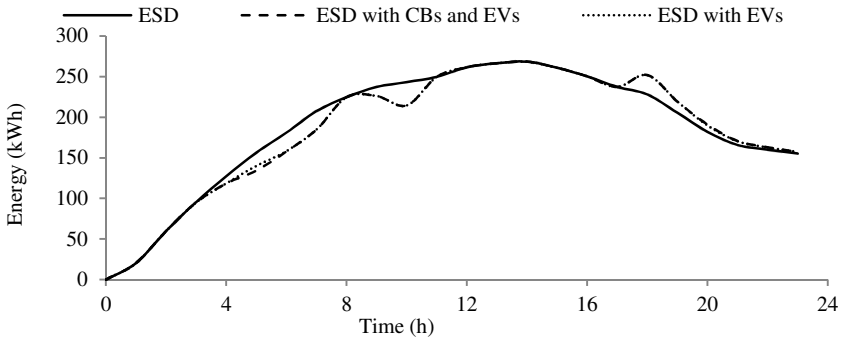

Fig. 4.22 The energy status of ESD for the rainy season

4.3.1.3 Summer season

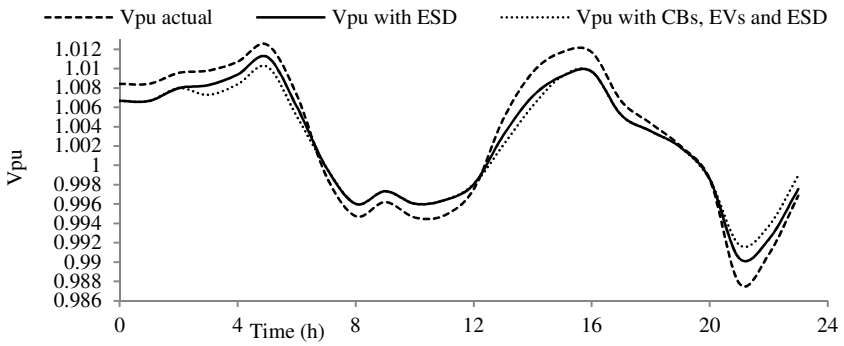

Fig. 4.23 Vpu profile of the grid with ESD only and 'ESD with CBs and EVs' for the summer season

The Vpu profiles of the grid with 'only ESD' and 'ESD with CBs and EVs' for the summer season are shown in Fig. 4.23. The 'Vpu with ESD' curve shows the improvement in Vpu profile during both, the off-peak and peak period. The 'Vpu with CBs, EVs and ESD' curve shows that the ESD is receiving more energy from the grid between 03:00 to 07:00 h and 13:00 to 15:00 h and also, sending more energy to the grid from 19:00 to 24:00 h. Comparing both the Vpu profiles such as: 'Vpu with CBs, EVs and ESD' curve and the 'Vpu with ESD' curve shows the further improvement in Vpu profile as that of ESD only and that can be observed from Fig. 4.23. The improvement in Vpu profile provides peak load relief to the grid during peak period. The Vpu profile with 'CBs, EVs and ESD' shows benefit to the grid, to the CBs, to the EVs, to the ESD and also, to the transportation network.

The energy behavior of ESD, the solar plant, ESD with EVs and the electric bus for the summer season is shown in Fig. 4.24. The energy behavior of 'ESD with EVs' curve shows that the ESD is receiving more energy from the grid between 03:00 to 07:00 h and 13:00 to 15:00 h with the presence of EVs and sending extra energy to the grid between 19:00 to 24:00 h. The energy behavior of the solar plant curve shows that the solar plant is sending energy (maximum solar energy is available in the summer season (ref. Fig. 4.11)) to ESD from 06:00 to 8:00 h and 13:00 to 18:00 h and also, sending energy to the grid from 08:00 to 13:00 h, as shown in Fig. 4.24.

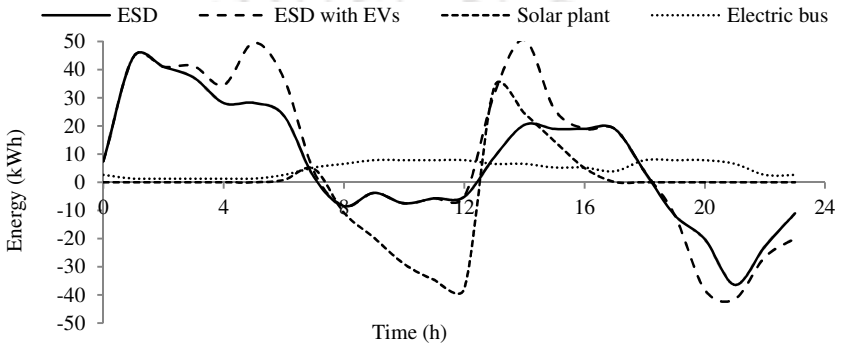

Fig. 4.24 Energy behavior of ESD, the solar plant, ESD with EVs and the electric bus for the summer season

The energy status of ESD, 'ESD with CBs and EVs' and ESD with EVs for the summer season are shown in Fig. 4.25. EVs are receiving energy from ESD between 03:00 to 07:00 h and 13:00 to 15:00 h. Vpu profile of the grid has stayed close to 1pu between 18:00 to 19:00 h (ref. Fig. 4.24), so that EVs are not receiving/sending energy from/to ESD. EVs are discharging energy to ESD according to the EV controller's command from 19:00 to 24:00 h, as shown in Fig 4.25.

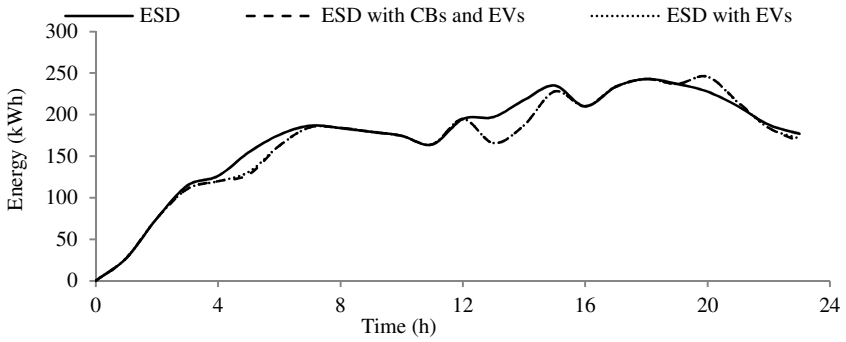

Fig. 4.25 The energy status of ESD for the summer season

The net energy status of EVs for all the three seasons of a year is shown in Fig. 4.26. EVs are not receiving energy up to 03:00 h due to the minimum criteria of EV controller is not satisfied (4.20). EVs receiving energy from ESD between 03:00 to 07:00 h and is represented

with the rising curve of EVnet. EVs utilizing energy from 07:00 to 09:00 h and from 15:00 to 17:00 h for transportation purpose and is represented with the falling curve of EVnet. After completion of travel, EVs are connected to ESD. EVs received/sent energy from/to ESD according to the Vpu profile of the grid as shown in Fig. 4.26 (4.23). In two situations, EVs do not receive energy from ESD: one is, if the grid stays under peak period from 09:00 to 15:00 h (observe EVnet for winter and summer in Fig. 4.26) and the other is, if EVs are in filled state (observe EVnet for rainy in Fig. 4.26). EVs are discharging energy to ESD after 18:00 h according to the Vpu profile of the grid (4.22), (4.24). If the grid stays under off-peak period after 18:00 h then EVs receive energy from ESD with respect to the EV controller's command.

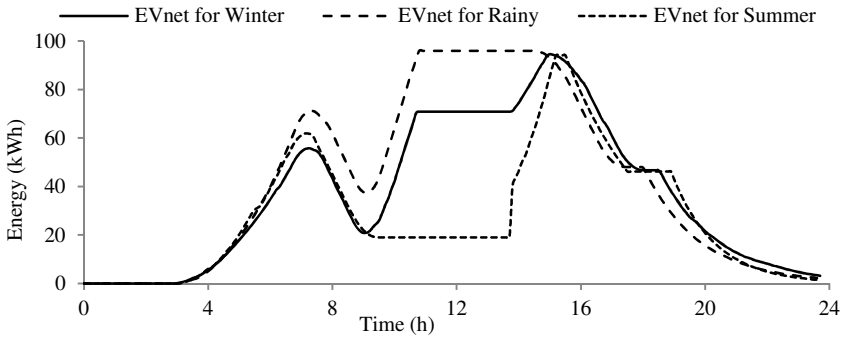

Fig. 4.26 The net energy status of EVs for three seasons of a year

4.3.2 Case-2: The smart public transportation network response for uncertain situations

Two types of uncertainties have been considered in the smart public transportation network: one is, if CB fails to receive energy from ESD and the other is EVs behavior when the grid stays continuously under peak/off-peak period during sunshine hours.

4.3.2.1 If CB fails to receive energy from ESD

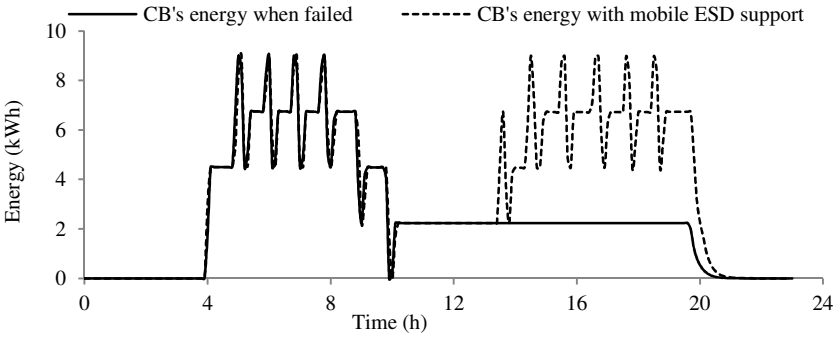

Fig. 4.27 CB's energy status when it is failed to receive energy from ESD

The energy status of CB when it is failed to receive energy from ESD is shown in Fig. 4.27. CB is failed to receive energy from ESD after 08:00 h, as shown in Fig. 4.27. However, CB managed the energy to complete three loops of travel with its maximum energy rating and is represented by solid line in Fig. 4.27. After 11:00 h, CB halted with regenerative braking energy and that energy is not sufficient to complete a loop of travel. In this situation, mobile ESD has been arranged at MEBS after 13:00 h. CB is receiving energy from the 'mobile ESD' with respect to (4.15), (4.16) and (4.17) as shown in Fig. 4.27. The energy requirement of CB is high after 11:00 h, but it received energy with respect to (4.15) (based on the maximum energy limit of CB) and is represented with the dotted line in Fig. 4.27.

4.3.2.2 EVs behavior when the grid is under peak period during sunshine hours

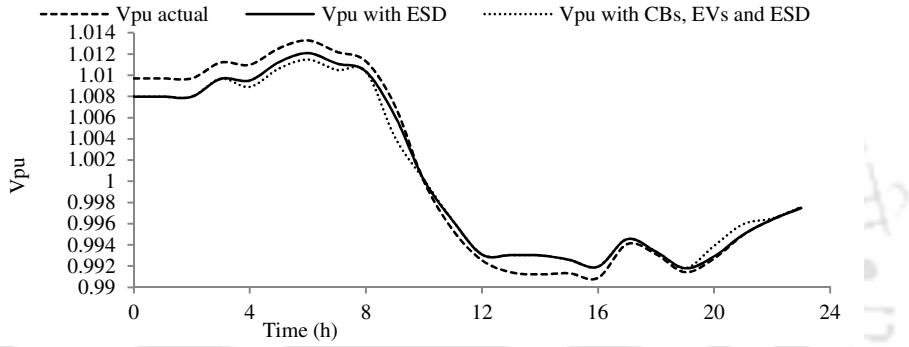

Fig. 4.28 Vpu profile of the grid when the peak period exist continuously in sunshine hours

The Vpu response of the grid, when the peak period exists continuously in sunshine hours is shown in Fig. 4.28. Vpu profile improvement with 'only ESD' and 'ESD with CBs and EVs' can be observed from Fig. 4.28.

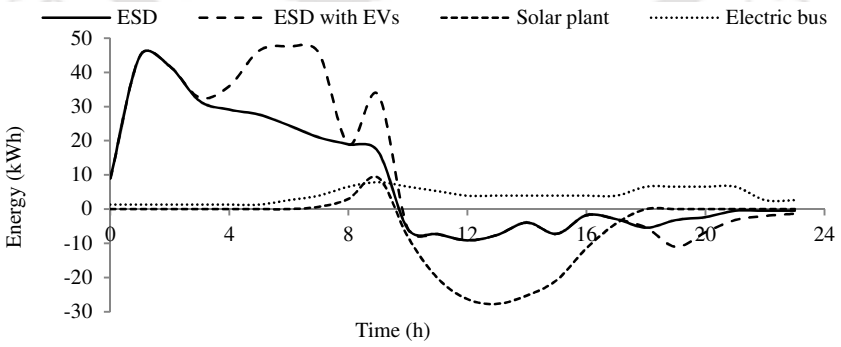

Fig. 4.29 Energy behavior of ESD, the solar plant, ESD with EVs and the electric bus when the grid is under peak period in sunshine hours

The energy behavior of ESD, the solar plant, ESD with EVs and the electric bus, when the grid stays under the peak period in sunshine hours is shown in Fig. 4.29. 'ESD with EVs'

curve shows that the EVs are receiving energy from ESD between 03:00 to 10:00 h. After 10:00 h, the grid has stayed under the peak period, so that EVs are not receiving energy from ESD. The solar plant curve shows that the solar plant is sending its total energy to the grid from 10:00 to 18:00 h. Therefore, ESD is sending less energy to the grid during this period and that can be observed from Fig. 4.29. The energy status of ESD when the grid stays under peak period during sunshine hours is shown in Fig. 4.30.

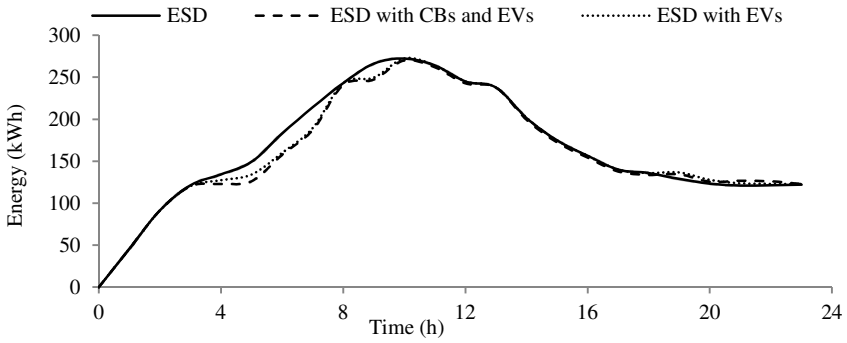

Fig. 4.30 The energy status of ESD when the grid is under peak period in sunshine hours

The net energy status of EVs when, the grid is under peak/off-peak period in sunshine hours (SH) is shown in Fig. 4.31.

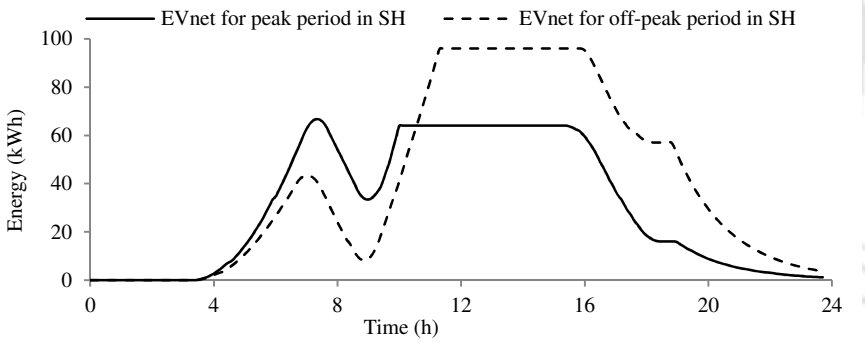

Fig. 4.31 The net energy status of EVs when, the grid is under peak/off-peak period in sunshine hours (SH)

The 'EV_{net} for peak period in SH' curve shows that the EVs are not receiving energy from ESD between 09:00 to 15:00 h (the grid has stayed under peak period). In this situation, EVs utilize total energy for transportation purpose. Therefore, EVs are sending less energy to ESD after 18:00 h and that can be observed from Fig. 4.31. The 'EV_{net} for the off-peak period in SH' curve shows that the EVs are receiving energy from ESD between 09:00 to 15:00 h (4.23) (the grid has stayed under off-peak period) until they reach to the fully charged state. Therefore, EVs are sending more energy to ESD after 18:00 h and that can be observed from Fig. 4.31. In this case, the solar plant sends its total energy to ESD, so that the

ESD receives less energy from the grid. Therefore, CBs and EVs utilize maximum solar energy in this case. The Vpu response of the grid and the energy behavior of ESD are not shown for this case.

4.4. Summary

- The proposed system has achieved the smooth performance of the smart public transportation network with the presence of ESD as well as the solar plat at every EBS and the complete system is coordinated with the grid.
- A specified EBS (MEBS) of the smart public transportation network has been considered to charge CBs and EVs, along with the electric buses.
- This system has performed two actions simultaneously: first one is, expanded the electrified transportation network using CBs and EVs along with electric buses in the Guwahati city, and the second one is, maintained the power quality in the grid during both, the off-peak and peak periods.
- Three controllers such as: FLC, CB controller and EV controller have been used to manage the energy at MEBS.
- The CB controller managed the energy flow between ESD and CBs.
- The EV controller managed the energy flow between ESD and EVs.
- FLC intelligently managed the energy flow between the grid, the solar plant and ESD.
- The smart public transportation network response has been verified for three seasons of a year and also, verified its behavior for the uncertain situations that exist in the system.
- The use of solar plants has reduced the transportation network dependence on the grid.
- The transportation network is operated with only solar energy, when the grid has stayed under off-peak period during sunshine hours.
- This system implementation is beneficial to the common citizen, to the transportation network, to the city regions and also, to the grid.

The proposed system is sustainable for different situations in all the seasons of a year. The benefits that Guwahati city gains, by the implementation of this system are therefore:

- The reduced usage of internal combustion engine vehicles in the city and as a result the improved air quality in the city region.
- This system brings the convenience to the common citizen to take part in the clean energy based transportation system in the city.

- Developing all the EBSs similar to that of MEBS in the Guwahati city transportation network, creates the possibility to transform the present transportation system from petroleum powered to the clean energy based.

Note: This work, 'Smart Public Transportation Network expansion and its interaction with the grid' is submitted to ELSEVIER Journal on 'Sustainable Energy, Grids and Networks'.

5

Conclusion and future works

Contents

5.1 Summary of the present work

The proposed work in this thesis focused on the coordination of solar assisted smart public transportation system with the grid. This system achieved the voltage profile improvement during both the off-peak and peak period and also, achieved the smooth performance of SPTS using energy from both the grid and the solar plant. The mass transportation has been performed using the e-buses in the Guwahati city. The e-buses received energy from the electric bus stops that are present through the ring road of the Guwahati city. The combined use of both ESD and SP at every EBS has reduced the SPTS dependence on the grid. ESD received energy form both the grid and SP during off-peak period and sent the stored energy back to the gird during peak period. The charging and discharging performance of ESD achieved the improvement in Vpu profile during both, the off-peak and peak period. The solar irradiance availability has been calculated based on the real time solar data and is used to determine the size of the solar plant. SPTS response has been verified for three seasons of a year based on the real time data of the dynamic profiles: load, solar and passengers. At every EBS, the fuzzy logic controller intelligently controlled the energy flow between ESD, the solar plant and the grid.

In Chapter-2, the small-scale solar plants coupled with SPTS and its coordination with the grid has been presented. The energy required by the e-bus to travel between the consecutive EBSs is calculated using the NYCC. The size of ESD is decided based on the number of e-buses required in SPTS for 24 h. An algorithm has been developed to calculate the solar irradiance availability throughout the year. The size of SP is decided based on the irradiance availability. An algorithm has been developed for the favorable energy support from both the grid and SP to the SPTS. The response of SPTS has been verified for three seasons of a year.

The optimal number of e-buses in the solar assisted smart public transit system and its failure analysis has been presented in Chapter-3. ONB is required to manage the passenger's traffic per hour in SPTS. Therefore, an algorithm has been developed to determine the ONB as a function of the load profile, passenger's profile, the energy status of ESD and the energy status of SP. The self-sustainability of SPTS is very important to overcome the failures that exist in SPTS. Therefore, the failure analysis of SPTS has been carried out by considering two types of failures such as: failures from hardware side and the failures from software side. Three isolation switch controllers (ISCs) (suitable algorithms have been developed), an

inductive charging system controller (ICSC) and an aggregator are responsible to manage the failure situations in SPTS. The performance of SPTS for ND and SDs with respect to ONB has been verified. Also, the SPTS response for both types of failures has been verified through simulations.

In Chapter-4, the smart public transportation network expansion and its interaction with the grid has been presented. CBs and EVs have been used along with the e-buses to expand the electrified transportation network in the Guwahati city. A specified EBS of the smart public transportation network has been considered to charge the CBs and EVs along with the e-buses. An algorithm has been developed for CB controller to control the energy flow between ESD and CBs. Also, an algorithm has been developed for EV controller to control the energy flow between ESD and EVs. The SPTS network response with 'only ESD' and 'ESD along with CBs and EVs' has been verified for three seasons of a year. Also, verified the SPTS network response for uncertain situations that exist in the system.

In all these works, the FLC is responsible to manage the energy flow between the grid, ESD and SP. The use of ESD in SPTS is responsible to perform the valley filling and peak shaving during off-peak and peak period. ESD acted as a load to the grid during off-peak period and acted as a source to the grid during peak period. Therefore, ESD has performed the Vpu profile flattening with the help of energy support from both the grid and SP during off-peak and peak period. All the works that are presented in this thesis are beneficial to the passengers, to the grid, to the transportation system and to the Guwahati city.

5.2 Contributions of the present work

The contribution of the presented work in this thesis is to introduce the self-sustainable solar assisted smart public transportation system in the Guwahati city. The main contributions are listed as follows:

i. The energy requirement of the e-bus to travel between the consecutive EBSs is determined using NYCC.

ii. The real time data based dynamic profiles such as: load, solar and commuters have been used in SPTS simulations.

iii. An algorithm has been developed (real time solar data is used) to determine the solar irradiance availability through all the seasons of a year. SP size is decided based on the solar irradiance availability.

iv. The size of ESD is decided with respect to the energy requirement of the e-bus.

v. An algorithm has been developed to minimize SPTS dependence on the grid using the favorable energy from both, the grid and SP.

vi. The results for this work have been explained through two types of case studies. First case explains the benefits of using 'ESD alone' and 'ESD along with SP' in SPTS and the second case explains the SPTS response for three seasons of a year

vii. An algorithm has been developed to determine ONB for normal and special days as a function of the load, SP energy status, commuters profile and ESD energy status.

viii. SPTS failure analysis has been carried out through the algorithm based controllers and aggregators. The complete system is integrated with the grid using FLC and simulated through MATLAB.

ix. Two types of case studies have been considered to explain the simulated results of this work. First case explains the SPTS performance for ND and SD with respect to ONB and the second case explains the SPTS response for different failures that exist in the system

x. The vehicle-dynamics including the road angle is calculated using EMPARX driving cycle and determined the amount of energy required by CB to travel between EBSs.

xi. SPTS network expansion has been performed using CBs and EVs along with the e-buses in the Guwahati city. Both CB's and EV's, charging/discharging performance from/to ESD during off-peak/peak period is controlled through the algorithm based controllers and aggregators.

xii. The entire system is integrated with the grid using FLC. SPTS response has been verified for three seasons of a year, with 'ESD alone' and with 'ESD along with CBs and EVs'. Also, the SPTS response has been verified for the uncertain situations that exist in SPTS.

5.3 Scope for the future research work

This section explains the scope for the future research work.

(i). The different approaches can be used to calculate the vehicle dynamics and to decide the energy requirement of EV.

(ii). Mathematical modeling of the supercapacitor.

(iii). Mathematical modeling of VRB.

(iv). Suitable algorithms can be developed to make SPTS less dependent on the grid.

(v). Optimization algorithms such as genetic algorithm approach and game theory approach can be used to determine the precise number of e-buses in SPTS and to predict the amount of energy transfer between the grid and the energy storage device.

(vi). The design of intelligent public transportation systems using energy consuming devices and energy storage devices.

(vii). Different approaches can be made to avoid the failures that exist in SPTS and make the SPTS self-sustainable.

(viii). SPTS functioning with only solar energy.

(ix). Algorithms can be developed to determine the solar irradiance availability using different methods and to estimate the difference in solar irradiance with these approaches.

(x). Solar energy based EVs operated in harmony with SPTS.

(xi). Renewable energy (solar, wind etc.) based public transportation systems development in city regions.

(xii). The communication technologies can be utilized to pre-detect the bus position, the number of seats available in the bus, the amount of energy required by the bus and bus schedule display based on real time data.

(xiii). The analysis can be carried out for the voltage regulation at the distribution node level using the reactive power control and its impact on the distribution system.

(xiv). SPTS can be utilized as a source for different kinds of transportation vehicles with proper controllers design.

(xv). A study can be carried out to show the benefits of multi input and multi output fuzzy logic controller in public transportation systems.

(xvi). A study can be carried out to show the power factor variations in the distribution network with the presence of SPTS.

The Vehicle dynamics and the e-bus energy requirement calculations

A.1 The vehicle dynamics calculations

The amount of energy required by the e-bus to travel between consecutive EBSs in the Guwahati city ring road circuit is determined using the New York City Drive Cycle (NYCC) [113, 123]. The e-bus travels through the city traffic conditions to cover the distance between EBSs in the Guwahati city. Also, an average speed of 11 km/h is suitable for the e-buses to cover the distance between consecutive EBSs in the Guwahati city ring road circuit. Therefore, NYCC is used as a reference to calculate the energy requirement of e-bus. The speed with respect to time graph of NYCC is shown in Fig. A.1.

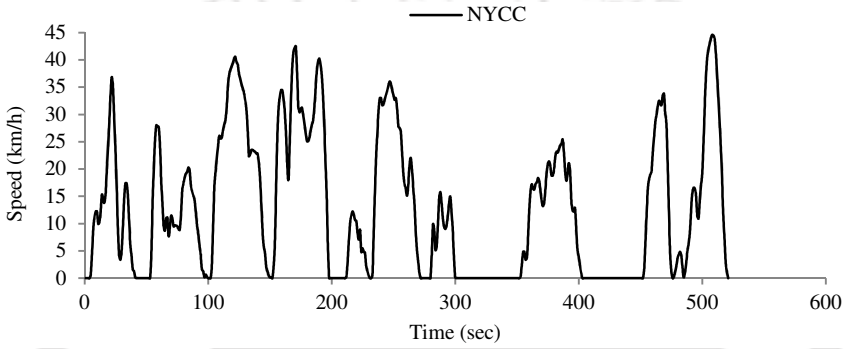

Fig. A.1 New York City Drive Cycle (NYCC)

The various resistive forces that oppose the motion of the e-bus are shown in Fig. A.2.

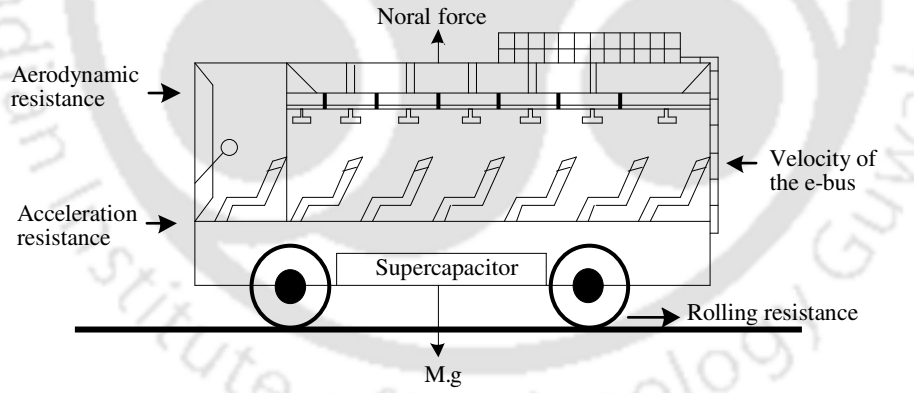

Fig. A.2 The resistive forces acting on the e-bus

The e-bus should overcome all these resistive forces to move on the surface of a road. The resistive forces usually include: the rolling resistance of the tire (F_R), the aero dynamic resistance (F_{AD}) and the acceleration resistance (F_A). The vehicle acceleration (Newton's second law) can be expressed as

$$\frac{dV}{dt} = \frac{\sum(F_t) - \sum(F_r)}{\delta M} \tag{A.1}$$

V is the speed of the vehicle, $\Sigma(F_t)$ is the tractive force required by the vehicle, $\Sigma(F_r)$ is the total resistive force, M is the vehicle mass, δ is the mass factor (converts the rolling component's rotational inertias into translational mass) [123]. The details of different resistive forces that act on the e-bus movement are explained in the following manner.

A.1.1 The rolling resistance (F_R):

The rolling resistance/ rolling friction/ rolling drag, is the force which resists the motion of a vehicle, when the wheels of a vehicle roll on a surface (the tires of a vehicle rolls in contact with the surface of the road. The friction is produced due to the relative motion of two hard surfaces. Both, the road and tires are not rigid. Therefore, both reflex slightly under the load. The gradual deformation exists between the tire and the road (more at the bottom and low at the entry and exit points). The slip of the tire on the road surface causes energy loss and which results in a resistance) [123]. The forward movement produced by the ground reaction force is the rolling resistance movement (T_r) and is given as

$$T_r = P \times a \tag{A.2}$$

P is the normal load acting on the center of the wheel and 'a' is the deformation of the tire. The balancing force of the rolling resistance movement (F_R) is therefore

$$F_R = \left(\frac{T_r}{r_d}\right) = \left(\frac{P \times a}{r_d}\right) = \left(M \times g \times \left(\frac{a}{r_d}\right)\right) = M \times g \times f_r \tag{A.3}$$

r_d is the dynamic radius of tire (m), M is the e-bus's mass (10^4 kg), f_r is the coefficient of rolling resistance (0.01), g is the gravitational acceleration (9.81 m/s^2). 'f_r' is the function of tire (structure, material and inflation pressure), road (material, roughness and presence/absence of liquids on the road) and tread geometry [123].

A.1.2 The aerodynamic resistance (F_{AD}):

The resisting force which acts on motion of a vehicle when it travels in the air is termed as the aerodynamic resistance (F_{AD}) (when an object moves in the dense medium, it collides with the molecules which are present in the medium. Therefore, the molecules absorb some of the energy from the object. The moving objects feel it as a resistance. This resistance is proportional to the medium density and the speed of an object) [123]. Therefore, F_{AD} is expressed as

$$F_{AD} = 0.5 \times \rho_a \times C_D \times A \times V^2 \quad \text{(A.4)}$$

where, ρ_a is the mass density of air (1.184 kg/m^3), C_D is the aerodynamic drag coefficient (0.5), A is the e-bus frontal area (6 m^2) and V is the speed of the vehicle (m/s).

A.1.3 The acceleration resistance (F_A):

The acceleration resistance is influenced by the inertia forces of a vehicle. The force required to overcome the acceleration resistance is more for the greater acceleration of the vehicle (the faster change in speed). Similarly, the accelerating force also rises with the mass of the accelerated vehicle [123]. Therefore, the force required to overcome the acceleration resistance is expressed as

$$F_A = M \times \delta \times \frac{dV}{dt} \quad \text{(A.5)}$$

where, δ is the rotational inertia factor (1.1) and dV/dt is the e-bus acceleration (m/s^2). The road angle is assumed to be zero in these calculations so that the gradient resistance is zero. The tractive force required by the e-bus ($F_{T\ e\text{-}bus}$) to overcome all these resistive forces is expressed as

$$F_{T\ e\text{-}bus} = (F_R + F_{AD} + F_A) = (Mgf_r + 0.5\rho_a C_D A V^2 + M\delta \frac{dV}{dt}) \quad \text{(A.6)}$$

A.2 The e-bus energy requirement calculations

The tractive energy ($E_{T\ e\text{-}bus}$) required by the e-bus is expressed as

$$E_{T\ e\text{-}bus} = \sum_{t=1}^{n} (F_{T\ e\text{-}bus})_t \times (D)_t \quad \text{(A.7)}$$

D is the displacement (m), t is the time instants of NYCC (t= 1, 2, --- n). The regenerative braking energy produced by the kinetic energy of the e-bus ($E_{R\ e\text{-}bus}$) [146] in deceleration/ breaking period is therefore

$$E_{R\ e\text{-}bus} = \gamma \times E_{T\ e\text{-}bus} \quad \text{(A.8)}$$

γ is the fraction of gravitational potential energy ($0 < \gamma < 1$) and is considered as 0.4. Actual e-bus energy ($E_{e\text{-}bus}$) is therefore

$$E_{e\text{-}bus} = E_{T\ e\text{-}bus} - E_{R\ e\text{-}bus} \quad \text{(A.9)}$$

The size of the supercapacitor in e-bus ($C_{e\text{-}bus}$) is expressed as

$$C_{e\text{-}bus} = (2 \times E_{e\text{-}bus}) / (V^2) \tag{A.10}$$

V is the super-capacitor's rated voltage. The energy quantity required by the e-bus to travel between the consecutive EBSs ($E_{e\text{-}bus\ T}$) is therefore

$$E_{e\text{-}bus\ T} = E_{e\text{-}bus\ \max} - E_{T\ e\text{-}bus} + E_{R\ e\text{-}bus} \tag{A.11}$$

$E_{e\text{-}bus\ max}$ is the e-bus maximum energy and is given as

$$E_{e\text{-}bus\ \max} = 2 \times E_{e\text{-}bus} \tag{A.12}$$

The factor 2 in (A.12) is considered to avoid the emergency situations (If the e-bus failed to receive energy from ESD then e-bus crosses consecutive EBSs with $E_{e\text{-}bus\ max}$).

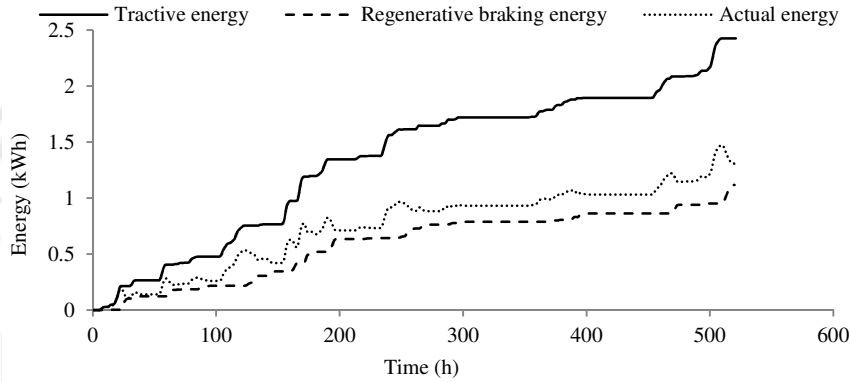

Fig. A.3 The tractive, regenerative and actual energy of the e-bus

The tractive energy needed by the e-bus, the regenerative braking energy produced by the e-bus and the actual energy needed by the e-bus is calculated using NYCC and are shown in Fig. A.3. The solid line represents the tractive energy needed by the e-bus to complete a 2 km distance between the consecutive EBSs. The medium dotted line represents the amount of energy produced by the e-bus during deceleration/braking period while travelling through 2 km distance. The small dotted line represents the actual energy required by the e-bus to complete the distance between the consecutive EBSs in the Guwahati city ring road circuit. The energy rating of the e-bus is given in Table 2.1 (ref. chapter-2). The time required by the e-bus to complete a round trip of travel through the ring road circuit (T_R) is expressed as

$$T_R = \sum_{i=1}^{Bp} (Tx_i + T_{C\ i}) \tag{A.13}$$

where, 'Tx' is the time required by the e-bus to travel from i^{th} EBS to $(i+1)^{th}$ EBS (i = 1, 2… Bp) and T_C is the time required to charge the supercapacitor at EBS.

A. The Vehicle dynamics and the e-bus energy requirement calculations

B

The working principle and equivalent circuit of the supercapacitor

This section explains the details of the supercapacitor working principle, the equivalent circuit model of the supercapacitor and the basic reasons for supercapacitors utilization in SPTS.

B.1 Introduction

The supercapacitors are complementary to the batteries, which deliver high power density (W/L) and low energy density (Wh/L). Also, the supercapacitors have long life cycle than batteries. The frequent stop and go pattern is the common feature for city transportation systems. This requires high power frequently. Therefore, the supercapacitors are well suited for this application rather than batteries (deliver low power density). The supercapacitors are used in the e-buses due to their salient features compared to batteries. The definitions of the basic terminology used in supercapacitor/battery are given in the following manner [149].

The power density (W/L): The maximum amount of power available per unit volume is termed as the power density. It plays major role in deciding the size (which is required to achieve the given target) of the supercapacitor/battery.

The energy density (Wh/L): The amount of energy per unit volume is termed as the energy density. It decides the size (which is required to achieve the given electric range) of the supercapacitor/battery.

The specific power (W/kg): The maximum power availability per unit mass is termed as the specific power (loading). This indicates the loading capability and determines the required weight of the supercapacitor/battery.

The specific energy (Wh/kg): Specific energy (capacity) is the amount energy per unit mass. This indicates the capacity of the supercapacitor/battery. Also, it determines the required weight of the supercapacitor/battery.

The technological growth of the capacitors can be classified into three generations such as: the electrostatic capacitors (first generation), the electrolytic capacitors (second generation) and the electric double layered capacitors/supercapacitors (third generation). The energy density is low in the electric double layered capacitors. Therefore, to overcome this difficulty, the researchers incorporated carbon along with the transition metal oxide (have a wide variety of surface structures) in the electrodes. The oxide electrode material consists of

a specific capacitance 10 to 100 times. In such situation the electric double layered capacitor is called as the supercapacitor or pseudo-capacitor [150].

B.2 The working principle of the supercapacitor

Supercapacitor is the fourth generation capacitor. The structure of the supercapacitor is shown in Fig. B.1. The supercapacitor consists of two electrodes, two collectors, an electrolyte and a separator. The electrolyte contains dissolved and solvated ions which connect the electrodes to each other electrically. The electrolyte contains the mixture of liquid/viscous conductive mixture of an organic solvent. The electrolyte defines the characteristics of the supercapacitor in terms of the peak current capability and the range of operating voltage and the temperature. The electrodes are separated by a separator which prevents the internal short circuits. The electrodes are connected to the outside terminals to access the power. The electrodes should show the following features: good conductivity, high resistant for corrosion, high surface area per unit volume and high stability for both chemical and temperature [150]. The capacitance of the supercapacitor is the function of electrode structure, ion mobility in electrolysis and the frequency.

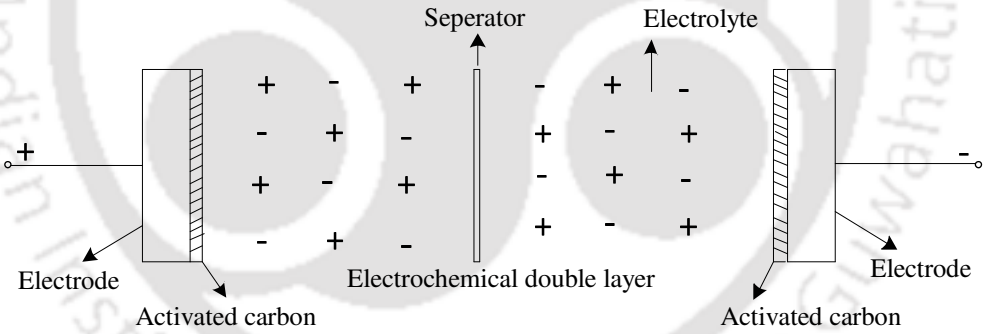

Fig B.1 Structure of the supercapacitor

The activated carbon is placed along with the electrodes of the supercapacitor as shown in Fig. B.1. The supercapacitor works based on the carbon (nanotube) technology (creates a very huge surface area with an extremely small distance of separation between the electrodes). The activated carbon in the supercapacitor creates a physical barrier and it acts as the dielectric material. A double layered electric field is generated in the supercapacitor when the electric charge is applied to the electrodes. Therefore, the electric double layer acts as a dielectric in the supercapacitor. The electric double layer's thickness is as thin as a molecule. The surface area is equal to several thousands of square meters per gram in the activated

carbon. Therefore, this large surface area allows the maximum amount of ions absorption as shown in Fig. B.2. Charging and discharging performance exists in an ion absorption layer formed on the electrodes of activated carbon [150, 151].

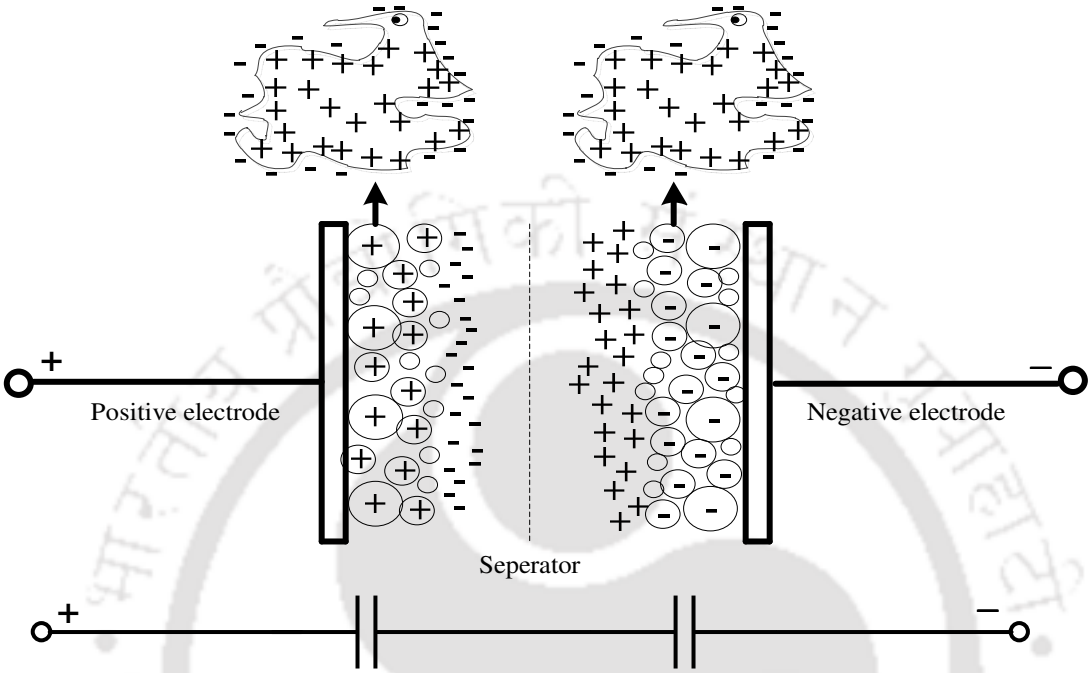

Fig B.2 The electrochemical action (double electric field) in the supercapacitor

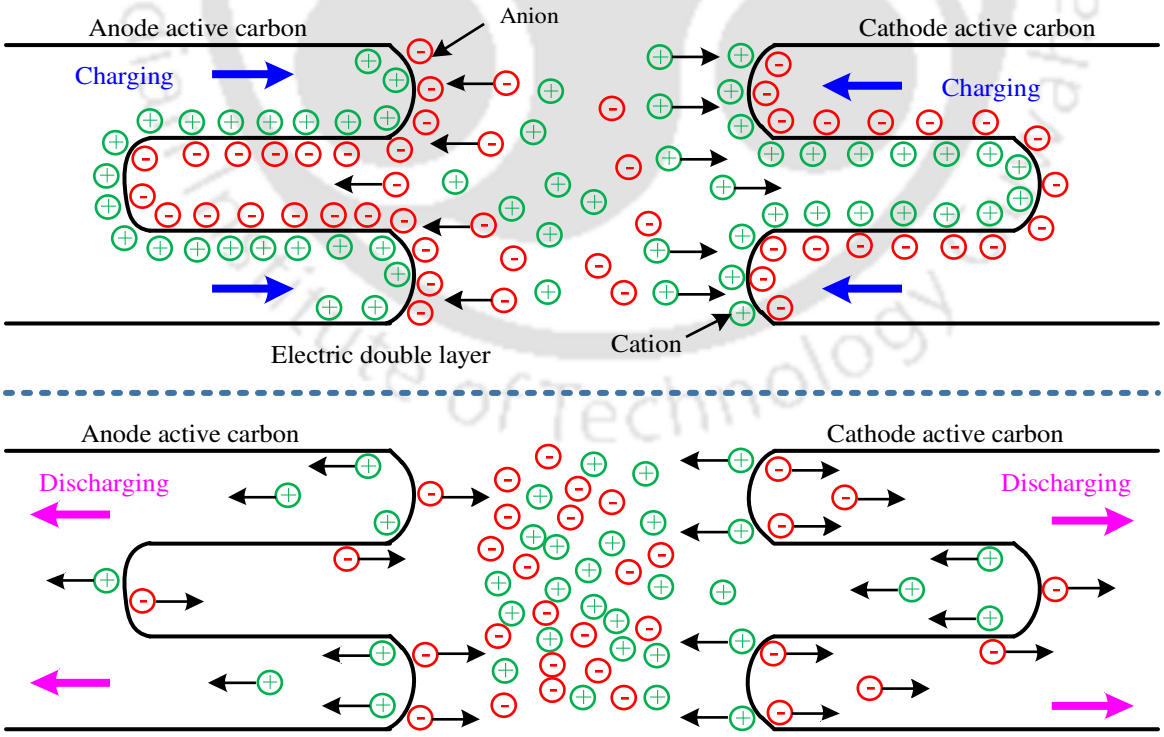

Fig. B.3 The charge separation in supercapacitor during charging and discharging mode

The activated carbon electrodes are impregnated with an electrolyte where the positive and negative charges are formed between the electrodes and the impregnate as shown in Fig. B.2. The electric double layer act as an insulator until a suitable voltage is applied and the current begins to flow. The voltage magnitude is, where the charges begin to flow and where the electrolyte begins to break down. Therefore, this voltage is the decomposition voltage. The supercapacitors can fulfill the gap between the batteries and the conventional capacitor. The supercapacitor can store electric charge in the order of 10^6 Farads [151, 152].

The charge separation in the supercapacitor during charging and discharging mode is shown Fig. B.3. In the charging mode all the anions from the electrolyte move towards the anode (positively charged electrode coated with activated carbon) and all the cations move towards the cathode (negatively charged electrode coated with activated carbon). At the interface between electrode and the electrolyte, an array of the charged particles exists. This array acts as a dielectric medium with a very thin layer. In discharging mode all the cations and anions are moving back to their original position in the electrolyte near from the electrodes and the charged particles are moving from the electrodes to the external circuits [152].

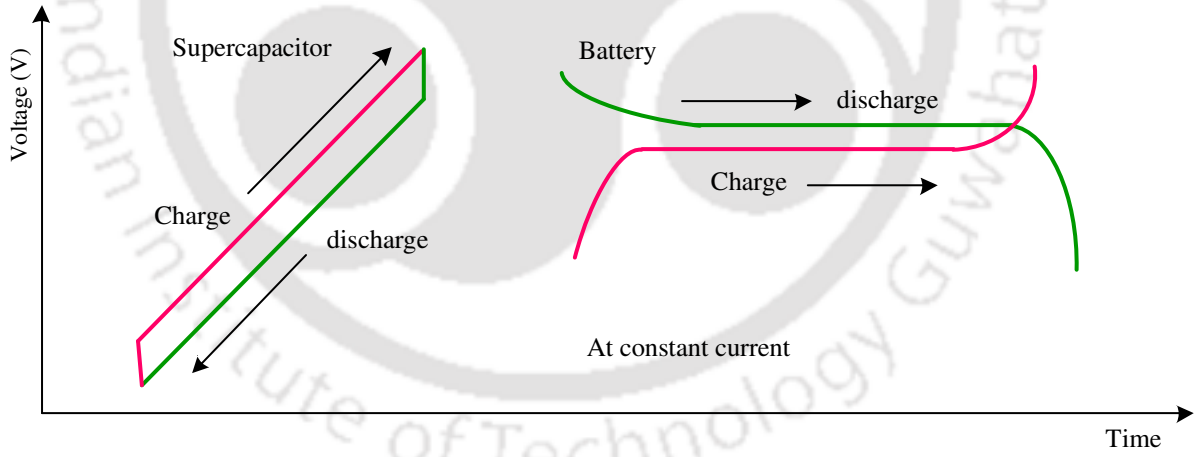

Fig. B.4 The rate of charge/discharge of the supercapacitor and the battery

The graph in Fig. B.4 shows the charge/discharge rate comparison of the supercapacitor with the battery. The supercapacitor performs the charging/discharging operation with a fast rise in voltage at constant current as shown in Fig. B.4. The battery performs the charge/discharge operation with exponential rise/fall of voltage at initial/final state, and then maintains a constant voltage between initial and final states as shown in Fig. B.4. The comparison of two graphs from Fig. B.4 shows that the supercapacitors are having fast

charge/discharge rate compared to batteries. The advantages that the supercapacitors show compared to rechargeable batteries are: long life time, higher power density, high peak currents, maximum charge/discharge cycles, low cost, low losses, less weight and high efficiency. The applications of the supercapacitors are: computer and ups systems, automobile regenerative breaking systems, power generators, welders, power conditioners, cameras, traction energy, space flight technology, power supplies and power electronics [149]-[152].

B.3 The equivalent circuit of the supercapacitor

The super-capacitor's equivalent circuit is shown in Fig. B.5. The supercapacitor performance can be represented by its terminal voltages during charging/discharging mode with different current ratings [152]. Three parameters are involved in the super-capacitor's equivalent circuit such as: the capacitance of the supercapacitor (C), the series resistance (R_S) and the dielectric leakage resistance (R_L) as shown in Fig. B.5. The supercapacitor performance in charging and discharging modes of operation are given in the following manner.

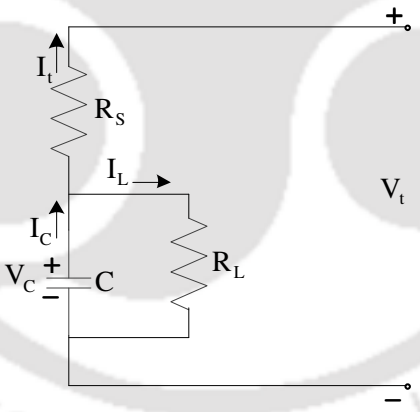

Fig. B.5 The equivalent circuit of the supercapacitor

B.3.1 Discharging mode:

The terminal voltage of the supercapacitor during the discharging mode (ref. Fig. B.5) is expressed as

$$-V_C + (I_t \times R_S) + V_t = 0 \tag{A.1}$$

$$V_t = V_C - (I_t \times R_S) \tag{A.2}$$

V_t is the terminal voltage, I_t is the current to/from the terminal and V_C is the voltage across the capacitor. The capacitor current (I_C) and the leakage current (I_L) can be expressed as

$$I_C = I_t + I_L \tag{A.3}$$

$$I_L = \frac{V_C}{R_L} \tag{A.4}$$

The electric potential of the capacitor is therefore

$$I_C = C \times \frac{dV_C}{dt} \;\Rightarrow\; \frac{dV_C}{dt} = \frac{I_C}{C} = \frac{(I_t + I_L)}{C} = \left(\frac{I_t}{C} + \frac{V_C}{C \times R_L}\right) \tag{A.5}$$

The operating efficiency in discharging mode (η_D) can be expressed as

$$\eta_D = \frac{V_t \times I_t}{V_C \times I_C} = \frac{(V_C - (I_t \times R_S)) \times I_t}{V_C \times (I_t + I_L)} \tag{A.6}$$

B.3.2 Charging mode:

The terminal voltage of the supercapacitor during charging mode (ref. Fig. B.5) is expressed as

$$-V_t + (I_t \times R_S) + V_C = 0 \tag{A.7}$$

$$V_t = V_C + (I_t \times R_S) \tag{A.8}$$

The capacitor current is therefore

$$I_C = I_t - I_L \tag{A.9}$$

The operating efficiency in charging (η_C) mode can be expressed as

$$\eta_C = \frac{(V_C \times I_C)}{(V_t \times I_t)} = \frac{V_C \times (I_t - I_L)}{(V_C + (I_t \times R_S)) \times I_t} \tag{A.10}$$

In actual operation 'I_L' is very small and can be ignored. Thus (A.6) and (A.10) becomes

$$\eta_D = \frac{(V_C - (I_t \times R_S))}{V_C} = \left(\frac{V_t}{V_C}\right) \tag{A.11}$$

$$\eta_C = \frac{V_C}{(V_C + (I_t \times R_S))} = \left(\frac{V_C}{V_t}\right) \tag{A.12}$$

The above equations indicate the energy loss caused by the series resistance in the supercapacitor. The efficiency of the supercapacitor decreases at maximum current rate and minimum cell voltage. The energy stored in the supercapacitor can be obtained as

$$E_C = \int_0^1 V_C \times I_C \times dt = \int_0^V V_C \times C \times dV_C = \frac{1}{2} C V_C^2 \quad \text{(A.13)}$$

Above equation shows, an increase in the supercapacitor voltage increases the stored energy of the supercapacitor. The specifications of the supercapacitor cell are given in Table B.1.

Table B.1: The specifications of the supercapacitor cell

Variable	*Cell rating*
Capacitance (F)	2600
The maximum series resistance ESR (mΩ)	0.7
Voltage (V)	2.5-2.8
The specific power (W/kg)	4300
The specific energy (Wh/kg)	4.3
Maximum current (A)	600
Weight (kg)	0.525
Volume (L)	0.42
Operating temperature (^{0}C)	-35 to +65
Leakage current (mA)	5

The specific power of the different storage devices are given in Table B.2.

Table B.2: The specific power of different storage devices

Storage material	*Specific power (W/kg)*
Li-ion battery	250-340
VRB	100-150
Normal capacitor	10
Supercapacitor	10000

The specific energy and the energy densities of different storage devices along with the supercapacitor are given in Table B.3.

Table B.3: The specific energy and the energy densities of different storage devices

Storage material	*Specific energy (MJ/kg)*	*Specific energy (Wh/kg)*	*Energy density (MJ/L)*	*Energy density (Wh/L)*
Petrol/diesel	46	12880	36	10080
Coal	24	6.72	-	-
Li-ion batteries	0.36-0.875	100-245	0.9-2.63	252-736
Ni-Hydride	0.288	80.64	0.504-1.08	141-302.4
Lead acid	0.17	47.6	0.34	95.2
VRB	0.1008	28	0.169	47
Normal capacitor	0.000036	0.01	-	-
supercapacitor	0.018	5.04	-	-

C

The working principle and equivalent circuit of Vanadium redox flow battery (VRB)

This section explains the working principle of the Vanadium redox flow battery (VRB), the importance of VRB in SPTS and the details of equivalent circuit model of VRB.

C.1 Introduction

The battery technology has been developed mainly for two purposes. One is for electric vehicles and the other is for the stationary applications. The details of battery technology and their use in different applications are given in the following manner.

C.1.1 Batteries for electric vehicles

Internationally, there is an increased interest in the development of modern battery powered electric vehicles. Batteries are the enabling technology for the electric drive vehicles. In 19th century almost of all the electric vehicles were powered with lead acid batteries [111]. In 20th century nickel iron battery has been developed with slight higher energy density. This battery has achieved an improved performance over lead acid battery. In 20th century, varieties of batteries have been developed for the electric vehicles such as: Nickel-cadmium batteries, Nickel-zinc batteries, Sodium-metal chloride batteries, Sodium-sulfur batteries, Zinc-bromine batteries, Zinc-chlorine batteries and Li-ion batteries. All these batteries support energy to the electric vehicle less than 100 miles. The large lithium-ion batteries were developed by Sony and Hitachi for electric vehicle applications in the early 1990s with high energy ratings. They designed thin electrodes in the lithium-ion battery to provide high power. With the introduction of lithium-ion battery the serious safety issues were mitigated and the battery technology has been improved to a significant level.

C.1.2 Batteries for stationary storage applications

The extended role of the energy storage systems in the transmission and distribution side of the electric grid started in late 1980s and in early 1990s [111]. These batteries were developed for the national benefits. The batteries for stationary energy storage applications can be divided into two categories. In the first category: the Sodium-beta high temperature battery and the Sodium/sulfur batteries were developed. The limitations with these batteries are: safety issues, durability and the thermal management. In the second category: the flowing electrolyte batteries were developed. The flow type battery (zinc/chlorine hydrate battery) is invented in 1968. Thereafter, the work on this type of batteries has been started.

The flow type batteries are of two types. First one is Zinc/bromine flow type batteries. These batteries have the following disadvantages such as: the temperature control issues, safety issues and improvements are needed to moderate power capability. Second one is Vanadium redox flow type batteries. NASA has conducted a development program to develop the redox flow batteries using ferric chloride ($FeCl_3$) as the oxidizing agent (positive) and chromium chloride ($CrCl_2$) as the reducing agent (negative)) for stationary energy storage applications. Thereafter, the work on the redox flow battery has been started. The words 'reduction' and 'oxidation' were decreased to the term 'redox'. These batteries are used in the electrochemical systems (oxidation and reduction involves in ionic species solution and the reactions take place on the inert electrodes). The active materials in these batteries are stored externally from the electrode cells.

The Vanadium Redox flow Battery (VRB) was introduced in the year 1988. Thereafter, a significant development has been achieved for the higher level electrical energy storage. The VRB is well suited for the large scale energy storage applications. VRB has the following features: high capacity, long life span, minimum maintenance and quick response to rapid changes [153, 154]. VRB is an electrochemical cell divided into two components. One is the ionic membrane (battery reactions exist) and the other is storage tanks (vanadium electrolyte (positive and negative) is stored).

VRB provides the voltage support and peak load relief to the load served by the distribution feeder and also, improves the power quality in the distribution grid. The working model of VRB is shown in Fig. C.1. The components that are involved in the VRB model are: the electrolyte (electrolyte stays at different valance states of vanadium sulfate in the positive and negative electrode components of VRB. The sulfuric acid is the supporting electrolyte for this solution and stays at 2 molar in concentration), the electrolyte storage tanks, cell stacks (electrodes), control unit and the converter unit. Electrolyte is the solution of Vanadium in dilute sulfuric acid and this solution is electrochemically oxidized or reduced to store energy. The nitrogen air pads are used to prevent the oxidation.

The VRB works in the following manner. The electrolyte is pumped from storage tanks through cell stacks (positive and negative electrodes) and the electrical energy is added to the cell stacks to charge the electrolyte. The charged electrolyte is pumped through cell stacks when the energy required as shown in Fig. C.1 [153, 154]. The converter unit is used to

convert ac-dc when charge energy from the source and dc-ac when discharge energy to the load. The control panel is used to operate the VRB remotely. The applications of VRB are: renewable energy and remote area power supplies, wind and solar energy storage coupled with diesel generation for fuel and emission reduction, commercial and industrial facilities, ancillary services for utilities, telecommunications and backup power systems.

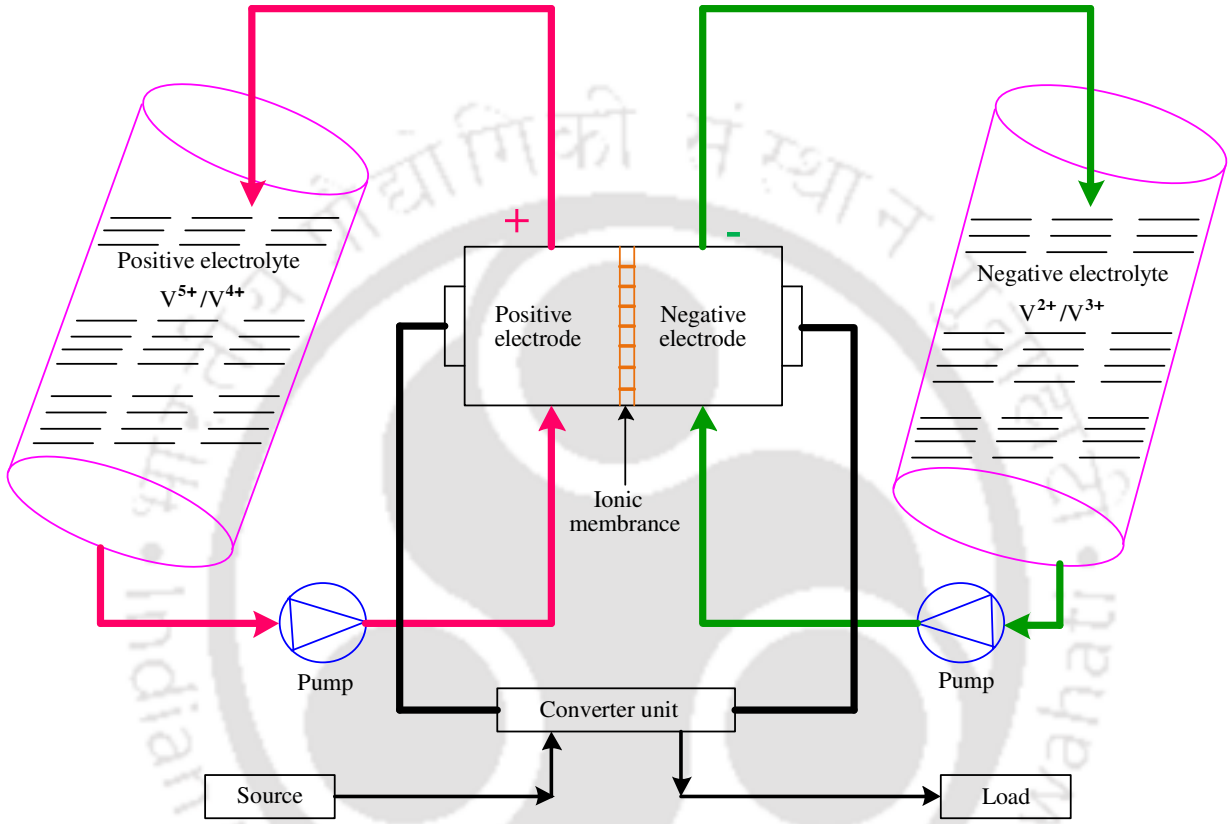

Fig. C.1 The working model of VRB

The power availability in VRB depends on the size of the electrodes in the cell stacks. The amount of energy stored in VRB is the function of active chemical substances and the state of charge (*SOC*). The chemical reactions that are taken place in VRB cell during charging and discharging operations are expressed as

$$V^{4+} - e^{-} \leftrightarrow V^{5+} \tag{C.1}$$

$$V^{3+} + e^{-} \leftrightarrow V^{2+} \tag{C.2}$$

(C.1) is for positive electrode and (C.2) is for negative electrode.

C.2 The equivalent circuit model of VRB

The equivalent circuit model of VRB is shown in Fig. C.2 [153, 154]. The terminal voltage of the battery is calculated by using the following equations. The battery cell EMF (V_{cell}) depends on *SOC* and according to 'Nernst equation' it is expressed as

$$V_{cell} = V_{equilibrium} + 2\times\left(\frac{RT}{F}\right)\times\ln\left(\frac{SOC}{1-SOC}\right) \tag{C.3}$$

$V_{equilibrium}$ is the normal battery EMF, R is the molar gas constant (R=8.314 j/mol. K), T is the temperature (K) and F is the faraday's constant (F=9.65x10^4 C/mol).

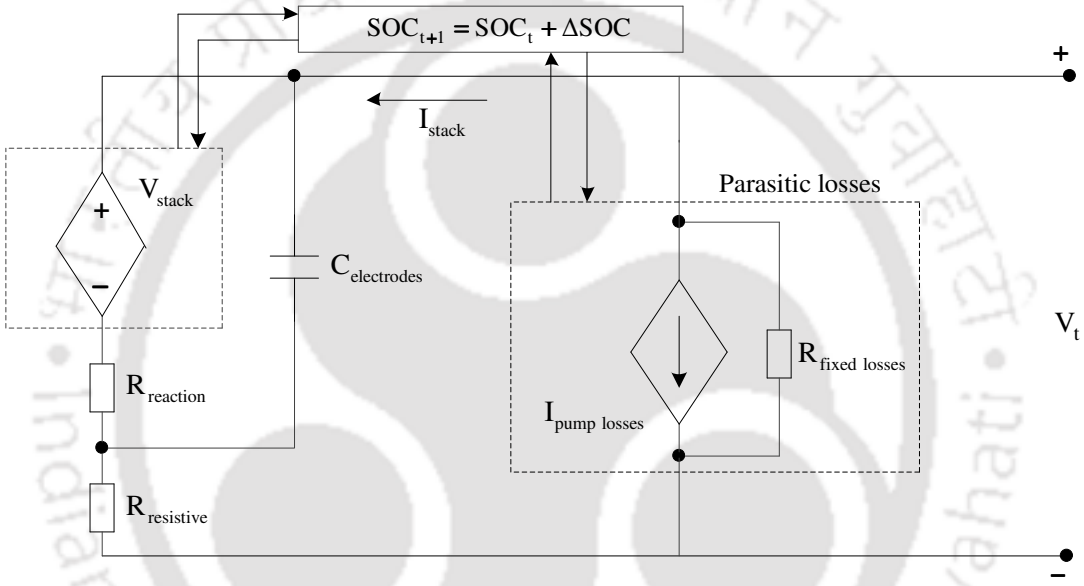

Fig. C.2 The equivalent circuit model of VRB

Total EMF of the battery stack for 'n' cells connected in series is therefore

$$V_{stack} = n\times V_{cell} \tag{C.4}$$

Stack of the battery is modeled as a controlled voltage source and is determined by the state of charge and the number of series connected battery cells.

$$V_t = V_{stack} - I_{stack}\times\left(R_{reaction} + R_{resistive}\right) \tag{C.5}$$

The equivalent internal resistance includes $R_{reaction}$ and $R_{resistive}$, which accounts for losses associated with the resistances (mass transport, membrane, solution, electrode and bipolar plate) and reaction kinetics. However, these losses are constant during overall battery operation. Assuming the power loss caused by all these resistances is σ_1% and the battery stack power (P_{stack}) loss is σ_2%, then $R_{reaction}$ and $R_{resistive}$ are expressed as

$$R_{reaction} = \left(\frac{\sigma_1 \% \times P_{stack}}{I_{\max}^2} \right) \tag{C.6}$$

$$R_{resistive} = \left(\frac{\sigma_2 \% \times P_{stack}}{I_{\max}^2} \right) \tag{C.7}$$

The parasitic losses include fixed power loss (P_{fixed}) modeled as fixed resistance (R_{fixed}) and variable power loss ($P_{variable}$) modeled as controlled current source (I_{pump}). Assuming that these losses occupy $\sigma_3\%$ and $\sigma_4\%$ of P_{stack} separately, then

$$P_{stack} = \left(\frac{P_{rating}}{1 - \sigma\%} \right) \tag{C.8}$$

P_{rating} is the rated power and $\sigma\%$ is the total power loss of the battery ($\sigma_1\%+\sigma_2\%+\sigma_3\%+\sigma_4\%$).

$$R_{fixed} = \left(\frac{V_{stack}^2}{P_{fixed}} \right) = \left(\frac{V_{stack}^2}{\sigma_3 \% \times P_{stack}} \right) \tag{C.9}$$

$$I_{pump} = \left(\frac{K}{V_{stack}} \times \frac{I_{stack}}{SOC} \right) \tag{C.10}$$

K (0.425) is the recirculation pump power loss constant. The battery terminal current is given as

$$I_t = \left(I_{stack} + \frac{V_t}{R_{fixed}} + I_{pump} \right) \tag{C.11}$$

The SOC is calculated from the following equation

$$SOC = \left(\frac{Current\ energy\ in\ the\ battery}{Total\ energy\ capacity\ of\ the\ battery} \right) \tag{C.12}$$

The change in SOC (ΔSOC) is therefore

$$\Delta SOC = \left(\frac{\Delta E}{E_{capacity}} \right) = \left(\frac{P_{stack} \times time\ step}{E_{capacity}} \right) = \left(\frac{I_{stack} \times V_{stack} \times time\ step}{P_{rating} \times time\ rating} \right) \tag{C.13}$$

The electrode capacitor is represented by measuring battery cell capacitor and is based on the connection type of the cell. The calculations of the VRB equivalent circuit parameters are based on the total losses of 21%, where the parasitic losses are 6% in worst operating conditions and the 15% loss is due to internal resistances. These losses can be varied based on the charge and discharge rate of VRB [153, 154].

Solar energy and the solar irradiance availability determination

D.1 The solar irradiance availability determination

The solar power generation is proportional to the solar irradiance availability of a particular region. The solar irradiance availability is calculated based on the real time solar data collected from the India Meteorological Department (IMD), Guwahati, Assam, India [124]. The collected solar data has the details of longitude (σ), latitude (Φ), relative humidity (RH) and air temperature (T). The details of the necessary steps that are required to calculate the solar irradiance (G) are listed in the following manner.

(i). Solar constant (S): Solar constant is the amount of energy received at the top of the Earth's atmosphere on a surface oriented perpendicular to the sun's rays (at the mean distance of the Earth from the Sun) [125]. The satellite measured yearly average solar constant is 1367 W/m^2 [125]. Therefore, the solar constant is

$$S = 1367 \ W/m^2 \tag{D.1}$$

The irradiance is defined as: the total power falling on the unit surface area from a radiant source. The total energy flux (E) incident on the Earth is expressed as

$$E = S \times \Pi R^2 \tag{D.2}$$

where, R is the Earth's radius. The average flux (F_{avg}) incident on the unit surface area is therefore

$$F_{avg} = \frac{S \times \Pi R^2}{4\Pi R^2} = 342 \ W/m^2 \tag{D.3}$$

(ii). Hour angle (ω): The hour angle is used to compute the Sun's path in the sky. The hour angle converts the local solar time into degrees to trace the Sun movement across the sky. At solar noon the hour angle is 0^0. The Earth rotates 15^0 per hour. Therefore, each hour away from solar noon (0^0) corresponds to an angular motion of the Sun in the sky. The hour angle is negative in the morning hours and positive in the afternoon hours [155]. Therefore, the hour angle is given as

$$\omega = 15^\circ \times (LST - 12) \tag{D.4}$$

LST is the local solar time and is defined when the sun is highest in the sky (twelve noon) [155]. The local time varies from LST. The details about the LST calculations are given in the following manner. The Local Standard Time Meridian ($LSTM$) is a reference meridian used for a particular time zone and is expressed as

$$LSTM = 15° \times \Delta T_{GMT} \tag{D.5}$$

15°= 360°/24 hours. ΔT_{GMT} is the difference of the Local Time (*LT*) from Greenwich Mean Time (*GMT*) in hours and is expressed as

$$\Delta T_{GMT} = LT - GMT \tag{D.6}$$

The equation of time (in minutes) (*EOT*) is used to correct the eccentricity of the Earth's orbit and the Earth's axial tilt [125]. Therefore *EOT* is expressed as

$$EOT = 9.87 sin\,(2A) - 7.53 cos(A) - 1.5 sin(A) \tag{D.7}$$

where, *A* (in degrees) is given as

$$A = \frac{360}{365}(d - 81) \tag{D.8}$$

where, *d* is the day number from the start of a year. The variation of *LST* and σ within the time zone is represented with the time correction factor (*TC*) and is expressed as

$$TC = 4 \times (\sigma - LSTM) + EOT \tag{D.9}$$

For every 4 minutes, the Earth rotates 1 degree. Therefore, the factor 4 is considered in (D.9). The *LST* is expressed as

$$LST = LT + \frac{TC}{60} \tag{D.10}$$

(iii). Solar declination (δ): Solar declination is the angle between the line joining the centers of the Sun and the Earth and the equatorial plane [125]. This angle varies in-between -23.45^0, 0^0, 0^0 and 23.45^0 for winter, vernal, autumnal and summer solstice respectively [125, 126]. The approximate solar declination is expressed as

$$\delta = \Pi \times \left(\frac{23.45}{180}\right) \times sin\left(2\Pi \frac{(284 + n)}{365}\right) \tag{D.11}$$

where, *n* is the day number in a year (*n*=2 on 2nd January, for example).

(iv). Zenith angle (θz)/solar elevation (α): The angle between the Sun's direction and the horizon is the solar elevation α, whose complement to 90^0 is zenith angle θ_z [125]. These angles define how high the Sun is. The solar elevation is expressed as

$$sin\alpha = (sin\delta \times sin\Phi) + (cos\delta \times cos\Phi \times cos\omega) = cos\theta_Z \tag{D.12}$$

where, Φ is the geographical latitude.

(v). Solar azimuth angle (ψ): This angle defines in which direction the Sun is. The solar azimuth is zero at solar noon and increases towards the east [125]. Therefore, the solar azimuth is expressed as

$$cos\psi = \left(\frac{(sin\alpha \times sin\Phi) - sin\delta}{cos\alpha \times cos\Phi} \right) \tag{D.13}$$

(vi). Sunrise hour angle (ω_S): The Sunrise hour angle is the angular measurement of time in degrees from the solar noon [125]. At solar noon ω_S is 0^0. Therefore, the Sunrise hour angle is given as

$$\omega_S = cos^{-1}(-tan\Phi \times tan\delta) \tag{D.14}$$

Irradiance (B_0) received by the unit horizontal area, outside the Earth's atmosphere is therefore

$$B_0 = \frac{24}{\Pi} \times S \times \left(1 + 0.33cos\left(\frac{2\Pi d_n}{365} \right) \right) \times \left((cos\Phi \times cos\delta \times sin\omega_S) + (\omega_S \times sin\Phi \times sin\delta) \right) \tag{D.15}$$

where, d_n is the day number in a year. The 'extraterrestrial irradiance' (G_{ex}) is the available solar irradiance at the outer edge of the Earth's atmosphere [126]. Therefore, G_{ex} is expressed as

$$G_{ex} = S \times sin\alpha \tag{D.16}$$

If α is greater than zero then proceed for further calculations, otherwise G_{ex} is zero. The solar irradiance on the Earth surface is 30% lower due to the scattering and reflection of irradiance. Therefore the average solar irradiance on the ground is expressed as

$$G_{avg} = 0.7 \times F_{avg} \times 24 \tag{D.17}$$

The clearness index (K_T) is therefore

$$K_T = \left(G_{ex} / B_0 \right) \tag{D.18}$$

The diffuse radiation (D) is given as

$$D = \left((1 - 1.13K_T) \times G_{ex} \right) \tag{D.19}$$

The beam radiation (B) is expressed as

$$B = \left(G_{ex} - D\right) \tag{D.20}$$

The beam radiation $B(\theta)$ with respect to panel angle (θ) is therefore

$$B(\theta) = B \times \left(\frac{(cos(\Phi - \theta) \times cos\,\delta \times sin\,\omega_0 + \omega_0 \times sin(\Phi - \theta) \times sin\,\delta)}{(cos\,\Phi \times cos\,\delta \times sin\,\omega_S + \omega_S \times sin\,\Phi \times sin\,\delta)} \right) \tag{D.21}$$

where: $\omega_0 = min\left(\omega_S, \omega_S^1\right);\ \omega_S^1 = cos^{-1}\left(-tan(\Phi - \theta) \times tan\delta\right)$

The diffusion radiation with respect to 'θ' ($D(\theta)$) is therefore

$$D(\theta) = 0.5 \times (1 + cos\theta) \times D \tag{D.22}$$

The irradiance reflected from the ground ($R(\theta)$) is given as

$$R(\theta) = 0.5 \times (1 - cos\theta) \times \rho \times G_{ex} \tag{D.23}$$

where, ρ is the reflectivity of the ground. Total global irradiance $G(\theta)$ on the inclined surface is expressed as

$$G(\theta) = B(\theta) + D(\theta) + R(\theta) \tag{D.24}$$

The atmospheric effect on the solar irradiance is calculated through the following expressions.

(vii). The cloud effect on irradiance from upper air humidity:

The atmospheric layer is divided into three sub-layers based on the pressure level [128]. The lower-layer stays between 800-1000 hpa (hpa is the hector Pascal, the unit for pressure and 1 hpa = 0.750061683 torr (1 torr = 133.3 Pascal's), the middle-layer stays between 400-800 hpa and the upper-layer stays below 400 hpa. The water vapor ($W.V$) content of air is termed as humidity. The cloud amount depends on the relative humidity (RH) rather than the specific humidity and is expressed as

$$RH = \frac{Actual\ W.V\ in\ the\ air}{Max.\ W.V\ \ the\ air\ can\ hold\ at\ a\ agiven\ T} \tag{D.25}$$

T is the temperature. The cloud exists when RH exceeds normal RH value (RH_n) and the cloud amount in three layers is expressed as

$$C_i = \left(\frac{1}{(P_{Li} - P_{Ui})} \right) \times \left(\int_{P_{Ui}}^{P_{Li}} Max\left(0.0, \frac{(RH - RH_{ni})}{(1 - RH_{ni})}\right) dp \right) \tag{D.26}$$

P_{Li} and P_{Ui} are the pressure at the lower and upper levels of individual layer 'i' (i= lower (l), middle (m) and upper layers (u)). RH_n values are assumed to be 66%, 50% and 40% for three layers respectively (j= l, m and u) for cloud generation. The following expression is used to express the variations in RH_n for three layers

$$RH_{ni} = RH_{nj} + \beta(45^0 - \Phi) \tag{D.27}$$

where, β is the optimized co-efficient and is considered as 0.003/deg, and Φ is the latitude (decrease in Φ causes the increase in RH_n). Since, the solar radiation passes through all these layers. Therefore, the clearness indicator (SCI) with respect to the total cloud effect is given as

$$SCI = \prod_{i=l}^{u}(1 - C_i) \tag{D.28}$$

where, i= l, m and u. SCI is used to calculate the cloud attenuation to the actual global solar irradiance and is expressed as

$$\frac{G}{G_0} = \frac{f(SCI)}{1 - r_s r_a} \tag{D.29}$$

where, G is the actual global solar irradiance (W/m^2), G_0 is the global solar irradiance (W/m^2) (D.24), r_s is the surface albedo to solar irradiance, r_a is atmospheric reflectivity from the surface of the earth. The surface albedo is a function of surface material. For the surface covered with snow, the albedo depends on snow existing time. Therefore r_s is expressed as

$$r_s = r_{sz} + r_{sm} \tag{D.30}$$

$$r_{sz} = 0.01 \times \left[\exp\left(0.003286\theta_z^{1.5}\right) - 1\right] \tag{D.31}$$

where, θ_z is the zenith angle, r_{sm} is the least albedo with θ_z = 0 (r_{sm} is 0.14 for bare soil and vegetation covered surface and 0.5 for the surface covered with snow). Therefore, r_a depends on cloud fraction (C_T) and is expressed as

$$r_a = 0.685 + 0.4195 C_T \tag{D.32}$$

where, C_T is given as

$$C_T = 1 - SCI \tag{D.33}$$

The quadratic polynomial is used to approximate the function $f(SCI)$ and included in (D.29).

D.2 Solar energy calculations

The characteristic equation of the diode is expressed as

$$I_D = I_S \times \left[exp\left(\frac{V_D}{n \times V_T} \right) - 1 \right] \tag{D.34}$$

where, I_D is the diode current, 'I_s' is the reverse bias current (for silicon diodes it is 10^{-12} A and for germanium diodes it is 10^{-6} A), V_D is the voltage across the diode (V_D=0.65 V for silicon diode and V_D=0.3 V for germanium diode), n is the ideal or quality factor (n=1) and V_T is the thermal voltage (approximately equal to 25.85 mV at 300 K) and is given as

$$V_T = \frac{kT}{q} \tag{D.35}$$

where, k is the Boltzmann constant (k=1.38 x 10^{-23} J/K or k=8.62 x 10^{-5} eV/K), T is the absolute temperature of the p-n junction (K) and 'q' is the charge magnitude of electron (q=1.602 x 10^{-19} C).

D.2.1 The solar cell's equivalent circuit

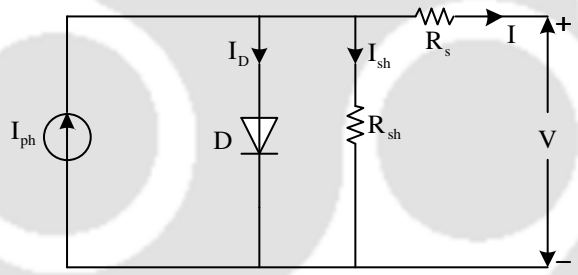

Fig D.1 The solar cell's equivalent circuit

The solar cell's equivalent circuit with the p-n junction (represented with an ideal current source I_{ph} in parallel with a diode), series resistance R_s and the parallel resistance R_{sh} is shown in Fig. D.1. Under open circuit condition without R_s and R_{sh}, the continuous equalization current flows through the circuit in such a manner: I_{ph} flows from n-side to p-side resumes flowing through the diode from p-side to n-side as current I_D [126]. This means the total current generated from the light flows through the diode in open circuit condition. Under short circuit condition all this current flows through the external load. The solar cell output current expression as a function of voltage 'V' is expressed as

$$I = I_{ph} - I_D - I_{sh} \tag{D.36}$$

I_{ph} is the photo current (proportional to the solar irradiance), I_D is diode current and I_{sh} is the current flows through R_{sh}. I_{ph} is expressed as

$$I_{ph} = \left(I_{SC} + k_i(T - 298)\right) \times \left(\frac{G}{1000}\right) \tag{D.37}$$

I_{SC} is the short circuit current (full current capacity of photo current), k_i is the short circuit current temperature co-efficient (k_i=0.0017 A/^{0}C) of the solar cell and G is the solar irradiance (W/m^2). The solar cell output current is therefore

$$I = I_{ph} - I_S \times \left[\exp\left(\frac{V_D}{n \times V_T}\right) - 1\right] - \left(\frac{(I \times R_s) + V}{R_{sh}}\right) \tag{D.38}$$

The open circuit voltage of the solar cell is given as

$$V = V_{OC} = n \times V_T \times \ln\left(1 + \frac{I_{SC}}{I_S}\right) \tag{D.39}$$

where, V_T is given as: $V_T = \dfrac{N_S \times k \times T}{q}$

'*Ns*' is the number of series connected solar cells. The output power is expressed as

$$P = V \times I \tag{D.40}$$

The amount of energy that the solar cell produces is given as

$$E = P \times dt \tag{D.41}$$

where, '*dt*' is the change in time (in hours).

The working principle of Fuzzy logic controller

This section explains the working principle of the fuzzy logic controller (FLC) and the step by step procedure to build the FLC in MATLAB.

E.1 Introduction

Two types of controllers are common in the power system control applications. One is, proportional plus integral controller (PI controller), and the other is proportional plus integral plus derivative controller (PID controller). An error signal is generated by comparing the standard signal with the reference signal. This signal is the input for these controllers. The gain should be adjusted to get the desired response by tuning the controller's parameters. This is the main drawback with these controllers. In SPTS, many controlling parameters are present. Therefore, it is difficult to control all these parameters by tuning the gains of every controller's parameter. Therefore, a suitable controller which is free from gain tuning is required in SPTS. FLC is more suitable to fulfill all the above mentioned criteria. Therefore, FLC is used in SPTS.

E.2 The working principle of FLC

The fuzzy logic is a logical system and it is an extension of multivalued logic. The fuzzy algorithms underlie much of human thinking. FLCs were developed to imitate the performance of human expert operators by encoding their knowledge in the form of linguistic rules. The structure of the fuzzy system is shown in the Fig. E.1. The input and the output values of FLC are the crisp set values and are denoted with the numbers (0, 1, 2 --- n). The crisp set values (input values) are converted into linguistic variables in the process of fuzzification. The rules are formed based on the linguistic variables and the decision making process can be performed based on the collective rules. The linguistic variables are converted into crisp set values using the Defuzzification process (this process is performed using the center of area method (COAM)). These crisp set values are the output values for FLC [156]. Output is applied to the processing unit of the system as shown in Fig. E.1. The advantages that the fuzzy logic controller shows are therefore [156]:

- The concept of fuzzy logic is very easy to understand. Simple mathematical concepts behind fuzzy reasoning. Also, the complexity is very less and more flexible.
- Fuzzy logic is capable to handle the imprecise data.
- Fuzzy logic simplifies the implementation of the conventional control techniques.

- Fuzzy logic works based on natural language.

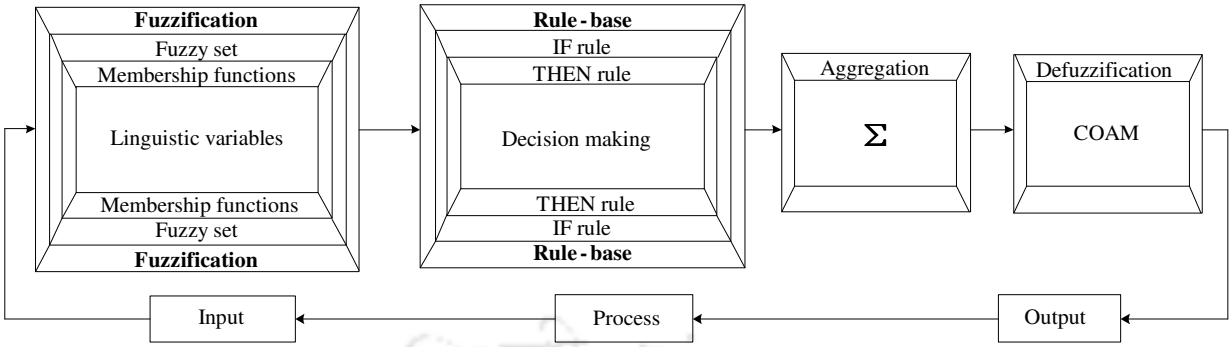

Fig. E.1 The structure of the fuzzy system

The descriptions of specific terms that are necessary in the Fuzzy system are given as follows:

Membership functions: A curve which defines the mapping of every point in the input space to a membership value (degree of membership) between 0 and 1 is termed as the membership function (MF).

Fuzzy set: A set of membership (characteristic) function which assigns to each object a grade of membership from 0 to 1 is called the fuzzy set.

Fuzzification: Every measure of input variable can be assigned with a degree of membership (membership value) for all the fuzzy sets defined in the universe of discourse (a fancy name of the input space is the universe of discourse).

Linguistic variables: The values of a variable represented with words/sentences in an artificial/natural language rather than numbers (0, 1, 2, --- n) is termed as the linguistic variable. It represents the process state and the control variable in FLC (represented with; negative high (NH), negative medium (NM), negative low (NL), zero (Z), positive low (PL), positive medium (PM), positive high (PH) etc.).

Rule base: A mechanism of dealing with fuzzy consequents (expressed by IF) and antecedents (expressed by THEN) is the fuzzy rule. The rule base plays a key role in most of the FLC applications. A rule in the fuzzy logic is formulated using the conditional statements (IF-THEN statements).

Defuzzification*:* This process can be used to generate the crisp output values for the FLC. The center of area method (COAM) is used to perform the Defuzzification process.

The working principle and the calculations that are required for the internal processing of the FLC have been explained through the following example.

E.3 Example for the working principle of FLC

Q) Consider the input values applied to FLC are: Vpu=0.99pu, E_{ESD}=140 kWh, EB_f=4 and E_{SP}=12 kWh (shown in Fig. E.2). Explain the working principle of FLC and also, explain the process of determining FLC output values ($P\pm$ and $SP\pm$) at these input values?

Explanation: The universe of discourse for each input is divided into three membership functions represented with linguistic variables low (L), medium (M) and high (H) as shown in Fig. E.2. The 'μ' (any variable) denotes the degree of membership of a linguistic variable and that can be observed from Fig. E.2.

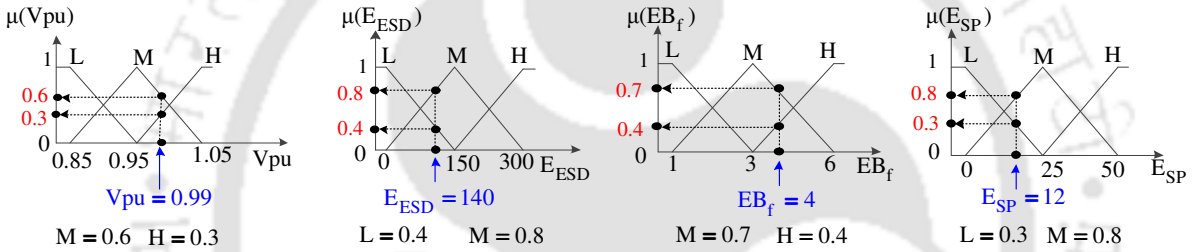

Fig. E.2 Input values of the fuzzy logic controller

- The degree of membership function (DMF) (μ(Vpu)) for the linguistic variable 'M' at 0.99pu is 0.6 and μ(Vpu) for H at 0.99pu is 0.3 as shown in Fig. E.2.
- $\mu(E_{ESD})$ for L at 140 kWh is 0.4 and for M at 140 kWh is 0.8.
- $\mu(EB_f)$ for M at 4 is 0.7 and for H at 4 is 0.4.
- $\mu(E_{SP})$ for L at 12 kWh is 0.3 and for M at 12 kWh is 0.8.

The DMFs for all the inputs are shown in Fig. E.2. Following steps are used to determine the output values of FLC at the given input values.

i. **Step-1:** At every input value two DMFs are involved as per Fig. E.2. Therefore, create the rules (use IF and THEN conditions) by using these DMFs of all inputs (form a total of 16 rules for 4 inputs). The rules formed by using DMFs for these inputs at specified input values are given in the Table E.1.

Table E.1: The rules associated for the given input values and their DMFs

S. no.	*Vpu*	E_{ESD}	EB_f	E_{SP}		*S. no.*	*Vpu*	E_{ESD}	EB_f	E_{SP}
1.	M(0.6)	L(0.4)	M(0.7)	L(0.3)		9.	H(0.3)	L(0.4)	M(0.7)	L(0.3)
2.	M(0.6)	L(0.4)	M(0.7)	M(0.8)		10.	H(0.3)	L(0.4)	M(0.7)	M(0.8)
3.	M(0.6)	L(0.4)	H(0.4)	L(0.3)		11.	H(0.3)	L(0.4)	H(0.4)	L(0.3)
4.	M(0.6)	L(0.4)	H(0.4)	M(0.8)		12.	H(0.3)	L(0.4)	H(0.4)	M(0.8)
5.	M(0.6)	M(0.8)	H(0.4)	M(0.8)		13.	H(0.3)	M(0.8)	H(0.4)	M(0.8)
6.	M(0.6)	M(0.8)	H(0.4)	L(0.3)		14.	H(0.3)	M(0.8)	H(0.4)	L(0.3)
7.	M(0.6)	M(0.8)	M(0.7)	L(0.3)		15.	H(0.3)	M(0.8)	M(0.7)	L(0.3)
8.	M(0.6)	M(0.8)	M(0.7)	M(0.8)		16.	H(0.3)	M(0.8)	M(0.7)	M(0.8)

ii. **Step. 2:** Now identify these rules from the rule base of FLC given in the Table E.2. The blue colored rules in Table E.2 are matched with the rules of Table E.1.

Table E.2: The rule base of FLC

Input				*Output*			*Input*				*Output*	
Vpu	E_{ESD}	EB_f	E_{SP}	*P*±	*SP*±		*Vpu*	E_{ESD}	EB_f	E_{SP}	*P*±	*SP*±
H	M	H	H	Z	PH		M	L	H	H	Z	NH
H	M	H	M	Z	PM		M	L	H	M	Z	NM
H	M	H	L	Z	PL		M	L	H	L	Z	NL
H	M	M	H	Z	PH		M	L	M	H	Z	NH
H	M	M	M	Z	PM		M	L	M	M	Z	NM
H	M	M	L	Z	PL		M	L	M	L	Z	NL
H	M	L	H	Z	PH		M	L	L	H	Z	NH
H	M	L	M	Z	PM		M	L	L	M	Z	NM
H	M	L	L	Z	PL		M	L	L	L	Z	NL
H	L	H	H	PL	PH		L	H	H	H	NH	NH
H	L	H	M	PL	PH		L	H	H	M	NH	NM
H	L	H	L	PL	PM		L	H	H	L	NH	NM
H	L	M	H	PL	PH		L	H	M	H	NH	NH
H	L	M	M	PL	PH		L	H	M	M	NH	NM
H	L	M	L	PL	PM		L	H	M	L	NH	NM
H	L	L	H	PL	PH		L	H	L	H	NH	NH
H	L	L	M	PL	PH		L	H	L	M	NH	NM
H	L	L	L	PL	PM		L	H	L	L	NH	NM
M	H	H	H	NH	NH		L	M	H	H	NM	NH
M	H	H	M	NH	NM		L	M	H	M	NM	NM
M	H	H	L	NH	NL		L	M	H	L	NM	NL
M	H	M	H	NH	NH		L	M	M	H	NM	NH
M	H	M	M	NH	NM		L	M	M	M	NM	NM
M	H	M	L	NH	NL		L	M	M	L	NM	NL
M	H	L	H	NH	NH		L	M	L	H	NM	NH
M	H	L	M	NH	NM		L	M	L	M	NM	NM
M	H	L	L	NH	NL		L	M	L	L	NM	NL
M	M	H	H	NH	NH		L	L	H	H	Z	PH
M	M	H	M	NH	NM		L	L	H	M	Z	PM
M	M	H	L	NH	NL		L	L	H	L	Z	PL
M	M	M	H	NH	NH		L	L	M	H	Z	PH
M	M	M	M	NH	NM		L	L	M	M	Z	PM
M	M	M	L	NH	NL		L	L	M	L	Z	PL
M	M	L	H	NH	NH		L	L	L	H	Z	PH
M	M	L	M	NH	NM		L	L	L	M	Z	PM
M	M	L	L	NH	NL		L	L	L	L	Z	PL

iii. **Step-3:** Now define the degree of fulfillment (*DOF*) for each identified rule (R) from the rule base (Table E.2). *DOF* for each rule is decided using the minimum/maximum method. Here minimum method (AND (∧) operator) is used. *DOF* for the output-1 (*P*±) of the FLC is therefore:

E. The working principle of fuzzy logic controller

- DOF_1=min {μ_M(Vpu), $\mu_L(E_{ESD})$, $\mu_M(EB_f)$, $\mu_L(E_{SP})$}=min { 0.6, 0.4, 0.7, 0.3}=0.3 → $\mu_Z(P\pm)$ (ref. Table E.1).

  DOF_3, DOF_{13}, DOF_{14}, DOF_{15}, and DOF_{16} are same as that of DOF_1. The contribution of R_1, R_3, R_{13}, R_{14}, R_{15} and R_{16} is shown in Fig. E.3(a).

- DOF_2=min {μ_M(Vpu), $\mu_L(E_{ESD})$, $\mu_M(EB_f)$, $\mu_M(E_{SP})$}= min {0.6, 0.4, 0.7, 0.8}=0.4 → $\mu_Z(P\pm)$.

  DOF_4 is same as that of DOF_2. The contribution of R_2 and R_4 is shown in Fig. E.3(b).

- DOF_5= min {μ_M(Vpu), $\mu_M(E_{ESD})$, $\mu_H(EB_f)$, $\mu_M(E_{SP})$}= min {0.6, 0.8, 0.4, 0.8}=0.4 → $\mu_{NH}(P\pm)$.

  The contribution of R_5 is shown in Fig. E.3(c).

- DOF_6= min {μ_M(Vpu), $\mu_M(E_{ESD})$, $\mu_H(EB_f)$, $\mu_L(E_{SP})$}= min {0.6, 0.8, 0.4, 0.3}=0.3 → $\mu_{NH}(P\pm)$.

  DOF_7 is same as that of DOF_6. The contribution of R_6 and R_7 is shown in Fig. E.3(d).

- DOF_8= min {μ_M(Vpu), $\mu_M(E_{ESD})$, $\mu_M(EB_f)$, $\mu_M(E_{SP})$}= min {0.6, 0.8, 0.7, 0.8}=0.6 → $\mu_{NH}(P\pm)$.

  The contribution of R_8 is shown in Fig. E.3(e).

- DOF_9= min {μ_H(Vpu), $\mu_L(E_{ESD})$, $\mu_M(EB_f)$, $\mu_L(E_{SP})$}= min {0.3, 0.4, 0.7, 0.3}=0.3 → $\mu_{PL}(P\pm)$.

  DOF_{10}, DOF_{11} and DOF_{12} are same as that of DOF_9. Fig. E.3(f) shows the contribution of R_9, R_{10}, R_{11} and R_{12}.

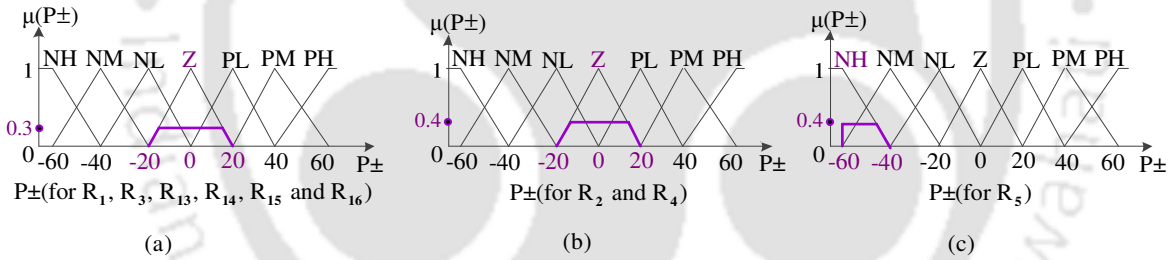

Fig. E.3(a): Contribution of R_1, R_3, R_{13}, R_{14}, R_{15} and R_{16}; (b): Contribution of R_2 and R_4; (c): Contribution of R_5.

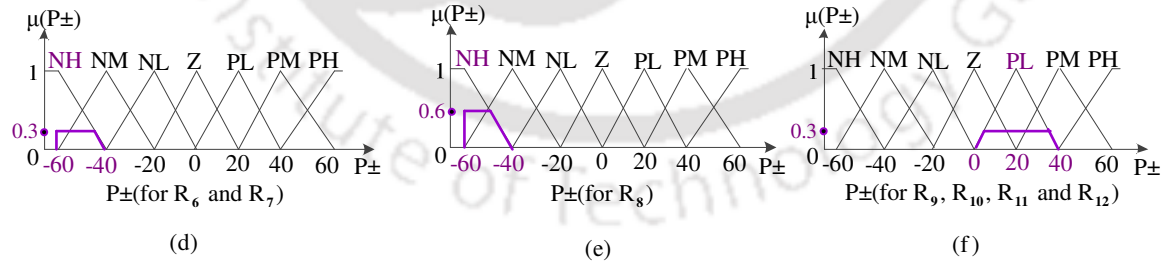

Fig. E.3(d): Contribution of R_6 and R_7; (e): Contribution of R_8; (f): Contribution of R_9, R_{10}, R_{11} and R_{12}.

DOF for the output-2 ($SP\pm$) of the FLC (ref. Table E.1) is therefore:

- DOF_1= min {μ_M(Vpu), $\mu_L(E_{ESD})$, $\mu_M(EB_f)$, $\mu_L(E_{SP})$}= min {0.6, 0.4, 0.7, 0.3}=0.3. → $\mu_{NL}(SP\pm)$.

  DOF_3, DOF_6 and DOF_7 are same as that of DOF_1. Fig. E.4(a) shows the contribution of R_1, R_3, R_6 and R_7.

- DOF_2= min {μ_M(Vpu), $\mu_L(E_{ESD})$, $\mu_M(EB_f)$, $\mu_M(E_{SP})$}= min {0.6, 0.4, 0.7, 0.8}=0.4. → $\mu_{NM}(SP\pm)$.

  DOF_4 and DOF_5 are same as that of DOF_2. The contribution of R_2, R_4 and R_5 is shown in Fig. E.4(b).

- DOF_8= min {μ_M(Vpu), $\mu_M(E_{ESD})$, $\mu_M(EB_f)$, $\mu_M(E_{SP})$}= min {0.6, 0.8, 0.7, 0.8}=0.6. → $\mu_{NM}(SP\pm)$.

  The contribution of R_8 is shown in Fig. E.4(c).

- DOF_9= min {μ_H(Vpu), $\mu_L(E_{ESD})$, $\mu_M(EB_f)$, $\mu_L(E_{SP})$}= min {0.3, 0.4, 0.7, 0.3}=0.3. → $\mu_{PM}(SP\pm)$.

  DOF_{11}, DOF_{13}, and DOF_{16} are same as that of DOF_9. The contribution of R_9, R_{11}, R_{13} and R_{16} is shown in Fig. E.4(d).

- DOF_{10}= min {μ_H(Vpu), $\mu_L(E_{ESD})$, $\mu_M(EB_f)$, $\mu_M(E_{SP})$}= min {0.3, 0.4, 0.7, 0.8}=0.3. → $\mu_{PH}(SP\pm)$.

  DOF_{12} is same as that of DOF_{10}. The contribution of R_{10} and R_{12} is shown in Fig. E.4(e).

- DOF_{14}= min {μ_H(Vpu), $\mu_M(E_{ESD})$, $\mu_H(EB_f)$, $\mu_L(E_{SP})$}= min {0.3, 0.8, 0.4, 0.3}=0.3. → $\mu_{PL}(SP\pm)$.

  DOF_{15} is same as that of DOF_{14}. The contribution of R_{14} and R_{15} is shown in Fig. E.4(f).

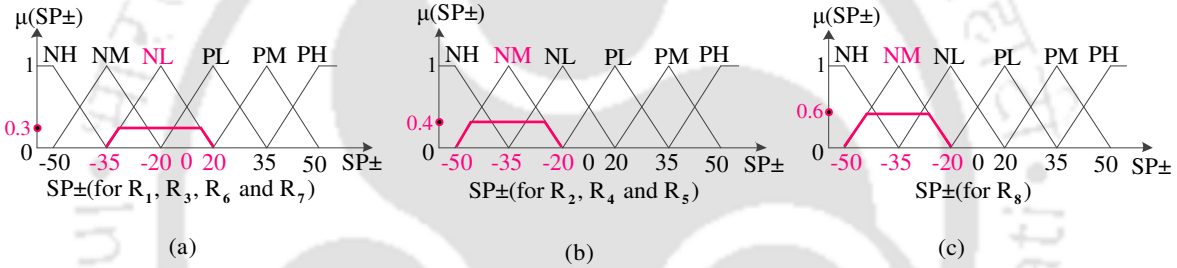

Fig. E.4(a): Contribution of R_1, R_3, R_6 and R_7; (b): Contribution of R_2, R_4 and R_5; (c): Contribution of R_8

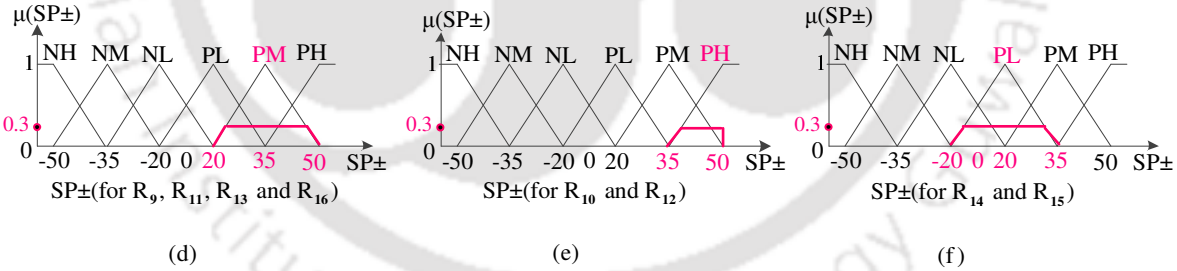

Fig. E.4(d): Contribution of R_9, R_{11}, R_{13} and R_{16}; (e): Contribution of R_{10} and R_{12}; (f): Contribution of R_{14} and R_{15}

iv. Step-4: Aggregate all the corresponding outputs of identified rules using union (∨) operator.

- $\mu(P\pm)$={$\mu_Z(P\pm) \vee \mu_Z(P\pm) \vee \mu_{NH}(P\pm) \vee \mu_{NH}(P\pm) \vee \mu_{NH}(P\pm) \vee \mu_{PL}(P\pm)$ }.

  Contributions from the corresponding outputs of all the identified rules for $P\pm$ are shown in Fig. E.5.

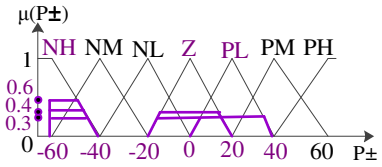

Fig. E.5: Corresponding output ($P\pm$) from the contribution of all the identified rules

- $\mu(SP\pm)=\{\mu_{NL}(SP\pm) \vee \mu_{NM}(SP\pm) \vee \mu_{NM}(SP\pm) \vee \mu_{PM}(SP\pm) \vee \mu_{PL}(SP\pm) \vee \mu_{PH}(SP\pm)\}$. Contributions from the corresponding outputs of all the rules for $SP\pm$ are shown in Fig. E.6.

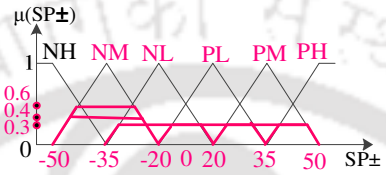

Fig. E.6: Corresponding output ($SP\pm$) from the contribution of all the identified rules

v. **Step-5:** Now perform the Defuzzification process.

The general expression for the Defuzzification using COAM is expressed as

$$(P\pm)=\frac{\sum_{i=1}^{n}\{P(\pm)_i \times \mu(P(\pm)_i)\}}{\sum_{i=1}^{n}\mu(P(\pm)_i)} \qquad \text{(E.1)}$$

where $(P\pm)_i$ is the output power value on x-axis (i=1, 2, --- n), $\mu(P\pm)_i$ is the degree of membership function for the corresponding output power on y-axis and $P\pm$ is the net output power for the corresponding input values. The area covered between $P\pm$ and $\mu(P\pm)$ with the contributions of all the identified rules is shown in Fig. E.7.

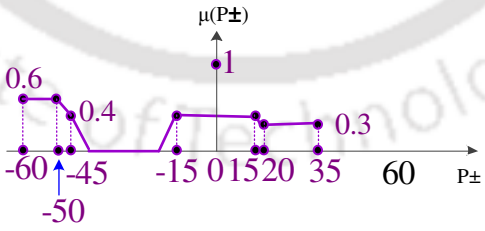

Fig. E.7: Defuzzification for $P\pm$

The area under the curve is evaluated by using (E.1) and is given as

$$P(\pm)=\frac{[(0.6\times\text{-}60)+(0.6\times\text{-}50)+(0.4\times\text{-}45)+(0.4\times\text{-}15)+(0.4\times15)+(0.3\times20)+(0.3\times35)]}{(0.6+0.6+0.4+0.4+0.4+0.3+0.3)}=\text{-}22.5\ kW \qquad \text{(E.2)}$$

The area covered between $SP\pm$ and $\mu(SP\pm)$ with the contributions of all the identified rules is shown in Fig. E.8.

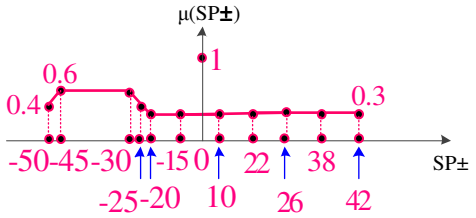

Fig. E.8: Defuzzification for $SP\pm$

The area under the curve is evaluated by using (E.1) and is given as

$$SP(\pm) = \frac{\begin{matrix}[(0.4\times -50)+(0.6\times -45)+(0.6\times -30)+(0.4\times -25)+(0.3\times -20)+(0.3\times -15)+(0.3\times 10)+\\ (0.3\times 22)+(0.3\times 26)+(0.3\times 38)+(0.3\times 42)]\end{matrix}}{(0.4+0.6+0.6+0.4+0.3+0.3+0.3+0.3+0.3+0.3+0.3)} = -11.61\ kW \quad \text{(E.3)}$$

In this way, FLC performs the internal process and decides the desired output of the system. Both, the output values of FLC are negative (ref. (E.2) and (E.3)) for the given input values. Therefore, FLC directs both, the ESD and SP to send power to the grid. If both, the output values are positive then FLC directs SP to send power to ESD and also, directs ESD to receive power from both the grid and SP.

E.4 The procedure to build FLC in MATLAB

Fig. E.9 shows the different steps required to build the Fuzzy Inference System (FIS) in the fuzzy logic tool box of MATLAB software [156].

FIS editor: In this editor, the number of input and output variables can be added or deleted. Also it has an option to define the name for both, input and output variables. The numbers of inputs are unlimited in the fuzzy logic toolbox. However, the complexity increases with the increase in the number of inputs.

Membership function editor: The shapes of all the membership functions associated with each variable can be defined in the membership function editor. It has an option to add or delete the membership functions. Also, the editing option is available to set the range of each membership function.

Rule editor: This editor has an option to edit the list of rules and also has the possibility to add or delete the rules.

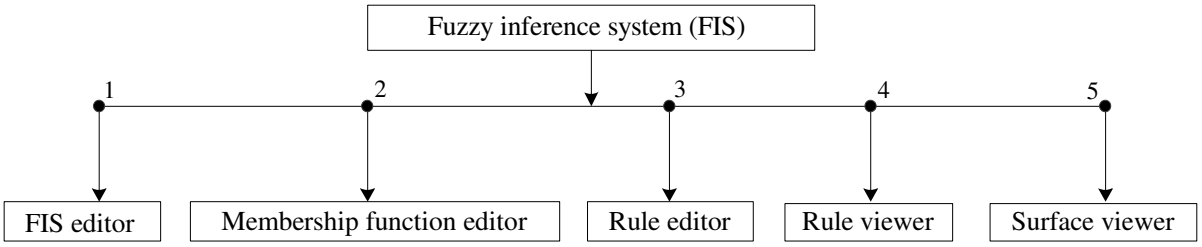

Fig. E.9: The different steps required to build FIS system in the MATLAB

Rule viewer: It shows the contribution of each rule for the output variable. The status of rules whether they are working/non-working can be checked in this viewer. Also it has the possibility to identify non-working rules.

Surface viewer: This viewer shows the output surface map with respect to the inputs.

Bibliography

[1] R. Shrivastava, S. Neeta and G. Geeta, "Air Pollution Due To Road Transportation in India: A Review on Assessment and Reduction Strategies", *J Environmental Research and Development*, Vol. 8, pp. 69-77, Sep. 2013.

[2] Ministry of Statistics and Programme Implementation Government of India. Available: www.mospi.gov.in; Ministry of Petroleum and Natural Gas Economic and Statistics Division, India. Available: www.petroleum.nic.in.

[3] L. Berzi, M. Delogu and M. Pierini, "A comparison of Electric Vehicles use-case scenarios: Application of a simulation framework to vehicle design optimization and energy consumption assessment", *Int. Conf. on Environment and Electrical Engineering (EEEIC'16)*, pp.1-6, Sep. 2016.

[4] CEA, Ministry of Power Central Electricity Authority, New Delhi, India. Available: www.cea.nic.in.

[5] ASEB, Assam State Electricity Board Guwahati, India. Available: *www.apdcl.gov.in.*

[6] E. Saberbaril, H. Sabooril, and S. Sabood, "Utilizing PHEVs for Peak-Shaving, Loss Reduction and Voltage Profile Improvement via V2B Mode", *IEEE Conf. on Electrical Power Distribution (EPDC'14)*, pp. 59-65, May 2014.

[7] Thomas B. Reddy, 'Linden's Handbook of Batteries', (McGraw-Hill, 4th edn. 2011), pp. 1.3-39.33.

[8] Andres Carvallo, "The Advanced Smart Grid: Edge Power Driving Sustainability", (Artech House, 2nd edn. 2015), pp. 1-9, Available: http://m.eet.com/media/1120982/c0792pt1.pdf.

[9] C. Kristen, E. Hasen and J. Driesen, "The Impact of Charging Plug-In Hybrid Electric Vehicles on a Residential Distribution Grid," *IEEE Trans. Power Syst.*, vol. 25, No. 1, Feb. 2010.

[10] S. Deilami, S. Masoum, S. Moses and M. Masoum, "Real-Time Coordination of Plug-In Electric Vehicle Charging in Smart Grids to Minimize Power Losses and Improve Voltage Profile," *IEEE Trans. Smart Grid*, vol. 2, pp. 456-467, March 2011.

[11] K. Qian, C. Zhou, M. Allan and Y. Yuan, "Modeling of Load Demand Due to EV Battery Charging in Distribution Systems," *IEEE Trans. Power Syst.*, vol. 26, pp. 802-810, May 2011.

[12] Y. Cao, S. Tang, C. Li, P. Zhang, Y. Tan, Z. Zhang and J. Li, "An Optimized EV Charging Model Considering TOU Price and SOC Curve," *IEEE Trans. Smart Grid*, vol. 3, pp. 388-393, March 2012.

[13] E. Sortomme, and M. Sharkawi, "Optimal Charging Strategies for Unidirectional Vehicle to Grid," *IEEE Trans. Smart Grid*, vol. 2, pp. 131-138, March 2011.

[14] M. Etezadi, K. Choma and J. Stefani, "Rapid-Charge Electric-Vehicle Stations," *IEEE Trans. Power Delivery*, vol. 25, pp. 1883-1887, July 2010.

[15] Z. Amjadi, and S. Williamson, "Prototype Design and Controller Implementation for Battery-Ultra capacitor Hybrid Electric Vehicle Energy Storage System," *IEEE Trans. Smart Grid*, vol. 3, pp. 332-340, March 2012.

[16] H. Li, X. Lin, H. Yang, X. Liang, R. Lu, and X. Shen, "EPPDR: An Efficient Privacy-Preserving Demand Response Scheme with Adaptive Key Evolution in Smart Grid," *IEEE Trans. Parallel and Distributed Systems*, vol. 25, pp. 2053-2064, April 2013.

[17] L. Gkatzikis, I. Koutsopoulos, and T. Salonidis, "The Role of Aggregators in Smart Grid Demand Response Markets," *IEEE J selected areas in communications*, vol. 31, No. 7, July 2013.

[18] K. Dyke, N. Schofield, and M. Barnes, "The Impact of Transport Electrification on Electrical Networks," *IEEE Trans. Ind. Electron*., vol. 57, pp. 3917-3926, Dec. 2010.

[19] M. Amoli, K. Choma, and J. Stefani, "Rapid-Charge Electric-Vehicle Stations," *IEEE Trans. Power Delivery*, vol. 25, pp. 1883-1887, July 2010.

[20] E. Schaltz, A. Khaligh, and P. Rasmussen, "Influence of Battery/Ultra capacitor Energy-Storage Sizing on Battery Lifetime in a Fuel Cell Hybrid Electric Vehicle," *IEEE Trans. Veh. Technol.*, vol. 58, pp. 3882-3891, Oct. 2009.

[21] H. Zhou, and M. Khambadkone, "Composite Energy Storage System Involving Battery and Ultra capacitor With Dynamic Energy Management in Micro grid Applications," *IEEE Trans. Power Electron.,* vol. 26, No. 3, March 2011.

[22] Y. He, B. Venkatesh and L. Gaun," Optimal Scheduling for Charging and Discharging of Electric Vehicles," *IEEE Trans. Smart Grid*, vol. 3, pp. 1095-1105, Sep. 2012.

[23] Y. Ma, T. Houghton, A. Cruden, and D. Infield, "Modeling the Benefits of Vehicle-to-Grid Technology to a Power System," *IEEE Trans. Power Syst.*, vol. 27, pp. 1012-1020, May 2012.

[24] M. Yilmaz, and T. Krein, "Review of Benefits and Challenges of Vehicle-to-Grid Technology," *IEEE Trans. Power Electron.*, vol. 28, pp. 5673-5689, Dec. 2013.

[25] M. Yilmaz, and T. Krein, "Review of the Impact of Vehicle-to-Grid Technologies on Distribution Systems and Utility Interfaces," *IEEE Trans. Power Electron*., vol. 28, pp. 5673-5689, Dec. 2013.

[26] S. Vazquez, M. Lukic, E. Galvan, G. Franquelo, and M. Carrasco, "Energy Storage Systems for Transport and Grid Applications," *IEEE Trans. Ind. Electron*., vol. 57, pp. 3881-3895, Dec. 2010.

[27] D. Gulas, A. Waraich and G. Andersson, "Integrating Power Systems, Transport Systems and Vehicle Technology for Electric Mobility Impact Assessment and Efficient Control," *IEEE Trans. Smart Grid*, vol. 3, pp. 934-949, March 2012.

[28] M. Singh, P. Kumar and I. Kar, "Analysis of Vehicle to Grid Concept in Indian Scenario," in *Proc. IEEE Int. Conf. on Power Electron. and Motion Control (EPE-PEMC'10)*, pp. 146-158, Sep. 2010.

[29] M. Singh, I. Kar and P. Kumar, "Influence of EV on Grid Power Quality and Optimizing the Charging Schedule to Mitigate Voltage Imbalance and Reduce Power Loss," in *Proc. IEEE Int. Conf. on Power Electron. and Motion Control (EPE-PEMC'10)*, pp. 196-203, Sep. 2010.

[30] M. Singh, P. Kumar and I. Kar, "A Model of Electric Vehicle Charging Station Compatibles with Vehicle to Grid Scenario," *IEEE Int. Conf. on Electric Vehicle (IEVC'12),* pp. 1-7, March 2012.

[31] M. Singh, P. Kumar and I. Kar, "Coordination of Multi Charging Station for Electric Vehicles and its Utilization for Vehicle to Grid Scenario," *IEEE Conf. on Transportation Electrification and Expo (ITEC'12)*, pp. 1-7, June 2012.

[32] M. Singh, P. Kumar and I. Kar, "Designing a Multi Charging Station for Electric Vehicles and its Utilization for the Grid Support," *IEEE Power and Energy Society General Meeting (PESMG'12)*, pp. 1-8, July 2012.

[33] M. Singh, P. Kumar, and I. Kar, "Implementation of Vehicle to Grid Infrastructure Using Fuzzy Logic Controller", *IEEE Trans. Smart Grid*, vol. I, pp. 565-575, March 2012.

[34] Robert N. Tweedy and H. Dudgeon, "Notes on overhead equipment of tramways", *IET J Institution of Electrical Engineers*, vol. 37, pp. 161-191, Sep. 1906.

[35] Alfred H. Gibbings, "The carriage of goods on electric tramways", *IET J Institution of Electrical Engineers*, vol. 32, pp. 1057-1085, Aug. 1903.

[36] J. Joachim, K. Thanatchai and A. Greyson, "Tram and Trolley bus Net Traction Energy Consumption Comparison", *IEEE Int. Conf. on Electrical Machines and Systems (ICEMS'15)*, pp. 2164-2169, Oct. 2015.

[37] P. Garcia, L. Fernandez and F. Jurado, "Energy Management System of Fuel-Cell-Battery Hybrid Tramway", *IEEE Trans. Ind. Electron*., vol. 57, pp. 4013-4023, Dec. 2010.

[38] J. Torreglosa, P. García and F. Jurado, "Predictive Control for the Energy Management of a Fuel-Cell–Battery–Supercapacitor Tramway", *IEEE Trans. Ind. Informatics*, vol. 10, pp. 276-285, Feb. 2014.

[39] F. Ciccarelli, D. Iannuzzi and L. Fratelli, "Line-Voltage Control Based on Wayside Energy Storage Systems for Tramway Networks", *IEEE Trans. Power Electron*., vol. 31, pp. 884-899, Jan. 2016.

[40] L. Streit and J. Talla, "Verification of stochastic tram model based on real traffic data", *IEEE European Conf. on Power electronics and applications (EPE'15ECCE-Europe)*, pp.1-5, Oct. 2015.

[41] J. Talla, L. Streit and V. Blahnik, "Fuzzy Energy Management Strategy for Tram with Supercapacitors", *IEEE Conf. on Ind. Electron. (IECON'16)*, pp. 003963-003968, Jan. 2016.

[42] H. Thomas, "The electric trolley bus", *IET Students' Quarterly J*, vol. 3, pp. 152-155, Feb. 1933.

[43] J.P. Senior, "The trolley bus", *IET Students' Quarterly J*, vol. 20, pp. 11-16, Sep. 1949.

[44] J. H. Gauss, "Can the Trolley Coach Compete Economically With the Gas or Diesel Bus Where No Overhead Facilities Exist", *IEEE Trans. American Institute of Electrical Engineers*, vol. 66, pp. 264-268, Jan. 1947.

[45] "Ninety Miles an Hour in a Trolley Car!", *IEEE Electrical Engineering*, vol. 50, pp. 49-49, Jan. 1931.

[46] M. Schreiber, "Development of the all-service vehicle**",** *IEEE Electrical Engineering*, vol. 55, pp. 236-240, March 1936.

[47] M. Falvo, R. Lamedica and A. Ruvio, "An environmental sustainable transport system: A trolley-buses Line for Cosenza city", *IEEE Int. Sym. on Power Electron., Electrical Drives, Automation and Motion (SPEEDAM'12)*, pp. 1479-1485, Aug. 2012.

[48] K. Kutsmeda, K. Fehrle and P. Trick, "Computer Modeling, Simulation, and Validation by Field Testing of a Traction Power System for Electric Trolley Buses", in *Proc. IEEE Conf. on Joint Railroad (RRCON'95)*, pp. 87-91, April 1995.

[49] A. Singh, "A new Design of Current Collector (ECC) for Electric Trolley Bus", *IEEE Int. Conf. on Transportation Electrification (ITEC'16)*, pp. 1-8, Jan. 2016.

[50] D. Vierling, J. Dworacek, and B. Schmuelling, "Smart Trolley-Bus Systems: Why a presumed dead relic makes the difference to re-electrify public transportation", *IEEE Int. Conf. on Energy (ENERGYCON'16)*, pp. 1-6, July 2016.

[51] A. Diez, E. Velandia and M. Restrepo, "Trolleybuses in Smart Grids as effective strategy to reduce greenhouse emissions," *IEEE Int. Conf. on Electric Vehicle (IEVC'12)*, pp. 1-6, March 2012.

[52] R. Barrero, V. Mierlo and X. Tackoen, "Energy savings in public transport", *IEEE Veh. Technol. magazine,* vol. 3, issue. 3, pp. 26-36, Sep. 2008.

[53] S. Barsali, A. Bechini and D. Poli, "Storage in Electrified Transport Systems", *IEEE Int. Conf. on Energy (ENERGYCON'12)*, pp. 1003-1008, Nov. 2012.

[54] M. Falvo, R. Lamedica and A. Ruvio, "Energy Storage Application in Trolley-Buses Lines for a Sustainable Urban Mobility", *IEEE Conf. on Electrical Systems for Aircraft, Railway and Ship Propulsion* (*ESARS'12)*, pp. 1-6, Dec. 2012.

[55] P. Barrade and A. Rufer, "Supercapacitors as energy buffers: a solution for elevators and for electric busses supply", in *Proc. IEEE Conf. on Power Convers., (PCC'02)*, vol.3, pp. 1160-1165, Aug. 2002.

[56] F. Mapelli, D. Tarsitano, and G. Bosia, "A study of urban electric bus with a fast charging energy storage system based on lithium battery and supercapacitors", *IEEE Int. Conf. on Ecological Vehicles and Renewable Energies (EVER'13)*, pp. 1-9, May 2013.

[57] M.Ayad, M.Becherif and M. Wack, "The use of Supercapacitors in electrical vehicle: modeling, sizing and control", *IEEE Conf. on Vehicle Power and Propulsion (VPPC'10)*, pp. 1-6, Sep. 2010.

[58] S. Avanzo, D. Iannuzzi and P. Tricoli, "A Sample Application of Supercapacitor Storage Systems for Suburban Transit", *IEEE Conf. on Electrical Systems for Aircraft, Railway and Ship Propulsion (ESARS'10)*, pp. 1-7, Dec. 2010.

[59] F. Ciccarelli, D. Iannuzzi and D. Lauria, "Supercapacitors-Based Energy Storage for Urban Mass Transit Systems", in *Proc. IEEE Conf. on Power Electronics and Applications (EPE'11)*, pp. 1-10, Sep. 2011.

[60] L. Battistelli, M. Fantauzzi, and D. Lauria, "Generalized approach to design supercapacitor-based storage devices integrated into urban mass transit systems", *IEEE Int. Conf. on Clean Electrical Power (ICCEP'11)*, pp. 530-534, Oct. 2011.

[61] P. Thounthong, M. Phattanasak and P. Sethakul, "Control of a Two-Port Supercapacitor Converter Based on Differential Flatness Principle for Transportation Applications", *IEEE Int. Conf. on Environment and Electrical Engineering (EEEIC'12)*, pp. 824-829, June 2012.

[62] G. Fabbri, C. Medaglia and M. Gallarate, "An Innovative System for a Clean and Sustainable Public Transport System in Smart Cities", *IEEE Int. Symposium on Ind. Electron. (ISIE'16)*, pp. 974-979, Nov. 2016.

[63] M. Camara, H. Gualous and B. Dakyo, "Supercapacitors Modeling and Integration in Transport Applications", *IEEE Annual Meeting on Industry Applications Society (IAS'11)*, pp. 1-7, Nov. 2011.

[64] S. Trieste, S. Bourguet, and J.Claire, "Accurate sizing of supercapacitors storage system considering its capacitance variation", in *Proc. IEEE European Conf. on Power Electronics and Applications (EPE'11)*, pp. 1-10, Sep. 2011.

[65] H. Yin, W. Zhou and C. Zhao, "An Adaptive Fuzzy Logic-Based Energy Management Strategy on Battery/Ultracapacitor Hybrid Electric Vehicles", *IEEE Trans. Transportation Electrification*, vol. 2, pp. 300-311, Sep. 2016.

[66] Yoichi Hori, "Novel EV Society based on Motor/ Capacitor/ Wireless – Application of Electric Motor, Supercapacitors, and Wireless Power Transfer to Enhance Operation of Future Vehicles", *IEEE Int. workshop on Innovative Wireless Power Transmission: Technologies, Systems, and Applications (IMWS'12)*, pp. 3-8, June 2012.

[67] W. Infante, A. Khan, "Performance Evaluation of Series Hybrid and Pure Electric Vehicles Using Lead-Acid Batteries and Supercapacitors", *IEEE Region 10 Conf. (TENCON'12)*, pp. 1-5, Nov. 2012.

[68] A. Allegre, A. Bouscayrol and S. Fassi, "Energy Storage System with Supercapacitor for an Innovative Subway", *IEEE Trans. Ind. Electron.*, vol. 57, pp. 4001-4012, Dec. 2010.

[69] J. Xie, J. Lu, and X. Chen, "A Practical Digital VRB Simulator for Power System and Smart Grid Applications", *IEEE Conf. on Power Engineering and Automation (PEAM'13)*, pp. 1-6, Sep. 2013.

[70] Z. Zhou, F. Scuiller, and J. Frederic, "Application of Flow Battery in Marine Current Turbine System for Daily Power Management", *IEEE Int. Conf. on Green Energy (ICGE'14)*, pp. 8-13, June 2014.

[71] G. Wang, M. Ciobotaru and G. Agelidis, "Power Smoothing of Large Solar PV Plant Using Hybrid Energy Storage", *IEEE Trans. Sustain. Energy*, vol. 5, pp. 834-842, July 2014.

[72] S. Miyake and N. Tokuda, "Vanadium Redox-Flow Battery for a Variety of Applications", in *Proc. IEEE Conf. on Power Engineering Society Summer Meeting (PESS'02)*, pp. 450-451, Aug. 2002.

[73] T. Shigematsu, T. Kumamoto and T. Hara, "Applications of a Vanadium Redox-flow Battery to Maintain Power Quality", *IEEE Conf. on Transmission and Distribution (TDC'02)*, pp. 1065-1070, Oct. 2002.

[74] L. Barote, C. Marinescu, and M. Georgescu, "VRB Modeling for Storage in Stand-Alone Wind Energy Systems", *IEEE Bucharest Power Tech (PTC'09)*, pp. 1-6, Oct. 2009.

[75] P. Alotto, M. Guarnieri, and Andrea Stella, "Redox Flow Batteries for Large Scale Energy Storage", *IEEE Int. Conf. on Energy (ENERGYCON'12)*, pp. 293-298, Nov. 2012.

[76] X. Binyu, Z. Jiyun and L. Jinbin, "Modeling of an All-Vanadium Redox Flow Battery and Optimization of Flow Rates", *IEEE Power and Energy Society General Meeting* (*PESMG'13)*, pp. 1-5, Nov. 2013.

[77] X. Binyu, J. Zhao and Z. Chenda, "State of Charge Estimation of an All-Vanadium Redox Flow Battery Based on a Thermal-Dependent Model", *IEEE Conf. on Asia-Pacific Power and Engineering (APPEEC'13)*, pp. 1-6, Dec. 2013.

[78] X. Qiu, T. Nguyen and A. Elmore, "A Field Validated Model of a Vanadium Redox Flow Battery for Micro grids", *IEEE Trans. Smart Grid*, vol.5, pp.1592-1601, July 2104.

[79] Y. Parvini, J. Siegel, and A. Vahidi, "Supercapacitor Electrical and Thermal Modeling, Identification, and Validation for a Wide Range of Temperature and Power Applications", *IEEE Trans. Ind. Electron*., vol. 63, pp. 1574-1585, March 2016.

[80] R. German, A. Hammar and P. Venet, "Novel Experimental Identification Method for a Supercapacitor Multipore Model in Order to Monitor the State of Health", *IEEE Trans. Power Electron*., vol. 31, pp. 548-559, Jan. 2016.

[81] R. German, P. Venet and J. Vinassa, "Improved Supercapacitor Floating Ageing Interpretation Through Multipore Impedance Model Parameters Evolution", *IEEE Trans. Power Electron*., vol. 29, pp. 3669-3678, July 2014.

[82] V. Yuhimenko, G. Geula and A. Kuperman, "Average Modeling and Performance Analysis of Voltage Sensor less Active Supercapacitor Balancer With Peak Current Protection", *IEEE Trans. Power Electron*., vol. 32, pp. 1570-1578, Feb. 2017.

[83] N. Rizoug, P. Bartholomeus and P. Moigne, "Modeling and Characterizing Supercapacitors Using an Online Method", *IEEE Trans. Ind. Electron*., vol. 57, pp. 3980-3990, Dec. 2010.

[84] P. Thounthong, "Model Based-Energy Control of a Solar Power Plant With a Supercapacitor for Grid-Independent Applications", *IEEE Trans. Energy Convers*., vol. 26, pp. 1210-1218, Dec. 2011.

[85] V. Musolino, L. Piegari and E. Tironi, "New Full-Frequency-Range Supercapacitor Model with Easy Identification Procedure", *IEEE Trans. Ind. Electron*., vol. 60, pp. 112-120, Jan. 2013.

[86] P. Thounthong, A. Luksanasakul and B. Davat, "Intelligent Model-Based Control of a Standalone Photovoltaic/Fuel Cell Power Plant With Supercapacitor Energy Storage", *IEEE Trans. Sustain. Energy*, vol. 4, pp. 240-249, Jan. 2013.

[87] D. Torregrossa, M. Bahramipanah and M. Paolone, "Improvement of Dynamic Modeling of Supercapacitor by Residual Charge Effect Estimation", *IEEE Trans. Ind. Electron.,* vol. 61, pp. 1345-1354, March 2014.

[88] R. Chai and Y. Zhang, "A Practical Supercapacitor Model for Power Management in Wireless Sensor Nodes", *IEEE Trans. Power Electron*., vol. 30, pp. 6720-6730, Dec. 2015.

[89] E. Reena, A. Dalal and P. Kumar, "Accurate Computation of Mutual Inductance of Two Air Core Square Coils with Lateral and Angular Misalignments in a Flat Planar Surface", *IEEE Trans. Magnetics*, vol. 50, pp. 7000209, Jan. 2014.

[90] R. Bosshard and J. Kolar, "Multi-Objective Optimization of 50 kW/85 kHz IPT System for Public Transport", *IEEE J Power Electron*., vol. 4, pp. 1370-1382, Dec. 2016.

[91] E. Reena and P. Kumar, "Impact of Circuit Parameters in Contactless Power Transfer System", *IEEE Int. Conf. on Power Electronics Drives and Energy (PEDES'14)*, pp. 1-6, Dec. 2014.

[92] E. Reena, K. Thirugnanam and P. Kumar, "AC Bus Distributed Bidirectional Contactless Charging Station", *IEEE Power and Energy Society General Meeting (PESMG'15)*, pp. 1-5, Oct. 2015.

[93] E. Reena and P. Kumar, "Analysis and Comparison of Four Compensation Topologies of Contactless Power Transfer System", *IEEE Int. Conf. on Electric Power and Energy Conversion Systems (EPECS'15)*, pp. 1-6, Nov. 2015.

[94] K. Thirugnanam, T. Reena and P. Kumar, "Modeling and Control of Contactless Based Smart Charging Station in V2G Scenario", *IEEE Trans. Smart Grid*, vol. 5, pp. 337-348, Jan. 2014.

[95] Bhim Singh, C. Jain and K. Haddad, "A Multifunctional Grid-Tied Solar Energy Conversion System With ANF-Based Control Approach", *IEEE Trans. Ind. Appl*., vol. 52, pp. 3663-3672, Oct. 2016.

[96] K. Shinozaki, N. Yamakawa and T. Inoue, "Areal Solar Irradiance Estimated by Sparsely Distributed Observations of Solar Radiation", *IEEE Trans. Power Syst.*, vol. 31, pp. 35-42, Jan. 2016.

[97] G. Wang, M. Ciobotaru and V.Agelidis, "Power Management for Improved Dispatch of Utility-Scale PV Plants", *IEEE Trans. Power Syst.*, vol. 31, pp. 2297-2306, May 2016.

[98] H. Shaker, H. Zareipour, and D. Wood, "A Data-Driven Approach for Estimating the Power Generation of Invisible Solar Sites", *IEEE Trans. on Smart Grid*, vol. 7, pp. 2466-2476, Sep. 2016.

[99] P. Kydd, J. Anstrom, And M. Crouse, "Vehicle-Solar-Grid Integration: Concept and Construction", *IEEE J Power and Energy Technology*, pp.81-88, Sep. 2016.

[100] E. Baleke, M. Anwar and E. Moursi, "Wind speed and solar irradiance forecasting techniques for enhanced renewable energy integration with the grid: a review", *IET J Renewable Power Generation*, pp. 885-898, March 2016.

[101] M. Alam, K. Muttaqi and D. Sutanto, "Effective Utilization of Available PEV Battery Capacity for Mitigation of Solar PV Impact and Grid Support with Integrated V2G Functionality", *IEEE Trans. Smart Grid*, vol. 7, pp. 1562-1571, May 2016.

[102] E. Pompodakis, A. Drougakis and C. Alexiadis, "Photovoltaic systems in low-voltage networks and overvoltage correction with reactive power control", *IET J Renewable Power Generation*, pp. 410-417, Sep. 2015.

[103] K. Qian, C. Zhou, M. Allan, and Y. Yuan, "Modeling of Load Demand Due to EV Battery Charging in Distribution Systems", *IEEE Trans. Power Syst*., vol. 26, no. 2, pp. 802-810, May 2011.

[104] C. Chan, "The Rise & Fall of Electric Vehicles in 1828–1930: Lessons Learned", *proc. IEEE*, vol. 101, Issue: 1, pp. 206-212, Jan. 2013.

[105] S. Deilami, A. S. Masoum, P. S. Moses and A. S. Masoum, "Real-Time Coordination of Plug-In Electric Vehicle Charging in Smart Grids to Minimize Power Losses and Improve Voltage Profile", *IEEE Trans. smart grid*, vol. 2, no. 3, Sep. 2011.

[106] A. Diez, E. Velandia and M. Restrepo, "Trolleybuses in Smart Grids as effective strategy to reduce greenhouse emissions," in *proc. IEEE, IEVC*, March 2012, pp. 1-6.

[107] H. Thomas, "The electric trolley bus," *J. IET*, vol. 3, issue. 11, pp. 152-155, Feb 1933.

[108] Supercapacitor based buses for urban transportation. [Online]. Available: http://www.slideshare.net/ResearchIndia/super-capacitor-buses-in-shanghai-5156990.

[109] R. Barrero, and X. Tackoen, "Energy savings in public transport," *IEEE Veh. Technol. Mag.,* vol. 3, issue. 3, pp. 26-36, Sep 2008.

[110] Y. Jang, E. Suh and J. Kim, 'System Architecture and Mathematical Models of Electric Transit Bus System Utilizing Wireless Power Transfer Technology', *IEEE Syst. J.*, 2016, 10 (2), pp. 495-506.

[111] Thomas B. Reddy, "Linden's Handbook of Batteries", 4th ed. McGraw-Hill, 2011, pp. 30.41-30.45.

[112] X. Qiu, A. Nguyen, and A. Elmore, "A Field Validated Model of a Vanadium Redox Flow Battery for Microgrids", *IEEE Trans. Smart Grid*, vol. 5, no. 4, July 2014.

[113] A. Agrawal and P. Kumar, "Smart Public Transit System Using an Energy Storage System and Its Coordination with a Distribution Grid", *IEEE Trans. Intell. Transp. Syst*., vol. pp, issue. 99, pp. 1-11, Feb. 2014.

[114] M. Zandi, A. Payman and F. Tabar, "Energy Management of a Fuel Cell/Supercapacitor/Battery Power Source for Electric Vehicular Applications", *IEEE Trans. Veh. Technol*., vol. 60, no. 2, pp. 433-443, Feb. 2011.

[115] A. Hammar, P. Venet, and G. Rojat, "Study of Accelerated Aging of Supercapacitors for Transport Applications", *IEEE Trans. Ind. Electron*., vol. 57, no. 12, pp. 3972-3979, Dec. 2010.

[116] A. Castaings,W. Lhomme and R. Trigui, "Practical control schemes of a battery/supercapacitor system for electric vehicle", *IET Elect. Syst. Transp.*, vol. 6, no.1, pp. 20–26, 2016.

[117] P. Khatun, C. Bingham, N. Schofield, and P. Mellor, "Application of Fuzzy Control Algorithms for Electric Vehicle Antilock Braking/Traction Control Systems", *IEEE Trans. Veh. Technol*., vol. 52, no. 5, pp. 1356-1364, Sep. 2003.

[118] N. Schouten, A. Salman and A. Kheir, "Fuzzy Logic Control for Parallel Hybrid Vehicles", *IEEE Trans. Control Syst. Technol*., vol. 10, no. 3, pp. 460-468, May 2002.

[119] M. Rohmanuddin, H. Liong, and S. Ahmad, "Simplifying Fuzzy Rule Base of Multiple Input Multiple Output Systems by Constructing Multi-Layer Fuzzy Controller", in *Proc. IEEE Int. Conf., SMC*, Oct. 2000, pp. 3728 – 3733.

[120] H. Ying, "Analytical Structure of a two-input two-output Fuzzy Controller", in *Proc. IEEE* 3rd Int. Conf., IFIS, Dec. 1993, pp. 123 – 127.

[121] ASEB, Assam State Electricity Board Guwahati, India. [Online]. Available: http://aseb.in/, 2012.

[122] Guwahati Electric Circle-1 and Guwahati electric circle-2 taken from Assam power Distribution Company limited. [Online]. Available: "http://www.mybijulibill.com/about_GEC1_profile.jsp".

[123] M. Ehsani, Y. Gao and A. Emadi, "Modern Electric, Hybrid Electric and Fuel Cell Vehicles Fundamentals, Theory and Design", 2nd ed. CRC press, Taylor and Francis Group, 2010, pp. 19-27.

[124] IMD, India meteorological department Guwahati, Assam, India. [Online]. Available: www.imd.gov.in.

[125] T. Markvart, "Solar Electricity", 2nd ed. John Wiley and Sons Ltd, 2005, pp. 1-45.

[126] H. Habberlin, "Photovoltaics System Design and Practice" 1st ed. John Wiley and sons Ltd, 2012, pp. 1-75.

[127] I. Baklouti, Z. Driss, and M. Salah, "Estimation of Solar Radiation on Horizontal and Inclined Surfaces in Sfax, TUNISIA", in *Proc. IEEE 1st Int. Conf.*, *REVET*, March 2012, pp. 131-140.

[128] K. Yang, and T. Koike, "Estimating Surface Solar Radiation From Upper-Air Humidity", *J. Solar Energy*, vol. 72, no. 2, pp. 177–186, 2002.

[129] N. Pandiarajan and R. Muthu, "Mathematical Modeling of Photovoltaic Module with Simulink", in *Proc. IEEE* 1st *Int. Conf., ICEES*, pp. 258 – 263, Jan. 2011.

[130] B. Borowy, and Z. Salameh, "Optimum Photovoltaic Array Size for a Hybrid Wind/PV System", *IEEE Trans. Energy Convers*., vol. 9, no. 3, pp. 482-488, September 1994.

[131] A. Hijazi, P. Kreczanik, and M. Loreto, "Thermal Network Model of Supercapacitors Stack", *IEEE Trans. Ind. Electron*., vol. 59, no. 2, pp. 979-987, Feb. 2012.

[132] M. Singh, P. Kumar, and I. Kar, "Implementation of Vehicle to Grid Infrastructure Using Fuzzy Logic Controller", *IEEE Trans. Smart Grid*, vol. 3, no. 1, pp. 565-577, March 2012.

[133] M. Bhaskar Naik, P. Kumar and S. Majhi, "Small-scale solar plants coupled with smart public transport system and its coordination with the grid', *J. IET Elect. Syst. Transp*., vol. 7, no. 2, pp. 135-144, May 2017.

[134] M. Kumar, B. Naik, and P. Kumar, "Analysis of Implementing the Electric City Bus and its Coordination with the Grid", in *Proc. IEEE, INDICON,* pp. 974-978, Dec. 2012.

[135] Optimal power flow problem and solution methodologies. Available at: http://shodhganga.inflibnet.ac.in/bitstream/10603/4566/13/13_chapter3.pdf.

[136] S. Hamacek, M. Bartłomiejczyk and St. yskala, "Energy recovery effectiveness in trolleybus transport", *Elsevier J. Electric Power Systems Research*, vol. 112, pp. 1–11, March 2014.

[137] D. Vierling, J. Dworacek, and B. Schmuelling, "Smart Trolley-Bus Systems: Why a presumed dead relic makes the difference to re-electrify public transportation", *IEEE Int. Conf. on Energy (ENERGYCON'16)*, pp. 1-6, July 2016.

[138] http://www.polisnetwork.eu/publicdocuments/download/1765/document/nimh-and-primove-systems-2-finalpolis.pdf.

[139] http://www.adelaidecitycouncil.com/assets/acc/Environment/energy/docs/tindo_fact_sheet.pdf.

[140] A. Lucas, S. Chondrogiannis, "Smart grid energy storage controller for frequency regulation and peak shaving, using a vanadium redox flow battery", *Elsevier J. Electrical Power and Energy Systems*, vol. 80, pp. 26–36, Feb. 2016.

[141] C. Brivio, S. Mandelli and M. Merlo, "Battery energy storage system for primary control reserve and energy arbitrage", *Elsevier J. Sustainable Energy, Grids and Networks*, vol. 6, pp. 152-165, June 2016.

[142] S. Heslop, I. MacGill, and J. Fletcher, "Maximum PV generation estimation method for residential low voltage feeders", *Elsevier J. Sustainable Energy, Grids and Networks*, vol. 7, pp. 58-69, Sep. 2016.

[143] K. Benmouiza and A. Cheknane, "Classification of hourly solar radiation using fuzzy c-means algorithm for optimal stand-alone PV system sizing", *Elsevier J. Electrical Power and Energy Systems*, vol. 82, pp. 233–241, March 2016.

[144] M. Moradi and S. Hosseinian, "Optimal siting and sizing of renewable energy sources and charging stations simultaneously based on Differential Evolution algorithm", *Elsevier J. Electrical Power and Energy Systems*, vol. 73, pp. 1015–1024, July 2015.

[145] T. J. Barlow, S. Latham and P. G. Boulter, "A reference book of driving cycles for use in the measurement of road vehicle emissions", Published project report PPR354, Version: 3, *TRL Limited*, pp. 6, 10, 15 and 162.

[146] X. Shen, S. Chen and T. Tjing, "Configure Methodology of Onboard Supercapacitor Array for Recycling Regenerative Braking Energy of URT Vehicles", *IEEE Trans. Ind. Applications*, vol. 49, issue. 4, pp. 1678-1686, Aug. 2013.

[147] R. Roofegari, S. Hakimi, and S. Moghaddas, "Smart virtual energy storage control strategy to cope with uncertainties and increase renewable energy penetration", *Elsevier J. Energy Storage*, vol. 6, pp. 80-94, March 2016.

[148] M. Esmaili, A. Goldoust, "Multi-objective optimal charging of plug-in electric vehicles in unbalanced distribution networks", *Elsevier J. Electrical Power and Energy Systems*, vol. 73, pp. 644-652, June 2015.

[149] Battery University, Available: batteryuniversity.com.

[150] IC, Illinois Capacitor, Des Plaines, USA. Available: www. illinoiscapacitor.com.

[151] A. Burke, "Cost-effective combinations of ultra- capacitors and batteries for vehicle applications", presented at the Second Int. Advanced Battery Conf., Las Vegas, NV, Feb. 2002.

[152] CDE, Cornell Dubilier (Energizing Ideas), East Rodney French Blvd, New Bedford. Available: www.cde.com/catalogues.

[153] J. Xie1, J. Lu1 and X. Chen, "A Practical Digital VRB Simulator for Power System and Smart Grid Applications", IEEE Power Engineering and Automation Conference (PEAC), pp. 1-6, Sep.2012.

[154] W. Wang, B. Ge, D. Bi and D. Sun, "Grid-connected wind farm power control using VRB-based energy storage system," *IEEE* Energy Conversion Congress and Exposition (ECCE), pp. 3772-3777, Sept 2010.

[155] Photovoltaic education network. Available: www.pveducation.org.

[156] B. K. Bose, "Modern Power Electronics and AC Drives", Eastern Economy ed. Pearson Education Inc., 2002, pp. 559-623.

Publications:

Published Journals

[1] **M. Bhaskar Naik**, P. Kumar and S. Majhi, "Small-scale Solar Plants coupled with Smart Public Transport System and its Coordination with the Grid", *J. IET Elect. Syst. Transp*., vol. 7, no. 2, pp. 135-144, May 2017.

[2] **M. Bhaskar Naik**, Praveen Kumar and Somanath Majhi, "Optimal number of e-buses in the Solar assisted Smart Public Transit System and its Failure Analysis", *J. IET Elect. Syst. Transp*., DOI: 10.1049/iet-est.2016.0071, Aug 2017.

Communicated Journals

[1] **M. Bhaskar Naik**, Praveen Kumar and Somanath Majhi, "Smart public transportation network expansion and its interaction with the grid", Submitted to *Elsevier journal* on '*Sustainable Energy, Grids and Networks*'.

International Conferences:

[1] **M. Bhaskar Naik**, Santayana Gonzalo, Praveen Kumar, S. Majhi, "Analysis of Sustainable Public Transportation System and Its Interaction with the Grid", *IEEE Power and Energy Society General Meeting,* pp. 1-5, Oct 2015.

[2] **M. Bhaskar Naik**, Ashish Ranjan, Vivek Gunawat, Praveen Kumar, S. Majhi, " A brilliant Public Transportation System linked with Electric Vehicles in coordination with the Grid", *Annual IEEE India Conference* (*INDICON)*, pp. 1-6, Dec 2014.

[3] **M. Bhaskar Naik**, Kumar P, Majhi, S, "Analysis of city-Capabus transportation system failures and solutions with FLC", *16th International IEEE Conference on Intelligent Transportation System (ITSC)*, pp. 1900-1905, Oct 2013.

[4] M. Kumar, **M. Bhaskar Naik**, V. Gunawat, S. Swami, D. Prajapati, M. Singh, P. Kumar, "Analysis of Implementing the Electric City Bus and its Coordination with the Grid," *Annual IEEE India Conference* (*INDICON)*, pp. 974-978, Dec 2012.